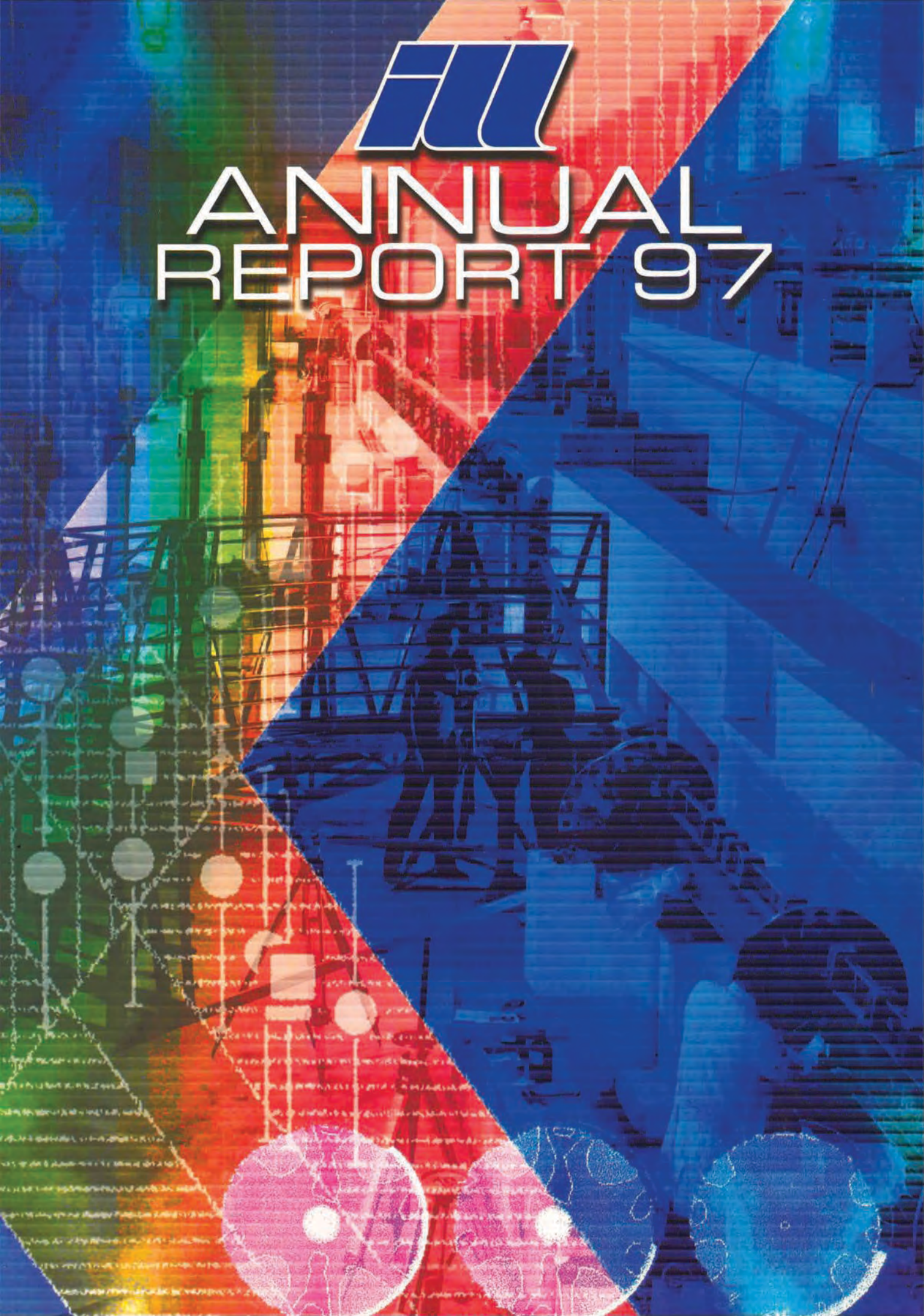
ANNUAL
REPORT 97

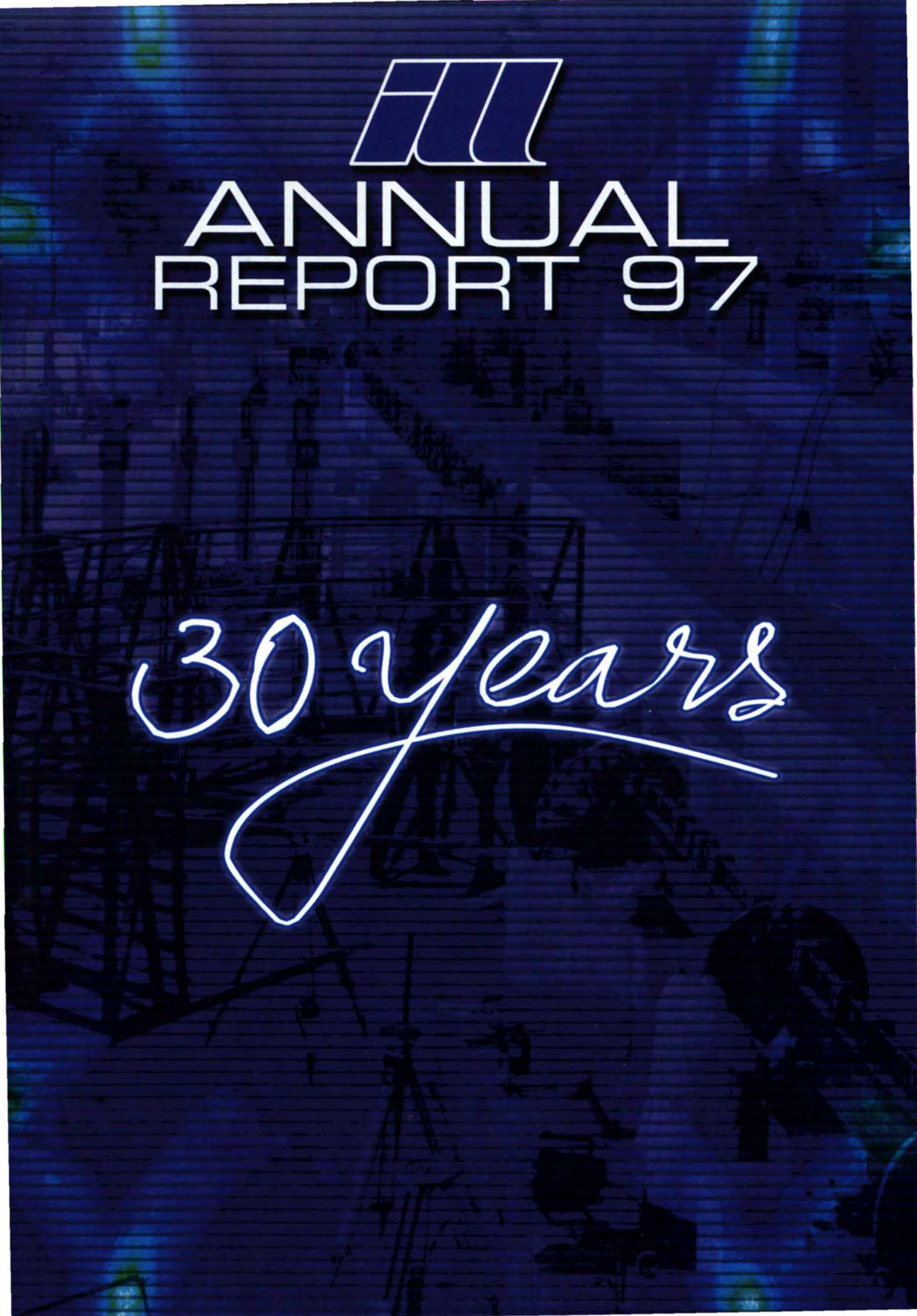
ANNUAL
REPORT 97
30 years

31 August 1971: the ILL's high-flux reactor goes critical; Bernard Jacrot, the French director at the time (blue pullover), now retired and living in Provence.

Over a quarter of a century later (on 21 April 1997), Bernard (left) attends a seminar «Les deux mondes de Bernard; reconciling Physics and Biology» – held in his honour (Mogens Lehmann on the right).

Bill Stirling, Univ. Liverpool, chairing the scientific council for the last time (10 April).

Klaus Yvon, Univ. Lausanne, (right) chairing his first scientific council meeting (23 October); from left: Dirk Dubbers, Philippe Leconte, Alan Leadbetter, Reinhard Scherm.

CONTENTS

CONTENTS

DIRECTOR'S REPORT

Science and instrumental development were a great success in 1997. However, the year brought some difficulties concerning the future uranium supply and the financial situation, and these problems will extend into the future. In order to ensure long-term provision of uranium for the reactor, agreements were signed with the Russian authorities in 1996 providing for the supply of uranium for nine years. As part of this agreement, Russia became a scientific member of the ILL and this membership was operational throughout 1997. However, no uranium has been delivered and the ILL has therefore decided with regret that, with effect from 1st January 1998, Russian scientific membership will be suspended until the uranium supply situation is successfully resolved. In the meantime the ILL is vigorously investigating alternative sources of fuel for the reactor.

At present, nearly all national research institutions are suffering budgetary constraints. This explains why also international large facilities like the ILL are under financial pressure. Currently, the ILL has to cope with an annual operating budget reduced by 6 MF compared to the original planning and with an additional reduction of 3.75 MF in 1998.

Nevertheless, now that the ILL has been in existence for 30 years with the reactor having restarted 3 years ago, it might be appropriate to take stock of ILL's current situation and future prospects. The success story of the ILL's operation is essentially based on 3 elements:

• The *high-flux reactor* with integrated cold and hot sources was and still is unrivalled as the world's best neutron source.

• As a *multinational* institute, the ILL plays host to scientific visitors from a truly international community. It has thus advanced the culture of collaboration across frontiers.

• ILL's *instrument suite* has put the institute at the forefront of neutron science. Moreover, it has been able to maintain its position thanks to continuous efforts to develop its instrumentation.

Which of these are still true today?

1. The refurbished reactor operates extremely reliably, even though we currently have to overcome problems concerning the long-term procurement of fuel.

2. As an international meeting place, « le carrefour des idées » ILL is booming. 1 400 scientists visit the institute every year. When examining proposals, we note an ever increasing « promiscuity ». Experiments are very often performed jointly by different groups. At ILL, « l'Europe vécue » comes true, and what is more, without any additional structural help!

3. ILL's instrument suite is still regarded as *the* reference in international comparisons.

The newly built thermal time-of-flight spectrometer IN4C is now being commissioned. Moreover, a moderate upgrade programme - spending some 28 MF over 5 years - will rejuvenate five instruments: with D17, ILL will - 10 years late - offer a proper up-to-date reflectometer. The diffractometer D16 and the extremely sought after TOF instrument IN5 will both benefit from a considerable flux increase. The liquids/amorphous diffractometer D4 will be equipped with a new set of multidetectors. This will increase the data rate by 10! Finally, the upgrade of the three-axis spectrometer IN8 - aiming at increased flux and flexibility - would not have been possible without the generous help of our Spanish partner.

There is, however, no reason to sit back with our arms folded. There is still tremendous scope for possible improvements. The guide hall with its neutron guides, integrated in the first design of the reactor, was a breakthrough 30 years ago. Since then much progress has been made in neutron beam-optics. The first supermirror guide at the ILL has been installed by the CEA for the CRG instruments D23 and IN22. Replacing some of the guides by supermirror guides - combined with a rearrangement of thermal beam-positions in the guide halls - would considerably increase flux or the available energy range and would thus create new opportunities, particularly in the thermal region.

But even without major rebuilds, there is plenty of opportunity for continuous improvement. Working towards improved monochromators and neutron optics will increase the flux on the sample. And the use of multidetectors can improve data rates often by more than an order of magnitude. A splendid example of this is the image-plate detector jointly developed by EMBL and ILL in collaboration with a German group, a technique which may well turn out to be revolutionary.

In addition to these developments, which concern the number of recorded neutrons, I wish to emphasise developments which aim to improve the quality of what neutron scattering can detect. Here I am thinking in particular about making use of polarisation and polarisation analysis. At present, 6 of the 25 (ILL-funded) instruments can, and do, make use of polarised neutrons. After a long development, « CRYOPAD » has entered a mature state and now permits polarisation analysis in all three directions. The prototype ^{3}He polarisation-filter has passed its first tests in real life with « bravura » and can now be developed into a routine tool. And complementary to this, a programme to grow improved « Heusler » polariser crystals has been established at ILL. One does not need to be a prophet to predict a brilliant future for the various techniques of polarisation analysis, provided sufficient support in terms of manpower and funds can be made available.

I am, of course, aware that this is not the moment to ask for expensive modernisation programmes or an « n-ième souffle ». However, ILL should not live without a vision. The reactor is good for two more decades; the problem of the end of the fuel cycle has been solved thanks to the generous help of the associates. The present problems of procurement of uranium can and will be solved. Even according to the most optimistic predictions, an alternative and more intense neutron-source will not be available for another dozen years. Finally, there is no reason not to expect warm rain after the present financial drought. As outlined above, developments are possible at a modest price compared to basic operating costs which will give renewed impetus to the ILL and to the science it supports. The ILL is still the world's leading facility in neutron research. It is worthwhile keeping a broader vision in mind and fighting to make this vision come true.

L'année 1997 a été particulièrement fructueuse sur le plan scientifique et instrumental. Cependant, cette année a été marquée par des difficultés concernant l'approvisionnement futur en uranium et par des difficultés financières, et ces problèmes se prolongeront dans les années à venir. Afin d'assurer à long terme l'approvisionnement du réacteur en uranium, des contrats avaient été signés avec les autorités russes en 1996, contrats qui prévoyaient la livraison d'uranium pendant neuf ans. Conformément à la convention signée avec Minatom, la Russie devenait membre scientifique de l'ILL. La participation scientifique de la Russie a été effective tout au long de l'année 1997. Cependant, aucun uranium n'a été livré, l'ILL a donc décidé, avec regret, de suspendre la participation scientifique de la Russie à compter du 1er janvier 1998 jusqu'à ce qu'une solution satisfaisante ait été trouvée au problème de l'approvisionnement en uranium. Entre-temps, l'ILL recherche activement des sources alternatives pour l'approvisionnement du réacteur en combustible.

A l'heure actuelle, presque tous les instituts de recherche nationaux sont confrontés à des contraintes budgétaires. Cela explique pourquoi les grands centres de recherche internationaux comme l'ILL subissent également des pressions financières.
Actuellement, l'ILL doit faire face à une diminution de 6 MF de son budget de fonctionnement annuel par rapport aux prévisions initiales, à laquelle s'ajoute une baisse supplémentaire de près de 4 MF en 1998.

Cependant, après 30 ans d'existence et le redémarrage du réacteur il y a 3 ans, il peut sembler approprié de faire le bilan de la situation actuelle et des perspectives futures de l'ILL. Le succès de l'Institut repose essentiellement sur 3 éléments :

• Le *Réacteur à Haut Flux*, avec ses sources intégrées de neutrons froids et chauds, était et reste la meilleure source neutronique au monde.

• En tant qu'institut *multinational*, l'ILL accueille des visiteurs scientifiques en provenance d'une véritable communauté internationale. Il a ainsi favorisé la culture de collaboration par delà les frontières.

• Le *parc instrumental* de l'ILL a permis de placer l'Institut à l'avant-garde de la science neutronique. De plus, l'ILL a réussi à maintenir sa position grâce aux efforts continus pour développer son instrumentation.

Que reste-t-il de vrai aujourd'hui ?

1. Le réacteur remis en état fonctionne de manière extrêmement fiable, même si nous devons actuellement surmonter des problèmes concernant l'approvisionnement à long terme en combustible.

2. En tant que lieu de rencontre international, l'ILL, « carrefour des idées », est en plein essor. 1 400 scientifiques viennent à l'Institut chaque année. Lors de l'examen des propositions d'expérience, nous notons une « promiscuité » de plus en plus grande. Les expériences sont très souvent réalisées conjointement par différents groupes. A l'ILL, « l'Europe vécue » est une réalité, et cela, sans aucune aide structurelle supplémentaire !

3. Le parc instrumental reste *la* référence au niveau international.

Le nouveau spectromètre thermique à temps de vol, IN4C, est en passe d'être opérationnel. D'autre part, un programme d'amélioration modéré - environ 28 MF sur 5 ans - permettra de rajeunir cinq instruments : avec D17, l'ILL proposera -avec 10 ans de retard - un réflectomètre réellement à la pointe du progrès. Le diffractomètre D16 ainsi que l'instrument à temps de vol IN5, toujours très demandé, bénéficieront tous deux d'une augmentation considérable de flux. Le diffractomètre liquides/amorphes, D4, sera équipé de nouveaux multidétecteurs, ce qui permettra de multiplier la vitesse d'acquisition des données par 10 ! Enfin, l'amélioration du spectromètre à 3 axes IN8 - visant à augmenter le flux et la flexibilité - n'aurait pas été possible sans l'aide généreuse de notre partenaire espagnol.

Il n'y a cependant pas de raison de rester assis les bras croisés. Les possibilités d'améliorations restent immenses. Le hall avec ses conduits de neutrons, intégrés lors de la conception initiale du réacteur, représentait il y a 30 ans une percée technologique. Depuis, de nombreux progrès ont été faits dans le domaine de l'optique des faisceaux neutroniques. Le premier guide multicouches a été installé à l'ILL par le CEA pour les instruments CRG D23 et IN22. Le remplacement de certains guides par des guides multicouches - combiné à un réarrangement des positions des faisceaux thermiques dans le hall des guides - augmenterait considérablement le flux ou la largeur du spectre en énergie disponible et créerait ainsi de nouvelles opportunités, en particulier dans le régime thermique.

Mais, même sans reconstructions majeures, il existe de nombreuses possibilités d'améliorer régulièrement les instruments. L'amélioration des monochromateurs et de l'optique neutronique permettrait d'augmenter le flux sur l'échantillon. L'utilisation de multidétecteurs peut améliorer la vitesse des données, souvent de plus d'un ordre de grandeur.

Développée conjointement par l'EMBL et l'ILL en collaboration avec un groupe allemand, la détection par phospho-imageur à plaques, une technique qui pourrait se révéler révolutionnaire, en est un splendide exemple.

Outre ces développements qui concernent l'augmentation du nombre de neutrons utiles, je voudrais souligner les développements qui visent à améliorer la qualité de ce qui peut être mesuré grâce à la diffusion de neutrons. Je pense en particulier à l'utilisation de la polarisation et de l'analyse de polarisation.

Actuellement, 6 des 25 instruments (financés par l'ILL) peuvent utiliser, et utilisent des neutrons polarisés. Après une longue période de développement, « CRYOPAD » est maintenant au point et permet une analyse de polarisation à trois dimensions. Le prototype de filtre à ^{3}He polarisé a passé 'con bravura' ses premiers tests dans des conditions réelles et peut maintenant être développé en tant qu'instrument 'de routine'. En complément, l'ILL a mis en place un programme visant à produire des cristaux polarisants « Heusler » de qualité améliorée. Il n'est pas nécessaire d'être prophète pour prédire un avenir brillant aux différentes techniques d'analyse de polarisation, à condition qu'elles puissent disposer d'un support suffisant en termes de main d'œuvre et de moyens financiers.

Je suis bien entendu conscient que ce n'est pas le moment de demander la mise en place de programmes d'amélioration coûteux, ou un « n-ième souffle ». Cependant, l'ILL de devrait pas vivre sans une vision d'avenir. Le réacteur est en état de fonctionner encore 20 ans ; le problème de la fin du cycle combustible est réglé grâce à l'aide généreuse des Associés. Les problèmes actuels concernant l'approvisionnement en uranium peuvent être, et seront résolus. Même en se fiant aux prédictions les plus optimistes, une source alternative de neutrons plus intense ne sera pas disponible avant 12 ans. Et, pour terminer, il n'y a aucune raison de ne pas espérer « une pluie bienfaisante » après « la sécheresse financière » actuelle. Comme souligné précédemment, des développements sont possibles pour un coût modeste comparé aux frais de fonctionnement de base. Ils redonneraient un nouvel essor à l'ILL et à la science qu'il soutient. L'ILL reste à la pointe de la recherche neutronique dans le monde. Cela vaut la peine d'avoir à l'esprit une vision plus large et de se battre pour que cette vision se concrétise.

1997 war ein erfolgreiches Jahr für die wissenschaftlichen Aktivitäten und die Instrumententwicklung. Es brachte jedoch auch einige Schwierigkeiten bei der Beschaffung von Uran und durch die etwas angespannte Finanzlage, Schwierigkeiten, die noch andauern werden. Um die Uranversorgung für den Reaktor langfristig zu sichern, sind 1996 mit den russischen Behörden Abkommen für die Lieferung von Uran für die Dauer von 9 Jahren abgeschlossen worden. Im Rahmen dieser Abkommen wurde Rußland wissenschaftliches Mitglied des ILL und diese Mitgliedschaft war auch im gesamten Jahr 1997 gültig. Es sind jedoch keinerlei Uranlieferungen beim ILL eingetroffen, und es wurde daher mit Bedauern entschieden, die russische Mitgliedschaft ab dem 1. Januar 1998 vorübergehend ruhen zu lassen, bis das Problem der Uranlieferungen erfolgreich gelöst ist. Inzwischen versucht das ILL intensiv, alternative Lösungen für die Beschaffung von Brennstoff für den Reaktor zu finden.

Zur Zeit werden an fast allen staatlichen Forschungseinrichtungen die Budgets gekürzt. Dies ist auch der Grund, warum internationale Grossforschungseinrichtungen wie das ILL unter finanziellem Druck stehen. Gegenwärtig ist das ILL mit einer Budgetkürzung für den jährlichen Betriebshaushalt von 6 MF gegenüber dem ursprünglich veranschlagten Haushaltsplan konfrontiert, und eine weitere Kürzung von 3,75 MF ist für 1998 vorgesehen.

Dennoch, nach 30-jährigem Bestehen des ILL und nachdem der Reaktor vor drei Jahren wieder startete, möchte ich eine Bilanz der gegenwärtigen Situation und der Perspektiven für die Zukunft des ILL ziehen. Der Erfolg des ILL beruht überwiegend auf drei Faktoren :

• Der *Hochflußreaktor* mit seiner integrierten kalten und heissen Quelle bleibt nach wie vor die beste Neutronenquelle der Welt.

• als *multinationales Institut* empfängt das ILL Gäste, die tatsächlich aus der ganzen Welt kommen und pflegt somit grenzübergreifendes Zusammenarbeiten.

• Dank des *Instrumentenparks* des ILL steht das Institut in der Neutronenforschung ganz vorn, und die ständigen Bemühungen, die Instrumentierung weiterzuentwickeln, haben es ermöglicht, diese Position beizubehalten.

Inwieweit trifft dies heute noch zu ?

1. Der sanierte Reaktor arbeitet äußerst zuverlässig, obgleich wir zur Zeit mit Problemen für die langfristige Beschaffung von Brennstoff konfrontiert sind.

2. Das ILL wird immer mehr zu einem internationalen Treffpunkt, einem sogenannten « carrefour des idées ». 1 400 Wissenschaftler besuchen es jährlich. Bei der Prüfung von Meßanträgen stellen wir fest, daß die Kooperationsbereitschaft der Wissenschaftler ständig zunimmt: häufig werden Experimente von verschiedenen Gruppen gemeinsam durchgeführt. Im ILL wird das « Europe vécue » verwirklicht und das ohne irgendwelche zusätzlichen Strukturhilfen!

3. Der Instrumentenpark des ILL ist nach wie vor *die* Referenz im internationalen Vergleich.

Das neu gebaute Flugzeitspektrometer IN4C wird zur Zeit in Betrieb genommen. Außerdem werden im Rahmen eines moderaten Modernisierungsprogramms - mit zirka 28 MF über einen Zeitraum von 5 Jahren - 5 Instrumente erneuert: mit D17 wird das ILL - nach zehn Jahren - ein Reflektometer bauen, das dem neuesten Stand der Technik entspricht. Sowohl das Diffraktometer D16 als auch das vielbegehrte Flugzeitinstrument IN5 werden von einer Neutronenflußsteigerung profitieren. Das flüssig/amorph Diffraktometer D4 wird mit neuen Multidetektoren versehen, was die Datenleistung um ein 10 faches steigert!

Weiterhin wird das Dreiachsenspektrometer IN8 verbessert - gesteigerter Fluß und größere Flexibilität - was ohne die großzügige Hilfe durch den spanischen Partner nicht möglich gewesen wäre.

Dies ist jedoch kein Grund für das Institut, sich auf seinen Lorbeeren auszuruhen. Es gibt unzählige weitere Verbesserungsmöglichkeiten. Die Leiterhalle mit den im ersten Reaktordesign integrierten Neutronenleitern stellte vor 30 Jahren einen Durchbruch dar. Seither wurden in der Neutronenstrahloptik große Fortschritte gemacht. Der erste Superspiegel-Neutronenleiter wurde am ILL vom CEA für die CRG Instrumente D23 und IN22 installiert. Wenn man einige der Leiter durch Superspiegel-Neutronenleiter ersetzt - kombiniert mit einer neuen Anordnung der thermischen Strahlpositionen in den Leiterhallen - könnte man den Neutronenfluß oder den zur Verfügung stehenden Energiebereich beträchtlich erhöhen und somit neue Möglichkeiten, insbesondere im thermischen Bereich, schaffen.

Aber sogar ohne größere Umbauten gibt es viele Modernisierungsmöglichkeiten. Verbesserungen der Monochromatoren und der Neutronenoptik gewährleisten einen besseren Neutronenfluß auf den Proben. Die Anwendung von Multidetektoren kann die Datenleistung häufig um mehr als eine Größenordnung verbessern. Ein hervorragendes Beispiel dafür ist der Image-Plate Detektor, der gemeinsam vom ILL und dem EMBL in Zusammenarbeit mit einer deutschen Gruppe entwickelt wurde, eine Technik, die sich als revolutionär erweisen könnte.

Zusätzlich zu diesen Entwicklungen, die die Anzahl der gemessenen Neutronen betreffen, möchte ich den Akzent auf Entwicklungen setzen, die das Ziel haben, die Qualität dessen zu steigern, was die Neutronenstreuung entdecken kann. Dabei denke ich insbesondere an die Anwendung von Polarisation und Polarisationsanalyse. Zur Zeit sind 6 der 25 (vom ILL finanzierten) Instrumente in der Lage, polarisierte Neutronen zu produzieren und zu benutzen. Nach einer langen Entwicklungsphase ist « CRYOPAD » nun reif für Polarisationsanalysen in alle drei Richtungen. Der Prototyp des ^{3}He-Polarisationsfilters hat seinen ersten Einsatz mit Bravour bestanden und kann nunmehr zum Routineinstrument ausgebaut werden. Ergänzend dazu hat das ILL ein Programm für die Zucht von verbesserten « Heusler » Polarisationskristallen begonnen. Auch ohne Prophet zu sein, kann man den verschiedenen Techniken der Polarisationsanalyse eine brillante Zukunft voraussagen, soweit ausreichende Mittel in Form von Manpower und Finanzen zur Verfügung gestellt werden können.

Mir ist selbstverständlich klar, daß der Zeitpunkt nicht geeignet ist, teuere Modernisierungsprogramme oder einen « n-ième souffle » für das ILL zu verlangen. Jedoch sollte das ILL nicht ohne Perspektiven leben. Der Reaktorbetrieb ist für die kommenden zwei Jahrzehnte gesichert; das Problem mit dem Brennstoffkreislauf wurde dank der großzügigen Hilfe der Gesellschafter gelöst. Die gegenwärtigen Probleme der Uranversorgung sind lösbar und werden gelöst. Auch nach optimistischsten Vorhersagen wird eine alternative und stärkere Neutronenquelle vor gut einem Jahrzehnt nicht zur Verfügung stehen. Schließlich gibt es keinen Grund, nach der gegenwärtigen finanziellen Trockenheit keinen warmen Regen zu erwarten. Wie oben beschrieben, sind Modernisierungen möglich, deren Kosten im Vergleich zu den Betriebskosten bescheiden sind und die dem ILL und seinen wissenschaftlichen Aktivitäten neue Impulse geben können. Das ILL ist nach wie vor die führende Forschungseinrichtung in der Neutronenforschung. Man sollte mit Weitblick in die Zukunft sehen und sich dafür einsetzen, Visionen wahrzumachen.

REINHARD SCHERM

Reinhard Scherm surrounded by the two ladies of his ILL director's life: his wife Gisela (right) and his secretary Barbara Standke.

Robert Comès, LURE Orsay, (centre), member of the steering committee, enjoys a drink and a bite at the buffet of the ILL scientific council (10 April); from left: Francis Tasset, Charles-Henri de Novion, LLB Saclay, Christian Vettier, ESRF, Jean Blétry, CEA Grenoble, Albert-José Dianoux and Barbara Standke.

I agree, but .... Subcommittee 3 discussing the proposals; from left Klaus Schreckenbach, TU München, Helmut Rauch, Atominstitut Wien, Dominique Goutte, service nucleaire Bruyère-le-Châtel, Vladimir Nazarenko, PNPI St. Petersburg, Mike Pendlebury, Univ. Sussex, Dave Warner, CLRC Daresbury, Hans Börner.

Willi Bührer, LNS Villigen, as we all remember him, here in action on IN3. He died in November; he will be greatly missed by all those who worked with him.

Another sad loss is Oskar Blaschko, Univ. Wien. Seen here sitting in April's subcommittee 4 meeting (2nd from left). Oskar's work was very much appreciated by the ILL and all his colleagues. From right: Burkhard Renker, FZ Karlsruhe, Hilbert von Löhneysen, Univ. Karlsruhe , Dieter Strauch, Univ. Regensburg, Joël Mesot, LNS Villigen.

SCIENTIFIC HIGHLIGHTS

1

In 1997 the reactor operated for the planned 225 days and more than 750 experiments were carried out in over 4600 days of scheduled beam time. Individual reports on these experiments will appear on the Web in 1998. In addition to these experiments there are also those carried out by the Collaborating Research Groups (CRGs) in their own beam time, which are not in general included in this report.

As always, a remarkable range of scientific projects and types of experiment have been undertaken this year. In the following pages we present about 30 brief accounts of research carried out during the year in order to illustrate both the breadth of activity at the ILL and its quality. Included are two contributions from the theory group, which plays such an important role in the scientific life of the Institute. Among the experimental highlights are two contrasting examples of the new types of experiment now possible using the new high-intensity diffractometer D20: stroboscopic measurements of kinetic processes and rapid texture measurements of structural materials. The long wait for this instrument with its large 160° linear multidetector is being rapidly compensated for by its outstanding success since scheduled operation began in June. Some early results from the new high-resolution gamma spectrometer in the study of nuclear structure are also presented. Another new facility is just coming into service: the 2π image-plate detector LADI, optimised for Laue measurements on biological crystals. The first results have already been published in 1997 but another example of recent work on vitamin B_{12} is included here. The contrast between this biological experiment and, for example, those on superconductivity or neutron β-decay, illustrates very well the range of scientific questions addressed through the use of ILL's neutron beams.

We thank all those who submitted highlights for this Annual Report, especially those whose contributions we have not included, and invite our users to start thinking now of submissions for next year's report.

Segmental dynamics in unusual core-shell macromolecules: amphiphilic dendrimers

H. Frey, C. Lach, K. Lorenz, B. Stark, B. Stühn (Univ. Freiburg),
B. Frick (ILL).

Dendrimers based on a flexible carbosilane scaffold with perfluorohexyl ($-C_6F_{13}$) endgroups were investigated using x-ray and quasielastic neutron-scattering. The microphase separation between the dendrimer core and the endgroups leads to mesostructure which is lamellar for generation g = 1 and columnar for g = 3. The lateral order between the endgroups decreases with g. From quasielastic neutron-scattering experiments two components of the dynamic structure-factor are found; coherent scattering from the end groups and incoherent scattering from the dendrimer core. The segmental diffusion of the core as well as the rotational diffusion of the end groups decreases with g.

Recent years have brought significant progress in the understanding of the segmental dynamics in polymers. Quasielastic neutron-scattering was a key experimental method as it provides information on both the spatial and the time correlation of the dynamics of segments. The main interest so far was in the dynamics of linear chain polymers in solution and in the melt. Questions concerning the impact of the hydrodynamic interaction and the effect of entanglements were studied in great detail.

Molecular architecture and static structure

In this report we consider the segmental dynamics in macromolecules which are of more complex but well defined architecture [1]. Dendrimers are highly regular cascade polymers [2]. They represent the first class of synthetic macromolecules that can be prepared absolutely monodisperse. In this respect, dendrimers resemble biological macromolecules. Numerous applications are discussed for dendrimers at present, e.g. catalysis, drug targeting as well as medical imaging techniques. Furthermore, dendrimers are discussed as precision standards for gel permeation chromatography. However, in contrast to their synthesis, their solid structure, supramolecular ordering and segmental dynamics have been little investigated so far.

The centre of a dendrimer (inset in Fig. 1) is (in the present case) a 4-functional unit from which branches of well defined length emanate. They end again in a 4-functional

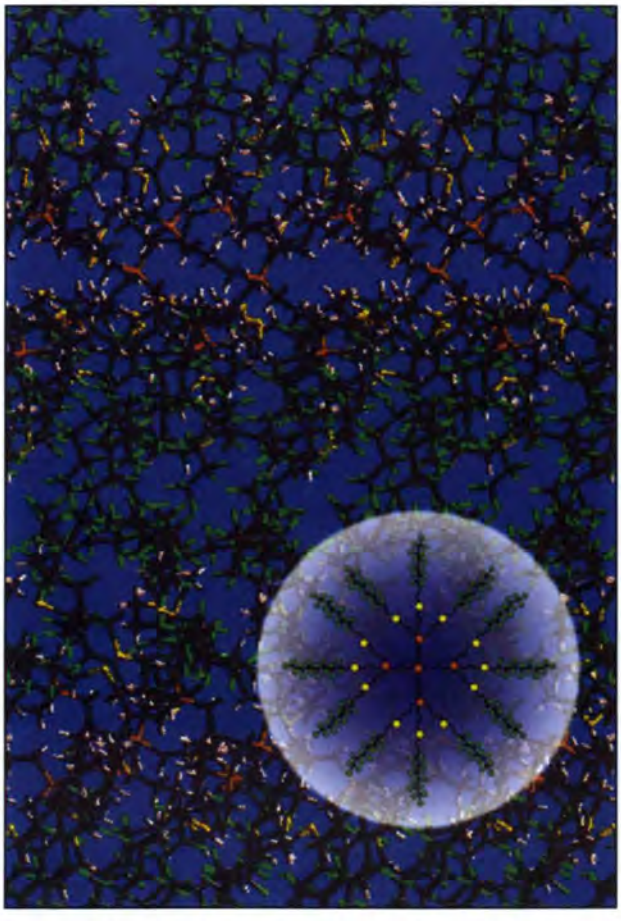

Figure 1: *The chemical structure (**inset :** • Si, • S, • F) and the lamellar superstructure of the first dendrimer generation. A bar in the dendrimer core structure denotes a $-C_3H_6$ group.*

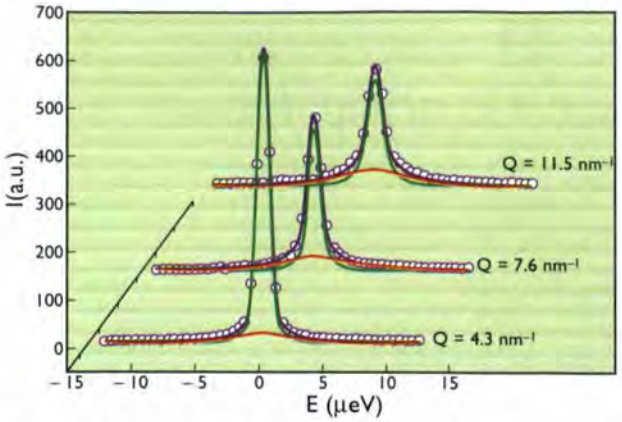

Figure 2: *The dynamic structure-factor as obtained on IN16. It consists of the sum of a narrow (green) and a broad (red) component.*

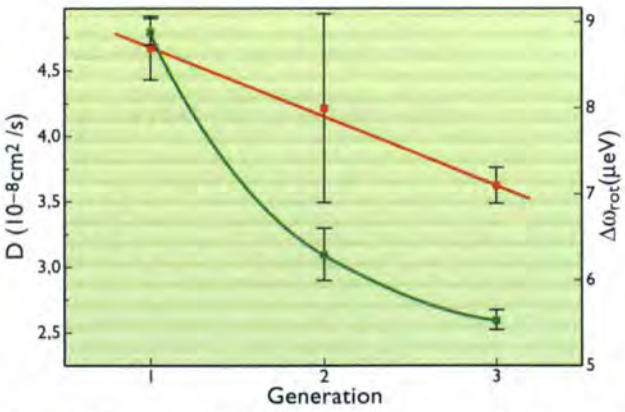

Figure 3: *The segmental diffusion coefficient D (green) and the rotational diffusion (red) (given in energy units) showing the decrease of both with the generation of the dendrimer.*

unit and thus complete the first generation (g = 1) of the dendrimer. Further branching leads to a perfect tree-like structure. We study the variation of structure and segmental dynamics with increasing number of generations. The inset of Fig. 1 shows the chemical structure of a generation 1 dendrimer based on carbosilane. The endgroups are $-C_6F_{13}$ units which may be thought of as stiff helical molecules. They microphase separate from the interior of the dendrimer which may therefore be considered a monomolecular micelle. In the bulk the spherical symmetry of the dendrimer is broken due to the superstructure caused by this microphase separation. In Fig. 1 we show the layered structure formed by the first generation of the dendrimer as deduced from analysis of x-ray scattering data. The $-C_6F_{13}$ groups form stratified double layers at the expense of a strong deformation of the carbosilane scaffold of the dendrimer. This layered structure is also found in crystals of C_nF_{2n+2}. The total thickness of a layer is 2.8 nm. The lateral packing of the endgroups is hexagonal but shows significant disorder. For g = 2 the superstructure is less well ordered, g = 3 shows columnar structure [1].

Quasielastic neutron-scattering

The quasielastic neutron-scattering profile as measured on the backscattering spectrometer IN16 clearly shows two contributions as shown for a selection of Q in Fig. 2. The full lines in the figure are a fit using two lorentzian lines convoluted with the experimentally determined resolution of the instrument. As a result we obtain the Q dependence of the full width at half maximum (FWHM) for both components of the dynamic structure-factor representing the space-time correlation of the segmental dynamics.

From the molecular structure of the dendrimer one indeed expects two separate contributions to the scattering. One component is coherent from F and C in the endgroups, the second arises from the incoherent scattering from H in the interior of the dendrimer. This interpretation is supported by the relative intensity of the two contributions. The broad component displays only very weak temperature and Q dependences and is related to the rotational diffusion of the $-C_6F_{13}$. The FWHM $\Delta\omega_{rot}$ is of the order of 10 μeV and thus of the same magnitude as observed for the rotational diffusion of $C_{20}F_{42}$ helices in the crystal [3].

The second component of the dynamic structure-factor displays a line broadening $\Delta\omega \propto Q^{\gamma}$. For $Q < 10\ nm^{-1}$ the data show $\gamma = 2$ in accordance with a simple diffusive motion and the resulting diffusion coefficient is given in Fig. 3. It decreases markedly with g and a decrease in the rotational diffusion is also found.

This decrease in mobility with g may be due to the variation in packing density associated with the increase in connectivity. It is only qualitatively explained by recent theoretical work [4].

The main result of this study is that the structure and the segmental dynamics of the core shell dendrimers are strongly influenced by the balance between the primarily spherical structure of the molecule and the layered superstructure enforced by its stiff endgroups.

References

■ [1] K. Lorenz, H. Frey, B. Stühn and R. Mülhaupt, Macromolecules 30 (1997) 6860 ■ [2] D.A. Tomalia, A.M. Naylor and W.A. Goddard, III. Angew. Chem. Int. Ed. Engl. 29 (1990) 138 ■ [3] M. Kimmig, R. Steiner, G. Strobl and B. Stühn, J. Chem. Phys. 99 (10) (1993) 8105 ■ [4] R. La Ferla, J. Chem. Phys. 106 (2) (1997) 688; C. Cai and Z.Y. Chen, Macromolecules 30 (1997) 5104.

Diffraction studies of alignment of plate-like particles under flow

A.B.D. Brown, S. M. Clarke, A.R. Rennie (Univ. Cambridge),
P. Convert, T. Hansen (ILL).

Neutron diffraction has been used to study the shear alignment of various plate-like particles. In contrast to other experimental techniques, the full angular orientation-distribution can be measured and this can be done at high volume fractions. Data for a sample of kaolinite lies between the calculations for a dilute fluid and a nematic liquid crystal. The time-resolved (stroboscopic) data-acquisition system on D20 can be used to follow relaxation processes on the time scale of less than a millisecond up to a number of seconds. The rate of ordering and relaxation under flow was studied using this technique.

Introduction

Many fluids such as polymers and colloidal dispersions display complicated rheological properties. The viscosity may decrease with increasing shear rate (shear thinning) or increase (shear thickening); changes in both elastic and viscous response can also be observed with amplitude of strain and shear history.

Many industrial processes are concerned with these non-linear properties though they are very poorly understood. In consequence, there is much research interest to understand this behaviour using computer simulation and experiment. To explain these phenomena and test theoretical models, it is important to determine and understand the particle motion, structure and orientation as well as the large-scale mechanical properties.

The Bragg diffraction from dispersions of crystallites is proportional to the number of crystallites in the correct orientation to diffract. If the sample is placed at different orientations then the number of crystallites at all orientations with respect to the sample can be measured (see Fig. 1a). This technique can be applied to a variety of flow geometries, particles and dispersing media [1].

Recent work has concentrated on dispersions of plate-like particles which are of widespread practical importance: for example as coatings in the paper industry and as drilling muds.

The penetration of the neutrons through both liquids and materials used to make flow cells is of particular advantage. A rotating disc shear cell has been constructed to fit within the Euler cradle on the diffractometer D20 and is shown in Fig. 1b.

The cell can be oriented in any direction with respect to the incident beam and the intensity of various Bragg peaks measured simultaneously on the 160° multidetector.

Measurements of diffraction under flow

The simplest experiments are on alignment in a continuous, uniform shear gradient. In kaolinite the $\{00\ell\}$ reflections are characteristic of the orientation of the plate normals and so were used to measure the orientation distribution of plates within the sample.

The intensity was investigated in many directions within the sample.

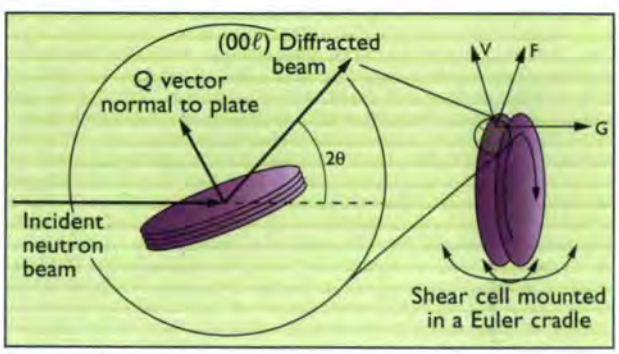

Figure 1a: *Schematic diagram of measurement of orientation from aligned crystallites in a dispersion. The Bragg diffraction from crystallites is proportional to the number of particles in a particular orientation. The diagram also shows the orthogonal, principal axes of flow: the flow direction, F, the shear gradient direction, G and the vorticity direction, V.*

Figure 1b: *Disc/disc cell for uniform shear mounted on the Euler cradle of D20. The cell is made from aluminium and has a diameter of 20 cm giving reasonably uniform shear gradients over an area of 1 cm² near the edge of the cell.*

Data are shown in Fig. 2 for a 50% w/w dispersion of kaolinite, displaying the distribution of the plate orientations for a number of shear rates. As shear rate is increased the particles become more aligned and the direction of alignment of the plate normals moves towards the shear gradient direction, i.e. the plates tend to align along the flow direction. Results in the form of plots of order parameter against the angle of alignment can be compared with theoretical models for dilute and liquid crystalline fluids [2]. This clay, at a high concentration, behaves between these extreme models. The high flux and large multidetector of D20 are important as it is necessary to measure many data points from fairly weak scattering samples. The ability to measure several Bragg peaks simultaneously allows the full particle-orientation distribution to be measured and improves the range and statistics of scattering patterns where one Bragg peak is obscured by the sample cell or cradle.

The stroboscopic collection of diffraction patterns as a series of repeating time slices, allowed the formation and relaxation of this order to be investigated on starting and stopping the flow. Measurements in a periodic, stepped flow are shown in Fig. 3. The rate of alignment and relaxation are clearly not the same, the former being much more rapid. The rate of reorientation can be measured as a function of volume fraction and gives a measure of the local rotation rates of particles in fluids subject to shear.

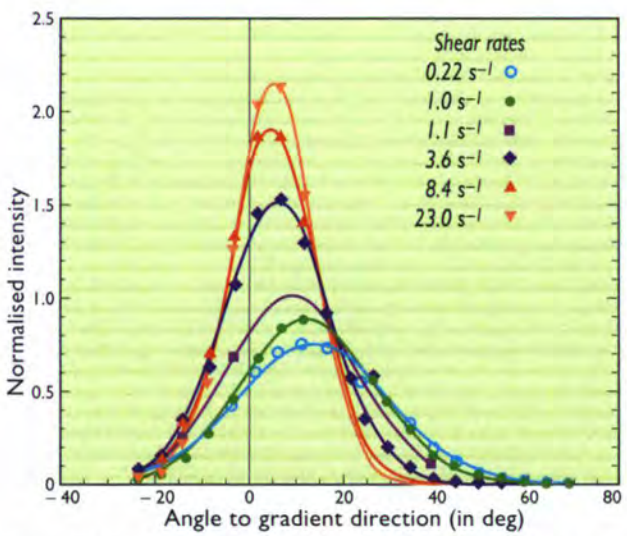

Figure 2: *Normalised diffracted intensity for the (002) and (004) Bragg peaks for kaolinite in D_2O at a number of shear rates. The angle is zero in the shear gradient direction, positive in the compressional quadrant and 90° in the shear flow direction. The data have been normalised to the incoherent scattering from the water.*

Conclusions

Only a small fraction of the data that can be obtained from time-resolved and continuous measurements of orientation in dispersions can be displayed in a short report. The high flux has allowed detailed measurements on regions of uniform flow.

This area of application of neutron diffraction now offers many exciting possibilities in the areas of pure science and engineering. Maps of non-uniform flow fields can be prepared using a small beam-size.

Re-orientation dynamics can be investigated in materials under the influence of magnetic or electric fields as well as mechanical stress.

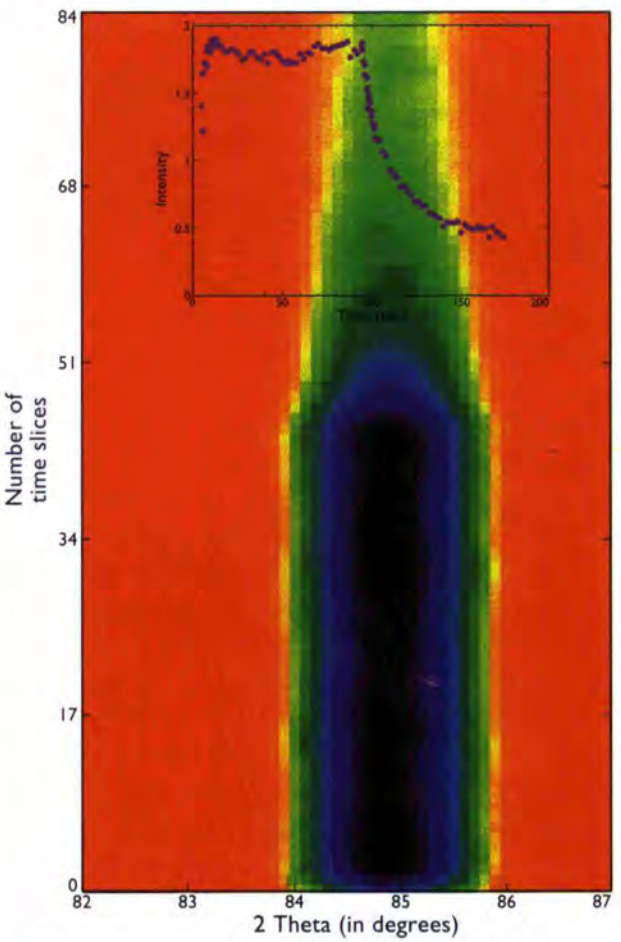

Figure 3: *Intensity map of diffraction against angle and time for 28% w/w kaolinite for a shear rate of 8 s^{-1} for 90 seconds and stop for 90 seconds (each time slice is 2 seconds). The analysis of this data is shown in the inset.* ***Inset:*** *Normalised intensity for the (004). The measurement was made close to the shear gradient direction and the plate normals align in this direction during flow.*

References

■ [1] S.M. Clarke, A.R. Rennie, P. Convert, Europhys. Letts. 35 (1996) 233 ■ [2] A.B.D. Brown, S.M. Clarke, A.R. Rennie, Prog. Coll. Pol. Sci. in press.

Homogeneous nucleation and growth studied by time-resolved small-angle neutron-scattering

- S.U. Egelhaaf (ILL),
- P. Schurtenberger (ETH Zürich),
- J. Morris, U. Olsson, H. Wennerstrom (Lund University).

Time-resolved small-angle neutron-scattering experiments were used in order to follow the nucleation and growth of big oil drops after an oil-in-water microemulsion consisting of spherical droplets is temperature-quenched into a two phase situation where excess oil separates out. The experiments provide detailed information on the temporal evolution of the size distribution of oil drops and small microemulsion spheres and demonstrate the power of time-resolved small-angle neutron-scattering experiments for studying pathways and kinetics associated with the relaxation to equilibrium in surfactant systems.

Oil and water can form thermodynamically stable phases in the presence of a surfactant. These microemulsions exhibit a range of nanoscale structures where water and oil domains are separated by a surfactant film. During the last decade a detailed understanding of the factors determining the stability of the phases and their structure has been established. This knowledge is now utilised so that microemulsions serve as model systems for studying a range of basic physical and chemical processes [1].

While we have seen significant progress in our understanding of equilibrium properties, much less is known about non-equilibrium or metastable states and the pathway and kinetics associated with the relaxation to equilibrium. One such process, namely the separation of an oil phase from oil-in-water microemulsion droplets, is the subject of the present study.

We start from an equilibrium system consisting of oligodisperse spherical droplets of oil (decane) covered with a surfactant film ($C_{12}E_5$), with structural and dynamic properties that closely follow those of a hard-sphere fluid [1,2]. The system is then temperature quenched into a two phase situation where excess oil separates out and coexists with a microemulsion of smaller droplets. To reach the equilibrium state the oil phase has to nucleate. From turbidity experiments we have evidence that this is a homogenous nucleation-process. The nucleation involves the growth of some of the droplets of the initial microemulsion, while the majority of droplets decrease in size (Fig. 1). The free-energy changes in this process are dominated by the curvature energy of the film. It was established both theoretically and experimentally that for moderate quenches a barrier for the nucleation exists, while for deeper temperature quenches the system is locally unstable [3,4]

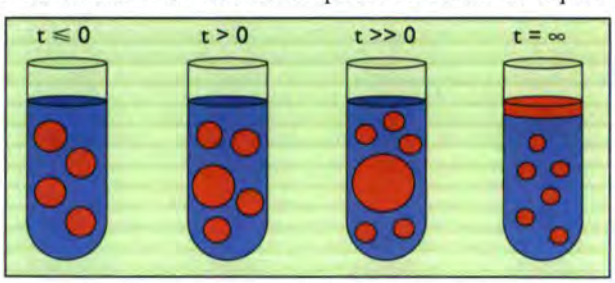

Figure 1: *At t = 0 an equilibrium system of oligodisperse oil-in-water microemulsion droplets is quenched into a two phase area where, at final equilibrium (t = ∞), smaller droplets coexist with an excess oil phase. The oil phase nucleates at a few of the initial droplets which subsequently grow (t > 0), allowing the majority of droplets to decrease in size. This growth phase proceeds with a constant number of large drops (t >> 0).*

However, while turbidity measurements may report on the onset of nucleation, alternative techniques are clearly needed to follow the phase separation process in more detail and to obtain structural information. We tried to use time-resolved dynamic light-scattering measurements in order to monitor the formation and growth of the larger oil drops, but these experiments were not very successful. The overall intensity was completely dominated by the contribution from the small microemulsion droplets, and the big oil drops became visible only in the late stages of phase separation.

However, with neutron scattering we can take advantage of the enormous changes in scattering contrast that can occur upon isotopic substitution. We worked with $C_{12}E_5$ and D_{22}-decane in mixtures of H_2O and D_2O and adjusted the H_2O/D_2O ratio in order to match out the contributions from the initial small droplets, therefore obtaining maximum sensitivity to the growth of the larger drops. The small-angle neutron-scattering experiments were performed on the instrument D22, which is particularly suited for time-resolved experiments [5]. Following a temperature quench into the unstable regime, scattering curves were measured for periods of 30 seconds over an observation period of more than two hours. Fig. 2 shows a sequence of scattering curves from one experiment, and it clearly demonstrates the dramatic changes in the scattering as time progresses.

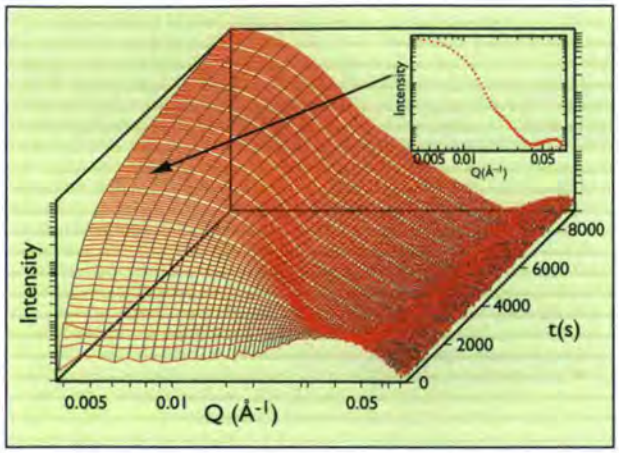

Figure 2: *Sequence of scattering curves from a time-resolved small-angle neutron-scattering experiment recorded during the nucleation and growth of an excess oil phase from oil-in-water microemulsion droplets. For clarity only every second measurement is shown. As an example the scattering curve obtained at t = 3150 s is added as an inset.*

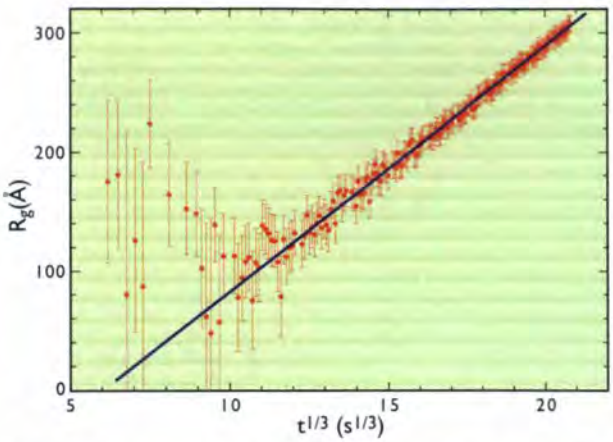

Figure 3: *Time-dependence of the radius of gyration $R_{g,big}$ as obtained from a Guinier fit. Also shown is the power law behaviour expected for a classical Ostwald ripening process.*

Although the isotope composition was adjusted in order to minimise the contributions from the small droplets of the initial system at low Q, it is not possible to obtain perfect matching since they have a certain degree of polydispersity. Therefore we observe a finite intensity at $Q \approx 0$ Å^{-1} even at time zero, i.e. before any large drops have been formed. The maximum observed initially at $Q \approx 0.04$ Å^{-1} reflects the average size of the small droplets of $R \approx 100$ Å. As time progresses it moves to higher Q-values, indicating a decrease of the microemulsion droplet size. At the end of the experiment the small droplets have still not reached their final equilibrium size of $R \approx 60 - 80$ Å.

The growing scattering amplitude at low Q-values is due to the few large drops. The large drops retain an oligodisperse ($\sigma_R = 0.3$) size distribution as can be seen qualitatively from the 'hump' in the scattering curves, which at later times appears at $Q \approx 0.02$ Å^{-1} and corresponds to the second peak in the form factor of a sphere. While a quantitative analysis of the intensity contribution from the small droplets will require explicit incorporation of interparticle interaction effects, the large drops are so few that their relative positions are completely uncorrelated and can be treated as an ideal gas of drops. A Guinier analysis of the behaviour at low Q yields the time-dependence of the radius of gyration $R_{g,big}$ of the large drops as shown in Fig. 3.

The following qualitative picture of the nucleation/growth process emerges from our time-resolved small-angle neutron-scattering study: there is an initial rapid nucleation phase, which ends when the depletion zones of oil monomers, that develop around each nucleus, overlap throughout the system. This is followed by a growth phase where individual dissolved oil molecules diffuse from the small droplets to the larger nuclei. This is supported by the time-dependence of $R_{g,big}$ which follows a power law of the form $R_{g,big} \sim t^{1/3}$ (the initial deviation is mainly due to the different contrasts of the deuterated oil core and the hydrogenated surfactant shell). The number of large drops remains constant, indicating that drop-drop coalescence is a negligible process under the circumstances. This is consistent with an Ostwald ripening of the nuclei that were formed during a short nucleation burst following directly after the temperature quench. This growth phase continues for long times.

The experiments provide us with data on the initial formation and subsequent growth of the oil drops initiated by a temperature quench of an oil-in-water microemulsion. For the first time we have access to the temporal evolution of the size distribution of oil drops and small microemulsion spheres, which will allow for a detailed, quantitative description of the underlaying processes.

This first series of experiments demonstrates the power of time-resolved small-angle neutron-scattering experiments for studying pathways and kinetics associated with the relaxation to equilibrium in surfactant systems.

References

■ [1] U. Olsson, H. Bagger-Jörgensen, M. Leaver, J. Morris, K. Mortensen, R. Strey, P. Schurtenberger, and H. Wennerström, Prog. Colloid Polym. Sci. 106 (1997) 6 ■ [2] U. Olsson and P. Schurtenberger, Langmuir 9 (1997) 3389 ■ [3] J. Morris, U. Olsson, and H. Wennerström, Langmuir 13 (1997) 606 ■ [4] H. Wennerström, J. Morris, and U. Olsson, Langmuir, 13 (1997) 6972 ■ [5] S. U. Egelhaaf and P. Schurtenberger, Physica B 234 - 236 (1997) 276.

Diffusion in zeolites

H. Jobic (IRC Villeurbanne),
M. Bée (UJF Grenoble).

Zeolites are widely used in industry for a wide range of applications including adsorption and separation of gases and hydrocarbons, catalysis, drying, etc. Shape-selective separation and catalysis are based on restricted molecular diffusion in the microporous network. A detailed characterisation of molecular migration in these materials is therefore essential to model their transport properties.

Introduction

Zeolites are crystallised microporous materials offering channels or cavities of molecular dimension, hence the term molecular sieve. In zeolites, the size of the molecules can be comparable to the size of the pores. This leads to diffusion limitations and diffusion coefficients are from 3 to 12 orders of magnitude lower compared to the gas phase. Quasielastic neutron-scattering has been used in recent years to characterise the diffusion process and to determine diffusion coefficients for molecules adsorbed in zeolites. Depending on the structure and on the adsorbate, different jump diffusion mechanisms have been encountered.

Xylenes/Faujasite

The industrial separation of para-xylene from C_8 aromatics (p-, o-, m-xylenes and ethylbenzene) is an important step in the large scale synthesis of petrochemicals. Xylenes are used as industrial solvents or intermediates for many derivatives. The para isomer is the most interesting, it is at the basis of the production of polyester films and fibres. Each derivative must be produced with a high purity for further use in synthesis. Classical methods of separation, e.g. distillation and crystallisation, are not efficient or economically attractive and the processes now in operation are based on zeolites of faujasite structure with barium as compensating cation. The industrial processes work in the liquid phase at a temperature of ≈ 150°C.

The faujasite structure leaves large cavities of about 12 Å in diameter, connected by windows about 8 Å wide (Fig. 1). Smaller cavities, the sodalite cages and the hexagonal prisms, are only accessible to small molecules like water. In all these cavities, several cation positions can be found: barium occupies mainly sites I and II whereas sites I , I', II, and III can be populated by sodium, with different occupation factors. Neutron diffraction reveals that xylene molecules are adsorbed at II cations, but the selectivity of BaX for para-xylene cannot yet be explained.

It seems that the selectivity involves both equilibrium properties and diffusion behaviour. Whereas neutron diffraction gives equilibrium positions of the molecules at low temperature, the dynamics of the molecules can be characterised by quasielastic neutron-scattering in a wide range of temperatures, including those used in the industrial process. Experiments were first performed on IN6 with an energy resolution (≈ 100 μeV) corresponding to relatively short time scales, $10^{-11} - 10^{-12}$ s. On this time scale, only rotational motions of the molecules within the supercages could be characterised.

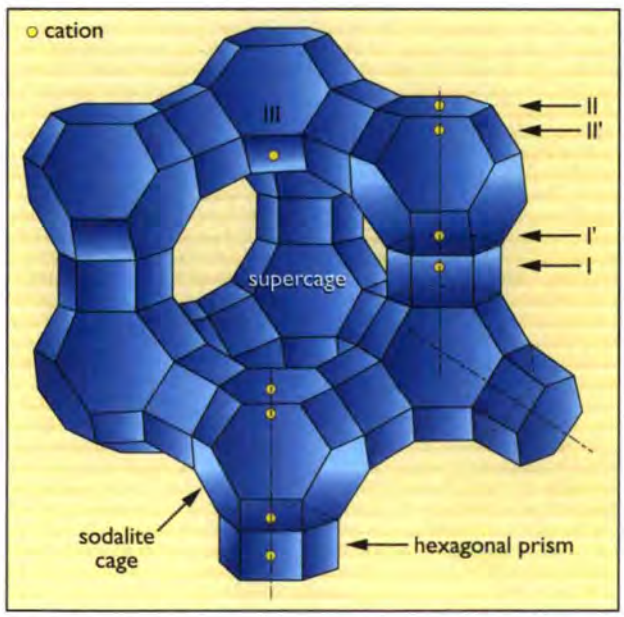

Figure 1: *Faujasite structure. Cation positions are indicated by roman numerals.*

In order to measure the diffusion from cage to cage, on a time scale of 10^{-9} s, the IN16 spectrometer, with a resolution of ≈ 1 μeV was used. The increased broadening of the elastic peak measured at different temperatures reflects the increase of the diffusivity of the molecules and it was found to be characteristic of a jump-diffusion process with jumps of a fixed length occurring in random directions, this is known as the Chudley-Elliot model (Fig. 2). All the spectra could be fitted simultaneously with this model. The jump length was found to be 5.5 Å, which indicates that the molecules jump from one site II position to another. This is the first time that this jump diffusion model has been so clearly observed in a zeolite. An influence of the cation on the dynamics of para and metaxylene was observed: the diffusion of both isomers is slower in BaX than in NaX, the para diffuses faster than the meta in NaX, but the reverse is found in BaX. This could explain the higher para/meta selectivity observed in this zeolite.

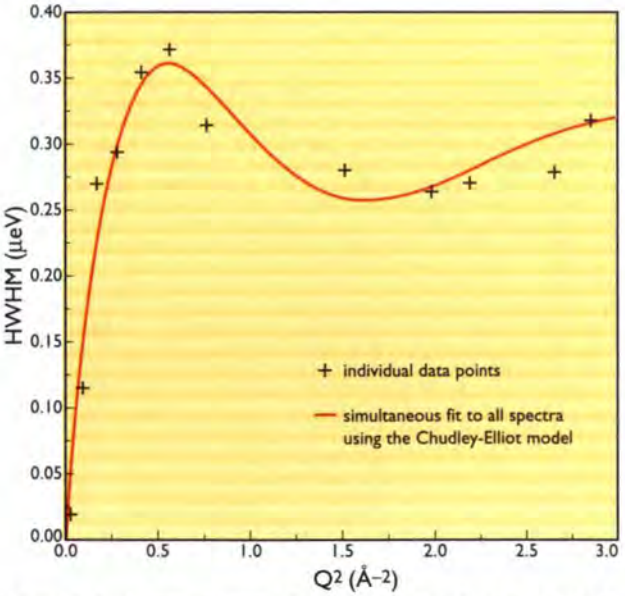

Figure 2: *Broadenings measured for para-xylene in NaX zeolite, at 355 K.*

Long alkanes/silicalite

Silicalite has already found several applications in the field of chemical and fuel processing. Zeolitic membranes, i.e. membranes incorporating silicalite crystals, are presently being studied in academic and industrial laboratories They have great potential interest for major processes, e.g. hydrocarbon recovery, steam reforming, hydrogen removal, etc. A schematic picture of the silicalite structure is shown in Fig. 3 (inset): there are straight channels running along the b axis, interconnected by zig-zag channels running along a, the size of both channels is ≈ 5.5 Å.

Various experimental techniques and simulation methods have been used to study the mobility of n-alkanes in this zeolite. Differences of up to 6 orders of magnitude have been observed in the diffusion coefficients. For short alkanes, quasielastic neutron-scattering, pulsed-field gradient NMR and molecular-dynamics simulations are in reasonable agreement, but large variations were noted with other methods like thermo-gravimetry, chromatography, frequency response, etc. For longer alkanes, no microscopic results are available and simulation was ahead of experiment: the mobility of these alkanes has recently been derived using a hierarchical approach [1], which draws upon concepts from Brownian motion and transition state theories and is capable of simulating very long times (>100 ns).

Quasielastic neutron-scattering experiments were recently performed on IN16 and the diffusion of C_8, C_{10}, C_{12}, and C_{14} could be characterised. Calculations and experiment are in agreement for the general trend: the self-diffusion coefficient decreases up to C_8 but shows only a slight decrease for longer alkanes. However, the diffusion coefficients measured by quasielastic neutron-scattering are smaller than the calculated values, by approximately a factor 10. This discrepancy can be attributed (i) to a larger loading in the quasielastic neutron scattering experiment and (ii) to a number of assumptions made in the calculations, e.g. rigid framework and coarse graining. For these long alkanes, there is no well defined absorption site and the spectra were fitted with a jump-diffusion model having a distribution of jump lengths. Diffusion in silicalite is anisotropic and information on the anisotropy of the diffusion can be obtained, as illustrated in Fig. 3 where it is shown that a better fit is obtained for 1D rather than 3D diffusion, when looking at distances corresponding to the length of a channel. The anisotropy is less pronounced when one looks at the diffusion over a distance of several channels.

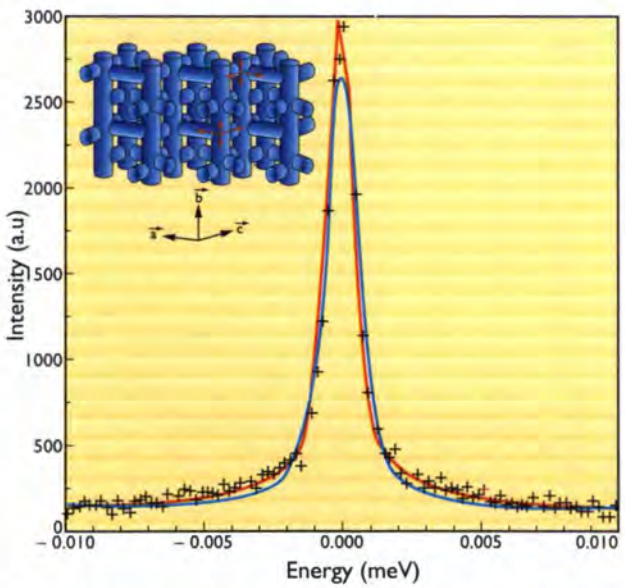

Figure 3: *Comparison between experimental (+) and calculated quasielastic neutron-scattering spectra obtained for octane in silicalite. The blue curve corresponds to isotropic diffusion, the red one to one-dimensional diffusion (Q = 1.3 Å⁻¹).* ***Inset:*** *Silicalite structure.*

References

[1] E.J. Maginn, A.T. Bell and D.N. Theodorou, J. Phys. Chem. 100 (1996) 7155.

The phase diagram of water/ice and a new metastable phase of ice

J.L. Finney, C. Lobban (Univ. College London),
W.F. Kuhs (Univ. Göttingen).

The ice phase diagram is extremely rich, comprising 11 confirmed crystalline phases, in which the water molecules link through hydrogen bonds to form tetrahedral frameworks. The structures and stabilities of many of these phases have been established definitively by means of neutron powder-diffraction in a British-German collaboration. This work is of importance to a large interdisciplinary group of researchers interested in the hydrogen bond, while the versatility of the water molecule in forming so many different structures is relevant to its biological importance.

15 years ago, little was known about the structures of ice under pressure, most information in the literature being obtained from samples 'recovered' to ambient pressure at liquid nitrogen temperatures. In the early 1980s, the high-pressure facilities at ILL, together with the Rietveld powder refinement technique, had developed to a stage where the structures of most of these phases could be studied *under their conditions of stability*. So began our collaboration which has, through neutron work both at ILL and ISIS, not only sorted out a good part of the phase diagram (Fig. 1), but has also led to new, unexpected results of wide significance.

The earliest work using clamped high-pressure cells [1] found that ice VIII was antiferroelectrically ordered with *non-bonded* oxygen-oxygen contacts *shorter* than the *bonded* distances. Although this might seem a strange result, it confirmed beautifully other ideas which stressed the importance of non-bonded repulsions in determining hydrogen bonded structures in general [2]. In addition to the expected hydrogen disorder, ice VII was shown to have

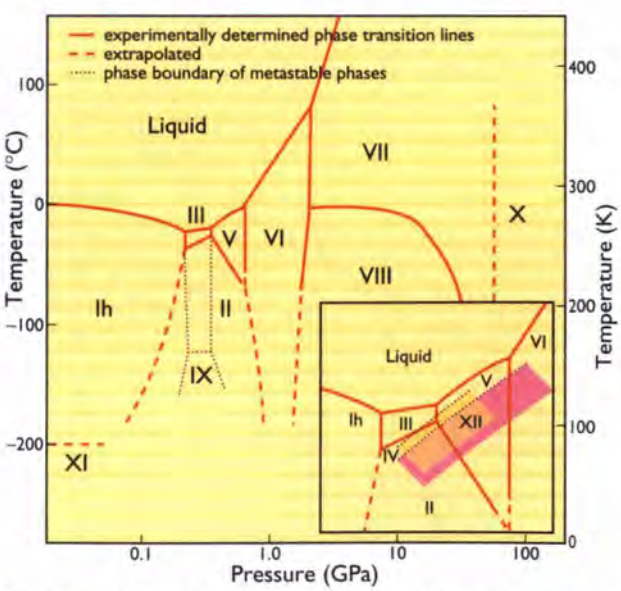

Figure 1: *The phase diagram of water/ice.* ***Inset:*** *The medium pressure range showing the melting curves of metastable ices IV and XII.*

oxygen disorder. Again, this was initially unexpected, though it has been found more generally since, e.g. in the disordered medium pressure phase ice VI. The lower pressure part of the phase diagram was probed using the He-gas cell. This raised many experimental difficulties: ice V was almost impossible to form and ice III was very difficult. The problem was resolved when it was discovered that the helium gas was stabilising a previously unknown He-hydrate with a water molecule topology identical to that of ice II [3] - another unexpected result and new structure.

The work on ice III and IX revealed that, in contrast to earlier assumptions, both ices are partially (dis)ordered [4]. Very recently, full sets of data on ices III and V under various conditions of temperature and pressure have been obtained, thus ending a long-standing uncertainty about H-ordering in these phases. Ice III and ice V both show partial ordering in the 20 to 30% range even close to the melting point [5].

However, the phase diagram is still not fully understood. On several occasions during the last 15 years, powder lines have been seen that could not be identified with any known ice or clathrate phase. As we have pinned down with increasing precision the preparation conditions for these phases, we have begun to back them into a corner. The first success has been ice XII, *a totally new structure* that we have found within the stability region of ice V and which was prepared by crystallisation from the liquid phase [6]. The topology of ice XII is unlike any of the known ice phases, and contains a mixture of 5 and 7 membered rings. The inset in Fig. 1 shows the tentative stability region and Fig. 2 the structure clearly exhibiting the 5 membered rings organised to form channels along the unique axis. Another metastable phase of ice, ice IV (Fig. 3), discovered in the 1930s by Bridgman, was obtained *in situ* in our experiments for the first time by following a slightly different preparation recipe. The density of ice V (1.402 $g \cdot cm^{-3}$ for D_2O) is smaller than the densities of ice IV and XII (1.436 and 1.437 $g \cdot cm^{-3}$ resp.), which are quite similar to

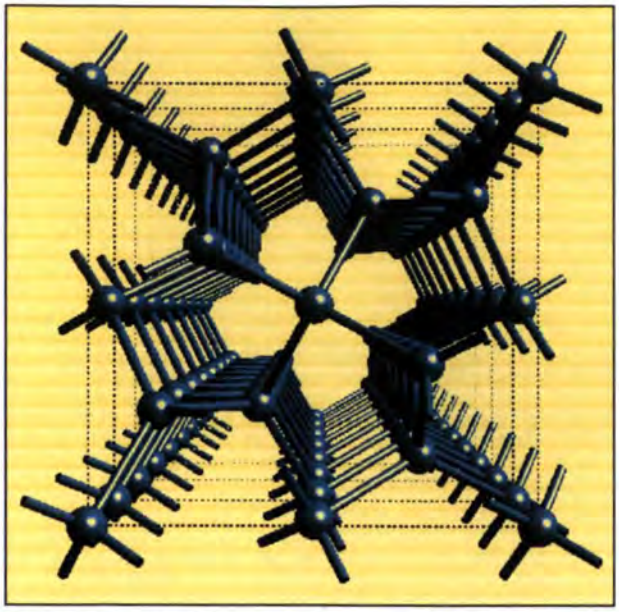

Figure 2: *The H-bond framework of tetragonal ice XII viewed down the c-axis. The spacegroup is I42d, lattice constants are a = 8.304 Å and c = 4.024 Å.*

each other. Both ice IV and XII are fully hydrogen disordered, while ice V is partially ordered as mentioned above. On the other hand, differences occur in the degree of hydrogen-bond bending: compared to ice V and XII the structure of ice IV shows distinctly smaller bending, yet exhibits interpenetration of the H-bond framework, a phenomenon sometimes referred to as auto-clathration. Clearly there are two ways of increasing the density in water structures: additional hydrogen bond bending as in ice V and XII or hydrogen bond interpenetration as in ice IV and also in the next highest pressure phase, ice VI. At present, ice XII is the densest known phase of the water substance without interpenetration. Yet in all these structures the non-bonded repulsive constraints [2] are active and confirmed by our neutron results.

Two lines of further research are now developing from these findings. First, the enhanced richness of the ice phase-diagram in the medium pressure range is an excellent demonstration of the versatility of the water molecule that enables the building of a variety of hydrogen-bonded structures sometimes in very close competition for occupying the same region of p-T space. The seemingly delicate balance of enthalpic and entropic contributions to the total energy will thus allow us to test very critically the viability of water potential functions used widely in computer calculations in chemical and biomolecular systems. Secondly, the fact that we have formed metastable phases directly

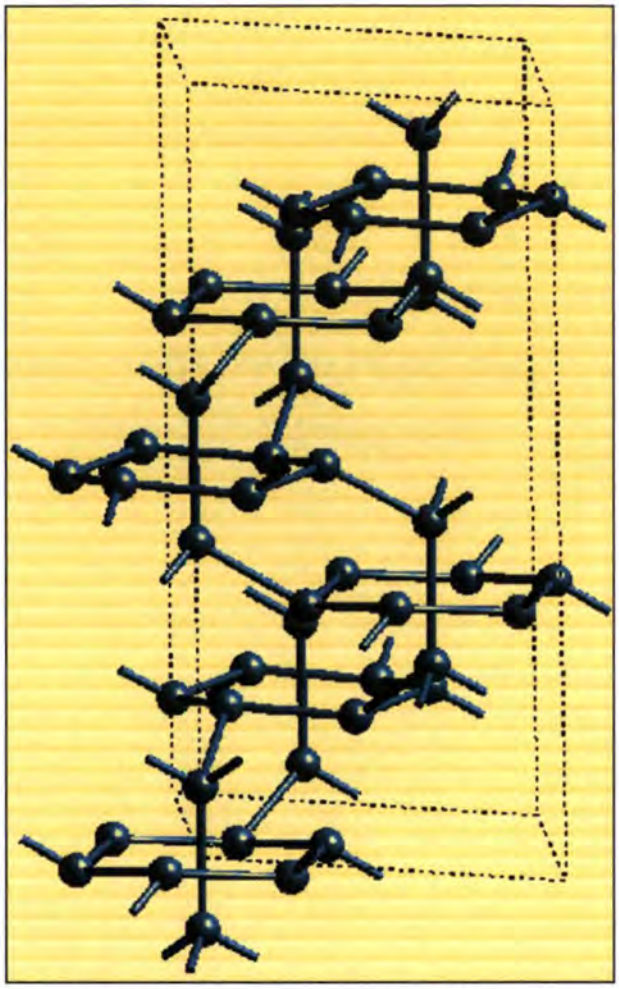

Figure 3: *The H-bond framework of rhombohedral ice IV showing the auto-clathrate arrangement with H-bonds passing through the centre of 6 membered rings.*

from the liquid makes the water system now an excellent candidate for studies of metastability, including both thermodynamic and kinetic aspects of phase formation.

This work has also demonstrated that neutron diffraction is by far the best method to explore the phase diagram of ice as it allows the detection of topological phase changes and any sudden or continuous changes in H-ordering. At the same time, information on expansivities and compressibilities is obtained which gives us further quantitative information on the details of the chemically and biologically important water-water intermolecular interaction.

Acknowledgement

We are very grateful for the very competent assistance of Louis Melesi in the high-pressure experiments over this whole period.

References

■ [1] W.F. Kuhs, J.L. Finney, C. Vettier, D.V. Bliss, J.Chem.Phys. 81 (1984) 3612 ■ [2] H. Savage, Water Science Reviews 2 (1986) 67 ■ [3] D. Londono, J.L. Finney, W.F. Kuhs, J.Chem.Phys. 97 (1992) 547 ■ [4] D. Londono, W.F. Kuhs, J.L. Finney, J.Chem.Phys. 98 (1993) 4878 ■ [5] W.F. Kuhs, C. Lobban, J.L. Finney, Rev. High. Press. Sci. & Techn. 7 (1998) in press. ■ [6] C. Lobban, J.L. Finney, W.F. Kuhs, Nature 391 (1998) 268.

Neutron diffraction studies of solvent regions in coenzyme Cob(II)alamin

P. Langan, M. Lehmann, S. Mason (ILL),
C. Wilkinson (EMBL),
G. Jogl, C. Kratky (Univ. Graz).

Diffraction data have been collected from a crystal of coenzyme Cob(II)alamin (B12r) using the high-resolution single-crystal diffractometer D19 and a recently designed medium resolution single-crystal diffractometer based on a Laue-concept, LADI. Difference density maps reveal the atomic positions of seven highly ordered water molecules and two partially disordered acetone molecules. These solvent molecules have important structural roles.

The Vitamin B12 coenzymes form a class of biological cofactors for several enzymes catalysing methyl-transfer and carbon-backbone rearrangement reactions. These cofactors have a very complicated chemical constitution, being the most complicated biological molecules known to date. The mechanism of the B12-dependent reactions are still a matter of dispute, although crystal structures of two B12-containing proteins were determined recently [1, 2]. We are interested in the 3D structure of isolated B12 cofactors in order to contribute to an understanding of their complicated biological role. Of special interest to us is coenzyme B12r, which is a crucial and highly reactive intermediate in reactions of coenzyme B12-dependent enzymes.

The x-ray crystal structure of B12r was determined several years ago [3], and we recently carried out neutron experiments on instruments D19 and LADI to elucidate the arrangement of solvent (water and acetone) molecules within these crystals. Elucidation of the structure of such solvent regions is one of the realms of neutron diffraction owing to the much larger scattering cross section of hydrogen and deuterium for neutrons as compared to x-rays. This permits the observation of hydrogen or deuterium positions which are normally invisible in x-ray electron density maps. For this experiment, we grew crystals of B12r from D_2O/D_6-acetone. A detailed comparison of the data collected on D19 to better than 1 Å resolution with those collected on LADI to 1.4 Å resolution as well as synchrotron x-ray data to 0.9 Å resolution is given in the technical section of this report.

Coenzyme B12r has a molecular weight of about 1500 Dalton and consists of a corrin ring and dimethylbenzimidazole nucleotide. In the crystal, neighbouring molecules are packed such that the phosphate groups of the nucleotides interdigitate forming relatively hydrophilic regions. Large open channels run through the crystal with the relatively hydrophobic corrin and benzimidazole fragments making its walls. There are about 20 water molecules plus two molecules of acetone per B12r moiety. Figs. 1 and 2 show details of difference density maps calculated from the LADI data with density representing ordered solvent.

Figure 1: *Solvent density in the hydrophilic region around the phosphate groups as revealed by a difference density map computed with phases based on the x-ray crystal structure of B12r.*

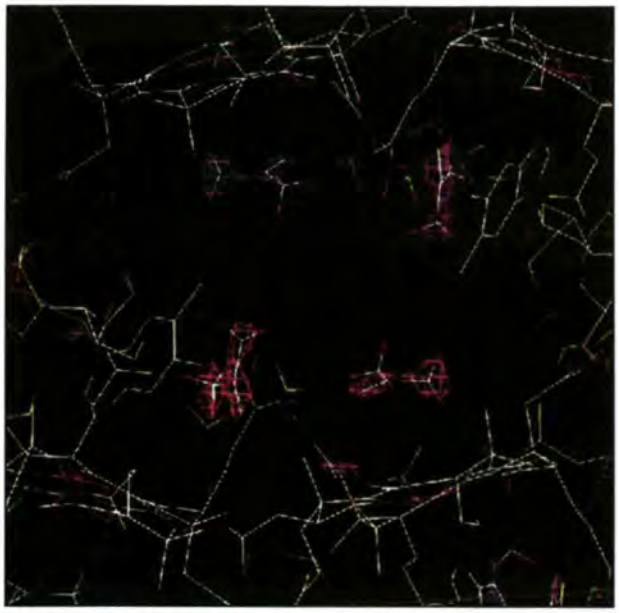

Figure 2: *Density from the two hexadeutero-acetone molecules which, together with ordered water molecules, line the walls of the large open solvent channels.*

Highly ordered water molecules are found in the hydrophylic regions which form single, double, triple and quadruple water bridges between neighbouring phosphate groups, Fig. 1. All of the hydrogen bonding donor potential of these water molecules and 90% of their hydrogen bonding acceptor potential is used with bond lengths and angles similar to those observed in small hydrate structures. This network of water mediates the interaction of the phosphate groups with their surrounding environment and is mainly responsible for linking neighbouring molecules.

This contrasts with the situation in crystals of coenzyme B12 [4] where there are more direct hydrogen bonds with groups from neighbouring molecules and fewer bonds through water. The difference in phosphodiester conformation between B12r and the coenzyme B12 is due to the different crystal packing environment of the phosphates and their interaction with this environment through water and hydrogen bonding.

Paul Langan (right) explaining the details of D19 to Gérard Fillion (CNRS Grenoble).

In the large open channels ordered water and acetone molecules line the walls with more disordered solvent molecules filling the channels. Ordered water molecules seem to anchor the acetone molecules over the corrin ring and dimethylbenzimidazole base thus interfacing the relatively hydrophic walls with the enclosed solvent. In crystals of the coenzyme B12 such a channel does not exist. The more disordered solvent molecules in this channel are being analysed in detail using the high resolution data collected on D19. The importance of knowing hydrogen atom positions in order to understand the relationship between solvation and structure in biological macromolecules cannot be overestimated and these results will be an important contribution.

References

■ [1] L.C. Drennan, S. Huang, J.T. Drummond, R.G. Mathews, M.L. Ludwig, Science 266 (1994) 1669 ■ [2] F. Mancia, N.H. Keep, A. Nakagawa, P.F. Leadlay, S. McSweeney, B. Rasmussen, P. Bosecke, O. Diat and P. Evans, Structure 4 (1996) 339 ■ [3] B. Krautler, W. Keller and C. Kratky, J. Amer. Chem. Soc. 111 (1989) 8936 ■ [4] H.F. Savage, P.F. Lindley, J.L. Finney and P.A. Timmins, Acta Cryst. B43 (1987) 280.

Interaction of the peptide penetratin with supported phospholipidic bilayers

E. Bellet-Amalric, G. Fragneto (ILL),
F. Graner, P. Dubos, T. Charitat (Univ. Grenoble).

Neutron reflection has been applied to the study of model lipid membranes and to their interaction with a 16-amino-acid peptide which possesses the unique feature to translocate across neuronal membranes without damaging them. The membrane, consisting of a phospholipid bilayer deposited on the surface of silicon crystals, has been fully characterised and the peptide has been found to interact mainly with the polar heads of the lipid molecules.

The incorporation of macromolecules in a cell presents a double interest. At a fundamental level, it allows the study of the mechanism of transport across the barrier constituted by the lipidic membrane. At a more applied level it can be used for conveying a drug to a specific target in the cell in small doses. Targeting hydrophilic compounds to the cytoplasm and nucleus of cells is, in principle, difficult because it requires the hydrophobic environment of the bilayer to be crossed. Classically this is obtained through a temporary disruption of the membranes. The peptide *penetratin* has recently been shown to translocate across neural cell membranes without damaging them, even when coupled to drugs [1]. This surprising 16-amino-acid peptide interacts directly with the lipids of the membrane, although it is not yet known how the lipids reorganise around the peptide to let it pass through without any water leakage.

We have used neutron reflection [2] to investigate the structure of model membranes and their interaction with the peptide. Measurements were made on an adapted configuration of D16. Collimation slits of constant width were employed and the reflectivity was measured down to $2 \cdot 10^{-7}$. Our reflectivity results are among the very first obtained from this traditional diffractometer. The technique has already proved to be very useful for studies of material adsorbed at interfaces, both air/liquid and solid/liquid. Although not yet commonly used in biological areas, it represents one of the most suitable techniques for systems, of interest in biology, such as asymmetric bilayers or highly hydrated double-bilayers.

The model membrane consisted of a phospholipid bilayer formed by 90% dipalmitoylphosphatidylcholine (DPPC) and 10% dipalmitoylphosphatidylserine (DPPS), dipalmitoylphosphatidylcholine being neutral and dipalmitoylphosphatidylserine negatively charged. Using the Langmuir-Schaeffer technique [3], bilayers were deposited on the highly hydrophilic surface of single crystals of silicon having a 13 Å thick oxide layer and 2 Å rms. roughness. The technique of deposition was found to be very reproducible and to lead to good quality layers stable over several days.

Measurements were made at the silicon/water interface, the beam passing through 5 cm of silicon. Reflectivity was measured for each system at several D_2O/H_2O ratios which provided different scattering contrasts in order to constrain the models used to fit the reflectivity profiles and to provide more detailed information on the different regions of the bilayer. The analysis of the measured

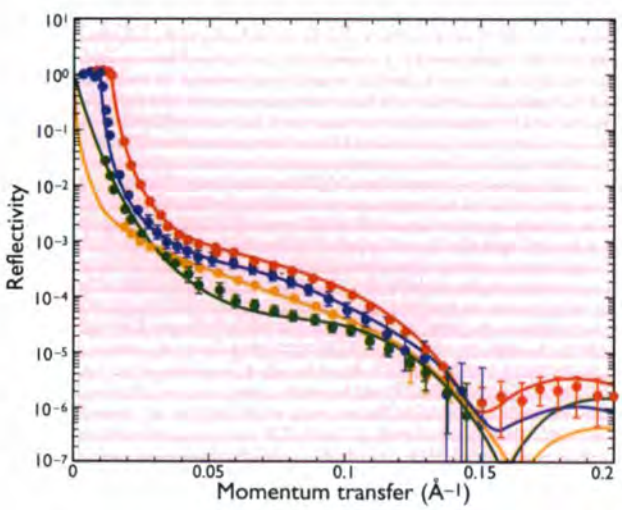

Figure 1a: *Reflectivity profiles (circles) and fitted curves (lines) of a bilayer of protonated lipids (90% DPPC + 10% DPPS) at the silicon/water interface. Water contrasts are as follows: (red) D_2O, (green) H_2O, (yellow) D_2O/H_2O mixture at the ratio 1:1.63 and (blue) D_2O/H_2O mixture at the ratio 1:0.52.*

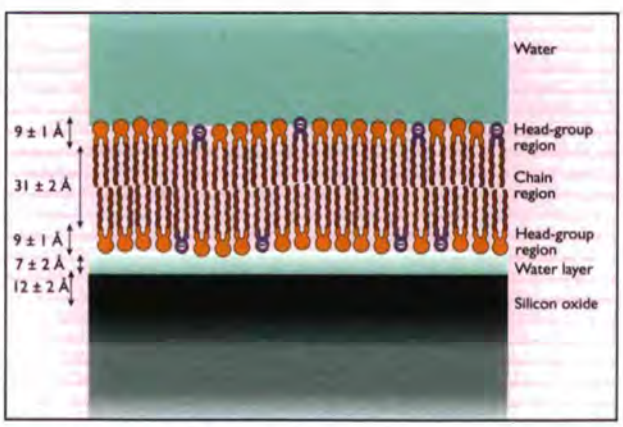

Figure 1b: *A sketch of the model bilayer.*

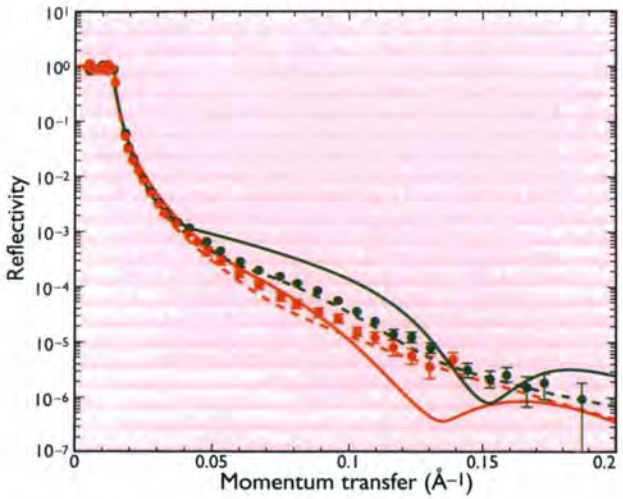

Figure 2a: *Reflectivity profiles (circles) and fits (dashed lines) from the systems silicon/H-lipids + peptide/D_2O (green) and silicon/D-lipids + peptide/D_2O (red). The concentration of the peptide is $7.21 \cdot 10^{-7}$ M. The continuous lines are the best fits of the corresponding profiles obtained without peptide and are included for comparison. Fig. 2b represents a sketch of a possible model.*

profiles was done using a new program written by A.R. Rennie (Cambridge Univ.) and R.E. Ghosh (ILL). This allows the refinement of a unique set of layer parameters by fitting simultaneously several sets of data from the same chemical system.

The lipid bilayer was studied first. Both protonated and deuterated lipids were employed. Fig. 1a shows the reflectivity profiles from a protonated bilayer in four water contrasts together with the fitted curves from which the model described below and shown in Fig. 1b was deduced. The membrane was found to have the structure of a symmetrical bilayer of overall thickness 47 ± 4 Å. 20% of water was detected in the interfacial region (atomic force microscopy and transfer rate measurements also indicate a coverage of the surface of about 80%). The head group regions were found to be adjacent both to the solid surface and to the bulk water, with the hydrocarbon chains being in the central part. The thickness of the head groups is 8 ± 2 Å and that of the chain region is 30 ± 2 Å.

The synthetic peptide *penetratin* was introduced below the lipid layer in the Langmuir trough before the deposition on the solid surface. Two concentrations were investigated and eight profiles were measured at each (four water contrasts on both protonated and deuterated lipids). Fig. 2 shows the results for one concentration of peptide in pure D_2O for both a protonated and a deuterated membrane.

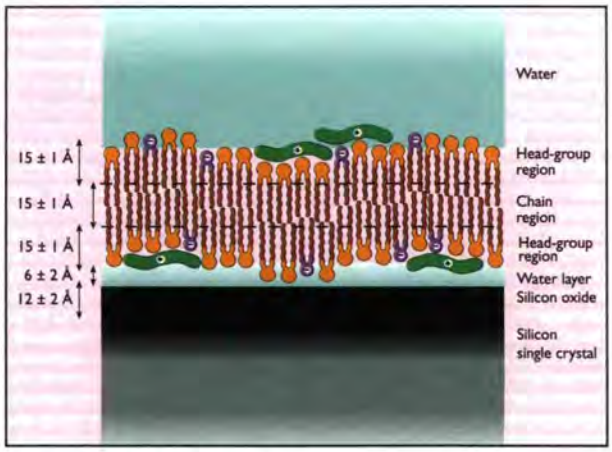

Figure 2b: *A sketch of the model bilayer.*

Also shown are the fits for a model which gives best agreement with all the eight measured profiles simultaneously. According to this model the presence of *penetratin* modifies the structure of the membrane. The head group region becomes thicker (15 ± 1 Å) and the tail group region thinner (15 ± 1 Å). All the interfaces are much rougher (14 ± 1 Å). A possible representation of the structure at the interface is given in Fig. 2b. These results shed new light on the lipid-peptide interaction, indicating that the peptide interacts with the polar heads of the lipid molecules, suggesting an interaction of electrostatic nature.
Double bilayers have also been investigated, their importance being related to the fact that the second bilayer interacts less strongly with the underlying solid surface and mimics more realistically a bio-membrane. This will be the direction of our future investigations.

D16 before its reconstruction. Edith Bellet-Amalric (left) and Miguel Castro, Sevilla, aligning a sample.

References

■ [1] A. Prochiantz, Curr. Opin. in Neurobiol. 6 (1996) 629 ■ [2] J. Penfold and R. K. Thomas, J. Phys. Condens. Matt. 2 (1990) 1369 ■ [3] L. Tamm and H. McConnell, Biophys. J. 47 (1985) 105.

Modelling milk: The structure of calcium phosphate nanoclusters

C. Holt (Hannah research Insitute, Ayr).
P. Timmins (ILL).

Milk contains a lot of calcium and phosphorus to sustain bone growth. New research at the ILL by small-angle neutron-scattering has helped to show the structure of milk calcium-phosphate nanoclusters.

Introduction

Milk is white largely because of light scattered by colloidal protein particles called casein micelles. In cows' milk, about two thirds of the calcium and half the phosphate is found in these casein micelles, largely as calcium-phosphate clusters bound to the phosphorylated residues of the α_{s1}–, α_{s2}– and β-caseins. The size of the micellar calcium-phosphate particles isolated from casein micelles by exhaustive proteolytic digestion has been shown by electron microscopy to be about 2.5 nm, the exact value depending on the thickness assumed for the carbon coating; other electron microscope studies have revealed electron dense nm-sized bodies distributed fairly uniformly throughout the protein matrix of the casein micelle. The biological significance of the structure of casein micelles is not easily established but it has been suggested that casein micelles allow the total calcium and phosphate concentrations in most, if not all milks to exceed the solubility of calcium phosphate, without causing uncontrolled precipitation of calcium phosphate in the mammary gland.

The highly phosphorylated caseins, along with many other phosphoproteins found in calcifying tissues, have been shown to be effective at inhibiting *in vitro* the precipitation of calcium phosphate from solutions of low to moderate supersaturation. Indeed, it has been suggested that the open and flexible conformation in solution of many of these highly phosphorylated phosphoproteins is an adaptive feature of peptides required to interact speedily with calcium-phosphate nuclei in order to control calcification in biological tissues.

Artificial casein micelles can be prepared in the laboratory by carefully mixing together the caseins and various milk salts in a prescribed sequence. With certain mixing sequences, stable colloidal particles resembling native casein micelles can form without at the same time producing a calcium-phosphate precipitate. The essential step in the formation of the micelle is the interaction of calcium phosphate with the highly phosphorylated peptide sequence. To avoid the complexities of other types of interactions a simplified model system was devised in which non-interacting calcium-phosphate nanoclusters are produced.

Using milk-like total concentrations of salts and phosphoserine residues in a short phosphopeptide, the colloidal concentrations at pH 6.7 - 6.8 are very similar to those found in milk at the same pH and the chemical composition of the nanoclusters is that of an amorphous dicalcium phosphate complexed to the phosphopeptide. The Ca, Mg, phosphate and phosphopeptide components of the nanoclusters were shown, by NMR line-width measurements, to exchange more-or-less rapidly between the colloid and the continuous phase and the apparent radius of gyration, is in the nm-range. Thus it was shown that in size, composition, short-range order and dynamics, the calcium-phosphate nanoclusters show a close similarity to native micellar calcium-phosphate. Here, we describe measurements on nanocluster preparations in order to derive the substructure, dimensions and densities of the particles.

Complementary techniques

X-ray small-angle scattering, NMR spectroscopy and sedimentation studies have all been important in the characterisation of casein nano particles but neutron scattering with the H_2O/D_2O contrast variation was the *key technique* which allowed us to unravel the internal structure of the particles [1]. This is because of the very different scattering-length densities of the amorphous calcium phosphate core and the casein shell. Fig. 1 shows how the scattering density of the particle varies as a function of the D_2O content of the solvent.

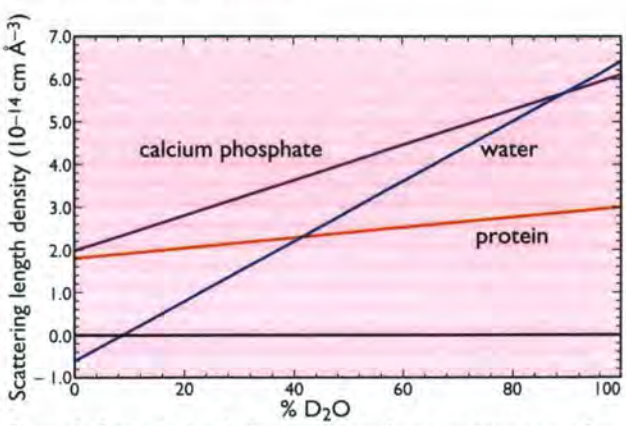

Figure 1: *Scattering length densities of nanocluster components as a function of D_2O/H_2O content.*

We see that in H_2O (0% D_2O) the shell and core have very similar scattering densities and the particles therefore appear homogeneous. In 40% D_2O however, the situation is very different for neutrons. Now the protein component of the particle is rendered invisible and only the calcium-phosphate core is seen. Similarly at 88% D_2O the core becomes invisible and only an empty protein shell is observed.

Small-angle neutron-scattering results

Scattering curves were measured for solutions of nanoclusters dissoved in solvents comprising various D_2O/H_2O mixtures from 0% to 100% D_2O. Via Guinier plots the radii of gyration (R_g) were obtained and are plotted in Fig. 2 as R_g^2 vs reciprocal contrast. It is striking that the radius of gyration is small at positive contrast where the phosphate dominates and large at negative contrast where the protein dominates. This shows that the phosphate is found in the core of the particle and the protein in the shell and allows us to calculate the outer radius of the core and the thickness of the protein shell.

These measurements, when put on an absolute scale, allow also the proportion of protein to calcium phosphate to be determined as well as the overall molecular weight of the nanoclusters to be estimated. Combined with the results obtained from small-angle x-ray scattering, sedimentation and chemistry the neutron-scattering results led us to propose the model shown in Fig. 3. This illustrates a hydrated amorphous calcium-phosphate core (grey) surrounded by a close-packed shell of casein phosphopeptides (red). The casein is fixed to the core via 4 phosphorylated serine residues. In contrast both C-terminus and N-terminus are arginyl residues. NMR suggests that one of them has a mobility similar to that found in the free peptide and is hence at the exterior of the particle.

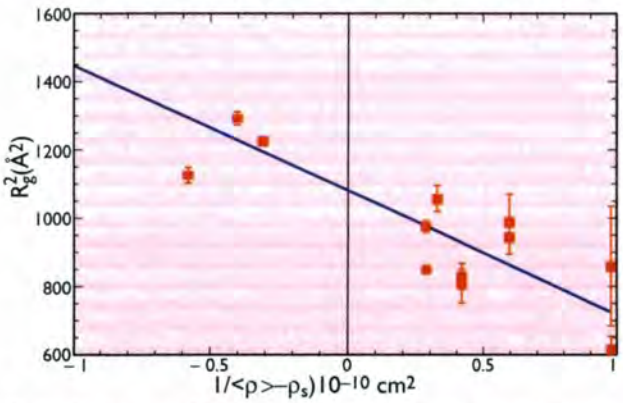

Figure 2: *Variation of R_g^2 with inverse contrast. Negative inverse contrast corresponds to D_2O/H_2O contents greater than 46.7% (the nanoparticle match point) whilst positive contrast corresponds to contents less than 46.7%.*

Conclusions

Neutron small-angle scattering along with other techniques has shown that casein nanoparticles synthesised in the laboratory have many of the characteristics of the native micellar calcium-phoshate and a core-shell structure.

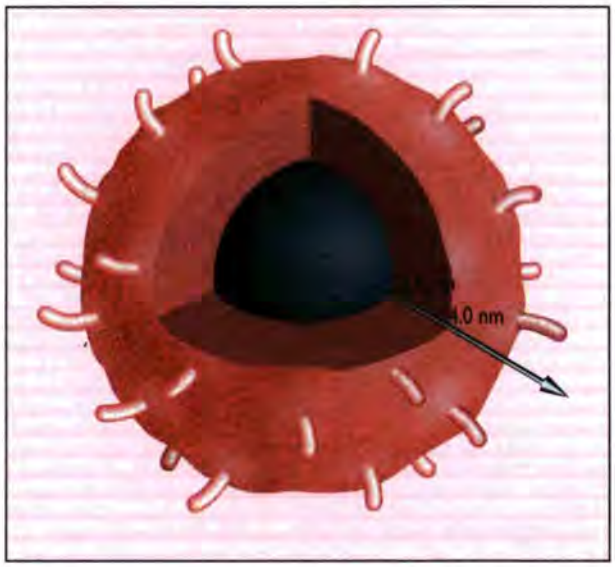

Figure 3: *Schematic representation of a nanocluster particle showing the calcium phosphate core surrounded by a dense shell of phosphoprotein.*

With hindsight we can see that such a structure is necessary. The mammary gland transports such a lot of calcium and phosphate that without effective control of the precipitation process, the gland would soon calcify and cease to function. Nanoclusters provide an illustration of a biological mechanism for the effective control of a phase transition. Moreover, it is a mechanism in which protein dynamics rather than protein structure plays the key part.

References

[1] C. Holt, P.A. Timmins, N. Errington and J. Leaver, Eur. J. Biochem. (1998) in press.

The diffusion of oxygen in silicon single-crystals

S. Rycroft and R.J. Stewart (Univ. Reading).

Silicon single-crystals grown by the Czochralski technique contain typically 30 parts per million of oxygen. This oxygen diffuses and agglomerates to form SiO_2 precipitates during the cooling of the crystal after growth and during the thermal treatments required in wafer processing. The control of the distribution and size of these precipitates is a crucial factor in the production of semiconductor devices. Small-angle neutron-scattering techniques have been used to study the growth of the SiO_2 precipitates and detailed analysis enables their size and shape to be determined. From these data the diffusion coefficient of oxygen in silicon can be determined very precisely.

The basis of nearly all micro chips used in electronic equipment ranging from computers to washing machines is silicon. In the computer field there is an insatiable demand for microchips with ever increasing numbers and densities of components. The 64 Megabyte RAM is now a reality and by the year 2010 64 Gigabyte RAM's are predicted and silicon wafers will still be the substrate on which such chips will be produced. This 1,000-fold increase will place very stringent limits on the quality of the single-crystal silicon from which the devices are made. To keep prices down larger and larger defect-free silicon crystals have to be grown. Currently 200 mm diameter by 2 m long crystals are the standard size from which wafers are cut. These have to be cooled very slowly so that large thermal gradients are avoided and thus few defects are introduced. Nearly all the silicon wafers used in the manufacture of semiconductor chips are cut from single crystals grown by the Czochralski method. All silicon grown by this method contains small amounts of oxygen, typically about 30 parts per million. This oxygen, which is located in interstitial sites, diffuses and agglomerates to form SiO_2 precipitates during the cooling of the crystal after growth and during the thermal treatments required in wafer processing. The control of the distribution and size of these precipitates is a crucial factor in the production of semiconductor devices.

Small-angle neutron-scattering techniques have been used to study the growth of the SiO_2 precipitates and data on the size, shape and form of the precipitates have been obtained from detailed analysis of the small-angle neutron-scattering data [1]. Fig. 1 shows the small-angle neutron-scattering from SiO_2 precipitates in a single crystal of silicon which has been heat treated for 500 hours at 600°C; the neutron beam was incident along a <100> direction. The central cross arises from the cushion shaped SiO_2 precipitates lying on (100) planes with their edges along <110> directions.

In the analysis the cushion shape is approximated as cuboids of size L × L × wL; for the pattern shown the precipitates have L = 17 nm with w = 0.18. The scattering seen at the corners of the detector disappears on cooling to

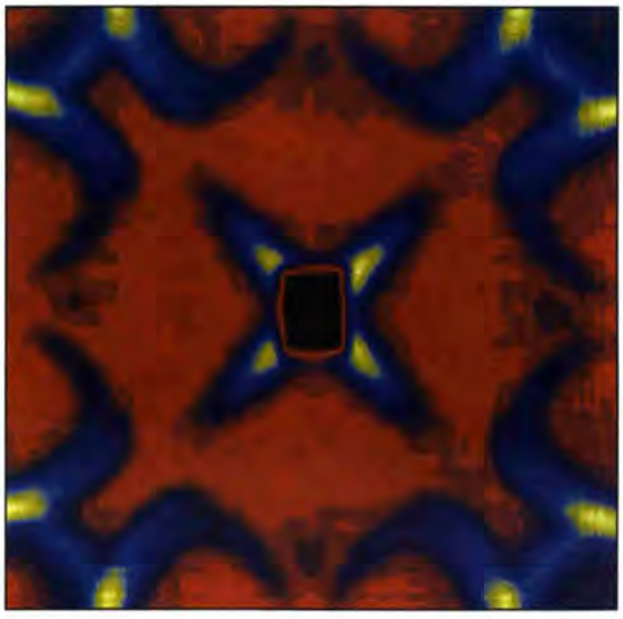

Figure 1: *Small-angle neutron-scattering from a silicon crystal heated at 600°C for 500 hours.*

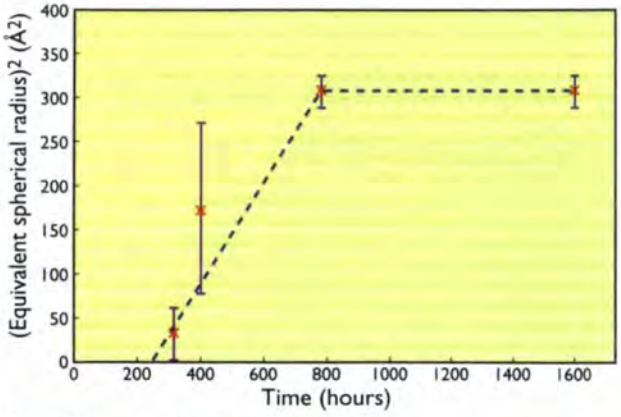

Figure 2: *Growth of precipitates at 550°C.*

100 K and probably arises from interactions of the long wavelength neutrons with phonons via an Umklapp process. The data on the size, shape and form of the precipitates as a function of heat-treatment time enables the diffusion coefficient of oxygen in silicon to be determined very precisely from the observed rate of growth of the precipitates as a function of time (Fig. 2) by applying Ham's theory. For temperatures above 600°C small-angle neutron-scattering data have made a significant contribution to the understanding of the rate of precipitation of oxygen as a function of both temperature and time (Fig. 3). However at temperatures below 600°C, small-angle neutron-scattering becomes progressively more difficult. This is because as the heat-treatment temperature is lowered, larger numbers of smaller precipitates are formed and the total concentration of oxygen available to form precipitates is extremely small (30 ppm). The smaller precipitates arise because the critical nucleus-size for a stable precipitate is lower the lower the temperature. The small-angle neutron-scattering intensity is directly proportional to the square of the volume of a precipitate, but only directly proportional to the number of precipitates. Thus for a given amount of oxygen in precipitates, if the volume of each precipitate is reduced by a factor of ten, then the number of precipitates would increase by a factor of ten and the small-angle neutron-scattering intensity would be reduced by a factor of ten. Fortunately the absorption of long-wavelength neutrons (1 nm) in silicon is very low and thus large samples (~ 20 cm along incident beam direction) can be employed to increase the small-angle neutron-scattering signal. The signal-to-noise ratio was also increased by carrying out the measurements in the evacuated sample vessel so that no window materials were in the beam to give parasitic scattering. A further major advantage is the increased intensity of the incident neutron-beam on D22 compared to D11 which coupled with the larger area-detector have enabled measurements in this lower temperature range to be attempted.

The low temperature region is crucial since the diffusion rate of oxygen in silicon at temperatures around 500°C is a hot topic at present. This is because different experimental techniques find diffusion coefficients differing in value by a factor of up to 100,000 as can be seen in Fig. 3. Our data at 600°C and 550°C show that the diffusion coefficient of oxygen in silicon is close to the value obtained if the high temperature data is extrapolated. Thus the larger values seen in the data by other techniques may be in doubt. This discrepancy has to be solved in order for the next generation of semiconductor devices to be produced efficiently. By 2010 300 mm diameter by 2 m long silicon crystals are likely to be the basis of the wafers on which memory chips are produced. Such crystals will have to be cooled over several days to avoid thermal stresses and during this time many more SiO_2 precipitates will be formed.

Acknowledgement

The help of Oliver Randl and Roland May in carrying out these experiments is gratefully acknowledged.

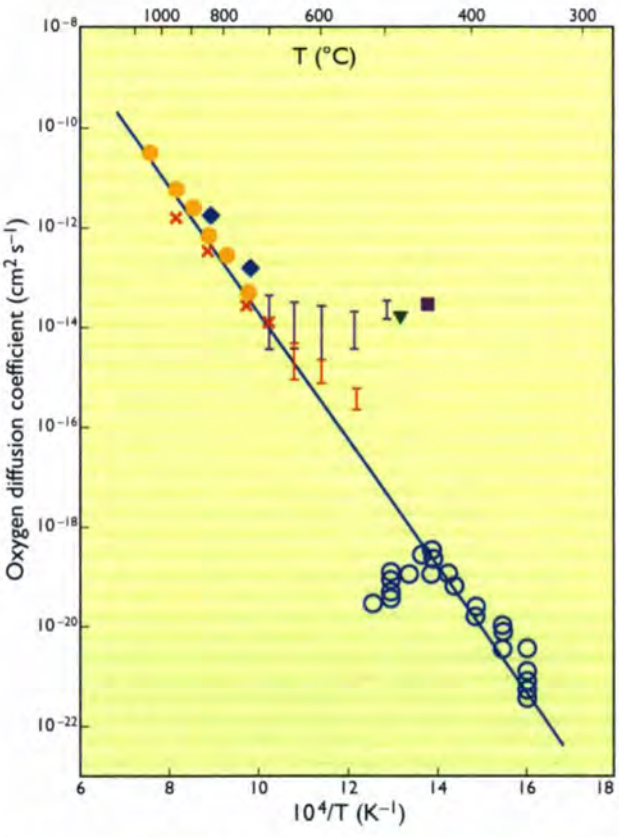

Figure 3: *Plot of normal diffusion, adapted from [2]. Also shown in red are data from recent small-angle neutron-scattering measurements.*

References

■ [1] R.J. Stewart, S. Messoloras and S. Rycroft, Proceedings of Oxygen '96, "The early stages of oxygen precipitation in silicon" R. Jones (ed). Kluwer Academic Publishers (1996) 381 ■ [2] R.C. Newman and R. Jones, in "Oxygen in Silicon", F. Shimura (ed.), Semiconductors and semimetals, 42 (1994) chapter 8, 289 .

Quantitative phase and texture-analysis on ceramic-matrix composites using Rietveld texture-analysis

- D. Chateigner (Univ. du Maine, Le Mans),
- L. Lutterotti (Univ. di Trento),
- T. Hansen (ILL).

Ceramic materials can be strengthened and toughened by the inclusion of a second phase in the form of short fibres. Specific anisotropic properties are achieved by fibre alignment along certain directions. To compare the resulting mechanical properties with the expected ones it is fundamental to determine the effective phase quantity along with the orientation distribution-function of both matrix and inclusions. At the present, if the texture of polyphase materials is a difficult task, there is no reliable method for quantitative phase analysis of strongly oriented bulk samples. By Rietveld texture-analysis both features can be analysed at the same time using special measurements affordable at the D20 beamline.

Ceramic materials are increasingly being utilised in structural applications due to their low density, high hardness, thermal stability and resistance to corrosion. However, one drawback of these materials is the occurrence of catastrophic failure due to their intrinsic brittle nature. Single-crystal whiskers or metallic inclusions can be used to increase the fracture toughness of these materials; with respect to the metallic inclusions, the whiskers have the advantage of increasing also the failure strength. In some cases it is desirable to maximise the mechanical properties along certain planes or directions for optimum design of the application. This can be achieved by alignment of the whiskers along the desired directions to obtain textured materials. For research purposes or quality control it is very important to check the texture obtained by the process and the effective quantity and homogeneity of the inclusions. Another important role is played by the residual stresses originating during the material fabrication-process. In most cases these are developed in response to the different thermal expansion coefficients of the matrix and fibres. The nature of the residual stresses (in compression or tension) play a fundamental role in promoting the resulting fracture toughness or so-called crack bridging or crack deflection. The Rietveld method [1] in connection with the measurement of a certain number of spectra collected at different tilting angles seems to be a good procedure to analyse at the same time phase quantity, texture and residual stresses. The first application was to incorporate the harmonic approximation of texture in a least-squares Rietveld analysis [2,3] but some limits appear, principally concerning the general applicability in connection with sharp texture. Subsequently the texture algorithm of WIMV [4] was included under the general name of Rietveld texture-analysis [5-7]. Here we try the application of the procedure to a composite material having a matrix of β-Si_3N_4 with SiC whiskers as inclusions. The material was obtained by a special procedure [8] in order to distribute the whiskers randomly in the basal plane of the sample; these whiskers have the (111) plane perpendicular to the fibre direction. In this manner, it is possible to maximise the in-plane fracture properties (strength, elastic modulus and toughness) of the material for applications where a high resistance to bending stresses are required. One purpose of the analysis is to check the angular dispersion of the whiskers from the basal plane and to obtain the residual stresses resulting from the fabrication process. A cubic sample obtained by piling up sheets of the original material was analysed at the D20 beamline. 720 spectra up to 157° in 2θ, were collected with the new position-sensitive detector, corresponding to a 10° × 10° grid on the χ and φ angles and two ω positions of the cradle. The data were analysed by the Rietveld texture-analysis procedure to obtain the texture and the whisker fraction in the sample.

The fitting results for some of the spectra are presented in Fig. 2. Fig. 1 reports the pole figures as obtained from the

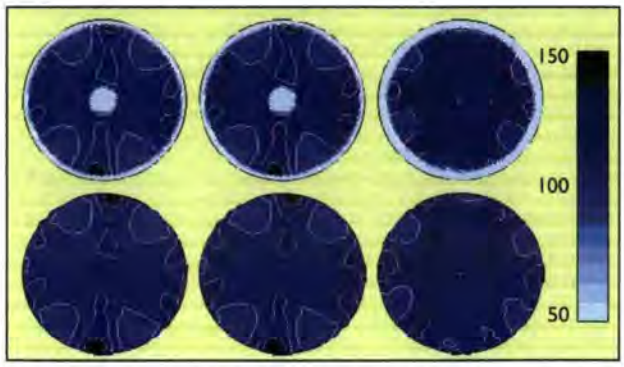

***Figure 1:** Experimental (upper) and reconstructed (lower), normalised pole figures for SiC. Linear intensity scale multiplied by 100, equal area projection. The pole figures are from left: (111), ($\bar{1}$11) and (220).*

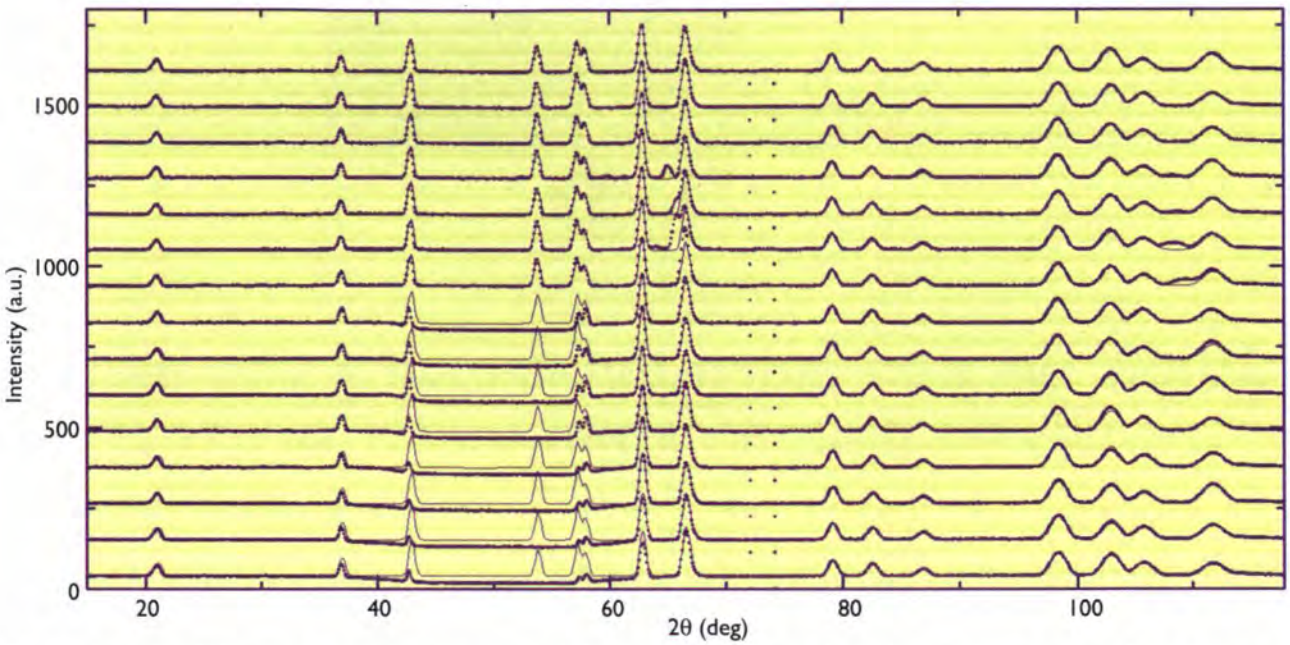

Figure 2: *Some of the 720 spectra fitted (thin lines) simultaneously by Rietveld texture-analysis to refine the texture and crystal structure for the silicon nitride sample with SiC whiskers. The low intensity range for the experimental data around 50° correspond to the presence of the Eulerian cradle masking part of the diffracted beam.*

Rietveld procedure and the recalculated ones using the WIMV algorithm for the SiC phase; these are labelled respectively experimental and reconstructed pole figures. The sample was positioned in the D20 instrument in a position for which the basal plane containing the whiskers is normal to the pole figure projection and along an ideal line connecting the lower and upper part of Fig. 1. As a result, the maximum polar density for the (1 1 1) and ($\bar{1}$ 1 1) planes is along that line with a sensible angular dispersion. The silicon nitride matrix was found to be completely random as expected from the fabrication process. The SiC phase fraction obtained by the analysis was 24.2% by volume in good agreement with the expected value and also the crystal-structure refinement on both phases was comparable to existing data. The effective elastic tensor (transversely isotropic) was computed from the phase fractions and orientation distribution function, confirming the expected higher modulus in the basal plane with respect to the normal direction [8].

The Rietveld method extended to texture analysis applied to data collected at the D20 beamline has enabled a two-phase composite to be analysed for the first time. The results are very encouraging and further work is in progress to obtain the residual stress field from the same data set.

The D20 beamline, thanks to the new position-sensitive detector, permits one to obtain all the required spectra, for a complete analysis, in a time at least two order of magnitude shorter than by traditional techniques, making this procedure of practical use.

View of D20.

References

■ [1] H. M. Rietveld, J. Appl. Cryst. 2 (1969) 65 ■ [2] N. C. Popa, J. Appl. Cryst. 25 (1992) 611 ■ [3] M. Ferrari and L. Lutterotti, J. Appl. Phys. 76 (1994) 7246 ■ [4] S. Matthies and G. Vinel, Phys. Status Solidi B 112 (1982) 111 ■ [5] H.-R. Wenk, S. Matthies and L. Lutterotti, Mater. Sci. Forum 157-162 (1994) 473 ■ [6] S. Matthies, L. Lutterotti and H.-R. Wenk, J. Appl. Cryst. 30 (1997) 31 ■ [7] L. Lutterotti, S. Matthies, H.-R. Wenk, A. S. Schultz and J. W. Richardson, Jr, J. Appl. Phys. 81 (1997) 594 ■ [8] M. Bosetti, Thesis (1997) University of Trento, Italy.

What we can learn by studying the glass transition phenomenon under pressure

A. Tölle, F. Fujara, (Univ. Dortmund),
H. Schober (ILL), J. Wuttke (TU München).

The slow dynamics (α-relaxation) in supercooled molecular liquids and the glass transition are two related topics which have received particular attention in the last ten years. The application of mode-coupling theory to glass forming liquids has stimulated many new experiments focusing on the previously uncovered microscopic time-range and on intermolecular distances. We present here the results of such investigations including pressure as an external control parameter. The complementary nature of temperature and pressure adds further evidence for an intrinsic coupling of fast microscopic and slow structural relaxation as predicted by the theory.

Why do structural relaxation times in some liquids change so dramatically within relatively small ranges of the external control parameters?

This is still one of the heavily debated questions of the glass transition [1]. The glass-transition phenomenon is quite general in all sorts of systems like supercooled van der Waals liquids, polymers, biomolecules and computer modelled hard spheres. It has been studied frequently by various experimental methods as a function of temperature and in relation to compositional changes in multicomponent systems. While temperature is an intensive variable changing both kinetic energy and density the hydrodynamic pressure primarily acts on the volume of the system. Therefore complementary information has to be expected from pressure experiments. The fact that pressure so far has been given only comparatively little attention certainly is related to the greater experimental difficulties involved.

We have tried to remedy this unsatisfactory situation by investigating as a function of pressure both the slow structural α-relaxation and its fast β-companion. Inelastic neutron-scattering experiments using backscattering (IN10, IN16) and time-of-flight (IN6) were performed on the supercooled van der Waals liquid orthoterphenyl [2]. Besides its model character for the study of the glass transition this compound has the advantage for the present purpose of possessing the highest pressure coefficient (dT_g/dP = 250 K/GPa) observed in any molecular liquid. Therefore small changes in pressure should lead to appreciable change in the dynamics.

Structural relaxation in liquids can be observed on all experimentally accessible time scales. It is a well established fact that the observed relaxation spectra at different temperatures can be mapped onto each other by rescaling the time axis. As this time-temperature superposition principle holds for a large number of substances (and particulary orthotherphenyl) there is no reason to assume that it breaks down with pressure. This we confirm experimentally.

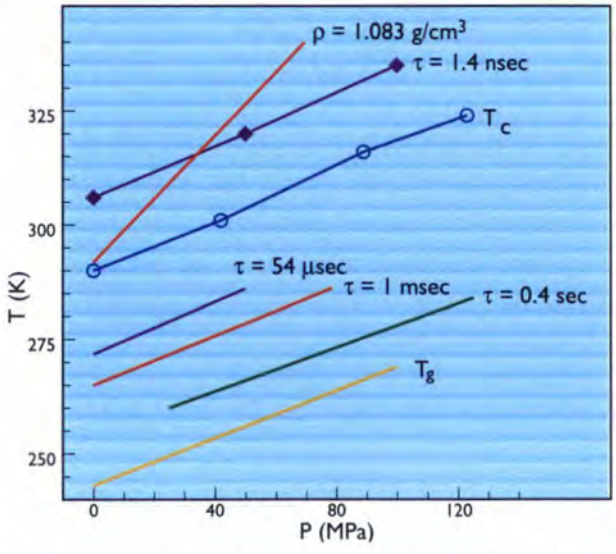

Figure 1: *Constant structural relaxation times in the (T, P)-plane. The line τ = 1.4 nsec corresponds to our backscattering measurements on IN16. Note, that over 15 decades (T_g corresponds to approximately 100 s) the slope (dT/dP) ≈ 250 K/GPa stays constant and the mode-coupling theory cross-over line from ergodic to non-ergodic behaviour $T_c(P)$ (see Fig. 3) lies parallel to the structural relaxation times.*

The mean relaxation times $\tau(T/T_g)$ which in many systems, including orthotherphenyl, can be identified with the macroscopic viscosity $\eta(T/T_g)$ (viscosity scaling, where T_g is the calorimetric glass transition temperature) is the single most important function for the classification of a glass (fragility scheme) [1]. *A priori* nothing can be said about the functional dependence of τ upon pressure. For the case of orthotherphenyl, in the temperature and pressure range investigated by us (0.1 – 120 MPa), relaxation times scale linearly with pressure as demonstrated in Fig. 1. Therefore, $\tau(T/T_g)$ is invariant as a function of pressure, or in other words the system in this range, does not change its fragility with pressure. Note that the relaxation times do not scale with the density ρ. Volume alone is not the driving force of the glass transition.

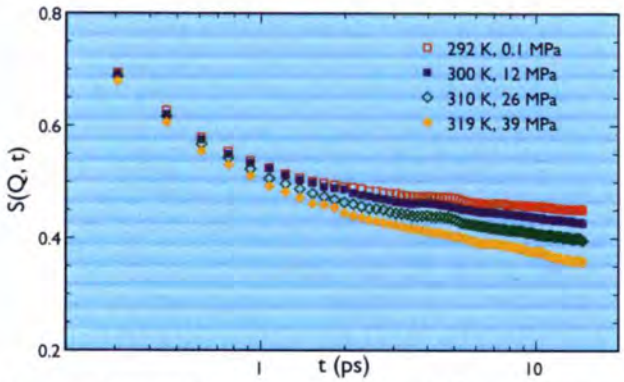

Figure 2: *Correlation functions S(Q, t) at Q = 1.8 Å^{-1} at fixed density ρ = 1.0834 g/cm^3 as obtained by Fourier transformation of IN6 spectra. The decay is more pronounced for higher temperatures underlining directly the improtant role of thermal effects.*

What is the connection of structural relaxation and fast relaxation on microscopic length and time scales?

Fast β-relaxation is a general feature observed in many supercooled liquids on microscopic length and time scales. A priori fast and structural relaxations could react independently to temperature and pressure.

The mode-coupling theory of the glass transition [3] establishes for the first time a firm theoretical link between the structural and the fast relaxation. Pressure experiments are, therefore, a good test of the theory. Within mode-coupling theory the supercooled liquid becomes non-ergodic when below a certain critical temperature T_c (or above a critical pressure P_c) the fast process is no longer able to promote the particle beyond the cage in which it becomes trapped. The fast processes can be observed in two ways: directly by time-of-flight experiments in the relevant time range or by an anomalous decrease of the elastic scattering recorded by backscattering instruments.

In Fig. 2 we show correlation functions S(Q, t) of the fast relaxation at Q = 1.8 Å^{-1} and a fixed density of ρ = 1.0834 g/cm^3 as measured on the instrument IN6. Again one immediately recognises that the decay explicitly depends on temperature. Within mode-coupling theory [3] the function S(Q, t) in the fast relaxation region is predicted to scale as $S(Q, t) = f_Q + H_Q g_\lambda(t/t_\sigma)$ (1). The scaling function $g_\lambda(t/t_\sigma)$ is fully determined by the equilibrium structure factor S(Q). From the temperature and pressure dependence of the coefficients H_Q and t_σ (Fig. 3) obtained by comparing expression (1) with the experimental data we are able to consistently extract the critical cross-over line from ergodic to non-ergodic behaviour $T_c(P)$.

As shown in Fig. 1 this line is parallel to the structural relaxation times $\tau(P)$. In conclusion, our results support the mode coupling senario which, via a highly non-linear feedback mechanism traces fast and structural relaxation back to a common origin.

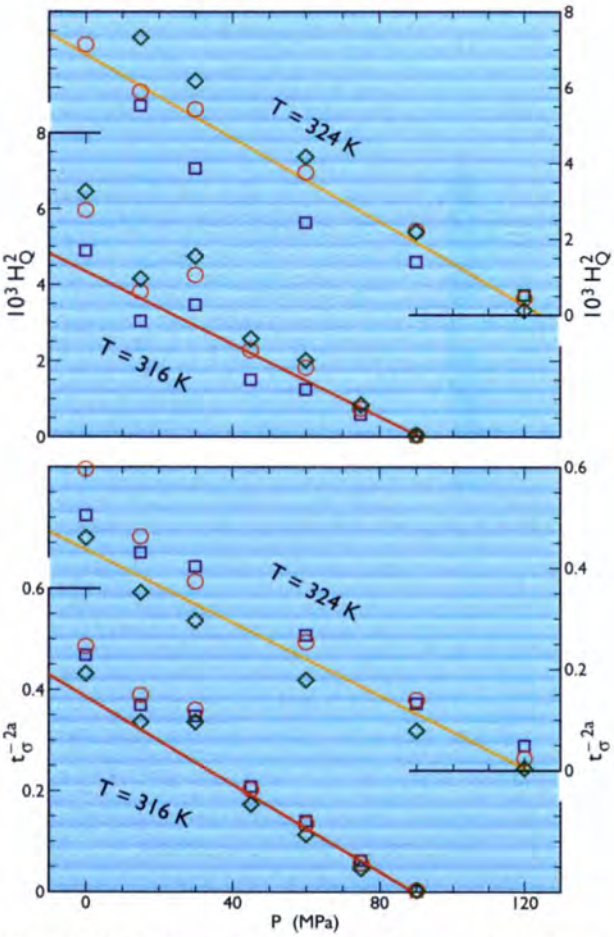

Figure 3: *Fast β-relaxation amplitude H_Q and cross-over time t_σ for two isotherms 316 and 324 K and three wave numbers Q = 1.2 (squares), 1.5 (circles) and 1.8 Å^{-1} (diamonds) as obtained from S(Q, t) using expression (1) (see text). According to mode-coupling theory H_Q is proportional to $\sigma^{1/2}$ and t_σ is proportional to $\sigma^{-1/2a}$ (a = 0.295) with the separation parameter $\sigma = (P_c - P)/P_c$. Extrapolation to zero gives consistent values for the critical pressures P_c as a function of temperature.*

References

■ [1] C.A. Angell, Science 267 (1995) 31 ■ [2] A. Tölle, H. Schober, J. Wuttke, O.G. Randl, F. Fujara, Phys. Rev. Lett., in press.
■ [3] W. Götze, L. Sörgen, Rep. Progr. Phys. 55 (1992) 241.

Structure and dynamics of liquid Ag_2Se

- A.C. Barnes, S.B. Lague and M. Hamilton (Bristol Univ.),
- H. Fischer (ILL),
- W.S. Howells (RAL Didcot),
- P.S. Salmon (Univ. East Anglia).

Understanding the relationship between the electronic properties, structure and dynamics of atoms in disordered materials is a fundamental challenge to condensed-matter physicists. In the case of binary liquids a good understanding of molten salts has been obtained using theoretical and computer-simulation methods based on ionic potentials. However, as the form of the interaction becomes more covalent or metallic in nature our theoretical understanding of binary liquids becomes progressively weaker. In this report we compare the results of a detailed study, using neutron-scattering techniques, of the structure and dynamics of a binary liquid semiconductor, Ag_2Se, and we compare the results with conventional and *ab initio* molecular-dynamics simulations.

Silver selenide (Ag_2Se) is an unusual material with a rich behaviour in both the solid [1] and liquid [2] phases. In the solid phase at a temperature of 416 K it undergoes a transition to a superionic phase in which the silver ions are able to move freely through a fixed Se lattice. It is also unusual as it shows a small but significant additional electronic contribution to its conductivity. Silver ions are also found to be highly mobile in some glassy materials, a property which has raised interest in the field of solid electrolytes for battery applications. On melting, the system continues to show unusual properties, for example, despite being a liquid semiconductor, the electrical conductivity decreases with temperature and shows an unusual enhancement precisely at the stoichiometric composition. It is believed that these properties are linked to an unusually high silver-mobility in the liquid.

In order to approach a full understanding of the properties of this liquid an important first step is to ascertain its microscopic structure. In a neutron diffraction-experiment the relationship between the differential scattering cross-section and the structure is given by

$$\frac{d\sigma}{d\Omega} = \sum_{i=1}^{n} c_i \overline{b_i^2} + \sum_{i=1}^{n} \sum_{j=1}^{n} c_i c_j \overline{b_i b_j} \left(S_{ij}(Q) - 1\right)$$

where $S_{ij}(Q)$ are the partial structure-factors that are related to the partial pair correlation-function $g_{ij}(r)$ between atoms of type i and j, and (c_i, c_j) and (b_i, b_j) are the concentrations and neutron scattering-lengths of atoms i and j respectively. $g_{ij}(r)$ is related to $S_{ij}(Q)$ by Fourier transform as

$$g_{ij}(r) = \frac{1}{2\pi^2 \rho r} \int_0^{\infty} Q \left(S_{ij}(Q) - 1\right) \sin(QR)\, dQ$$

As the $S_{ij}(Q)$ are smooth functions over all Q space it is not possible, in a single diffraction-experiment, to unambiguously determine the individual partial structure-factors. However, the technique of isotopic substitution (for certain elements) allows us to vary the value of the scattering length in the above expression so that the diffraction pattern for otherwise chemically identical samples can be varied. In the case of a binary system three separate diffraction measurements are sufficient to determine unambiguously the partial structure-factors provided the contrast in the scattering lengths is high enough.

Fig. 1 shows the partial structure-factors of liquid Ag_2Se determined from the diffraction patterns from three isotopically labelled samples of liquid silver-selenide

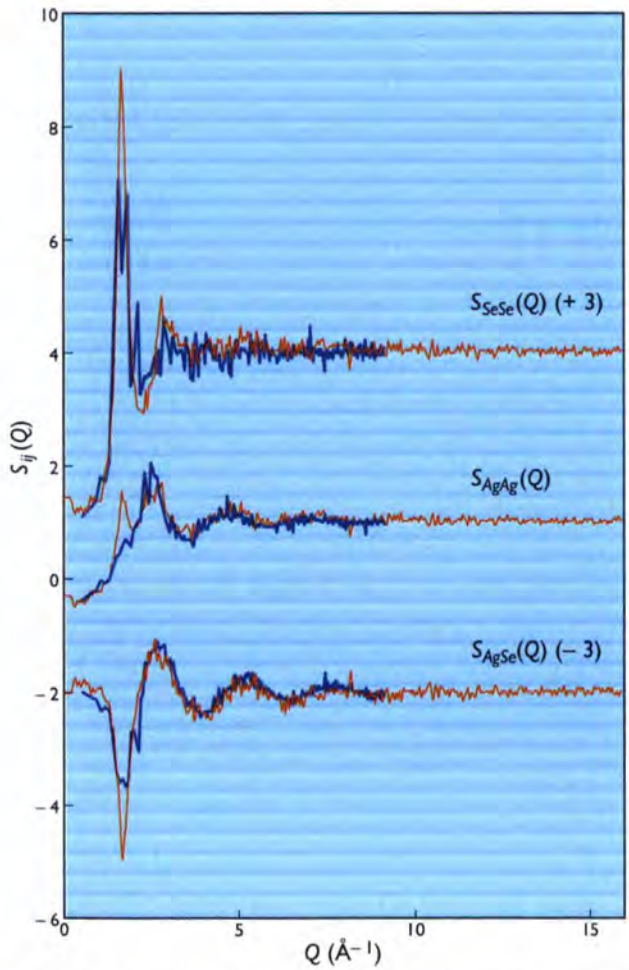

***Figure 1:** The experimental $S_{ij}(Q)$ (red line) and the ab initio molecular dynamics $S_{ij}(Q)$ (blue line) of Kirchhoff et. al. 1996.*

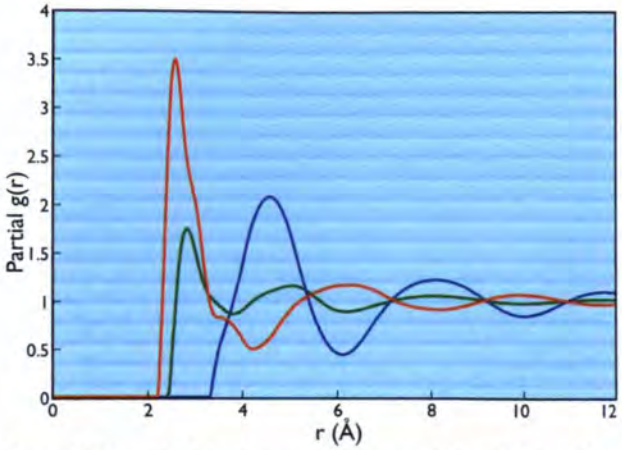

Figure 2: *The $g_{ij}(r)$ obtained from the $S_{ij}(Q)$ shown in figure 1. The red line is $g_{AgSe}(r)$, the blue line $g_{SeSe}(r)$ and the green line $g_{AgAg}(r)$.*

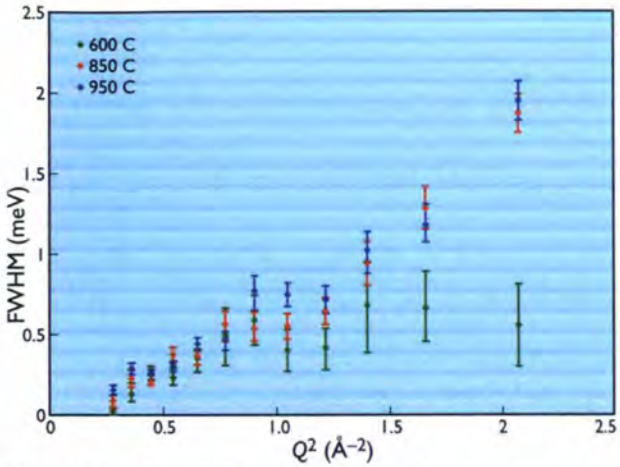

Figure 3: *The full width half maximum (FWHM) of the coherent quasielastic scattering from silver in the solid state (600°C (green) and 850°C (red)) and the liquid state (950°C (blue)) Ag_2Se.*

($^{107}Ag_2{}^{76}Se$, $^{109}Ag_2{}^{nat}Se$ and $^{nat}Ag_2{}^{76}Se$) collected using the D4 diffractometer. Fig. 2 shows the corresponding $g_{ij}(r)$. From Fig. 2 it is apparent that the selenium atoms are well ordered in the liquid and form a close-packed structure. The general weakness of the features in $g_{AgAg}(r)$ indicates that the silver atoms occupy the interstitial spaces between the selenium atoms and is consistent with a picture in which the silver atoms are highly mobile in the liquid. A comparison of the experimental partial structure-factors with those determined from a molecular- dynamics simulation [3] based on ionic potentials shows a good agreement apart from the tendency to underestimate the relative strength of the silver-silver interaction. Fig. 1 also shows the partial structure-factors determined from an *ab initio* molecular dynamics (AIMD) simulation [4]. The advantage of these methods is that the forces between the ions are calculated using first principles quantum methods with no adjustable parameters apart from the establishment of suitable atom core pseudopotentials. As a result the atomic structure, dynamics *and* electronic structure are calculated simultaneously.

Due to the demanding computational requirements the number of atoms that can be treated is small (69 in this case) and the currently obtain-able precision of the $S_{ij}^{AIMD}(Q)$ is limited. With these limits the agreement with the experimental data is good apart from the small pre-peak in $S_{AgAg}(Q)$. This discrepancy is most likely due to the limited box size in the simulation and demonstrates the need to experimentally verify the simulation results wherever possible. Despite the limitations of the *ab initio* molecular dynamics it correctly predicts the semiconducting behaviour of the liquid and it is able, unlike the conventional molecular-dynamics techniques, to simulate structures at off-stoichiometric compositions.

It has been postulated that the unusual electronic properties of liquid Ag_2Se may be associated with a high mobility of the silver ions as seen in the superionic phase before melting. The structure measurements reported above are consistent with such a high silver-mobility but are not conclusive. Measurements using coherent quasielastic neutron-scattering have been made on Ag_2Se in the liquid phase and the superionic phase just before melting.

Fig. 3 shows the quasielastic linewidth as a function of Q^2 associated with the silver motion in both these phases. At the lowest temperature a behaviour is observed where the silver ions show a jump diffusion at short distances (high Q) which tends to diffusional behaviour (FWHM $\propto Q^2$) at longer distances (low Q). As the temperature is raised the motion is characterised by a purely diffusional picture over the whole Q-range. It can be noted that the disorder induced on melting does not appear to drastically reduce the silver mobility in the liquid and no diffusional motion of the Se atoms could be observed at the experimental (IN6) resolution. With these results our aim is to build a more complete understanding of the electronic processes in this material. As part of this work it is also intended to study Ag_2Te; a material which appears to be very similar to Ag_2Se but shows more conventional liquid semiconducting behaviour.

References

■ [1] M. Kobayashi, Solid State Ionics, 39 (1990) 121 ■ [2] S. Ohno, A.C.Barnes and J.E.Enderby, J.Phys.: Condens. Matter 6 (1994) 5335 ■ [3] J.P. Rino, Y.M.M. Hornos, G.A.Antonio, I Ebbsjö, R K Kalia and P Vashishta, J. Chem. Phys. 89 (1988) 7542 ■ [4] F. Kirchhoff, J.M.Hollender and M.J. Gillan, Phys. Rev. B 54 (1996) 190.

A quantitative determination of the dynamic structure factor of a glass in the Brillouin scattering region

M. Foret, B. Hehlen, E. Courtens, and R. Vacher (Univ. Montpellier),
H. Casalta, R. Currat, A.-J. Dianoux, and B. Dorner (ILL).

The relatively large density of modes generally found in glasses around a few meV, and the contribution to it of strong acoustic scattering by structural disorder, are topics of considerable current interest. Two neutron Brillouin scattering techniques were used to clarify this issue in glassy selenium, g-Se. With cold-neutron time-of-flight spectroscopy on IN5, a pronounced boson peak is observed. With thermal-neutron three-axis spectroscopy on IN8, Brillouin scattering is clearly seen in addition to other spectral components. The quantitative comparison of the results obtained with both spectroscopies allows the various contributions to the boson peak to be unravelled.

Glasses are quenched liquids that remain structurally disordered on the scale of a few atoms. Their vibrational and relaxational spectrum on this scale is very different from that of crystalline matter. For example, the disorder is responsible for the existence of two-level systems, soft potential modes, and strong scattering of acoustic excitations. This is an important spectral region as it controls many singularities of glasses, such as their unique thermal properties. It might even be crucial to the actual kinetics of glass formation. However, in spite of the long active interest in the subject, the unravelling of the spectral components is still a matter of active debate. A central reason is that, owing to the lack of periodicity, coherent spectroscopy of glasses in the appropriate range of momentum exchange Q and energy ω has remained technically difficult [1].

In the experiments reported here, results of time-of-flight spectroscopy on IN5 are being combined with those of three-axis spectroscopy on IN8 to gain significant information on the dynamical structure factor, S(Q, ω), in a range where acoustic phonons become strongly scattered by disorder. Fig. 1 illustrates the energy-momentum relation of both instruments. The parabolic-like curves represent the energy, $\hbar\omega = E_f - E_i$, and momentum,

$$\hbar^2 Q^2/2m = E_i + E_f - 2\sqrt{E_i E_f}\,\cos\theta,$$

conservation relations traced at the smallest scattering angles θ that were effectively achieved. Two values of the initial energy E_i were selected on IN5, corresponding to wavelengths λ_i = 3.5 and 2.5 Å, respectively. A constant final energy E_f, corresponding to k_f = 4.1 Å^{-1}, was used on IN8. The small angle θ = 1.3° could be reached on IN8 with tight collimation and appropriate filtering. The ω(Q)-region covered in the experiments lies to the right of these parabolic-like limit curves. The energy resolution is 0.35 meV on IN5 with λ_i = 3.5 Å, and 1.45 meV on IN8, with triangular-shaped and gaussian resolution functions, respectively.

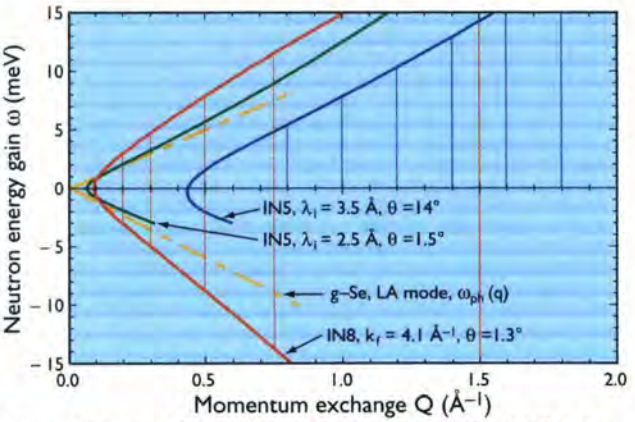

Figure 1: *Regions of {Q, ω}-space explored with both IN5 and IN8 in these experiments. The parabolic-like curves correspond to the smallest accessible scattering angles, and the explored regions lie to the right of these curves. The expected acoustic dispersion of g-Se, $\omega_{ph}(q)$, is also shown. The vertical lines correspond to data cuts displayed in Fig. 2, or to scans in Fig. 3.*

Glassy selenium, g-Se was selected for study because of its unusually low longitudinal acoustic velocity. The anticipated phonon-dispersion curve, $\omega_{ph}(q)$, is also shown in Fig. 1. With this low velocity, the kinematic condition $\{Q, \omega\}=\{q, \omega_{ph}\}$ is fulfilled on IN8 and nearly fulfilled on IN5. Se forms a well-known polymer-like glass in which the atoms are mostly two-fold co-ordinated in chains and rings of various sizes and mean length around five. Intuitively, one expects that the associated floppiness produces strong scattering of the longitudinal acoustic phonons plus a distribution of low frequency optic-like local modes. Both should contribute to a spectral feature generally known as the boson peak. The favourable {Q, ω}-region accessible in the present experiments, and the possibility to calibrate S(Q, ω) in neutron scattering, allow for the first time to identify clearly the longitudinal acoustic scattering spectrum of a glass and to separate it from the local modes contribution.

Fig. 2 illustrates results obtained on IN5 at λ_i = 3.5 Å on the neutron energy-gain side. The scattered intensities are corrected for absorption and empty cell scattering, and

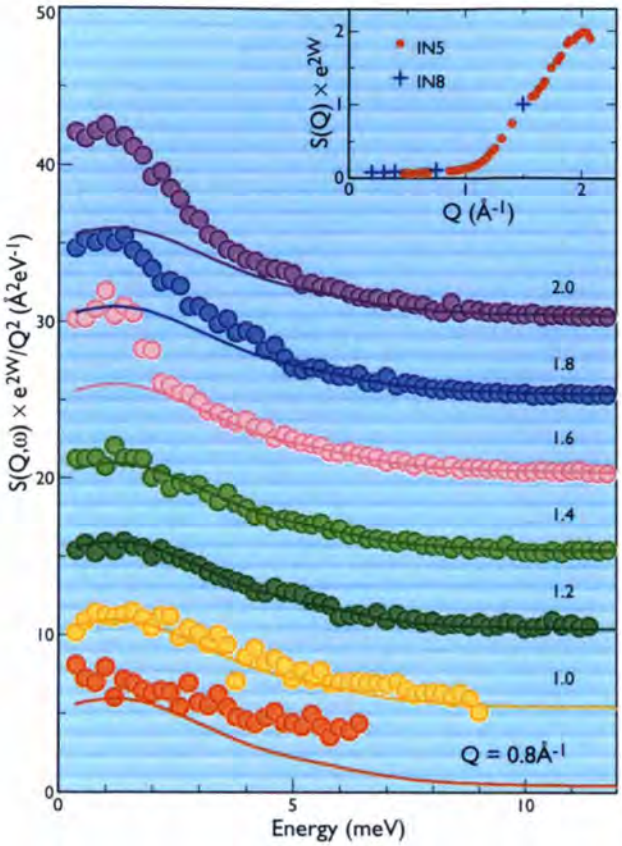

Figure 2: *Scaled structure factor for constant Q-cuts obtained on IN5 with λ_i = 3.5 Å, and at room temperature. Curves of increasing Q are displaced vertically in steps of 5, and labelled with the Q-value in Å^{-1}. The shifted lines are guides to the eye representing the value of the signal at intermediate Q-values. Departures from the lines are due to acoustic contributions, owing to the Brillouin signal at low Q, and to Umklapp processes at high Q. The inset shows the measured elastic structure factor, S(Q) on both IN5 and IN8, demonstrating the satisfactory agreement of the calibrations.*

calibrated against vanadium. The structure factor is scaled by the Debye-Waller factor, e^{-2W}, and divided by Q^2 to emphasise the near proportionality of S(Q, ω) to Q^2 over a broad range of Q-values. In this presentation, one notes an additional intensity appearing at the smaller Q's (0.8 and 1.0 Å^{-1}), but one fails to identify a clear acoustic contribution of well-defined $\omega_{ph}(q)$. Results obtained with λ_i = 2.5 Å are very similar. At large Q, there also appears an additional intensity at small ω in Fig. 2. It grows in Q with the elastic peak, S(Q), shown in the inset. Such a feature is already known for polybutadiene, a standard polymer. [2] We return to its interpretation below.

Fig. 3 shows S(Q, ω) × e^{2W} from three-axis-spectroscopy, for the vertical scans drawn on Fig. 1. For small Q, Brillouin peaks are immediately identified on the raw data (3a) previous to any treatment. Fig. 3b shows a scan at Q = 1.5 Å^{-1}, together with data from IN5. One notices the satisfactory match between the two independent measurements. Small differences can easily result from calibration and resolution effects. Comparing vertical scales on Figs. 3a and b, it is clear that the signal that grows with Q^2 on Fig. 2 has overwhelmed the LA-spectrum already at Q = 1.5 Å^{-1}. It gives a substantial relative contribution to spectra at 0.75 and 0.5 Å^{-1} in Fig. 3a, whereas its share drops to ~ 1% or less at the lower Q-values. This signal can be interpreted as scattering from local modes in the incoherent approximation. Under this assumption, the local modes scattering can be determined self-consistently and subtracted from the total signal, to provide pure longitudinal acoustic spectra.

To adjust the resulting Brillouin signals we use as a model a crossover spectral function already successful for high frequency acoustic spectra in vitreous silica [3].

The idea is that beyond a certain crossover ω_{co}, the acoustic excitations become so strongly perturbed by disorder that they *cease to propagate* as plane waves [4]. They enter then a regime where q loses its wave-vector meaning, only ω characterises the acoustic eigenmodes, and Q determines which Fourier component of all these modes is detected by the measuring apparatus. This situation prevails for Q larger than a crossover wave vector q_{co}. The latter is simply given by $\omega_{co} = c_0 q_{co}$, where c_0 is the sound velocity. The fitted acoustic components for the spectra of Fig. 3a are shown in Fig. 3c. These curves include the convolution with the 4-dimensional resolution ellipsoid of the three-axis spectrometer, calculated with a standard Monte-Carlo procedure. The Stokes-Antistokes asymmetries seen on Fig. 3c are not due to the Bose factor alone, but include resolution effects. This emphasises the considerable importance of proper spectrometer calibration and data analysis. The entire fits are the solid lines of Fig. 3a.

These correspond to a crossover at ω_{co} = 3.4 meV, or $q_{co} \approx 0.3$ Å^{-1}. In this interpretation the spectrum at Q = 0.2 Å^{-1} is in the phonon regime, that at Q = 0.3 is near crossover, while the others were above crossover. This is also clearly apparent with the ω/Q scale used in Fig. 3a : the peak positions are nearly identical for the two smallest Q values, while they move to lower ω/Q at higher Q.

We return to the additional low-ω feature appearing at high Q-values in Fig. 2. Umklapp processes can take place on the elastic structure-factor of a glass [5] as for a reciprocal lattice point for a crystal, which gives a doubly peaked acoustic signature. At low Q one sees the usual Brillouin signal, whereas at high Q one finds a contribution of all acoustic modes whose mean-free path is sufficient, approximately multiplied by $Q^2S(Q)$ (see Fig. 2).

The additional contribution at small ω for the three highest Q-values are large where S(Q) is large (see inset), but it disappears where the acoustic waves become strongly scattered, i.e. for $\omega > \omega_{co}$.

The observed size of the effect is in excellent qualitative agreement with that predicted by a simple model calculation in [4]. This interpretation is also quantitatively confirmed by a more detailed analysis of the data. The disappearance of the Umklapp signal for $\omega > \omega_{co}$ is a nice

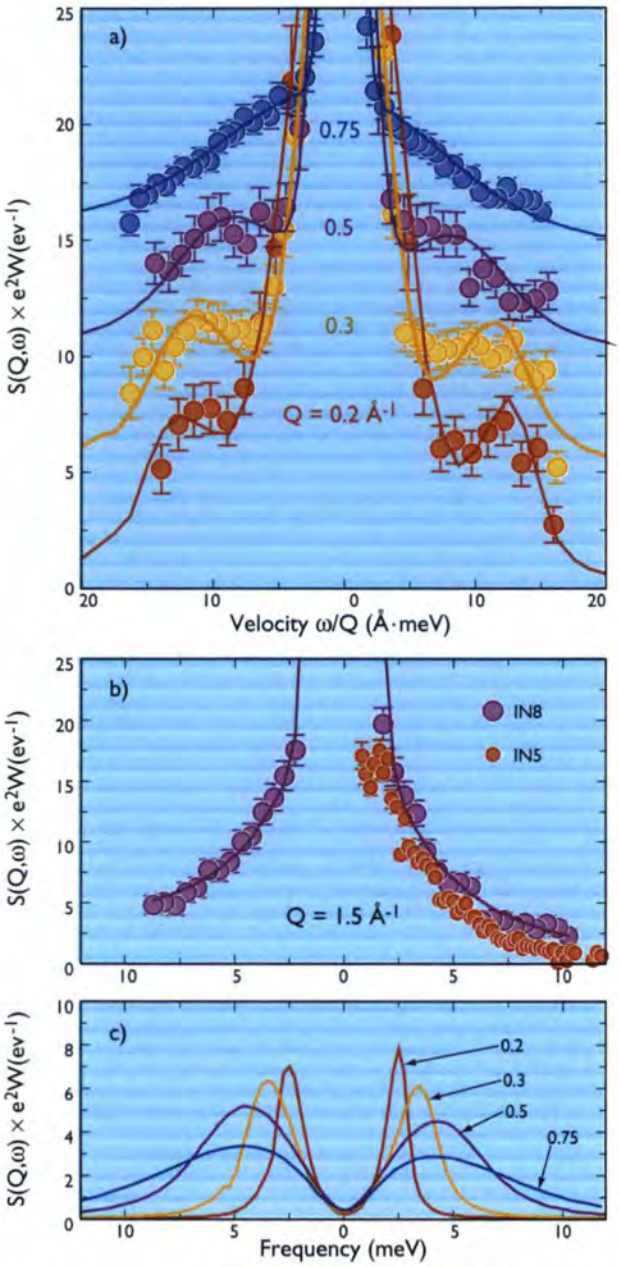

Figure 3: *Results from IN8 measurements at room temperature: (a) Q-scans at 0.2, 0.3, 0.5, and 0.75 Å^{-1}, the curves of increasing Q being displaced vertically in steps of 5. The fits are explained in the text ; (b) an IN8-scan at Q = 1.5 Å^{-1} compared to a corresponding cut of the IN5 data; (c) the fitted acoustic part of the spectra shown in (a) with the same color code.*

confirmation that the acoustic waves cease to propagate beyond that frequency.

In summary, we have for the first time clearly unravelled distinct spectral components contributing to the boson peak of a glass, including the acoustic signal. This became possible because coherent Brillouin scattering could be observed at low Q-values. Contrary to the case of the strong glass silica, for which the spectra could be described with just an acoustic crossover to strong scattering, other local modes play an important role in g-Se. If these other modes are "molecular reorientations", it is clear that the models that are used are somewhat crude. In particular, one would expect that resonant translational-rotational couplings could modify the spectral shapes, as well-known in some much simpler Brillouin scattering examples. Clearly, the present experiments constitute a beginning to be followed by many more investigations.

References

■ [1] J.-B. Suck, P.A. Egelstaff, R.A. Robinson, D.S. Sivia, and A.D. Taylor, Europhys. Lett. 19 (1992) 207 ■ [2] U. Buchenau, A. Wischnewski, D. Richter, and B. Frick, Phys. Rev. Lett. 77 (1996) 4035 ■ [3] M. Foret, E. Courtens, R. Vacher, and J.-B. Suck, Phys. Rev. Lett. 77 (1996) 3831; id. 78 (1997) 4669 ■ [4] J. Jäckle and K. Froböse, J. Phys. F: Metal Phys. 9 (1979) 967 ■ [5] J.M. Carpenter and C.A. Pelizzari, Phys. Rev. B 12 (1975) 2391.

Influence of magnetic order on superconducting properties of $Ho_xY_{1-x}Ni_2{}^{11}B_2C$

M. Loewenhaupt, A. Kreyssig, C. Sierks (TU Dresden),
K.-H. Müller, J. Freudenberger (IFW Dresden),
C. Ritter, H. Schober (ILL Grenoble).

The Borocarbide family RNi_2B_2C (R = Sc,Y,Th or lanthanides) exhibits a variety of interesting physical properties, especially the co-existence of magnetism and superconductivity. We report a correlation between magnetic ordering and superconductivity in the system $Ho_xY_{1-x}Ni_2{}^{11}B_2C$ as well as a correlation between magnetic ordering and the low energy magnetic excitations (spin waves from the low lying crystal field states).

The discovery of superconductivity in quaternary intermetallic RNi_2B_2C compounds (R = Sc, Y, Th or lanthanides) has attracted growing interest since the superconductivity is observed not only for the RNi_2B_2C compounds with nonmagnetic R, but also for the ones with magnetic rare-earths Tm, Er, Ho, and Dy which order magnetically at low temperatures [1]. This makes these systems suitable for a study of the interplay between superconductivity and magnetism. The systems where the Néel-temperature T_N and the superconducting transition-temperature T_c are of the same order of magnitude seem to be the most interesting since they show effects which are not yet completely understood [2].

A system with this property is $HoNi_2B_2C$ with $T_N \approx T_c \approx 8$ K. Furthermore, it exhibits a reentrant behaviour, this means that the superconducting properties do not strengthen with decreasing temperature but weaken in a narrow temperature range. We investigated the origin of the reentrant behaviour by comparing the temperature dependence of the magnetic ordering, of the low energy magnetic excitations, and of the superconducting properties. To study in a systematic way the correlation between the different properties, we prepared a series of samples where we diluted magnetic Ho with nonmagnetic Y.

$HoNi_2B_2C$ crystallises in the tetragonal $ThCr_2Si_2$ structure with the space group I4/mmm. The structure can be visualised as a framework of alternating R-C and Ni_2B_2 layers as shown in Fig. 1a. Three types of magnetic order are observed in $HoNi_2B_2C$ and the diluted samples: a commensurate antiferromagnetic structure with wave vector τ_1 = (0 0 1), an incommensurate structure with τ_2 = (0 0 0.915), and an incommensurate structure with τ_3 = (0.585 0 0) [1]. In certain temperature regions two or three of these structures seem to coexist. The commensurate antiferromagnetic c-axis modulated structure with τ_1 consists of Ho-moments ferromagnetically ordered in

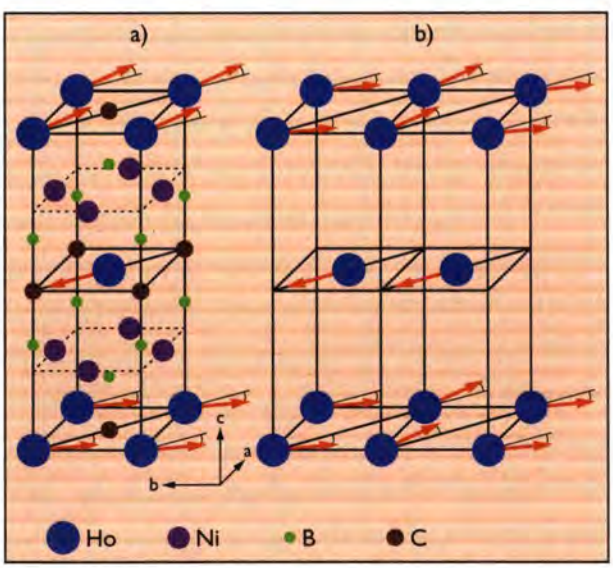

Figure 1: a) *Crystal and magnetic structure of $HoNi_2B_2C$. The red arrows show the Ho magnetic moments corresponding to the incommensurate c-axis modulated structure (moments in (a, b)-plane).* ***b)*** *Proposal for the incommensurate a-axis modulated magnetic order (moments with oscillating component perpendicular to (a, b)-plane).*

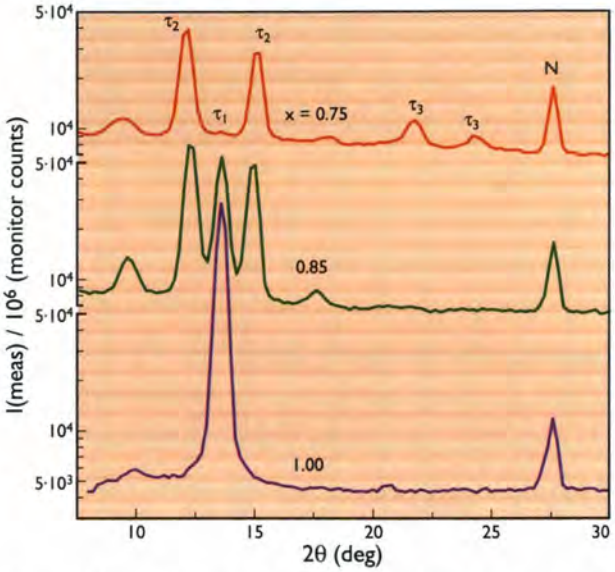

Figure 2: *Low-angle part of diffraction pattern for $Ho_xY_{1-x}Ni_2{}^{11}B_2C$ at 3 K with marked nuclear (N) and magnetic (τ_1, τ_2, τ_3) reflections.*

the (a, b)-planes pointing along (1 1 0) and stacked antiferromagnetically in the c-direction. In Fig. 1a the incommensurate c-axis modulated structure with τ_2 is illustrated. It consists of ferromagnetically ordered (a, b)-planes stacked along c-direction with a turning angle of approximately 165°. The incommensurate a-axis modulated structure with τ_3 is still under discussion. A proposal for it is shown in Fig. 1b.

To determine the behaviour of these three types of magnetic order, temperature-dependent neutron powder-diffraction experiments were carried out at the multidetector instrument D1B [3].

The powder samples of $Ho_xY_{1-x}Ni_2{}^{11}B_2C$ were first cooled down to the lowest temperature of 1.5 K and then heated in narrow temperature steps of 0.15 K up to 10 K. In Fig. 2 the low-angle parts of the diffraction patterns are shown for a temperature of 3 K.

In Fig. 3a-c the temperature dependence of peak intensities corresponding to the three types of magnetic order is presented. Peak intensities connected to the commensurate c-axis modulated structure decrease with decreasing Ho content and are below the detection limit for x = 0.75. The incommensurate a-axis modulated structure with τ_3 exists for all investigated samples only in a narrow temperature range. For x = 1 the temperature dependence of the incommensurate c-axis modulated structure with τ_2 is similar to that for τ_3, but for x < 1 the peak intensities increase monotonically with decreasing temperature down to the lowest measured temperatures.

To characterise the superconducting properties, we determined the upper critical field H_{c2} of the type-II-superconductor by measuring the electrical resistivity as a function of magnetic field and temperature in the range between 1.7 K and the critical temperature [3]. The upper critical

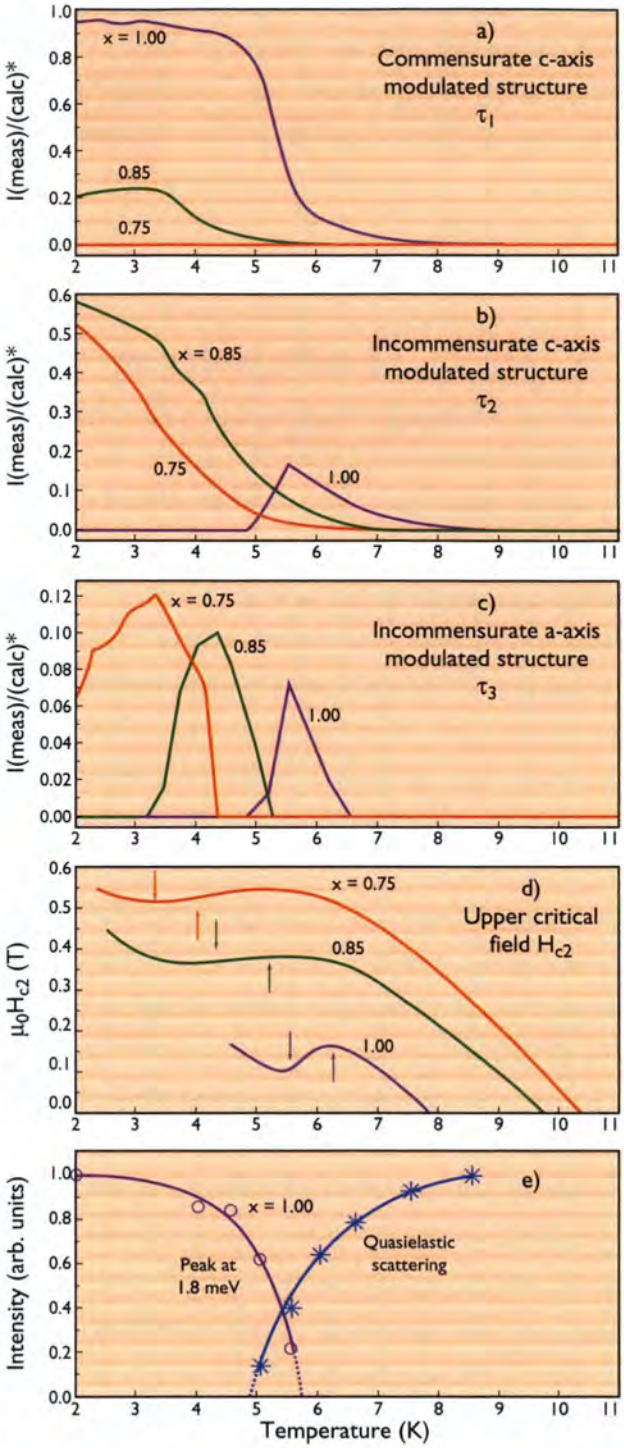

Figure 3: *Temperature dependence of intensities of magnetic reflections for $Ho_xY_{1-x}Ni_2{}^{11}B_2C$ normalised by calculated intensities for fully magnetically ordered phases with 10 μ_B for Ho^{3+} (free ion) for (a) τ_1, (b) τ_2, and (c) τ_3. The arrows (↑ and ↓) in the $H_{c2}(T)$ dependence (d) indicate onset and maximum temperature of τ_3-structure, respectively. In (e) the intensities of the magnetic excitation at 1.8 meV and of the quasielastic scattering are shown.*

field H_{c2} of the samples increases with decreasing temperature from zero at T_c up to a local maximum (see Fig. 3d). As a direct consequence of the reentrant behaviour H_{c2} decreases in a narrow temperature range and increases again monotonically to the lowest measured temperature for all investigated samples.

We observe the peculiar behaviour that although T_c increases with increasing dilution the temperature range

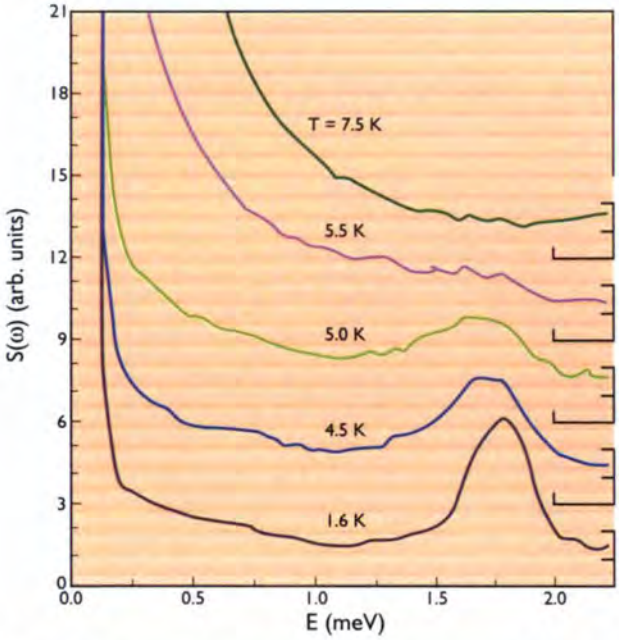

Figure 4: *Temperature dependence of the magnetic response of $HoNi_2{}^{11}B_2C$ in the magnetically ordered phases.*

where the reentrant behaviour can be observed is shifted to lower temperatures. This correlates for all three samples only with the temperature dependence of the incommensurate a-axis modulated structure which is indicated by the arrows in Fig. 3d.

Inelastic neutron-scattering experiments were carried out at the time-of-flight spectrometer IN6 [4]. No Q-dependence of the spectra could be detected for separate groupings of detectors. In the magnetic response function shown in Fig. 4 a sharp peak at 1.8 meV and a very broad one at 0.6 meV can be found for T = 1.6 K. Up to 5 K there is no significant change of the excitation spectrum. For higher temperatures the peak at 1.8 meV vanishes and a strong quasielastic scattering develops (see Fig. 3e). This is also the temperature region where the magnetic Bragg peaks of the commensurate c-axis structure decrease drastically (Fig. 3a). For x = 0.85 we could barely observe the 1.8 meV peak and for x = 0.75 we did not find it at all. It seems that the low-energy excitation at 1.8 meV is

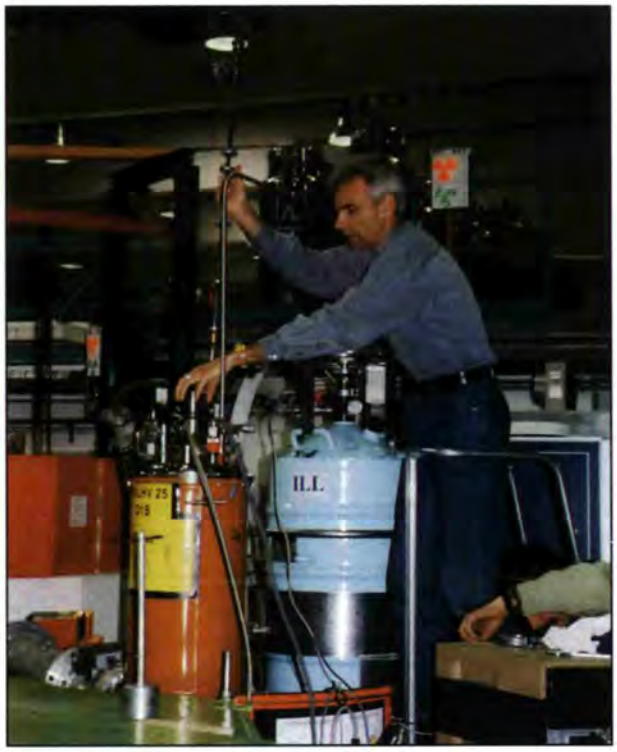

Clemens Ritter changes the sample on D1B.

correlated to the existence of the commensurate c-axis modulated structure.

In summary we can state the following: In the system $Ho_xY_{1-x}Ni_2{}^{11}B_2C$ the correlation between the reentrant behaviour and the temperature dependence of the incommensurate magnetic structure along the a-axis strongly suggests that the a-axis structure (τ_3) is responsible for the suppression of superconductivity.

Both magnetic structures with c-axis wave vectors (τ_1, τ_2) do not interfere with superconductivity, as their temperature dependencies and the reentrant behaviour are uncorrelated for x = 0.85 and x = 0.75. For the pure Ho-compound, however, τ_2 and τ_3 coexist in nearly the same temperature region. Similar investigations which have been undertaken by us in the system $Ho_xLu_{1-x}Ni_2{}^{11}B_2C$ yield qualitatively the same results but with more pronounced effects for the dilution [5,6].

References

■ [1] J.W. Lynn, S. Skanthakumar, Q. Huang, S.K. Sinha, Z. Hossain, L.C. Gupta ■ [2] H. Schmidt and H.F. Braun, Phys. Rev. B 55 (13) (1997) 3497 ■ [3] A. Kreyssig, M. Loewenhaupt, K.-H. Müller, G. Fuchs, A. Handstein and C. Ritter, Physica B 234-236 (1997) 737 ■ [4] M. Loewenhaupt, C. Sierks, P. Tils, A. Kreyssig, J. Freudenberger, A. Handstein, K.-H. Müller, C. Ritter and H. Schober, Physica B, in press ■ [5] A. Kreyssig, C. Sierks, M. Loewenhaupt, J. Freudenberger, G. Fuchs, K.- H. Müller and C. Ritter, Physica B, in press ■ [6] J. Freudenberger, G. Fuchs, K. Nenkov, A. Handstein, M. Wolf, A. Kreyssig, K.-H. Müller, M. Loewenhaupt and L. Schultz, J. Magn. Magn. Materials, in press.

Magnetic polarons in colossal magnetoresistance perovskites

M.R. Ibarra, J.M. De Teresa (Univ. Zaragoza and CSIC),
C. Ritter (ILL).

The intrinsic huge magnetoresistance observed in manganese oxide perovskites takes place in the paramagnetic phase in the neighbourhood of the transition to the ferromagnetic state at T_c. By using small-angle neutron-scattering under magnetic fields up to 5 T, we have shown the existence of ferromagnetic clusters in the paramagnetic phase which are responsible for the colossal magnetoresistance and disappear at T_c. These entities, formed by localised charge on Mn ions and shared by neighbouring Mn ions, are called magnetic polarons. The experiments allowed us to determine the thermal and field dependence of the magnetic correlation-length (ξ), which is interpreted as the average size of the magnetic polaron. The microscopic parameters ξ and the number of scattering centres have been correlated with macroscopic properties such as thermal expansion and resistivity.

In colossal magnetoresistance manganese perovskites, an extra contribution in the volume thermal expansion that adds to that of the anharmonic lattice was considered to be a signature of charge localisation above T_c in the form of small lattice polarons [1]. This extra contribution disappears at T_c as can be observed in Fig. 1b (all the results shown in this report correspond to the archetypal colossal magnetoresistance compound $La_{0.6}Y_{0.07}Ca_{0.33}MnO_3$). Application of a magnetic field tends to suppress the polaronic contribution to the volume thermal expansion. This seems to reflect the magnetic character of the polaron, which has been demonstrated by small-angle neutron-scattering measurements (on D16). Previous experiments on D1B had shown an anomalous small-angle neutron-scattering in the paramagnetic phase [2]. The new experiments carrried out on the diffractometer D16, and shown in Fig. 1a, have measured the effect more accurately to lower Q-values. The thermal and magnetic-field dependence of the small-angle neutron-scattering intensity, is similar to that of the extra contribution to the volume thermal expansion and confirms the magnetic nature of the polarons (see Fig. 1).

By fitting the small-angle neutron-scattering intensity to a lorentzian-type Q dependence $\{I = I_0/[Q^2 + (1/\xi)^2]\}$, ξ was obtained and interpreted as the average size of the magnetic polaron (Q is the scattering vector). In Fig. 2 one can observe that above T_c ξ is almost constant with temperature, defining ferromagnetic clusters of around 12 Å. As we approach T_c from above, a divergence in ξ is observed, which is interpreted as the percolation of the ferromagnetic clusters as the compound goes into the ferromagnetic phase. This is also reflected in the sharp drop in the small-angle neutron-scattering intensity at T_c (see Fig. 1a). Application of a magnetic field leads to a shift of T_c towards higher values.

At fixed temperature above T_c, the field dependence of ξ and the small-angle neutron-scattering intensity (see Fig. 3) correlate with the behaviour of the volume and the

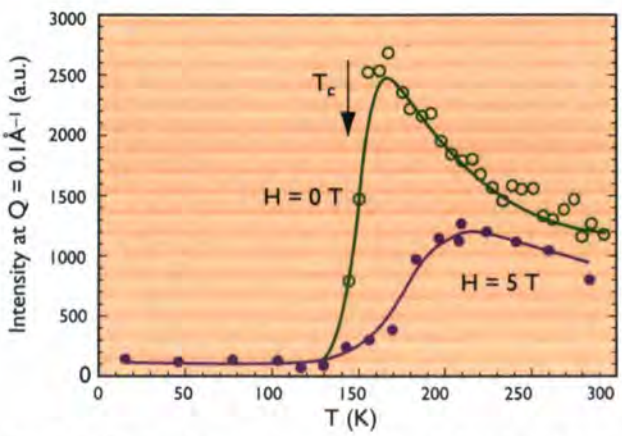

***Figure 1a:** Small-angle neutron-scattering intensity at fixed Q = 0.1 Å^{-1} in arbitrary units as a function of temperature without and under an applied magnetic field of 5 T in the compound $La_{0.6}Y_{0.07}Ca_{0.33}MnO_3$.*

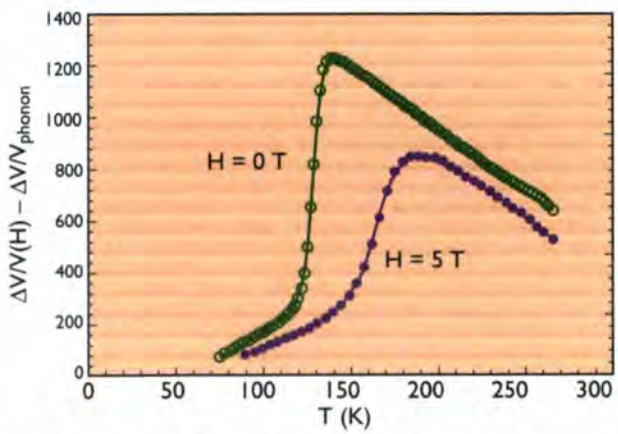

***Figure 1b:** Extra contribution to the volume thermal expansion without and under 5 T due to polaronic effects in the same compound.*

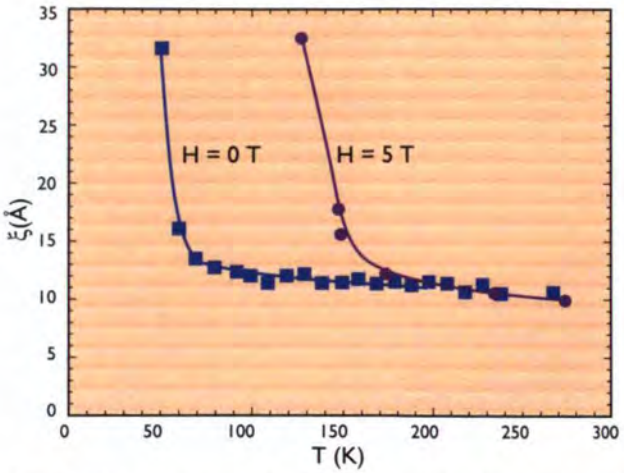

Figure 2: *Magnetic correlation-length, ξ, interpreted as the average size of the magnetic polarons, as a function of temperature without and under an applied magnetic field of 5 T in the compound* $La_{0.6}Y_{0.07}Ca_{0.33}MnO_3$.

resistivity when a magnetic field is applied [3]. The field increases the size of the polarons, whose number decreases. This implies a delocalisation of the charge carriers in larger ferromagnetic clusters, bringing about a drop in resistivity (several orders of magnitude) and a volume shrinkage. Percolation of the clusters causes the crossover from the polaronic to the metallic state.

This seems to be the first evidence in real systems of the identification of trapped carriers in magnetic clusters, which can open a new chapter in solid-state physics as mentioned by J.B. Goodenough and J.-S. Zhou [4].

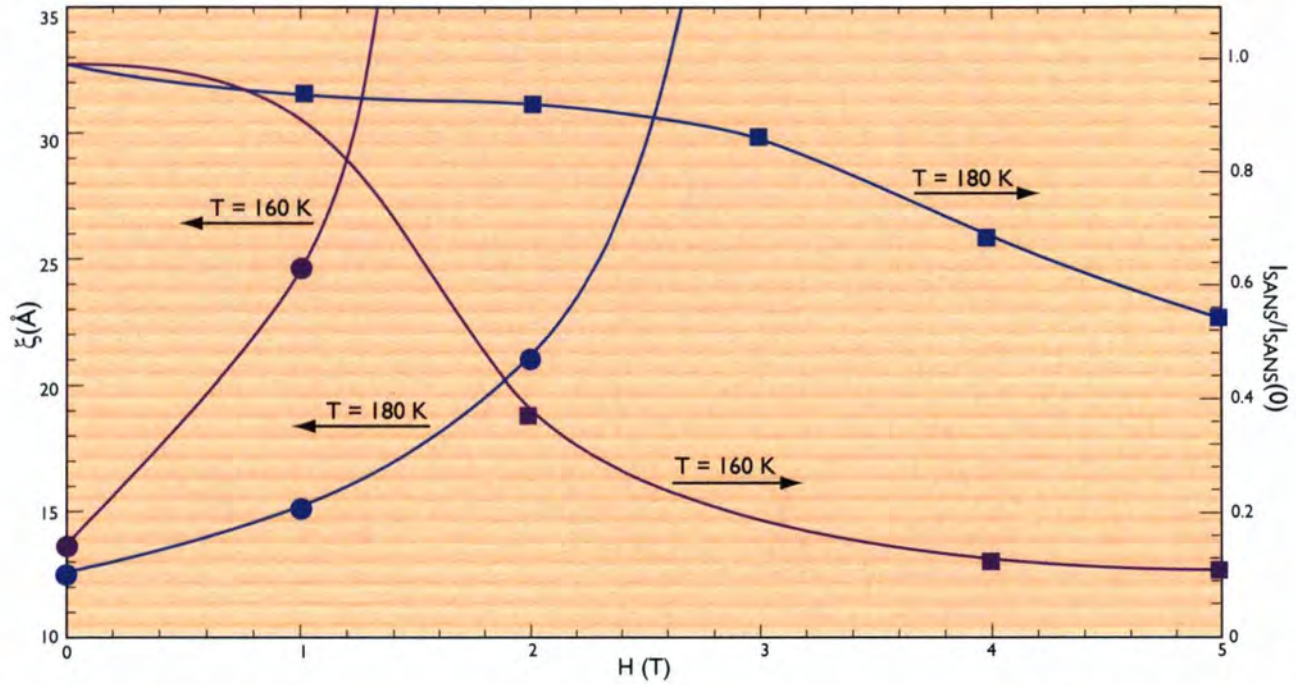

Figure 3: *Field dependence of the magnetic correlation-length, ξ, and the small-angle neutron-scattering intensity at fixed q = 0.1 Å⁻¹ normalised to the value at zero field, at constant temperatures, 160 and 180 K, in the compound* $La_{0.6}Y_{0.07}Ca_{0.33}MnO_3$.

References

■ [1] M.R. Ibarra, P.A. Algarabel, C. Marquina, J. Blasco, and J. García, Phys. Rev. Lett. 75 (1995) 3541 ■ [2] J.M. De Teresa, M.R. Ibarra, J. Blasco, J. García, C. Marquina, P.A. Algarabel, Z. Arnold, K. Kamenev, C. Ritter, and R. von Helmolt, Phys. Rev. B 54 (1996) 1187 ■ [3] J.M. De Teresa, M.R. Ibarra, P.A. Algarabel, C. Ritter, C. Marquina, J. Blasco, J. García, A. del Moral, and Z. Arnold, Nature 386 (1997) 256 ■ [4] J.B. Goodenough and J.-S. Zhou, Nature 386 (1997) 230.

Magnetic excitations in the ladder and chain subsystems of $Sr_{14}Cu_{24}O_{41+\delta}$

- L.P. Regnault (CEA Grenoble),
- H. Moudden (LLB Saclay),
- J.P. Boucher (UJF Grenoble),
- J.E. Lorenzo (CNRS Grenoble),
- A. Hiess (ILL),
- A. Revcolevschi (Univ. Paris-Sud).

At the boundary between dimensions one and two, spin-ladder systems are conceptually interesting as they exhibit rather "exotic" properties. In particular, the spin-pairing expected to develop in a 2-leg ladder could give rise, upon doping, to a charge pairing and finally to a non-conventional (i.e. non phonon-mediated) superconductivity. In this report, we present recent inelastic neutron-scattering results obtained on a single crystal of the undoped 2-leg spin-ladder compound $Sr_{14}Cu_{24}O_{41+\delta}$.

After the discovery of high-T_c superconductivity, a renewed interest in low-dimensional quantum magnetism has emerged, motivated by the possible rôle played by the magnetic interactions in the charge-pairing mechanism. One-dimensional antiferromagnets are particularly interesting to consider as they often exhibit unconventional phenomena. The first striking effect was discovered in the early 80's by Haldane [1], who suggested that Heisenberg antiferromagnetic chains with half-integer (S = 1/2, 3/2, ...) and integer (S = 1, 2, ...) spin values behave completely differently at low temperatures. Whereas the former is expected to be gapless, the latter should have a non-magnetic singlet ground-state and a quantum gap should open in the magnetic excitation spectrum. This non-intuitive prediction has been further very comprehensively verified from inelastic neutron-scattering experiments performed on the spin-1 antiferromagnetic chain compound $Ni(C_2H_8N_2)_2NO_2ClO_4$ [2]. On the other side, the spin-1/2 square lattice with antiferromagnetic nearest-neighbour Heisenberg exchange couplings exhibits «classically» an ordered gapless ground state at T = 0.

Spin-ladders can be viewed as an array of a finite number of coupled chains allowing therefore the study of the crossover between space dimensions 1 and 2. While spin-ladders with an odd number of legs behave like the spin-1/2 antiferromagnetic chain (gapless excitation spectrum, power-law spin correlations, ...), those with an even number of legs exhibit an exponential decay of the spin-correlations due to the opening of a spin-gap (with energy Δ) in the excitation spectrum [3]. Of particularly high interest is the 2-leg spin-ladder system, because of the prediction that charge doping could induce a non-conventional superconductivity, in which a d-wave pairing could be achieved, driven by the magnetic fluctuations [3]. Indeed, superconductivity has been recently discovered in the Ca-doped spin-ladder family $Sr_{14-x}Ca_xCu_{24}O_{41+\delta}$ for x > 11, under high pressure in the range 30-45 kbar [4]. The understanding of the mechanism leading to superconductivity in this material requires an accurate determination of both the temperature and doping dependencies of the magnetic excitation spectra. This can be achieved by inelastic neutron-scattering investigations on undoped and doped single crystals.

As a first step, we have recently undertaken such a determination on the undoped compound $Sr_{14}Cu_{24}O_{41+\delta}$. The structure of this material is a misfit stacking of layers of two distinct quantum spin systems: linear chains and 2-leg ladders [5]. Fig. 1 shows a "3D" view of the crystallographic structure, which emphasises the chain and ladder subsystems.

Magnetic excitations in the ladder subsystem

Following the theoretical predictions, the ground state of a 2-leg spin-ladder system in the case $J_\perp < J_{//}$ (where $J_{//}$ and

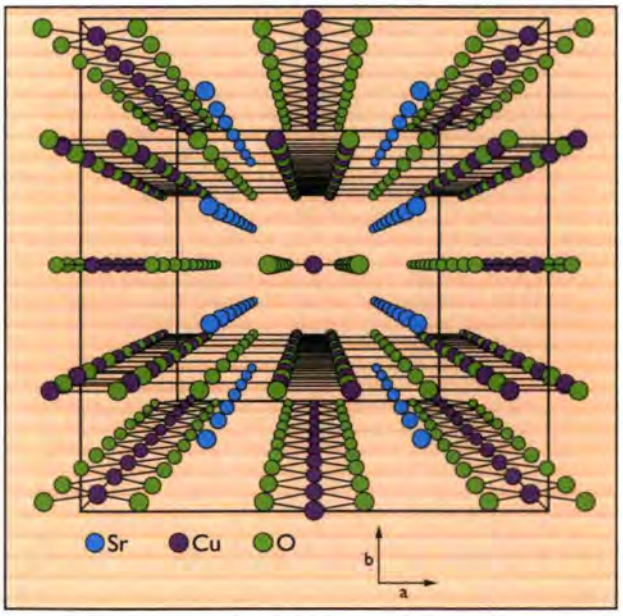

Figure 1: *Crystal structure of $Sr_{14}Cu_{24}O_{41+\delta}$ showing the chain and ladder subsystems (viewed along the c axis).*

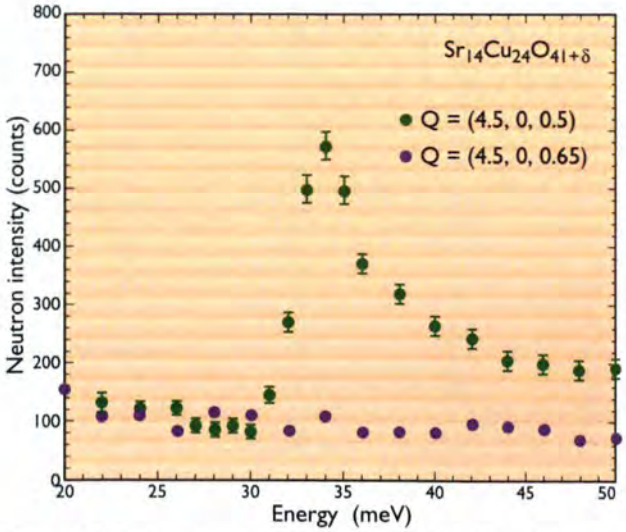

Figure 2: *Inelastic neutron-scattering response of the ladder subsystem at 1.5 K, showing the presence of a quantum spin-gap with energy 33 meV.*

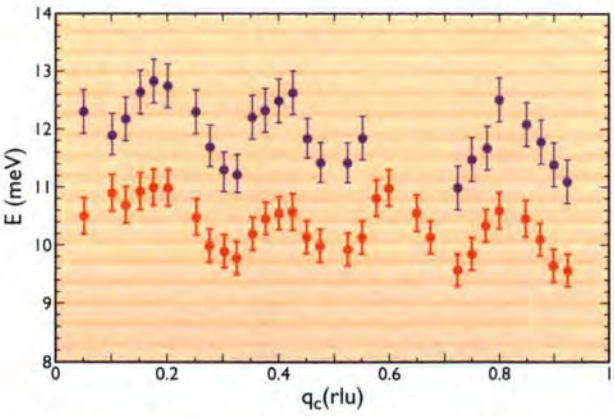

Figure 3: *Dispersion relation of magnetic excitations in the chain subsystem, showing the existence of two gapped and weakly dispersed branches of magnetic excitations.*

$J_\perp$ represent respectively the exchange coupling constants along the legs and along the rungs) should be a non-magnetic singlet ground-state, well separated from the first excited states by an energy gap $\Delta \approx 0.4\, J_\perp$. These two features have been unambiguously observed from inelastic neutron-scattering experiments carried out on the three-axis spectrometer IN8. We show in Fig. 2 two typical energy scans performed at scattering vectors **Q** = (4.5,0,0.5) (where one expects a strong signal originating from the ladders) and **Q** = (4.5,0,0.65) (where one expects a vanishing contribution of the ladders). The observed line shape is characteristic of a gapped magnetic response, with no signal detected around zero energy and a gap value Δ = 33 meV. At higher energy, the magnetic response persists without any sign of splitting (at least up to 90 meV), a fact which indicates the presence of large intra-leg exchange coupling constants $J_{//}$. From the quantitative analysis of our data, one estimates $J_\perp \approx 80$ meV and $J_{//} \approx 160$ meV.

Magnetic excitations in the chain subsystem

Concerning the magnetic CuO_2 chain, the present investigation broadly complements previous neutron scattering results [6] in showing a gapped response in contrast to the gapless spectrum mentioned above. As shown in Fig. 3, the dispersion of the elementary excitations along the chain direction is now determined in the whole Brillouin zone. The presence of two distinct branches in the energy range 10-12 meV is confirmed. However, the observed periodicity differs appreciably from what has been proposed before [6,7]. Accordingly, a new model describing the spin distribution along the chain has to be found for this undoped material. Our neutron data are consistent with a picture according to which the spins in the CuO_2 chains are forming dimers, with an intra-dimer coupling constant of the order of 10 meV and weak inter-dimer and inter-chain couplings.

The physical origin of the unconventional magnetic properties of the chain subsystem in $Sr_{14}Cu_{24}O_{41+\delta}$ is attributed to the presence of a large amount of "holes" in the CuO_2 chains (about 0.6/CuO_2 unit in the undoped material), whereas the ladders are still remaining undoped and magnetically "inert" due to the existence of a large spin gap. Upon Ca-doping, electrons are progressively transfered from the Cu_2O_3 ladders to the CuO_2 chains. This charge-transfer mechanism leads to a hole doping in the ladders and to a hole pairing and finally to superconductivity under pressure.

The next stage of our work is therefore to study the evolutions of the magnetic excitation spectra of both the ladder and chain subsystems upon Ca-doping and by applying a strong pressure. This should help in the understanding of the physical properties of these very promising materials.

References

■ [1] F.D.M. Haldane, Phys.Lett.A93 (1983) 464 ■ [2] L.P. Regnault, I. Zaliznyak, J.P.Renard and C. Vettier, Phys.Rev.B53 (1994) 5579 ■ [3] E. Dagotto and T.M.Rice, Science 271 (1996) 618 ■ [4] M. Uehara, T. Nagata, J.Akimitsu, H. Takahashi, N.Môri and K. Kinoshita, J. Phys. Soc. Jpn 65 (1996) 2764 ■ [5] E.M. McCarron, M.A. Subramanian, J.C.Calabrese and R.L. Harlow, Mat. Res. Bull. 23 (1988) 1355 ■ [6] M. Matsuda, K. Katsumata, H. Eisaki, N. Motoyama, S. Uchida, S.M. Shapiro and G. Shirane, Phys. Rev. B54 (1996) 1219 ■ [7] M. Takigawa et al, Phys. Rev. B (1998) in press.

Quantum fluctuations in a quasi-1D magnet in an applied field

R. Coldea, D.A. Tennant, R.A. Cowley (Univ. Oxford),
B. Dorner (ILL).

Magnetic excitations of the quasi-one-dimensional S = 1/2 Heisenberg antiferromagnet Cs_2CuCl_4 have been measured as a function of applied field using neutron scattering. At low temperatures and zero field the weak interchain coupling produces 3D incommensurate ordering. Fields greater than B_c = 1.66 T but less than the field required to fully align the spins (≈ 8 T) are observed to decouple the chains and the system has a disordered intermediate-field phase. This phase is dominated by quantum fluctuations which give rise to a continuum of excitations and field-dependent incommensurate correlations. These have been observed in the neutron-scattering experiments and are inconsistent with linear spin-wave theory.

The magnetic properties of the one-dimensional S = 1/2 Heisenberg antiferromagnetic chain are very different from those of three-dimensional magnetic systems because of the importance of quantum fluctuations. It has been known since the early 1930's that there is no long-range order even at T = 0 K. More recently, in the 1980's, it was realised that the excitations are not the doubly degenerate $\Delta S^z = 1$ spin waves, but S = 1/2 so-called spinons and that the neutron scattering from such systems is three fold degenerate and consists of a continuum in (Q, ω) space corresponding to the creation of pairs of spinons. This continuum has now been observed in quasi-1D, S = 1/2 Heisenberg antiferromagnetic chains and the results are in agreement with the theoretical predictions [1].

Another manifestation of the effect of quantum fluctuations occurs when a magnetic field is applied. Classically, magnets with antiferromagnetic Heisenberg interaction form a spin-flop phase in which the spin moments along the field are aligned ferromagnetically and those perpendicular to the field are aligned antiferromagnetically. Quantum theory, however, predicts that a number of spins become fully aligned by the field and those are distributed approximately regularly along the chain. This produces an incommensurate-like short-range order with a periodicity given by the average distance between the aligned spins, which decreases with increasing field. The triplet excitation continua in zero field are split by the applied field into separate continua which come down to zero energy at positions corresponding to the incommensurate ordering wavevector [2], as illustrated in Fig. 1. The positions of the continua alter as the applied field increases until at high fields $B > B_0$ the spins are all aligned parallel to the field and the excitations have a well-defined magnon dispersion relation.

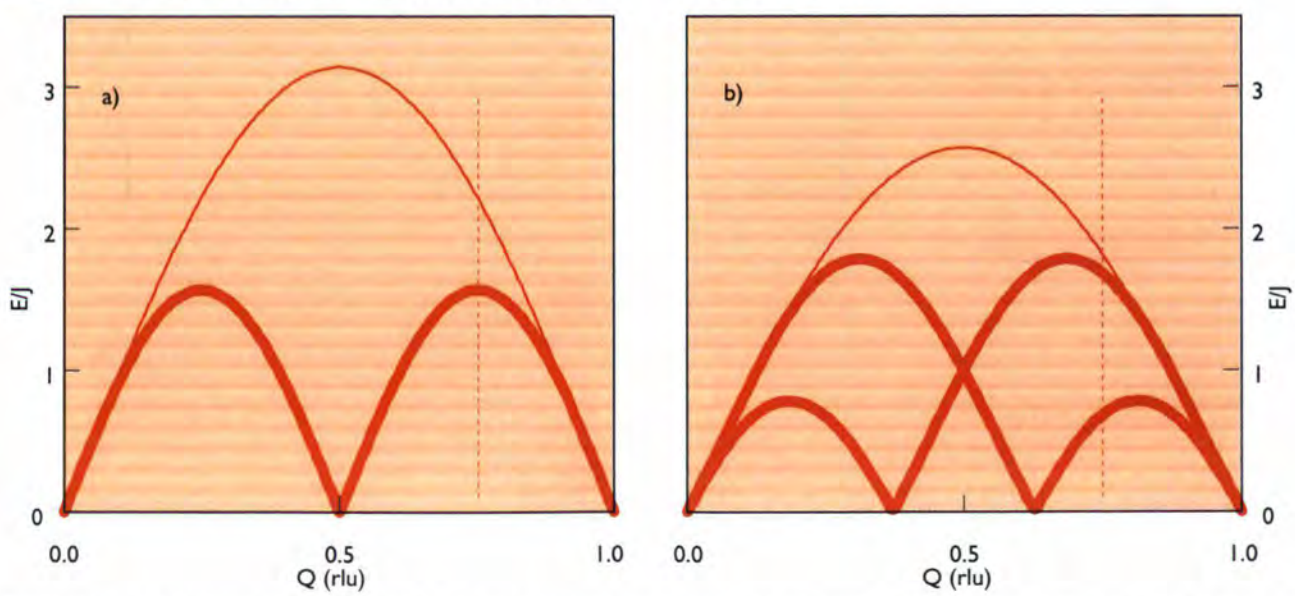

Figure 1: *Spectrum of longitudinal excitations in the 1D S=1/2 Heisenberg antiferromagnetic chain in* ***a)*** *zero and* ***b)*** *an applied field $B = J/g\mu_B$. The heavy and light lines are the boundary of the continua with the heavy lines indicating where strong scattering is expected. The dotted vertical lines show the direction of constant-Q scan in Fig. 3. The transverse modes also show similar effects [2] but have been omitted for the sake of clarity.*

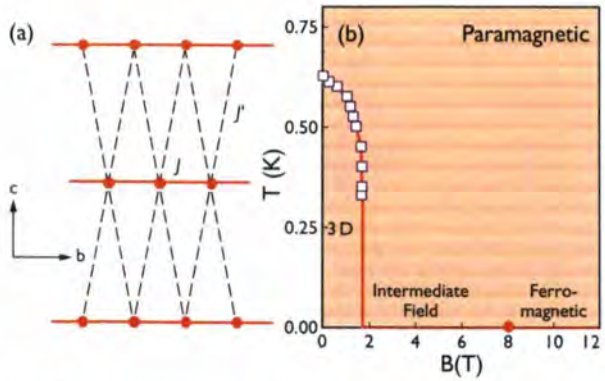

Figure 2: a) *Magnetic chains and exchange paths in Cs_2CuCl_4.* ***b)*** *Magnetic phase diagram in a field applied along c showing the measured boundary of the 3D cycloidal phase (open squares) and the regions of the intermediate-field and ferromagnetic phases.*

Cs_2CuCl_4 is one of the few quasi-1D systems with a sufficiently low exchange interaction (J = 0.41 meV) that it is possible to apply large enough magnetic fields to produce the fully aligned ferromagnetic phase [3]. The S = 1/2 Cu^{2+} spins are coupled into chains along the b-axis and the chains interact along the c-direction through a small exchange J' = 0.175 J as depicted in Fig. 2(a) (all other interchain exchanges are negligible) [4]. The frustration caused by the staggering of the chains produces 3D incommensurate cycloidal ordering below T_N = 0.62 K with the spins rotating mainly in the (b, c) plane. A field B > 1.66 T along the c-axis decouples the magnetic chains and the system has a structure in which no long-range incommensurate or antiferromagnetic order could be detected [3]. This phase occurs up to B ≈ 8 T where spins become ferromagnetically aligned by the field [5]. A summary of the phase diagram is shown in Fig. 2b.

The magnetic excitations were measured on a single crystal of Cs_2CuCl_4 using the cold neutron three-axis spectrometer IN14. The magnetic field was provided by a 6 T vertical magnet and the sample was cooled to temperatures below 0.1 K using a dilution-fridge insert. Fig. 3 summarises the results of constant-wavevector scans at Q = (0,0.75,0), which correspond to the dashed line in Fig. 1. The well-defined inelastic peak observed in zero field broadens above the transition to the disordered phase at 1.66 T where the lineshape can be described by two independent peaks (the fit is shown as a solid line in the figure). The observed splitting of the inelastic scattering and its behaviour in a field are well reproduced by the calculation for quantum chains shown by the vertical arrows above the scans. The strong field dependence of the low-energy scattering results from the field dependence of the short-range ordering wavevector as it varies across the zone with increasing field.

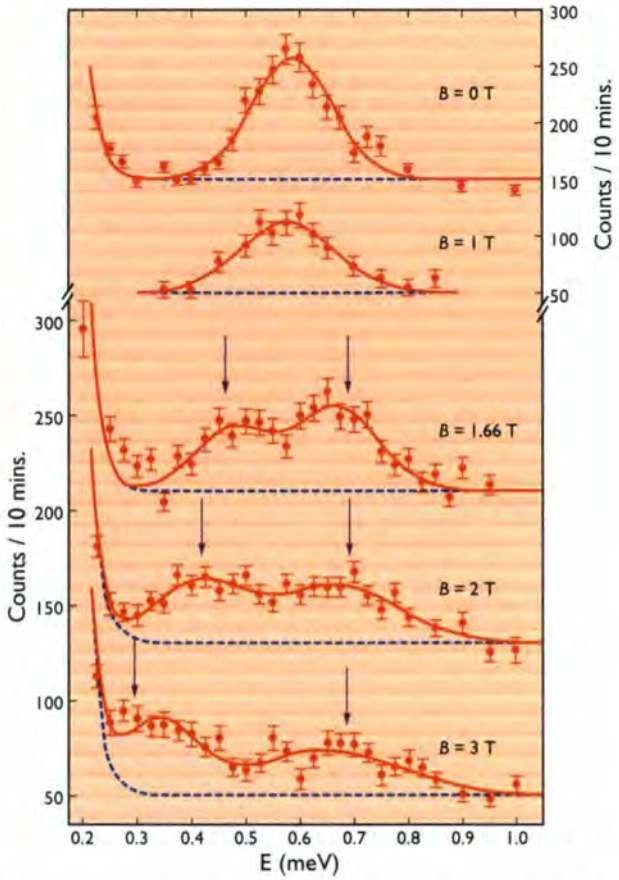

Figure 3: *Intensity observed at Q = (0, 0.75, 0) as a function of energy and field at T = 0.1 K. Two different scales are used and scans are shifted upwards by 100 (0 T) (right axis) 160 (1.66 T), and 80 (2 T) (left axis). Solid lines are fits as described in the text, and dotted lines represent the nonmagnetic background. The energies at which the intensity is expected to be large for quantum chains are shown by the vertical arrows above the scans.*

The experiments are inconsistent with a conventional antiferromagnetic spin-flop phase which would give a single peak at an energy of 0.64 meV and long-range antiferromagnetic order, which is not observed. It is concluded that the magnetic field produces the short-range incommensurate phase predicted by the quantum theory and neither the spin-flop nor any other long-range ordered structure predicted by classical theories of magnetism is consistent with the observed behaviour.

References

■ [1] D.A. Tennant, R.A. Cowley, S.E. Nagler, and A.M. Tsvelik, Phys. Rev. B 52 (1995) 13368 ■ [2] G. Müller, H. Thomas, H. Beck, and J.C. Bonner, Phys. Rev. B 24 (1981) 1429 ■ [3] R. Coldea, D.A. Tennant, R.A. Cowley, D.F. McMorrow, and Z. Tylczynski, Phys. Rev. Lett. 79 (1997) 151 ■ [4] R. Coldea, D.A. Tennant, R.A. Cowley, D.F. McMorrow, and Z. Tylczynski, J. Phys. Condens. Matter 8 (1996) 7473 ■ [5] R. Coldea, D.A. Tennant, R.A. Cowley, D.F. McMorrow, and Z. Tylczynski, J. Magn. Magn. Mater, 177-181 (1998) in press.

Giant ^{16}O-^{18}O isotope effect on the metal-insulator transition of $RNiO_3$ perovskites (R = rare earth)

M. Medarde, A. Furrer (LNS, Villigen), K. Conder (ETH, Zürich),
P. Lacorre (Lab. Fluorures, Le Mans), F. Fauth (LNS, Villigen and ILL).

The metal to insulator transition displayed by all the members of the perovskite family $RNiO_3$ (R = 4f rare earth different from La) has attracted a lot of interest since it constitutes one of the few examples of this phenomenon in perfectly stoichiometric compounds. In spite of the great deal of work performed during the last six years, the mechanism responsible for the electronic localisation is still a matter of controversy. The observation of unusually large O isotope shifts on the metal-insulator temperature T_{MI} reported in this study represents an important advance since it clearly proves the dominant role of the electron-lattice interaction as driving force for the transition. Moreover, the good agreement between this observation and a simple model based on the existence of Jahn-Teller polarons in the metallic state gives further qualitative and quantitative support to the polaronic picture recently suggested to account for O isotope effects in other 3d transition-metal oxides containing Jahn-Teller ions.

Since its discovery in 1991 [1], several mechanisms have been proposed to explain the occurrence of a metal-insulator transition in Ni perovskites [2]. Together with a magnetic origin (disregarded after recent studies on $SmNiO_3$ and $EuNiO_3$ [3]), a rather appealing possibility was a gap opening due to a Jahn-Teller induced distortion. However, though Ni^{3+} displays in these compounds the low spin, potentially Jahn-Teller active $t_{2g}^6\, e_g^1$ configuration, the NiO_6 octahedra appeared to be nearly perfect in previous high-resolution neutron-diffraction studies. In a first stage it was then believed that the Jahn-Teller effect was either drastically reduced, dynamic in character or simply non existent in Ni perovskites. However, the unusual magnetic structure reported for these compounds (they display a propagation vector $\mathbf{k}$ = (1/2 0 1/2) which is unprecedented in an oxide with perovskite structure [2]) strongly suggested the existence of an ordering of the $d_{x^2-y^2}$ and $d_{3z^2-r^2}$ orbitals.

Since in the neutron diffraction studies reported up to now no evidence of superstructure peaks related to the orbital ordering could be observed [3], we decided to try an alternative way to investigate the role of the Jahn-Teller effect as possible motor for the transition. For this purpose we synthesised two series of nickelates, one prepared using natural oxygen (99.76% ^{16}O) and the other using the heavier isotope ^{18}O, and we explored the influence of the O mass on the metal-insulator temperature using both differential scanning calorimetry and neutron powder-diffraction.

The neutron diffraction experiments were performed at the ILL on the diffractometers D1A and D1B. Fig. 1 shows the temperature dependence of the unit-cell volume and the ordered Ni^{3+} magnetic moment for the two $PrNiO_3$ samples. The metal-insulator temperature is indicated by the volume anomaly at T_{MI}, as well as by the sudden suppression of the magnetic ordering above this temperature. To be noted is the huge displacement of the transition by increasing the mass of the O isotope ($\approx$ + 8.2 K), clearly visible in both sets of data. A final proof that the change in T_{MI} due to the substitution of ^{16}O by ^{18}O was obtained

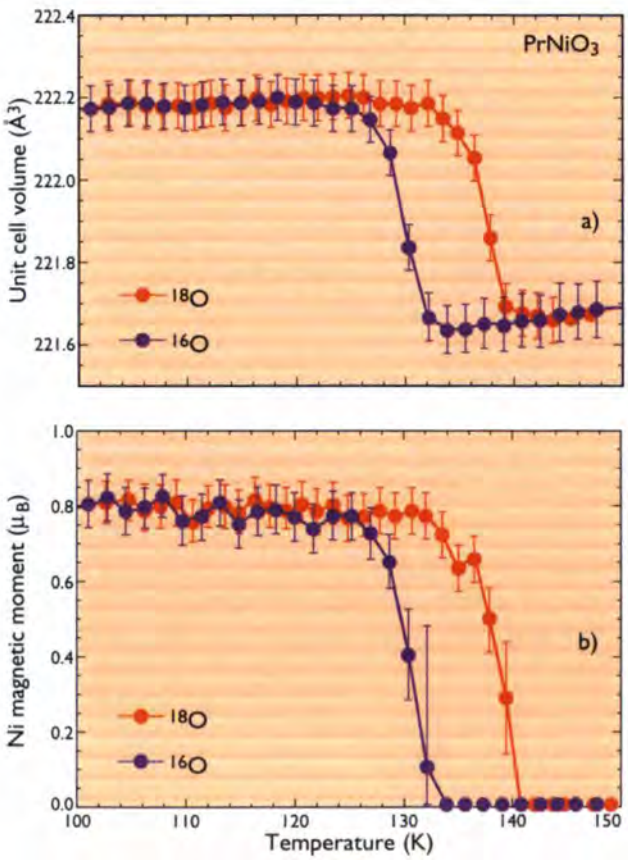

Figure 1: a) *Temperature dependence of the unit-cell volume and* ***b)*** *the Ni^{3+} magnetic moment across T_{MI} for $PrNi^{16}O_3$ and $PrNi^{18}O_3$. The neutron diffraction-data were recorded on D1B by heating at a constant rate of 0.1 K/minute.*

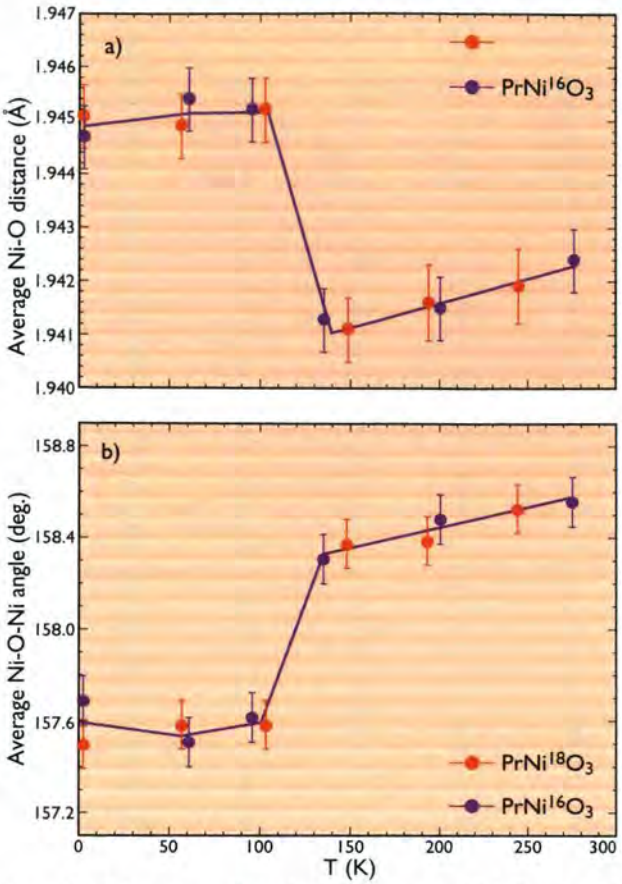

Figure 2: *a) Temperature dependence of the average Ni-O distance and b) the Ni-O-Ni superexchange angle across T_{MI} for $PrNi^{16}O_3$ and $PrNi^{18}O_3$. The neutron diffraction-data were recorded on D1A.*

by O back exchange. Furthermore, the values of the Ni-O distances, the Ni-O-Ni superexchange angles and the O content obtained from the high resolution D1A data (see Fig. 2) indicate that, within the experimental accuracy, no structural changes are induced by exchanging the O isotope.

Shifts on T_{MI} ranging between + 1.7 K (for $EuNiO_3$) and + 10.3 K (for $La_{0.1}Pr_{0.9}NiO_3$) have been measured for the remaining members of the series (see fig. 3 and refs [4], [5]), the last being the largest *positive* O isotope-shift ever reported for any kind of transition temperature. Larger absolute values have been recently reported for the Curie temperature of hole-doped magnetoresistive manganites, but both the sign of ΔT_c and its evolution with the radius of the rare-earth ion were opposite [6].

The origin of the O isotope effect in cuprates and manganites is actually a matter of discussion. However, several recent studies [6], [7] strongly suggest an interpretation based on the existence of Jahn-Teller polarons (electrons dressed by their associated Jahn-Teller distortion [8]). The present work gives strong support to this picture since this concept is also able to give a qualitative explanation of the isotope effect in Ni perovskites [4,5]. Moreover, it constitutes an important advance since, for the first time, a quantitative explanation which perfectly reproduces the experimental observations is proposed. The model, based on Jahn-Teller polarons in a charge-transfer system (see refs. [4] and [5] for details), implies the following dependence of the metal-insulator transition temperature T_{MI} on the oxygen isotope mass:

$$k_B T_{MI} = \Delta - \alpha \exp(-\gamma E_{JT}/\hbar\omega) \cos\phi$$

Here Δ is the charge-transfer energy, E_{JT} the Jahn-Teller energy, α is the proportionality constant between cos ϕ and the bandwidth Wb ($Wb = \alpha \cos\phi$), ϕ is the tilt angle of the NiO_6 octahedra and ω is the phonon frequency which depends on the O isotope mass (ω is proportional to $1/\sqrt{m_{oxygen}}$). Fig. 3 shows the evolution of ΔT_{MI} along the nickelate series together with the fit obtained with this model using ω = 80 meV (for ^{16}O) and E_{JT} = 400 meV. To be noted is the excellent agreement between the experiment and the calculation, as well as the fact that the values of the parameters involved in the model (the charge transfer energy $\Delta \approx$ 3eV and the bare band width Wb $\approx$ 8 eV) are of the same order of magnitude as previously published estimates from spectroscopic techniques [9].

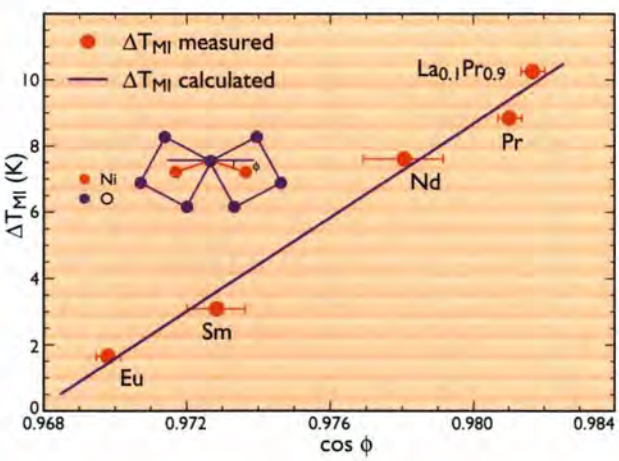

Figure 3: *Evolution of the isotope shift ΔT_{MI} along the nickelate series from DSC and neutron diffraction data. The cosine of the tilting angle of the NiO_6 octahedra represented in the abcissa axis is a measure of the distortion of the perovskite structure. The straight line is the fit mentioned in the text.*

References

■ [1] P. Lacorre, J.B. Torrance, J. Pannetier, A.I. Nazzal, P.W. Wang and T. C. Huang,, Solid State Chem. 91 (1991) 225 ■ [2] M. Medarde, J. Phys.: Condens. Matter 9 (1997) 1679 ■ [3] J. Rodríguez-Carvajal, S. Rosenkranz, M. Medarde, P. Lacorre, M. T. Fernández-Díaz, F. Fauth, and V. Trounov, Phys. Rev.B57 (1998) 456 ■ [4] M. Medarde, P. Lacorre, K. Conder, F. Fauth and A. Furrer, Phys. Rev. Lett. 80 (1998) in press. ■ [5] M. Medarde, P. Lacorre, K. Conder, J. Rodríguez-Carvajal, Stephan Rosenkranz, F. Fauth and A. Furrer, Physica B, in press. ■ [6] G.M. Zhao, K. Conder, H. Keller and K.A. Muller, Nature 381 (1996) 676 ■ [7] J. M. D. Teresa et al., Nature 386 (1997) 256 ■ [8] K.-H. Höck, H. Nickish and H. Thomas, Helv. Phys. Acta 56 (1983) 237 ■ [9] T. Mizokawa, A. Fujimori, T. Arima, Y. Tokura, N. Mori and J. Akimitsu, Phys. Rev. B52 (1995) 13865.

Structural investigation of the new inorganic spin-Peierls system α'-NaV_2O_5

T. Chatterji (ILL and MPI Dresden),
G.J. McIntyre (ILL),
K.D. Liss (ESRF).

Neutron and synchrotron x-ray diffraction experiments have been performed on the newly discovered inorganic spin-Peierls system α'-NaV_2O_5 above and below the spin-Peierls phase-transition temperature T_{SP}. Superstructure reflections corresponding to the cell doubling along a and b and quadrupling along c have been observed in both neutron and x-ray experiments. By comparing the relative intensities of substructure and superstructure reflections in the neutron and x-ray data we conclude that the modulation below T_{SP} is due predominantly to displacements of vanadium atoms.

Ever since the discovery of high temperature superconductivity in doped antiferromagnetic cuprate materials there has been a renewed interest in low-dimensional quantum antiferromagnets. A linear S = 1/2 chain with antiferromagnetic interaction along the chain interacting with the three-dimensional phonons can lead to a spin-Peierls (SP) phase transition. A dimerisation of the spin chain below the transition temperature T_{SP} leads to the formation of a non-magnetic singlet ground-state [1-4]. The transition is called a spin-Peierls transition because it is a magnetic analog of a Peierls transition in quasi-one-dimensional conductors. The transition was initially observed only in a few organic compounds [4]. The discovery of a SP-state in the inorganic compound $CuGeO_3$ [5] has renewed strong interest in this phenomenon. Recently Isobe and Ueda [6] have discovered a new inorganic spin-Peierls system α'-NaV_2O_5. Magnetic susceptibility measurements on both polycrystalline samples [6] and single crystals [7] have shown that a spin gap opens below T_{SP} = 34 K and Raman scattering measurements [7] also show a crystallographic distortion at the SP transition. It is now established that α'-NaV_2O_5 is a spin-Peierls compound with the highest critical temperature so far known T_{SP} = 34 K.

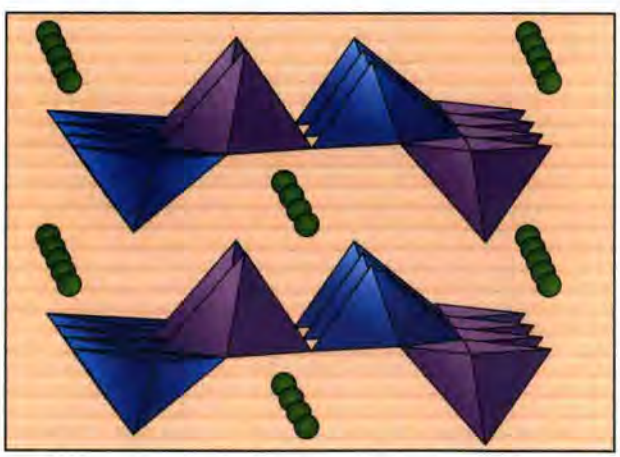

Figure 1: *The crystal structure of α'-NaV_2O_5. The V atoms are coordinated by O atoms to form square pyramids. Na atms are surrounded by a bi-capped trigonal prism of O atoms.*

According to Reference [8] α'-NaV_2O_5 crystallises in the orthorhombic space group $P2_1mn$. The non-centrosymmetric structure allows two independent V atoms in the unit cell. This led to the belief that the crystal structure contains V^{4+} (S = 1/2)-chains along the b axis, in which spins are antiferromagnetically coupled. These chains are separated from the non-magnetic V^{5+}-chains, which results in a quasi-one-dimensional behaviour. The coordination of the O atoms around V^{4+} and V^{5+} can be described in terms of square pyramids. Na atoms are surrounded by a bi-capped trigonal prism of O atoms.

We have performed neutron and synchrotron x-ray diffraction experiments on the same good quality single crystal of α'-NaV_2O_5. The crystal was small by neutron standards, but large by x-ray standards. A neutron diffraction study was possible due to the very low intrinsic background on D10; an x-ray study of the entire crystal was possible on the high-energy beam line ID15 at the ESRF. Our room temperature data showed that the non-centrosymmetric space group $P2_1mn$ proposed in [8] is not right and the real space group is the centrosymmetric Pmmn. There is only one symmetry independent V-atom in the unit cell. Therefore the description that the structure contains both magnetic V^{4+} and nonmagnetic V^{5+} chains along the b axis is not valid, at least not at room temperature. Fig. 1 shows schematically the crystal structure of α'-NaV_2O_5 obtained on the basis of our neutron diffraction data at room temperature. We have observed superstructure reflections by both techniques below T_{SP} = 34 K corresponding to cell doubling along a and b and quadrupling along c. Fig. 2 shows the temperature variation of

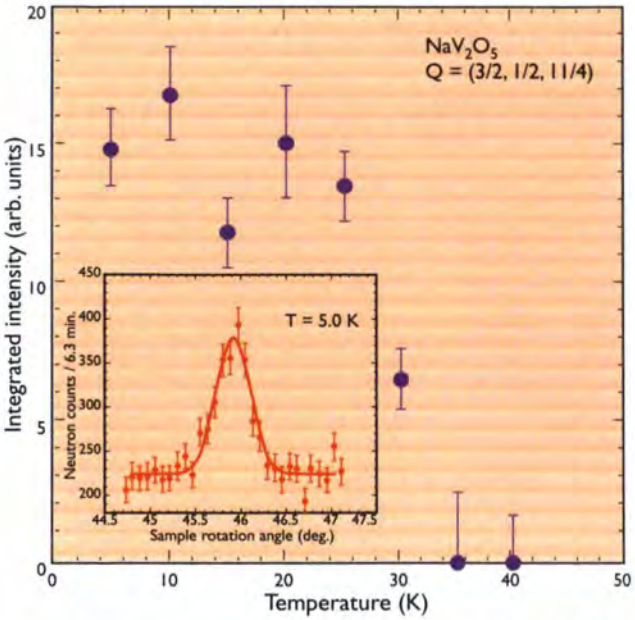

Figure 2: *Temperature variation of the integrated intensity of the 3/2, 1/2, 11/4 superstructure reflection of α'-NaV_2O_5 measured by neutron diffraction. The intensity of this reflection decreases with increasing temperature and becomes zero at T_{SP} = 34 K. The* ***inset*** *shows a typical scan of the 3/2, 1/2, 11/4 reflection at T = 50 K.*

the integrated intensity of the 3/2, 1/2, 11/4 superstructure reflection measured by neutron diffraction. The intensity of this reflection decreases with increasing temperature and becomes zero at $T_{SP} \approx 34$ K. The superstructure reflections are very weak in intensity in the neutron experiment but much stronger in the x-ray case (Fig. 3). We have measured intensities of both substructure and superstructure reflections at 5 K both by neutrons and x-rays.

The results of these experiments allow us to reach a very important conclusion about the structural modulation of α'-NaV_2O_5 below T_{SP}. The very fact that the intensities of the superstructure reflections in the x-ray diffraction experiment are of the order of 10^{-1} those of substructure reflections whereas in the neutron diffraction the corresponding ratio is of the order of 10^{-4} implies that the structural modulation below T_{SP} is essentially due to vanadium atoms. This is because the neutron scattering-length of V atoms is only $-0.0382(1)\cdot10^{-12}$ cm, whereas those of Na and O atoms are $0.363(2)\cdot10^{-12}$ and $0.5805(4)\cdot10^{-12}$ cm, respectively. The x-ray atomic scattering factors in the forward direction for V, Na and O are 23, 11 and 8 electrons, respectively. Thus the V atoms contribute very strongly to

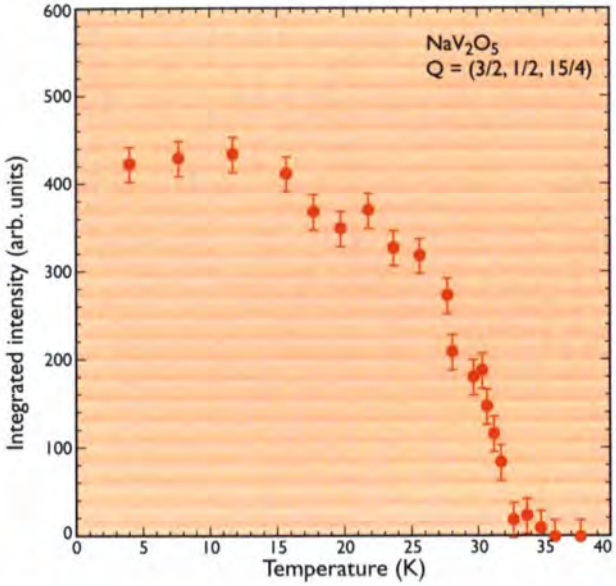

Figure 3: *Temperature variation of the intensity of the 3/2, 1/2, 15/4 superstructure reflection of α'-NaV_2O_5 by synchrotron x-ray diffraction.*

the x-ray intensities but very weakly in the neutron case. Indeed for this reason we could refine the neutron-diffraction substructure intensity data (both from polycrystalline and single crystal α'-NaV_2O_5) collected at 5 K with parameters essentially of the high-temperature structure. This further supports the conclusion that the structural modulation of α'-NaV_2O_5 below T_{SP} is essentially due to the displacements of V atoms.

A possible model for the low temperature structure can be obtained by "decorating" the zig-zag vanadium chains parallel to the crystallographic b axis. The doubling of the b axis can be easily realised by modulating the V-V distance (short S and long L). In the room temperature phase they are equal (D) along the zig-zag chain. So if one has the S-L-L-L-S-L... sequence at the low temperature instead of the sequence D-D-D-D-D-D... of room temperature then the unit cell is doubled along b. If we also decorate the next parallel chains as we move along the a axis like L-S-L-L-L-S..., L-L-S-L-L-L-S... and L-L-L-S-L-L-L-S... we get cell doubling along the a axis.

Now it is easy to stack these chains in the a-b plane along c in order to get the cell quadrupling along the c axis, although there are several ways of doing this. One such a model has indeed given a reasonable fit to the low-temperature diffraction data. The details of this model will be published elsewhere.

References

■ [1] L.N. Bulaevskii, Soviet Phys. - Solid State 11 (1969) 921 ■ [2] M.C. Cross, Phys. Rev. B 20 (1979) 4606 ■ [3] E. Pytte, Phys. Rev. B 10 (1974) 4637 ■ [4] J.W. Bray et al. Phys. Rev. Lett. 35 (1975) 744 ■ [5] M. Hase, I. Terasaki and K. Uchirtokura, Phys. Rev. Lett. 70 (1993) 3651 ■ [6] M. Isobe and Y. Ueda, J. Phys. Soc. Jap. 65 (1996) 1178 ■ [7] M. Weiden et al., Z. Phys. B 103 (1997) 1 ■ [8] A. Carpy and J. Galy, Acta Cryst. B 31 (1975) 1481.

Strong coupling between the structure and magnetism of manganese perovskites

K.V. Kamenev, A.J. Campbell, D. McK Paul, M. R. Lees, G. Balakrishnan (Univ. Warwick), G.J. McIntyre (ILL).

The pressure-temperature phase diagram of $La_{0.835}Sr_{0.165}MnO_3$ is found to exhibit extremely unusual features which include pressure independence of the Curie temperature in the orthorhombic phase, a re-entrance of the rhombohedral phase at low temperatures, and a change of the type of the magnetic phase transition from second to first-order at the intersection of the structural and magnetic phase boundaries. Comparison of the x-T, H-T and P-T phase diagrams reveals a common trend in the behaviour of $La_{1-x}Sr_xMnO_3$ ($x \sim 0.165$), i.e. increase in Sr content, magnetic field or pressure leads to a crossing of the temperatures of the structural and magnetic phase transitions. We conclude that the unique observation that the structural transition may be driven by application of a magnetic field is due to strong coupling between the magnetic and structural transitions near the intersection.

The system $La_{1-x}Sr_xMnO_3$ belongs to the family of doped manganese perovskites which exhibit colossal magnetoresistance near the ferromagnetic spin-ordering temperature. Samples with $x = 0.165$ undergo a first-order phase-transition from the high-temperature rhombohedral ($R\bar{3}c$) to a low-temperature orthorhombic (Pbnm) phase at $T_S = 295$ K, and a second-order phase transition from the para- to the ferromagnetic state at $T_C = 261$ K. Doping by Sr also results in a change in the ordering; with increasing x, T_C increases from 238 K for $x = 0.15$ to 283 K for $x = 0.175$, whereas T_S decreases from 380 K to 190 K. The magnetic and structural phase-transitions intersect on the x-T-phase diagram for a critical doping level $x_c \approx 0.165$ at about 270 K [1]. Application of a magnetic field to samples with $x \approx 0.165$ induces the structural transition from the orthorhombic to rhombohedral state at room temperature [2,3]. The same phenomenon also occurs on application of pressure. A recent strain-gauge dilatometric study showed that $T_S = T_C$ at a pressure of approximately 3 kbar in $La_{0.835}Sr_{0.165}MnO_3$ [4]. However, only isobaric temperature scans were possible in this study, and the type of transition, structural or magnetic, is only inferred indirectly. Here we report a more comprehensive investigation of the P-T phase diagram of $La_{0.835}Sr_{0.165}MnO_3$ by means of neutron diffraction.

Neutron-diffraction measurements were carried out on a sample of $La_{0.835}Sr_{0.165}MnO_3$ on the single-crystal diffractometer D10. A high-pressure cell using gaseous helium as pressure-transmitting medium allowed continuous variation of the temperature and pressure *in situ* over a temperature range of 1.2-310 K and pressure range of 0-5 kbar. The orthorhombic (2 0 0) and (4 0 5) reflections were chosen to monitor the magnetic and structural phase-transitions, respectively. The results of this investigation are summarised in the pressure-temperature phase diagram in Fig. 1.

The P-T phase diagram of $La_{0.835}Sr_{0.165}MnO_3$ is defined by the lines of the structural and magnetic phase-transitions. The first-order structural phase-transition, T_S, is shown by the two "Z"-shaped curves which enclose a metastable region where, depending on the history of the sample, either the rhombohedral or the orthorhombic phase can occur. The single line which starts at $T_C = 261$ K at ambient pressure and ends at 282 K at a pressure of 5 kbar corresponds to the (normally) second-order para- to ferromagnetic phase-transition. The hatched area indicates the intersection of T_S and T_C, and separates the four phases given by all possible different combinations of the two structural and two magnetic phases. These phases are marked on the diagram as Pr, Po, Fo or Fr, where "P" or "F" specifies the magnetic state as paramagnetic or ferromagnetic and "r" or "o" denotes the structure as rhombohedral or orthorhombic.

One of the key features of the phase diagram is that, due to the peculiar "Z"-shape of the structural phase-bounda-

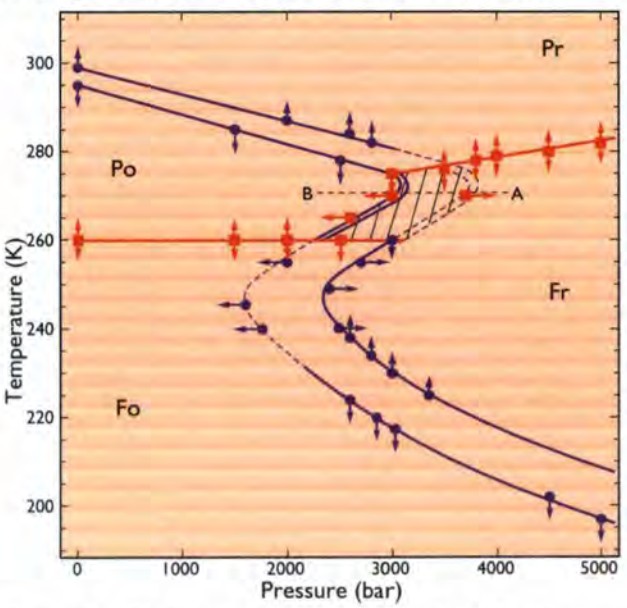

Figure 1: *The P-T phase diagram of $La_{0.835}Sr_{0.165}MnO_3$. The phases are described in the text. The observed T_C and T_S are denoted by squares and circles, respectively.*

ries near the intersection, some of the lines of the phase-transitions cannot be seen by pure temperature variations. The phase boundaries which can be found during temperature variations at a constant pressure are delineated by solid lines in Fig. 1; the phase boundaries shown by broken lines represent the transitions which can only be seen on isothermal pressure changes.

By observing the temperatures and pressures of the phase transitions found during pressure variations we could connect the phase boundaries which were invisible in heating-cooling runs, and had gone undetected in the dilatometric study. Isothermal pressure variations allowed us to establish the "Z"-shape. It is also clear that the magnetic phase-transition mirrors the hysteresis of the structural phase-transition in the crossing region which leads us to conclude that the structural change is a primary effect with respect to the magnetic one, and that the type of the ferro- to paramagnetic phase-transition switches from second-order to first-order, a most unusual phenomenon. Pressure scans at 270 K (Fig. 2) illustrate clearly the locking together of the structural and magnetic transitions in the region of intersection of the phase boundaries.

Due to the hysteretic character of the first-order structural and, locked to it, the magnetic phase-transition, the intersection occupies the hatched area on the P-T-phase diagram. In this area the sample can be in any one of the Pr, Po, Fo, or Fr phases depending on the pressure-temperature path by which it was brought to the area.

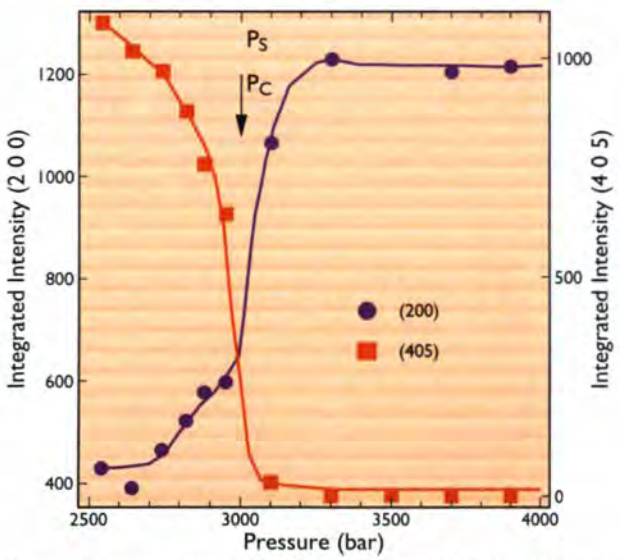

Figure 2: *Pressure dependencies of the intensities of (4 0 5) and (2 0 0) at 270 K on pressure release, along the path AB of Fig. 1.*

In sharp contrast to the pressure-independent T_C seen in the orthorhombic phase below 3 kbar, the Curie temperature in the rhombohedral phase increases with applied pressure with $dT_C/dP = 3.5°C/kbar$. Given that the cell volumes are almost identical in the two structural phases, the change in the pressure dependence is particularly intriguing. To understand this we note that T_C is sensitive to the Mn-O-Mn bond angle. When the crystal is compressed in the orthorhombic phase, the Mn-O-Mn angle is 180° by symmetry, and pressure cannot affect it, changing instead the inter-planar distances. In the rhombohedral phase the "easy" direction of compression is the three-fold axis, which is at an angle to the Mn-O-Mn bonds, so that the Mn-O-Mn bond angle is more easily affected by applied pressure.

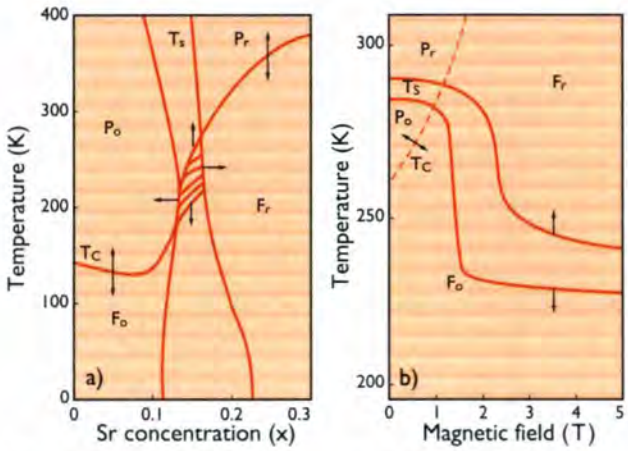

Figure 3: ***a)*** *The x-T phase diagram of $La_{1-x}Sr_xMnO_3$ (based on [1]), and* ***b)*** *the H-T phase diagram of $La_{0.835}Sr_{0.165}MnO_3$ (based on [2], and experiments on D3 [3]).*

Finally, comparison of the x-T [1], H-T [2,3], and P-T-phase diagrams reveals a common trend in the behaviour of $La_{1-X}Sr_XMnO_3$ ($x \sim 0.160$), i.e. increase in Sr-content, magnetic field or pressure leads to intersection of T_S and T_C. Even though it is impossible to give a definition of the Curie temperature in a magnetic field, we can suppose that the abrupt decrease of T_S near $H = 2$ T is related to the intersection with the magnetic phase-transition in the plane of magnetic field and temperature [3] (Fig. 3). A comprehensive study of the intersection region can only be done if both the temperature and another parameter, one of x, H or P, is varied. Since isothermal variations of Sr-content (x) are obviously impossible and because of the difficulty with the definition of T_C in magnetic field, use of pressure as a second variable is the only practical means to probe this complicated phase diagram.

References

■ [1] H. Kawano, R. Kajimoto, M. Kubota, H. Yoshizawa, Phys. Rev. B 53 (1996) R14709 ■ [2] A. Asamitsu, Y. Moritomo, Y. Tomioka, T. Arima, Y. Tokura, Nature, 373, (1995) 407 ■ [3] A.J. Campbell, G. Balakrishnan, M. R. Lees, D. McK Paul, G.J. McIntyre, Phys.Rev.B 55 (1997) R8622 ■ [4] K. Kamenev, G. Balakrishnan, M. R. Lees, D. McK. Paul, Z. Arnold, O. Mikulina, Phys. Rev. B 56 (1997) 2285.

Quantum critical behaviour in a high-temperature superconductor

- T.E. Mason (Univ. Toronto),
- G. Aeppli (NEC Research Inst.),
- J. Kulda (ILL),
- S.M. Hayden (Univ. Bristol),
- H.A. Mook (Oak Ridge Nat. Lab.),

We have used polarised (IN20) and unpolarised (TAS6, Risø) neutron scattering to measure the wavevector and frequency-dependent magnetic fluctuations in the normal state (from the superconducting transition temperature, T_c = 35 K, up to 350 K) of single crystals of $La_{1.86}Sr_{0.14}CuO_4$. The incommensurate peaks which dominate the fluctuations have amplitudes that decrease as $1/T^2$ and widths that increase in proportion to the thermal energy (k_BT) and energy transfer added in quadrature. The nearly singular fluctuations are consistent with a nearby quantum critical point. [1]

The normal state of the high T_c cuprates is as unusual as their superconductivity. This has been well known for many years and is strikingly manifested in the resistivity which is linear in temperature from above 1,000 K to just above T_c. The charge degrees of freedom display a variety of peculiar properties including some quite simple scaling behaviour often invoked as a signature of novel physics responsible for superconductivity. The fact that electrons also carry spin, together with the proximity of superconductivity to magnetic ordering (see Fig. 1) suggests that similar behaviour might be expected in the magnetic properties of high T_c superconductors. However, magnetic measurements have generally yielded complex and less universal results than those which probe charge. We have used inelastic neutron-scattering to study the magnetic fluctuations of the simplest high T_c material, $La_{2-x}Sr_xCuO_4$, over a much wider range of temperature and frequency than has previously been possible. We have found a nearly singular behaviour, in the sense of diverging amplitudes and length scales for $T \rightarrow 0$, indicating the presence of a low-T or zero-T phase transition. The latter is usually referred to as a quantum critical point.

We have studied the magnetic response of $La_{2-x}Sr_xCuO_4$ for x = 0.14, close to the optimal doping for superconductivity (Fig. 1). The magnetic response of this system is peaked at incommensurate wavevectors determined by the geometry of the Fermi surface for this quasi-two-dimensional metal [2]. Fig. 2 shows that this response occurs only in the spin flip channel, confirming its magnetic origin.

By combining the unambiguous determination of the magnetic signal provided by a polarised beam (on IN20) with more rapid unpolarised measurements carried out on the TAS6 spectrometer at Risø we have been able to characterise the magnetic response of $La_{2-x}Sr_xCuO_4$ between T_c and 350 K for energies between 2.5 and 15 meV. Full polarisation analysis of the signal and background up to 300 K on IN20 was used to verify background subtraction used to extract magnetic scattering from the unpolarised

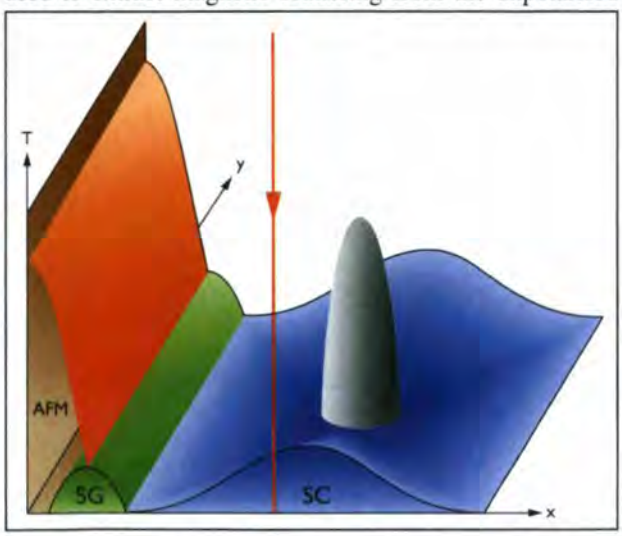

Figure 1: *Schematic phase diagram of $La_{2-x}Sr_xCuO_4$ showing the evolution from antiferromagnetism (AFM) through spin glass ordering (SG) to superconductivity (SC). Stripe ordering (shown in grey) occurs for double doping with both Sr (x) and Nd (y). The current measurements were for x = 0.14, shown as a red arrow along the T axis.*

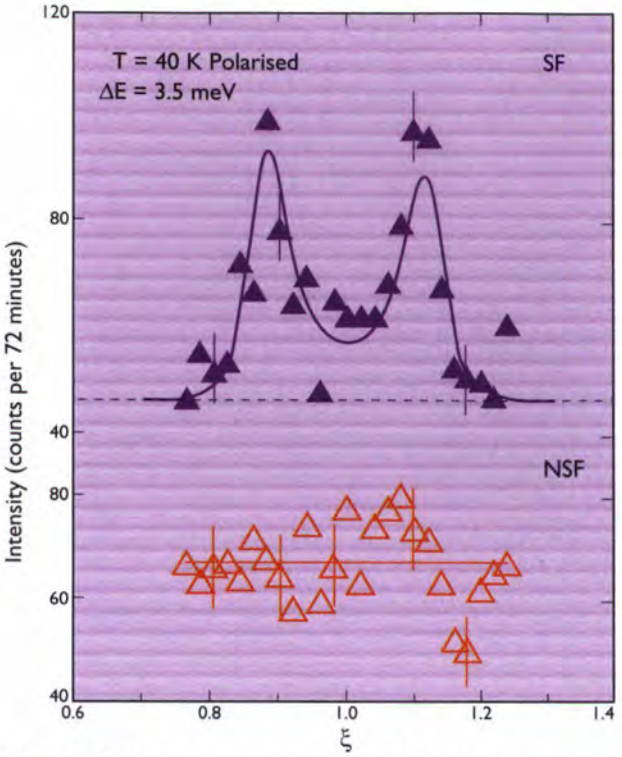

Figure 2: *Polarised beam data collected on IN20 showing constant energy scans for 3.5 meV at T = 40 K (> T_c). The incommensurate response occurs only in the spin flip channel, confirming the magnetic origin of the signal.*

data (Fig. 3a). The observed profiles were then fitted to a model, convoluted with the spectrometer resolution. The peak height (extracted from the fits) is proportionate to the imaginary part of the dynamical susceptibility $\chi''(\mathbf{Q}, \omega)$, being itself proportionate to ω as most of the measurements took place in a low-energy regime.

The peak value of the response is thus characterised by a single parameter $\chi_P''(\mathbf{Q}, \omega)/\omega$, varying as $1/T^2$ over the whole range of temperatures and energies probed (Fig. 3b). Its integral $\langle\chi''(\omega)\rangle/\omega$ falls off more slowly due to the increasing width (decreasing correlation length) as temperature is increased.

The linewidths (in momentum space), resulting from the fits, were found to scale linearly with the temperature and energy added in quadrature (not shown). This ω/T scaling, together with the implied dynamical exponent, Z = 1 are consistent with expectations for a quantum critical point [4]. As for ordinary critical points the state of the system is characterised by the inverse coherence length κ, whose value is obtained from the linewidths. The inset to Fig. 3a shows that the susceptibility varies as $1/\kappa^3$ which is

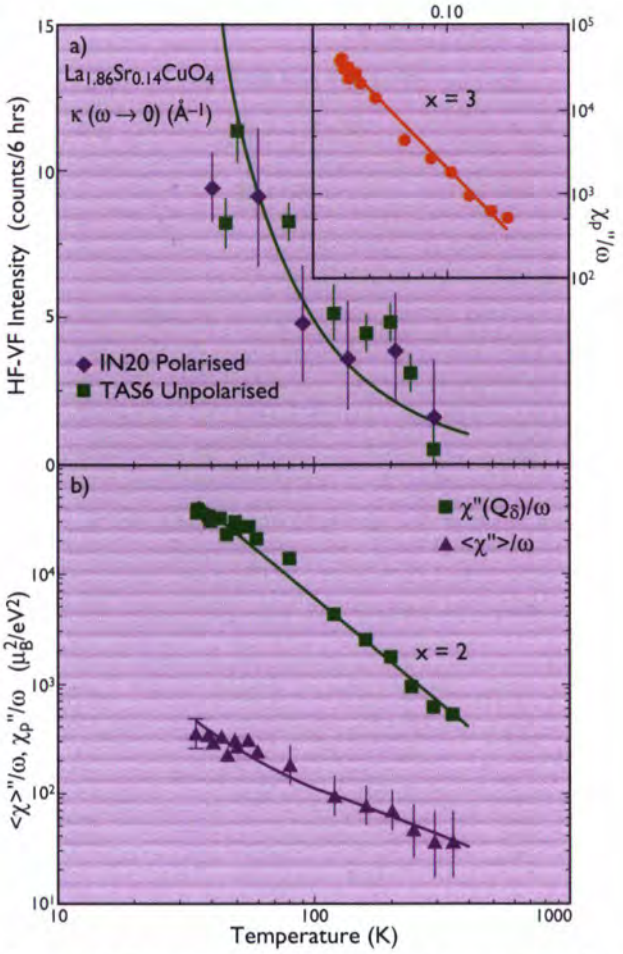

Figure 3: a) *Temperature dependence of the peak intensity derived from full polarisation analysis (difference between spin flip intensity for horizontal (HF) and vertical (VF) neutron polarisation) compared to unpolarised intensity from Risø.* ***b)*** *Peak amplitude of intensity for the response. The* ***inset*** *shows the $1/\kappa^3$ variation of the amplitude consistent with the quantum critical point prediction.*

consistent with the expected critical exponents for a quantum critical point in a 2D insulating magnet.

The nearly singular behaviour which could indicate a quantum critical point implies that there is a magnetic instability nearby in phase space. The antiferromagnetic state is far removed in doping from the superconducting phase and occurs at a commensurate wavevector so it is an unlikely candidate. However, as shown in Fig. 1, doping with Nd on the La site results in stripe ordering, so named due to the stripes of antiferromagnetic material separated by lines of charges [5]. This may be the instability which dominates the response at the temperatures and frequencies probed in these measurements, prior to the suppression of the low frequency response by superconductivity [2].

References

■ [1] G. Aeppli, T.E. Mason, S.M. Hayden, H.A. Mook, and J. Kulda, Science 278 (1997) 1432 ■ [2] S.-W. Cheong, G. Aeppli, T.E. Mason, H. Mook, S.M. Hayden, P.C. Canfield, Z. Fisk, K.N. Clausen, and J.L. Martinez, Phys. Rev Let Lett. 67 (1991) 1791; T.E. Mason, G. Aeppli, and H.A. Mook, Phys. Rev. Lett. 68 (1992) 1414 ■ [3] S.M. Hayden, G. Aeppli, H.A. Mook, T.G. Perring, T.E. Mason, S.-W. Cheong, and Z. Fisk, Phys. Rev. Lett. 76 (1996) 1344 ■ [4] S. Sachdev and J. Ye, Phys. Rev. Lett. 69 (1992) 2411 ■ [5] V. J. Emery and S.A. Kivelson, Physica 209 (1993) 597; J. Zaanen and O. Gunnarsson, Phys. Rev. B 40 (1989) 7391.

Spin dynamics at the magnetic instability in $CeCu_{6-x}Au_x$

- O. Stockert, H. von Löhneysen (Univ. Karlsruhe),
- N. Pyka (ILL),
- M. Loewenhaupt (TU Dresden).

The heavy-fermion system $CeCu_{6-x}Au_x$ orders antiferromagnetically for Au concentrations $x > 0.1$. At the critical Au concentration $x_c \approx 0.1$ remarkable deviations from Fermi-liquid behaviour are observed in thermodynamic and transport properties below ≈ 1 K. To investigate the dynamics of this phase transition from a non-magnetic to a magnetically ordered ground-state in $CeCu_{6-x}Au_x$ we performed inelastic neutron scattering experiments on single crystalline $CeCu_{6-x}Au_x$ ($x = 0, 0.1, 0.2$) on the IN14 spectrometer at very low temperatures $T \leq 100$ mK and magnetic fields up to $B = 5$ T. The dynamic correlations found for $x = 0.1$ together with the observed magnetic ordering for $x = 0.2$ provide a possible explanation for a scenario of the non-Fermi-liquid behaviour for $x = 0.1$.

The concept of Fermi liquids has greatly contributed to the understanding of the low temperature properties of metals with interacting electrons. Even unusual metals such as heavy-fermion systems can often be described within the scope of this concept. Recently, a number of these materials have been found to exhibit striking deviations from Fermi-liquid behaviour. One of the scenarios to explain this non-Fermi-liquid behaviour is the proximity to a magnetic instability arising from the competition between the intersite interaction between localised magnetic moments and the onsite moment screening by conduction electrons. This leads to either a non-magnetic or a magnetically ordered ground-state. The exemplary system $CeCu_{6-x}Au_x$ exhibits long-range antiferromagnetic order above the critical Au concentration $x_c = 0.1$, while pure $CeCu_6$ remains non-magnetic down to very low temperatures. At the concentration $x_c = 0.1$, where the Néel temperature is just suppressed to $T_N = 0$, the specific heat C depends on temperature T as $C \propto T\ln T$, the magnetic susceptibility χ varies as $\chi \propto 1 - a\sqrt{T}$ and the T-dependent electrical resistivity as $\Delta\rho \propto T$ instead of the Fermi-liquid behaviour, i.e. $C/T \sim \chi \approx$ const and $\Delta\rho \propto T^2$ [1]. The observed unusual temperature dependencies for the specific heat and the electrical resistivity of $CeCu_{5.9}Au_{0.1}$ can be described by a model [2] based on the scenario of 2D spin fluctuations driving the magnetic to non-magnetic quantum phase-transition. This spin-fluctuation theory assumes a coupling of 3D strongly renormalised conduction electrons to 2D critical fluctuations at the magnetic instability. In order to shed light on the microscopic origin of this unique low temperature behaviour of $CeCu_{5.9}Au_{0.1}$, we performed inelastic neutron-scattering experiments on single crystals of $CeCu_{6-x}Au_x$ ($x = 0$, 0.1, 0.2), since inelastic neutron-scattering is a unique tool for the investigation of magnetic fluctuations.

Q-scans along [1 0 0], taken at comparable temperatures $T < 100$ mK but different energy transfers $\hbar\omega$, are shown in Fig.1. In previous experiments on $CeCu_6$ only one broad commensurate correlation peak was found along [1 0 0] at Q = (1 0 0) for $\hbar\omega = 0.3$ meV [3]. Due to a largely enhanced Q-resolution on IN14 and a smaller energy transfer we could resolve a pronounced double-peak structure that is visible in all investigated alloys. With increasing x the double-peak structure is shifted towards $\hbar\omega = 0$ and appears in $CeCu_{5.8}Au_{0.2}$ as an elastic feature which represents short-range ordering evidenced by the large linewidth in Q. The shoulders near the magnetic peaks in

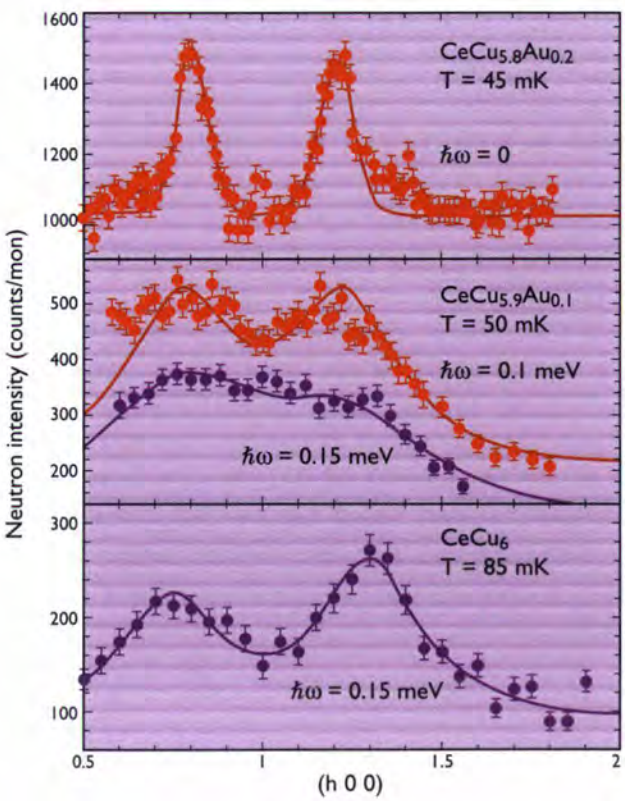

Figure 1: *Q-scans along [1 0 0] at different energy transfers $\hbar\omega$ in $CeCu_{6-x}Au_x$ ($k_f = 1.15$ Å^{-1}). Solid lines represent fits to the data with Lorentzian ($x = 0, 0.1$) and Gaussian line shape ($x = 0.2$). The asymmetry for $x = 0$ needs further investigation.*

$CeCu_{5.8}Au_{0.2}$ might be attributed to reminiscent correlations of $CeCu_{5.9}Au_{0.1}$. In Fig. 2 we present energy scans for the non-ordering $CeCu_{6-x}Au_x$ alloys, again at T < 100 mK, at Q ≈ (1.2 0 0) where the pronounced intersite correlations are observed (Fig. 1). The magnetic response can be described by a quasielastic Lorentzian line shape. Upon alloying with Au the response becomes much narrower for x = 0.1 indicating the vicinity to magnetic ordering. The intersite fluctuations in $CeCu_{5.9}Au_{0.1}$ are also sensitive to magnetic fields (B ∥ [001]) like in $CeCu_6$ [3]. A broadening and overall decrease of the quasielastic response is observed and at B = 3 T the intersite fluctuations are strongly suppressed as displayed in the inset of Fig. 2. This is in line with the Fermi-liquid recovery in the thermodynamic and transport properties in this field range [1].

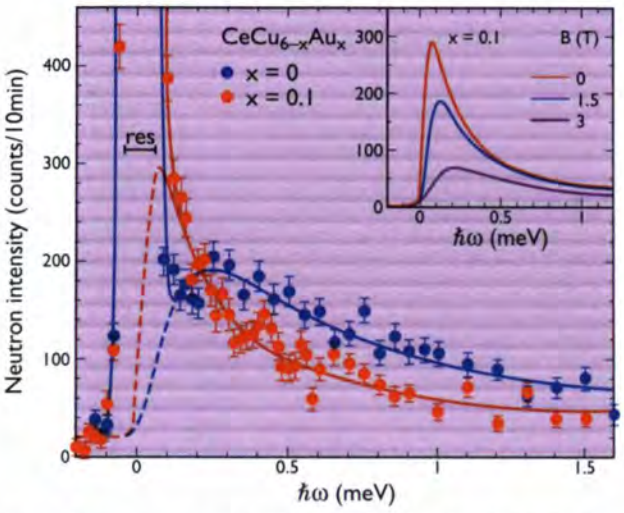

Figure 2: *Energy scans at Q ≈ (1.2 0 0) and T < 100 mK in $CeCu_{6-x}Au_x$ (instrumental background subtracted, k_f = 1.15 Å^{-1}). Solid lines are fits to a sum of a quasielastic Lorentzian and a resolution limited incoherent Gaussian. The inset shows the magnetic field dependence of the quasielastic response in $CeCu_{5.9}Au_{0.1}$ (the instrumental background and the resolution limited elastic line are subtracted for clarity).*

The correlation peaks found along a* (Fig. 1) are in fact part of a more complicated structure located in the a*c* plane. Q-scans along [h_0 0 ξ] with h_0 = const in $CeCu_{5.9}Au_{0.1}$ reveal a double-peak structure with only minor changes in the maximum intensity as one moves away from the a* axis. In Fig. 3 the observed peak positions together with the linewidths are displayed by closed circles with vertical bars. An analysis of these peaks shows the presence of rod-like features of the dynamical magnetic response in the a*c* plane. This dynamical magnetic structure for x = 0.1 evolves for x = 0.2 into both short-

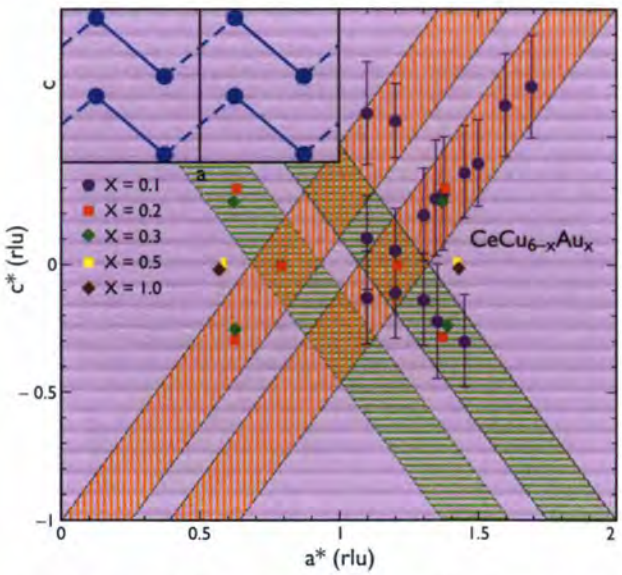

Figure 3: *Positions of the dynamic correlations (x = 0.1) and magnetic Bragg peaks (x = 0.2 – 1.0) in the reciprocal ac-plane in $CeCu_{6-x}Au_x$, for x = 0.5 from [4]). The vertical bars indicate the linewidth. The* ***inset*** *shows a schematic projection of the $CeCu_{6-x}Au_x$ structure (orthorhombic notation) on the ac-plane, in which only the Ce atoms are shown. The vertically (horizontally) hatched bands in reciprocal space correspond to the directions in real space marked by solid (dashed) lines (see inset).*

range ordering as described above (Fig. 1) and long-range incommensurate magnetic order with Q = (0.625 0 0.275). At higher Au doping the wave vector remains nearly unchanged until x = 0.5, where a sudden reorientation takes place to Q = (0.59 0 0) [4] which is then roughly constant up to x = 1. The magnetic structure of the heavily doped $CeCu_{6-x}Au_x$ alloys (x = 0.5, 1.0) can be described by moments aligned along the c axis with a sinusoidal modulation along the a direction whereas the structure for x = 0.2, 0.3 has yet to be determined. Fig. 3 summarises these results obtained in the different $CeCu_{6-x}Au_x$ crystals.

We recall that a 1-D feature in Q-space is related to a 2-D feature in real space. Hence, the observed quasi 1-D dynamical correlations in $CeCu_{5.9}Au_{0.1}$ correspond to a quasi 2-D coupling between the Ce moments. The vertically (horizontally) hatched rods in Fig. 3 can therefore be identified with planes in real space, the projection of which onto the ac plane is indicated by solid (dashed) lines between the Ce atoms, shown in the inset of Fig. 3. The observed quasi 2-D fluctuations strongly support the proposed scenario [2] with 2-D spin fluctuations coupled to 3-D quasiparticles leading to non-Fermi-liquid behaviour in $CeCu_{6-x}Au_x$.

References

■ [1] H.v. Löhneysen, J. Phys.: Condens. Matter 8 (1996) 9689 ■ [2] A. Rosch, A. Schröder, O. Stockert and H.v. Löhneysen, Phys. Rev. Lett. 79 (1997) 159 ■ [3] Rossat-Mignod, L.P. Regnault, J.L. Jacoud, C. Vettier, P. Lejay, J. Flouquet, E. Walker, D. Jaccard and A. Amato., J. Magn. Magn. Mater. 76-77 (1988) 376 ■ [4] A. Schröder, J.W. Lynn, R.W. Erwin, M. Loewenhaupt, H.v. Löhneysen, Physica B 199 & 200 (1994) 47.

Quasiparticles in the heavy-fermion superconductor UPd_2Al_3

- N. Bernhoeft, A. Hiess (ILL),
- N. Sato, N. Aso, Y. Endoh, T. Komatsubara (Tohoku Univ., Sendai),
- B. Roessli (ETHZ and PSI Villigen),
- G.H. Lander (EITU Karlsruhe).

Experiments with the IN14 three-axis spectrometer on a single crystal of UPd_2Al_3 have shown that a low-energy diffuse response in this heavy-fermion superconductor interacts strongly with the local spin-waves. Below T_N this response contributes a quasielastic peak (of width varying between 0.6 and 0.2 meV), and the real-space correlation length increases on lowering temperature. Below T_c the quasielastic response becomes inelastic; with a gap of ~ 0.35 meV at 0.15 K. A polarisation analysis experiment has verified that the response is predominantly transverse at low temperatures.

The observation of gaps, or pseudo-gaps, in the magnetic fluctuation spectrum has, of course, been reported previously in representative materials of the high T_c class of superconductors, in which the superconductivity develops out of a strongly correlated, but paramagnetic, state. To our knowledge previous explorations of this phenomenon in the heavy fermions have been hampered by the small magnitude of the magnetic diffuse scattering cross-section. The 5f states in uranium heavy-fermion materials are often antiferromagnetically polarised even when the material becomes superconducting. Despite much effort, the only clear evidence obtained from neutron scattering of a connection between the 5f states and the superconductivity is a small change that occurs in the Bragg peak intensity as the materials enter the superconducting state [1].

The compound UPd_2Al_3 is unusual in that the T_c is high at ~ 2 K (our samples have T_c = 1.9 K) and the magnetic ordering which occurs at T_N ~ 14 K is characterised by a relatively large moment of 0.8 μ_B per U atom. Conflicting evidence has been presented on the change of the antiferromagnetic Bragg peaks below T_c in this compound [2-4]. More recently, it appears that some small effect may occur at the level of < 1% [5]. Equally, the initial study of the *dynamical* properties [6] yielded an strongly damped spin-wave with *no* change seen in the response on entering the superconducting state. These experiments were performed at Risø with a resolution of 0.35 meV FWHM.

Our first experiments were conducted in Sept. 1996 at IN14 with constant k_f = 1.3 Å^{-1} (final energy of 3.5 meV) and an energy resolution of 0.12 meV (FWHM).

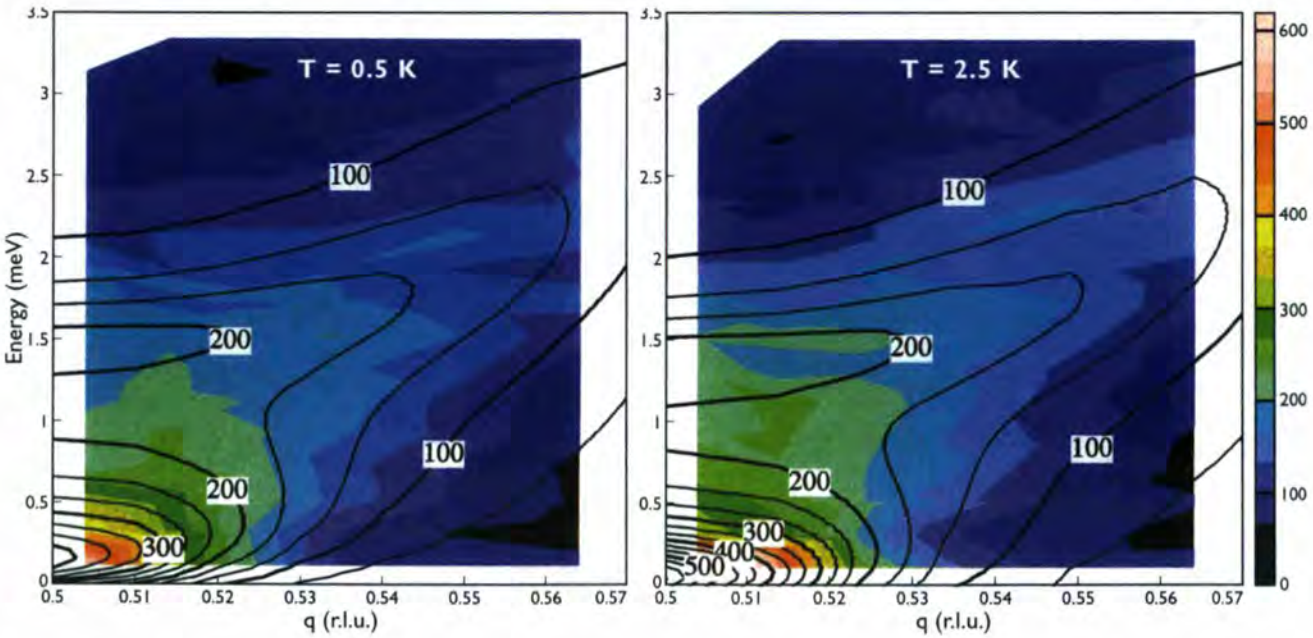

Figure 1: *Contour plots of the intensity of the scattered neutrons per fixed monitor time as a function of q around* **Q** *= [0, 0, 1/2], the ordered wavevector, and energy transfer for two temperatures, below (0.5 K) and above (2.5 K) T_c. The solid lines represent the theory discussed in the text.*

The important results of this experiment [7] are shown in Fig. 1 in terms of contour plots illustrating the intensity as a function of energy and wavevector *around the ordered wavevector* [0 0 1/2]. The intense resolution-limited Bragg peak appears at E = 0, **Q** = [0 0 1/2], i.e. in the left-hand bottom corner of the plot. Far away from this point may be seen the damped spin-wave [6]. In the lower left-hand corner may be seen additional intensity. This is *not* the Bragg intensity, but represents additional low-energy spectral response that is localised around the ordered wavevector. From its measured dispersion one may associate this mode with the quasiparticle response in the normal state. An approximate calculation indicates that this mode contributes the major part to the low-temperature heat capacity, and is associated with the transition to superconductivity.

As the temperature is lowered, this quasielastic response *sharpens* in q-space. Below T_c (Fig. 2) we have observed (October 1997 with k_f = 1.15 Å and a resolution of 0.09 meV) what appears to be the opening of a gap. The centre frame shows that at low temperature the quasiparticle mode exhibits a gap of ~ 0.35 meV and has a width of ~ 0.24 meV, considerably greater than the resolution. In contrast to the strong renormalisation at low energy on passing into the superconducting state, the higher energy response (> 1 meV) changes little between 0.15 and 3.5 K (compare lower two panels of Fig. 2).

To address the question concerning the polarisation of *both* these modes we performed a full polarisation experiment on IN14. The results are shown in the top panel of Fig. 2. The response at the lowest temperature for *both* modes is predominantly transverse.

A preliminary data-analysis has been performed assuming that the two modes (initially quasielastic and spin wave) are coupled via a mean-field interaction. Implicit in such an interaction is the transverse nature of both modes. Within this approximation, the mutual coupling between modes leads to an enhancement of the low frequency part of the susceptibility, and a concomitant renormalisation of the effective low-energy quasielastic linewidth. With few parameters, the theory gives the solid curves in Fig. 1, which are a reasonable representation of the data. As mentioned, the analysis allows an estimate of the extrapolated normal state heat capacity which is within ~ 20% of the measured value. The dramatic fall in the superconducting state implies the opening of a gap – which is indeed seen experimentally in Fig. 2. These experiments have, for the first time, identified a contribution in the f-electron dynamical response that is connected with the superconductivity in a heavy-fermion metal. Without the simultaneous high flux, energy resolution, and polarisation analysis available on IN14 such effects would be difficult to observe, which explains why, despite much effort, they have not been reported previously.

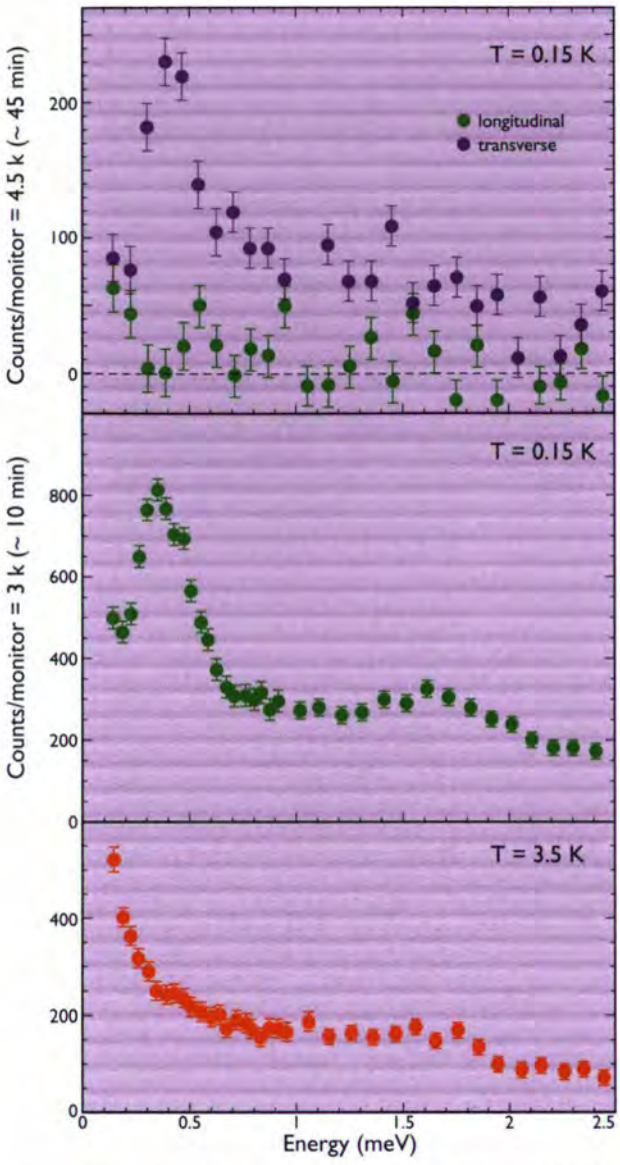

Figure 2: *Data taken in October 1997 on IN14 with k_f (fixed) = 1.15 Å^{-1} at the magnetic zone centre* **Q** *= [0, 0, 1/2]. Top two panels are at T = 0.15 K, whereas the lowest panel is at T = 3.5 K. Recall that T_c = 1.9 K. The top panel is taken with full polarisation analysis on IN14 (a background of 80 counts has been subtracted and corrections made for imperfect polarisation) and shows that the magnetic response is transverse in nature.*

References

■ [1] G. Aeppli and C. Broholm, eds. K.A. Gschneidner, L. Eyring, G.H. Lander, and G.R. Choppin, North Holland Physics, Amsterdam 19 (1994) 123 ■ [2] A. Krimmel et al., Solid State Commun. 87 (1993) 829 ■ [3] H. Kita et al., J. Phys. Soc. Japan 63 (1994) 726 ■ [4] B.D. Gaulin et al., Phys. Rev. Lett. 73 (1994) 890 ■ [5] N. Metoki et al., J. Phys. Soc. Japan 66 (1997) 2560 ■ [6] T. Petersen et al., Physica B 199 & 200, (1994) 151 ; T. Mason et al., Risø National Laboratory Annual Reports, 1992 and 1994 ■ [7] N. Sato et al., J. Phys. Soc. Japan 66 (1997) 1884.

Phonon-assisted tunnelling of hydrogen trapped in niobium: a two-state polaron

A. WÜRGER (ILL).

Interstitial hydrogen trapped by an oxygen or nitrogen impurity in Nb is confined to two states and shows a rich dynamic behaviour due to quantum tunnelling. At temperatures below 10 K, the hydrogen impurity performs coherent oscillations about the trap atom. At higher T, adiabatic interaction with conduction electrons drives a crossover to overdamped motion; the relaxation rate decreases with temperature according to the law $\Gamma \propto T^{2K-1}$, as derived first by Kondo. At about 60 K, however, the rate shows a minimum as a function of T and increases on further rising the temperature. We report strong evidence for the behaviour above 60 K being due to coupling to lattice vibrations; the resulting rate is governed by multiphonon processes.

Hydrogen in metals shows a variety of quantum phenomena. In clean samples, it diffuses through the whole crystal through jumps between well-defined interstitial sites. On the other hand, oxygen or nitrogen impurities may capture the hydrogen atom, thus forming a two-state tunnelling centre on equivalent tetrahedral sites [1]. The resulting tunnel matrix-element in niobium has been measured by inelastic neutron-scattering; it takes a value of $\Delta = 2.4$ K for H trapped by an oxygen impurity, and $\Delta = 1.9$ K for a nitrogen trap [2, 3].

Interaction with conduction electrons gives rise to dissipation and leads to overdamped, or incoherent, tunnelling above $T = 10$ K. Quasielastic neutron-scattering [3] confirmed Kondo's prediction for the rate [4],

$$\Gamma_{el} = \frac{\Delta}{\hbar}\,\frac{1}{K}\left(\frac{2\pi k T}{\Delta}\right)^{2K-1} \qquad (1)$$

that decreases with rising temperature as T^{2K-1}, with a Kondo parameter $K \approx 0.055$. This law describes quantitatively measurements on several impurity systems at various concentrations [1].

In real metals, however, coupling to lattice vibrations provides a second damping mechanism that prevails at sufficiently high temperature [5].

Fig. 1 shows the potential energy landscape of a two-state defect as a function of the defect position q and one phonon coordinate x_k. Due to the linear coupling term $\lambda q x_k$, the energy minima occur no longer at $x_k = 0$, but are shifted to finite values of the vibrational coordinate. As a consequence, the tunnelling motion involves both defect and lattice modes; when tunnelling from one well to the other, the hydrogen impurity drags its phonon cloud. This may be viewed as a two-state polaron, in analogy to the diffusion of a light particle in a solid [6].

This polaron effect gives rise to an effective potential that changes shape for the particle dwelling in the left or right well, as shown in Fig. 2. At very low T, phonon dressing results in an apparent increase of the barrier height and

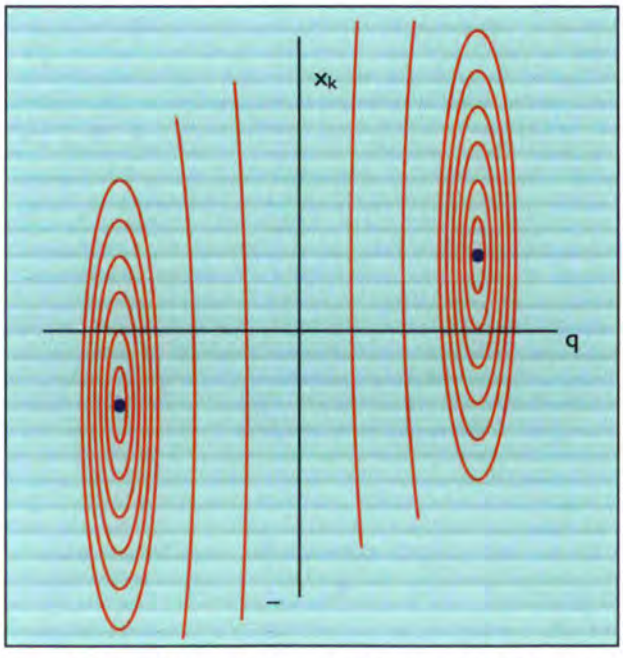

Figure 1: *Potential energy landscape as a function of the defect position q and the elastic mode x_k.*

hence slows down the tunnelling motion. Recently, we have pointed out a few subtleties concerning the phonon damping rate [7]. With rising temperature, the rigid phonon cloud 'melts', thus lowering the effective barrier and enhancing the jump rate.

When summing an infinite series of multiphonon contributions, we find a temperature-dependent correction factor to the electron-driven rate (1),

$$\Gamma = \Gamma_{el}[1 + F(T)] \qquad (2)$$

In the limit of low temperature, $T << T_0$, the additional term in brackets vanishes, $F(T) \to 0$, whereas in the opposite case, $T >> T_0$, it exceeds unity and hence governs the temperature dependence of the rate. The cross-over temperature is given by $kT_0 = \sqrt{\hbar^3 \rho v^5 / 3\gamma^2}$, with sound velocity v, mass density ρ, and the elastic deformation potential γ. There are well-known analytic expressions for $F(T)$, valid for T both well below and above the Debye temperature [7]. For hydrogen in Nb, none of these limits is satisfied, and the correction factor $F(T)$ has to be evaluated numerically. Details will be given in [8].

In Fig. 3 we plot quasielastic neutron-scattering data for $Nb(OH)_x$ and $Nb(NH)_x$, observed by Wipf and co-workers [1-3]. Because of the smaller tunnel energy, the relaxation is slower at nitrogen traps. The dashed lines account for damping by conduction electrons only, according to Eq. (1). The solid lines (2) take phonon coupling into account. The parameters used for the fit are $v = 2\,260$ m/s, $\rho = 8.4$ g/cm^3, and $\gamma = 0.2$ eV, resulting in $T_0 = 23$ K. The minimum in the rate occurs at about $2\,T_0$.

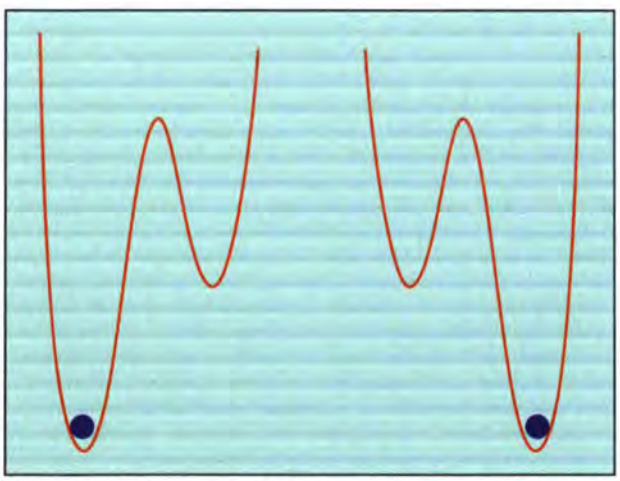

Figure 2: *Effective potential for the hydrogen dwelling in the left or in the right well.*

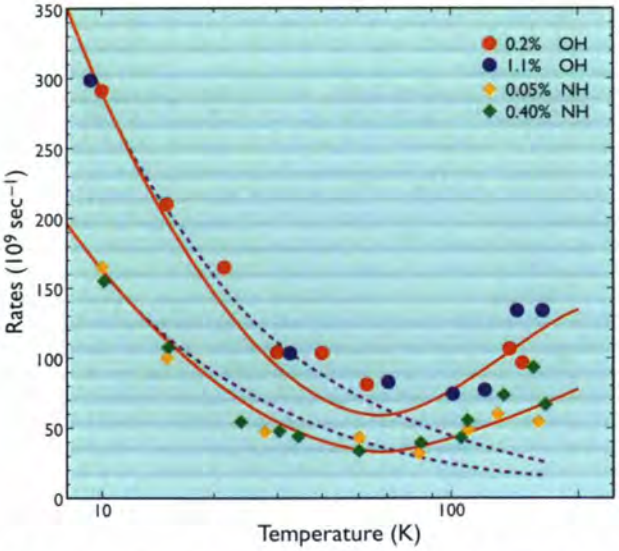

Figure 3: *Jump rates for hydrogen impurities for N and O traps. Dashed lines give the rate (equation 1) driven by conduction electrons only; solid lines (equation 2) take phonon coupling into account.*

Below 20 K, the solid lines differ little from the dashed ones, i.e., dissipation is driven by conduction electrons only. Between 30 and 70 K, the polaron effect reduces the rate slightly below the undressed value. Above 70 K, however, multiphonon processes prevail, and the rate increases with T. This behaviour is characteristic for phonon-assisted tunneling. At still higher T, the rate levels off towards the high-temperature result $\Gamma \propto T^{-1/2}$ [8]. In the whole range, the data agree well with the theoretical curve. In particular, the constant ratio of the rates for N and O traps assures that we are in the quantum regime, where $\Gamma \propto \Delta^{2-2\,K}$ holds true.

In summary, Fig. 3 shows how the polaron effect influences the damping rate. At low T, screening by conduction electrons results in a decreasing Γ with rising temperature. Above T_0 phonon coupling causes a strong increase of the rate. Comparison with quasielastic neutron-scattering data proves the relevance of phonon-assisted tunnelling for the dissipative dynamics of trapped hydrogen impurities above about 60 K.

References

■ [1] H. Wipf (ed.), Springer Berlin Heidelberg New York (1997) ■ [2] A. Magerl, A.-J. Dianoux, H. Wipf, K. Neumeier, I.S. Andersen, Phys. Rev. Lett. 56 (1986) 159 ■ [3] D. Steinbinder, H. Wipf, A.-J. Dianoux, A. Magerl, K. Neumeier, D. Richter, R. Hempelmann, Europhys. Lett. 16 (1991) 211 ■ [4] J. Kondo, Physica 125 B (1984) 279; Physica 126 B (1984) 377 ■ [5] H. Grabert, Phys. Rev. B 46 (1992) 12753 ■ [6] T. Holstein, Ann. Phys. (New York) 8 (1959) 325 and 343 ■ [7] A. Würger, Phys. Rev. Lett. 78 (1997) 1759; Phys. Rev. B 57 (1998) 347; Phys. Lett. A 236 (1998) 571 ■ [8] A. Würger, in: Tunneling in Solids, P. Esquinazi (ed.), Springer Berlin Heidelberg New York (1998).

Theory and data analysis for excitations in liquid ^{4}He beyond the roton minimum

F. Pistolesi (ILL).

The hybridisation of the single-particle branch with the two particle continuum in the region beyond the roton is reconsidered by including the effect of the interference term between one and two quasiparticle excitations. Fits to the latest data by B. Fåk and J. Bossy with our model allow us to extract the dispersion relation of the final part of the ^{4}He spectrum for momenta between 2.3 Å^{-1} and 3.6 Å^{-1} with improved accuracy. In contrast with previous measurements and data analysis we find that it never crosses the line of two times the roton energy as expected theoretically. Moreover, evidence for an attractive interaction between rotons in this range of momentum is found.

It is well known that the branch of the excitations in ^{4}He flattens out for momentum $Q \sim 2.4 - 3.4$ Å^{-1}, where one excitation can decay into two excitations (specifically two rotons) fulfilling energy and momentum conservation.

This phenomenon was first predicted by Pitaevskii [1] who exploited the logarithmic divergence of the two-roton density of states to find the exact form of the Green functions in a restricted region of energy around 2Δ (Δ is the roton energy). The explicit value of the parameters entering the Green functions cannot be inferred from the theory and should be extracted from the experimental data. In particular a crucial parameter of the theory is the two-roton interaction potential V_4 as it determines qualitatively the termination of the spectrum. As a matter of facts for an attractive interaction, due to the effective bi-dimensionality of the decay process, we always have a bound state ($E_B < 2\Delta$), and in this case the hybridisation between the one particle branch and the two-roton excitations gives rise to a one particle branch that approaches asymptotically E_B with a decreasing weight. For positive V_4, instead, the spectrum terminates with an essential singularity at a critical value of momentum Q_c at energy 2Δ. In both cases we should never observe a sharp peak at energy larger than 2Δ as for such energy excitations become unstable towards decay into two rotons.

The experimental data (for a recent review see Ref. [2]) show clearly that the hybridisation does take place, but they leave open questions. The position of the peak at momentum larger than 2.6 Å^{-1} seems to be above the 2Δ line in contrast with theoretical expectations. The experimental resolution is not enough to guarantee that the peak is really sharp, so it could also be a weakly damped peak at energy slightly larger than 2Δ, but again this would not agree with theory. Moreover, a satisfying quantitative agreement between experiment and theory has not been found so far [3] as even the sign of V_4 is still undetermined.

The validity of Pitaevskii's theory (extended successively by many authors [5] is restricted to the small region in energy where the logarithmic singularity dominates, and it cannot be applied to higher energies. So one encounters difficulties to analyse data for large value of Q because most of the spectral weight of $S(Q, \omega)$ is moving to higher energies. Moreover, so far no theory has taken into account the interplay between the one- and two-quasiparticle response function that becomes more and more important for large Q and ω.

We have thus considered this effect by studying a simple model where two real numbers α and β parametrise the coupling of neutrons to one and two roton excitations. We thereby include interference effects in neutron scattering parametrised on the hybridisation amplitude V_3 and the interaction V_4. The theory depends on the exact *roton-roton* response function $\chi(\omega)$ and on the bare one roton Green function. It applies, in principle, to a larger energy range than the Pitaevskii's one, as far as one can guess the form of $\chi(\omega)$. In particular in the narrow region of energy around 2Δ we can use the explicit expression for $\chi(\omega)$

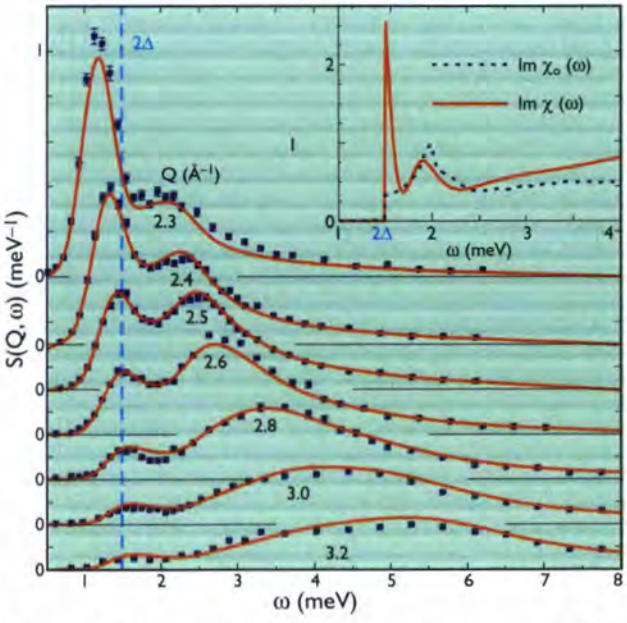

Figure 1: *Data from [6] and best fit for sets of data with $Q = 2.3 - 3.2$ Å^{-1}. In the* ***inset*** *the fitted $\mathrm{Im}\chi(\omega)$ is compared with the free one.*

given by Pitaevskii's theory. Outside this region $\mathrm{Im}\chi(\omega)$ should be related to the joint density of states of two noninteracting rotons but as it is not easy to have a reliable estimate of the exact one we preferred to extract also $\chi(\omega)$ from the data.

We have performed different kinds of fits to the data by Fåk and Bossy [6] with our expression for $S(Q, \omega)$. We performed our fits by assuming no dependence on Q of all the parameters, apart from the bare dispersion relation which is expected to be the only parameter strongly dependent on Q. The fits have been done by minimising *globally* the χ^2 for $S(Q, \omega)$ over the bi-dimensional region Q and ω and not by minimising it separately for each value of momentum. We find that this procedure reduces greatly the error bars on the fitted parameters and it gives more confidence in the reliability of the theory.

We studied two different problems. First we wanted to determine V_4 and for this purpose we performed a fit with a cut-off in energy of 1.7 meV (slightly larger than $2\Delta \approx 1.5$ meV). In this region the modified Pitaevskii theory should work quantitatively, as effectively we find. The interaction potential turns out to be attractive with a $V_4 \approx -4.7\mathrm{meV\AA^3}$ and a tiny $E_B \approx 2\Delta - 1.3\ \mu\mathrm{eV}$.

Second, we wanted to study the applicability of the theory to the whole region of energy $0 < \omega < 12$ meV and extract from the data $\chi(\omega)$. This has been possible with a second fit to the data without any cutoff and minimising the χ^2 also over the possible shapes of $\chi(\omega)$. In Fig. 1 we report the result of the fit compared with the data and the fitted $\mathrm{Im}\chi(\omega)$ compared with the non-interacting one $\mathrm{Im}\chi_0(\omega)$.

The peak at 2Δ is due to the attractive interaction. Note that the β parameter is crucial to obtain a good fit, also if we have completely free $\chi(\omega)$. The fit with a cutoff in energy (not shown) turns out to be even more accurate.

The two different fits suggest nearly the same dispersion relation for the quasiparticles as shown in Fig. 2 together with the one taken from Ref. [2].

In conclusion experiments agree with theory when data

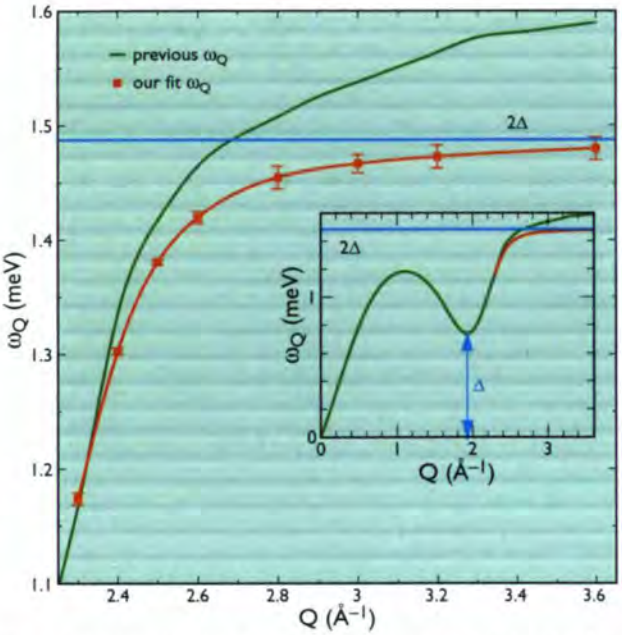

Figure 2: *New dispersion relation for the region $2.3 < Q < 3.6$ Å^{-1} compared with previous measurements. In the* ***inset*** *the complete dispersion relation is reported.*

are properly analysed. In fact within the resolution of the data it is not possible to extract the position of the sharp peak without a suitable analysis. The identification of the energy at which 2Δ has a maximum with the position of the pole in the quasiparticle Green function is *wrong* as continuum and discrete contributions are of the same order of magnitude. The convolution with the experimental resolution leads to a broad peak at energy slightly higher than 2Δ that has been previously interpreted as the quasiparticle energy. Experiments at higher resolution in this region would be useful to verify the presence of a sharp peak at the position suggested by our analysis.

Acknowledgement

I am indebted to P. Nozières for many suggestions and discussions. I gratefully acknowledge B. Fåk and J. Bossy for giving me data prior to publication. I also acknowledge B. Fåk, N. Cooper, N. Manini and H. Glyde for useful discussions.

References

■ [1] L.P. Pitaevskii, Sov. Phys. JETP 36 (1959) 830 ■ [2] R.J. Donnelly et al., J. Low Temp. Phys. 44 (1981) 471 ■ [3] A.J. Smith, et al., J. Phys. C10 (1977) 543 ■ [4] A. Zawadowski, J. Ruvalds, and J. Solana, Phys. Rev. B 5 (1972) 399; K. Bedell, D. Pines, and A. Zawadowski, Phys. Rev. B 29 (1984) 102 ■ [5] K. Juge and A. Griffin, J. Low Temp. Phys. 97 (1994) 105 ■ [6] B. Fåk and J. Bossy, J. Low Temp. Phys., in press.

Investigation of storage of ultra-cold neutrons (UCN) in traps

V.V. Nesvizhevsky, P. Geltenbort (ILL),
A.V. Strelkov (JINR, Dubna),
P.S. Iaydjiev (RAL Didcot/INRNE Sofia).

UCNs stored in traps are used in many experiments in fundamental physics such as the measurements of the neutron lifetime or electric dipole-moment. It is known that losses of neutrons from such traps are due to the β-decay, up-scattering and absorption on a surface but we have identified for the first time a complementary mechanism. This arises from an increase in energy of the neutrons (probability ~10^{-5} per collision with trap wall) resulting in a higher energy spectral cut-off which is about twice that for the initial stored neutrons. This is a different process from normal up-scattering to thermal energies but the result is that higher energy neutrons can then escape in the bulk of material by the known processes of up-scattering and absorption or penetrate through the trap wall if it is thin enough. Further experiments will show whether this effect is relevant to the anomalous UCN loss puzzle known for many years.

One of the most attractive features of UCNs (energy ~ 10^{-7} eV which corresponds to a jumping height in the Earth's gravitational field ~ 1 m) is that they can be stored in traps due to total internal reflection from a surface if the energy of UCNs is lower than the Fermi-potential barrier of the surface material (specific to each material). Long (theoretically predicted) storage times of UCNs in traps which correspond to long observation times in experiments (~ 900 sec, the neutron β-decay life time) are very attractive for experiments in fundamental physics. The investigation of this phenomenon itself revealed an interesting physical behaviour: large additional temperature-independent so-called "anomalous" losses [1]. Anyway the best storage times of UCNs in traps are always much shorter than theoretical expectation. The investigation of UCN storage is a long-term project involving a PNPI-JINR (Russia) collaboration. More recently an increase of international scientific collaborations, particularly with ILL, has led to an intensive experimental programme on the ILL UCN facility PF2.

One of our recent results was the observation of "anomalous" penetration of UCNs through the thin wall of a storage volume [2]. In the present experiment we investigated the nature of this effect using a gravitational spectrometer (Fig. 1). This consists of a vertical stainless steel cylinder (0.6 m diameter and 2 m height, in some measurements the internal surfaces are coated with Fomblin oil) and a plane polyethylene absorber that provides an upper cut-off (height = energy) to the UCN spectrum. A thin foil separated the storage volume from a curved neutron guide that connected it to a UCN gaseous detector. A very low background count-rate of ~ $5 \cdot 10^{-4}$ counts/sec was achieved by careful design of shielding configuration and detector electronics. The set-up guaranteed that, without penetration of the UCNs through the thin foil, there would be no correlation between the count-rate in the detector and the UCN flux in the storage

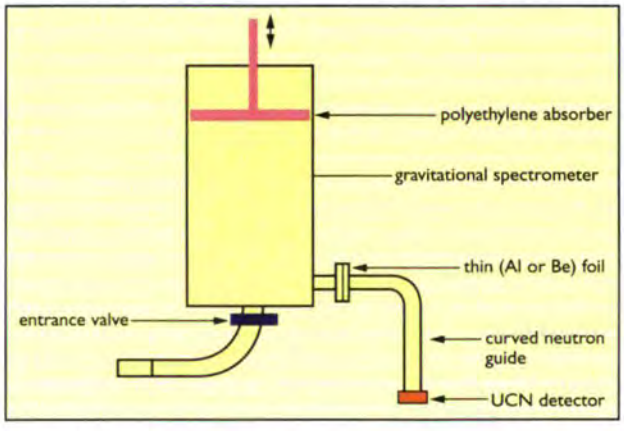

Figure 1: *Diagram of the installation.*

volume. If neutrons penetrate the foil then the count-rate should increase proportionally to the UCN flux at the foil position. False effects which could be related to above-barrier neutrons (neutron energy higher than the Fermi-potential barrier of the foil) in the initial UCN spectrum are avoided by tailoring the spectrum by means of the above mentioned polyethylene absorber. Fig. 2 shows the time dependence of the count rate. The spectrometer is filled with UCNs for 110 sec, then the entrance valve is closed (0 sec in Fig. 2). During the filling the absorber is always at such a height that the spectrum cut-off is at an energy significantly lower than the Fermi-potential barrier of the foil. In the first 70 sec after closure the initial UCN spectrum is cleaned from above-barrier neutrons (above-barrier for the foil). The dashed green line corresponds to the extrapolation of the count-rate of above-barrier neutrons in the initial spectrum. Neutrons counted after 80 sec. are penetrating "anomalously" through the foil. The red line is the normalised time dependence of the sub-barrier UCN flux at the foil position. The time dependence of the UCN flux inside the trap was calibrated in a separate experiment with a small hole in a thick foil. We checked and eliminated the most probable experimental errors: the effect of residual above-barrier neutrons; a significant probability for specular reflections at trap walls; pin holes in the thin foils; possible broadening of the UCN spectrum due to vibrations.

The energy dependence of the probability for penetration (ratio of the penetrating flux to the initial flux at the foil position) of UCNs through foils with different absorber heights was measured for a 11.5 μm Al foil (Fig. 3, circles), a 15.0 μm Be foil and for two 17.8 μm Al foils (Fig. 3, squares). All three curves show similar behaviour: 1. the higher is the initial UCN energy the higher is the probability for penetration, 2. simple linear extrapolation of the data shows that there is no penetration if there are

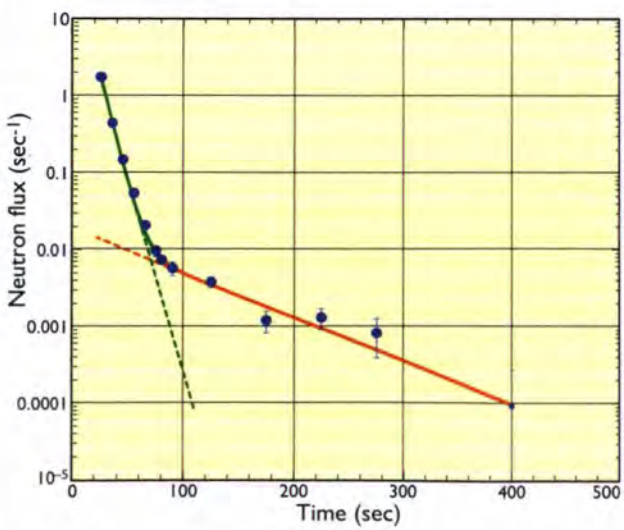

Figure 2: *The time-dependence of the flux of neutrons penetrating through 17.8 μm-thick Al foil.*

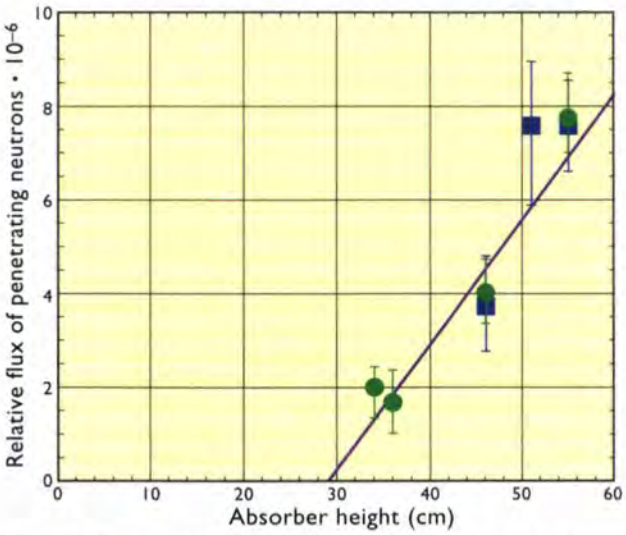

Figure 3: *The dependence of the penetration probability versus the absorber height. Single 11.5 μm Al foil (circles), two 17.8 μm Al foils separated by a polyethylene ring (squares). The squares are scaled to account for the differing thickness of Al in the beam.*

no neutrons in the initial spectrum with an energy higher than about half of the potential barrier of the thin foil (the barrier corresponds to an absorber height from the bottom of ~ 60 cm for Al). This result is valid both for Al and Be foils although the heights of their potential barrier are almost 5 times different.

The two Al foils (in Fig. 3, squares) were separated by a polyethylene ring mounted in such a way that it is out of the direct beam. While for above-barrier UCNs the transmission through two foils or one foil of double thickness are almost equivalent, sub-barrier neutrons (if they penetrate through the first foil) would be trapped in the inter-foil region (small probability of penetration per one collision) and therefore almost all of them would have been totally lost in the polyethylene ring. This measurement gave a key to the interpretation: it clearly showed that above-barrier neutrons are penetrating through foils! This seems to be a contradiction as no residual above-barrier neutrons are in the initial UCN spectrum, but it actually yields the explanation: UCNs are gaining in energy by interacting with a surface. This idea was also verified by an additional variation of the detector height (above what would correspond to the initial spectrum cut-off) and counts were still seen. This small gain in energy is a different process from " normal " up-scattering to thermal energies, but it is in line with a general hypothesis by A.V.Strelkov and A.D.Stoika proposed for the explanation of anomalous UCN losses [3]. Thus the probability of scattering the UCNs to a very narrow energy range (10^{-7}eV) is about as large as the total probability of up-scattering at clean surfaces to all other energies.

As soon as the stored UCNs gain in energy, most of them are lost in our set-up immediately in the polyethylene absorber. Indeed when the neutron absorber is lifted by

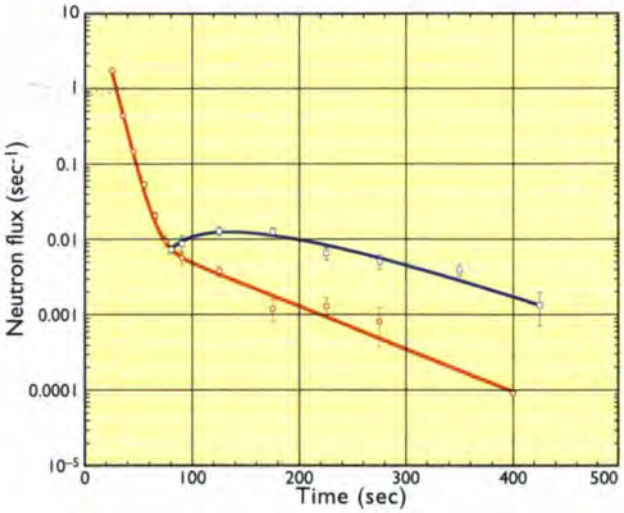

Figure 4: *The same dependence as in Fig. 2 but also with the data and blue line corresponding to the raising the absorber by 0.5 m after the spectrum cleaning (t > 80 sec).*

half a meter after having established the initial spectrum (i.e. after 70 sec) the penetrating UCN flux increased by a factor of about 25 (as shown in Fig. 4; blue squares)! The solid blue line in Fig. 4 was calculated using the measurement of the time dependence of the UCN flux at the foil position and the assumption of a constant probability for the generation of above-barrier neutrons created from sub-barrier ones. The absorber movement itself does not produce a noticeable false "heating effect". The spectrum of such "energised" UCNs has been measured by raising the absorber to different heights during the UCN storage (after the spectrum cut-off). One also observes an energy cut-off in the integral spectrum, i.e. no higher energies for higher absorber heights which corresponds to the maximum energy in the final spectrum which is about twice the maximal energy in the initial spectrum. In future experiments it will be important to identify the process and the experimental conditions which are responsible for this energy change.

Today there is no clear theoretical explanation but such a process would help to understand many puzzles in UCN physics. Therefore it is important to continue investigations with careful simultaneous control of all alternative channels of escape of UCNs from a trap.

The main result of the present experiment consists in the observation of a new escape channel of UCNs from traps resulting from the presence of constant admixture of above-barrier neutrons in the UCN spectrum which can not be eliminated even by the most efficient known method of spectrum cleaning (by means of the "almost perfect absorber" - polyethylene, installed above the storage volume). It is caused by a change in the energy of UCNs.

This energy increase caused the penetration of UCNs through 56 μm Be foil as seen in our previous experiment [2]. It could be relevant to explain the additional temperature-independent anomalous losses of UCNs [1] which have about the same rate but were measured at lower temperature and with different surface material. The relation of the current observation to this and other experiments involving UCNs needs to be tested by future experiments.

References

■ [1] V.P. Alfimenkov, V.V. Nesvizhevsky, A.P. Serebrov, A.V. Strelkov, R.R. Tal'daev, A.G. Kharitonov, V.N. Shvetsov, LNPI-1729 (1991) also JETP Lett. 55 (1992) 84 ■ [2] P. Geltenbort, A.G. Kharitonov, V.V. Nesvizhevsky, J.M. Pendlebury, K. Schreckenbach, A.P. Serebrov, V.N. Shvetsov, A.V. Strelkov, R.R. Tal'daev, V.E. Varlamov, Physics Lett. A (1997) submitted ■ [3] ILL proposal 3-14-51, 1996.

Right-handed currents and symmetry breaking

H. Abele (Univ. Heidelberg).

Parity is maximally violated in weak interaction: only left-handed fermions take part in the interaction. In the modern grand-unified theories, the universe originally is left-right symmetric. Parity violation arises only due to a spontaneous symmetry breaking at some intermediate energy scale. Recent neutron-decay measurements from various mixed American-British-French-German-Russian collaborations try to shed light on this question.

Left and right

Asymmetries are common in daily life. We find more screws with a right-handed thread than screws with a left-handed thread. This has something to do with the fact that more people (up to 95%) use the right hand rather than the left one. If we look at bio-chemistry we realise that fundamental to life is another left-right asymmetry: proteins, common to all living creatures, are made of amino acids. In general, amino acids exist in the "left-hand" L-alanine and the "right-hand" D-alanine. As a surprise proteins consist exclusively of L-alanine. The widely accepted assumption is this: "a particular historical accident was one-sided, and ever since then the lopsidedness has propagated itself" [1].

Now let us consider particle physics. Neutrinos are exclusively left-handed. A right-handed neutrino has not been found, yet. As a consequence neutron decay generates a β-asymmetry, where electrons show chirality. At first glance particle physics shows a feature similar to bio-chemistry. However, there is, as we believe, a fundamental difference between the left-handed neutrino and the left-hand amino acid: in particle physics a particular physical law itself is not symmetrical under reflection in space. Otherwise laws of nature tend to be symmetric with respect to mirror inversion or parity transformation. Electromagnetism, gravity and strong interaction show invariance. Also the biochemical examples do not show a lack of symmetry taking the physical laws as a basis. Nevertheless some authors [15] state that it was within bounds of possibility that the bio-chemical asymmetry might be induced by the parity violating weak interaction.

After the discovery of parity violation, weak currents were considered to have vector minus axial vector structure. As a consequence, only left-handed fermions take part in charged-current weak interaction. This peculiarity is incorporated into the standard model of particle physics. On the other hand, most grand unification theories favour the existence of a left-right symmetry in the early universe. Then parity violation is a consequence of the spontaneous breakdown of this symmetry. In contrast to the standard model, parity is not violated to 100% and right-handed neutrinos would be reminiscent of the initial symmetry. A left-right symmetry is incorporated in the following way: a left-handed W_L and a right-handed W_R replace the left-handed W gauge boson of the standard model. W_L and W_R are combinations of two mass states W_1 and W_2 with masses m_1 and m_2 and a mixing angle ζ:

$$W_1 = W_L \cos\zeta - W_R \sin\zeta$$

$$W_2 = W_L \sin\zeta - W_R \cos\zeta$$

The dominance of left-handed currents requires $m_1 \ll m_2$. Neutron experiments try to shed light on the origin of parity violation.

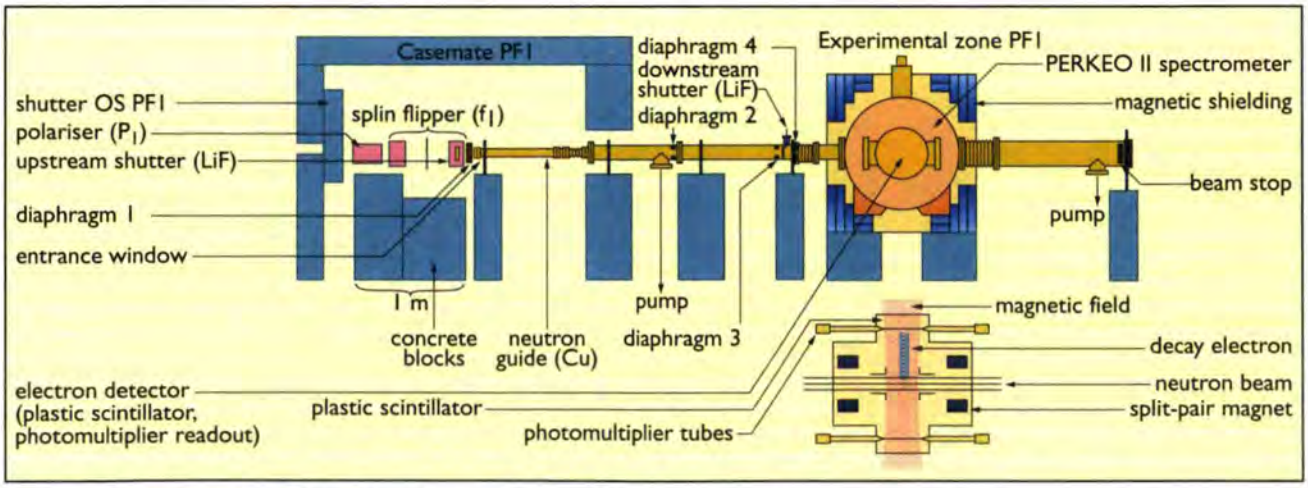

Figure 1: Experimental set-up of the PERKEO II instrument on the PF1 cold neutron position.

Experimental details

Observables in neutron decay are neutron lifetime, neutron spin and spin and momentum of proton and electron. Up to 1990, all results from neutron decay were in agreement with the standard model [2]. Then in 1991, a new value of the β-asymmetry A was published [3]. The experiment was done at LNPI (Gatchina). Decay events were recorded by a scintillation detector for electrons and a photomultiplier tube with CsI(Ti) layer for protons. The absolute value for A was significantly lower than in earlier measurements and in disagreement with the standard model. It is not surprising that this result of [3] was frequently interpreted as a possible signature of the existence of right-handed currents in weak interaction [4-6]. A more recent publication of Schreckenbach et al. [7] on A, on the other hand, gave a value which was slightly higher than the previous values, so that the situation was far from satisfactory. In that experiment the tracks and the energies of the decay electrons were measured with a time projection chamber and with plastic scintillators.

We present a new measurement of the β-asymmetry A, which, here, is the difference of electron count rate in two hemispheres for two opposite neutron polarisation states. The instrument PERKEO II has two electron detectors in each hemisphere and was installed at the PF1 cold neutron beam-position at the ILL (Fig. 1). The detector solid-angle of acceptance is $2 \times 2\pi$ and the energy threshold is 60 keV. The main component of the PERKEO II spectrometer is a superconducting 1 T magnet in a split-pair configuration, with coil diameter of about one meter. The decay electrons are guided by the magnetic field to either one of two scintillation detectors with photomultiplier readout. An unpolarised β-spectrum is shown in Fig. 2a. The measured electron spectra $N^{\uparrow}_i(E)$ and $N^{\downarrow}_i(E)$ in the two detectors (i = 1,2) for neutron spin up and down, respectively, define the experimental asymmetry as a function of kinetic energy E.

$$A_{exp} = \frac{N^{\uparrow}_i(E) - N^{\downarrow}_i(E)}{N^{\uparrow}_i(E) + N^{\downarrow}_i(E)}$$

The asymmetry data, fitted between 325 keV and 675 keV are shown in Fig. 2b. We obtain A = – 0.1189(12) [8]. The maximum correction we had to apply to the raw asymmetry A_{exp} is about one order of magnitude smaller than in all previous work. This value differs by more than three standard deviations from the value – 0.1139(11) adopted by the particle data group in 1996 [9]. The consequences for physics within or beyond the standard model will be discussed in the next paragraph.

Right-handed currents

Several recent evaluations of neutron decay data favoured the existence of a right-handed weak gauge-boson with a mass state m_2 between 207 GeV/c² and 369 GeV/c² at 95% confidence level [5]. Here we present a new evaluation of this question, based on the new neutron decay data and β–decay measurements [10].

In our search for a right-handed W boson, we concentrated on two parameters, the mass-squared ratio $\delta = (m_1^2/ m_2^2)$ and the mixing angle ζ. Fig. 3 shows an

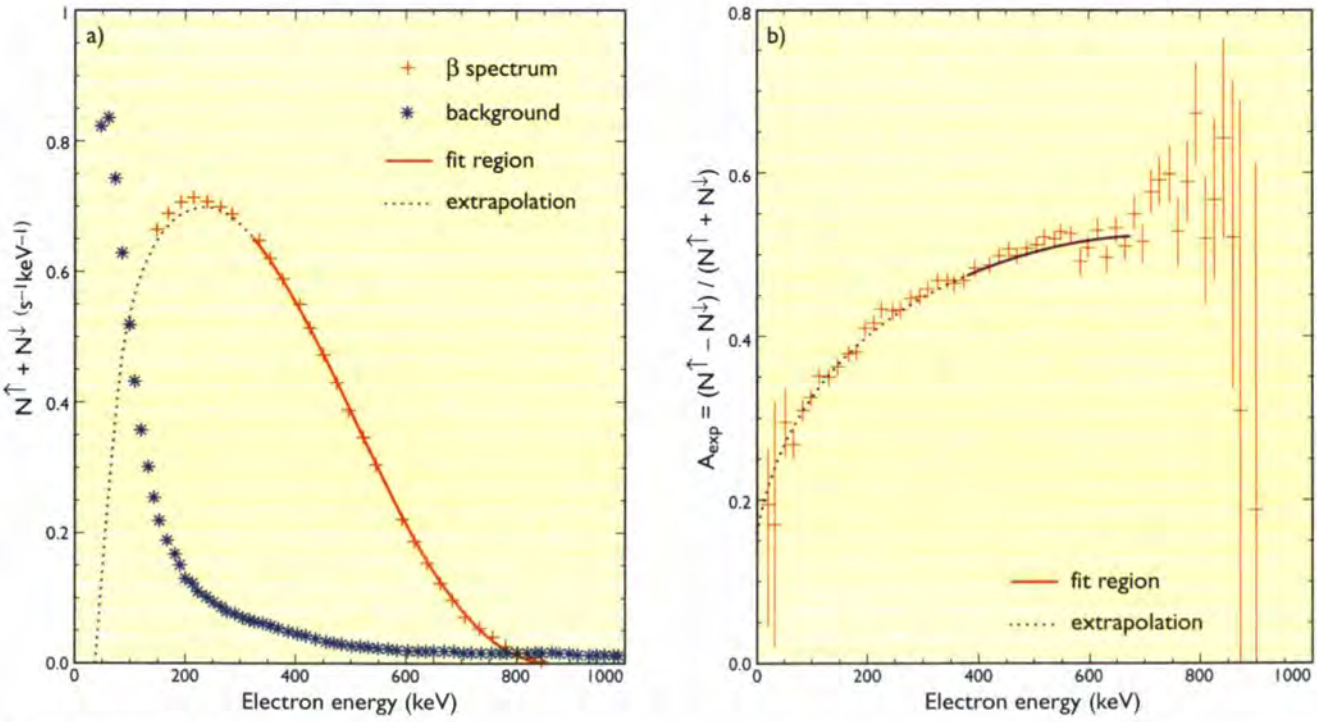

Figure 2: a) *Neutron β-spectrum. +: Electron energy spectrum after adding opposite neutron spin orientation $N^{\uparrow}$ and $N^{\downarrow}$. ∗: background which was subtracted from the raw data. The solid line shows a fit in the energy range between 325 keV and 675 keV and the dotted line shows an extrapolation to lower energies.* ***b)*** *Neutron β-asymmetry. The solid line shows a fit to the experimental asymmetry A_{exp} and the dotted line shows an extrapolation to lower energies.*

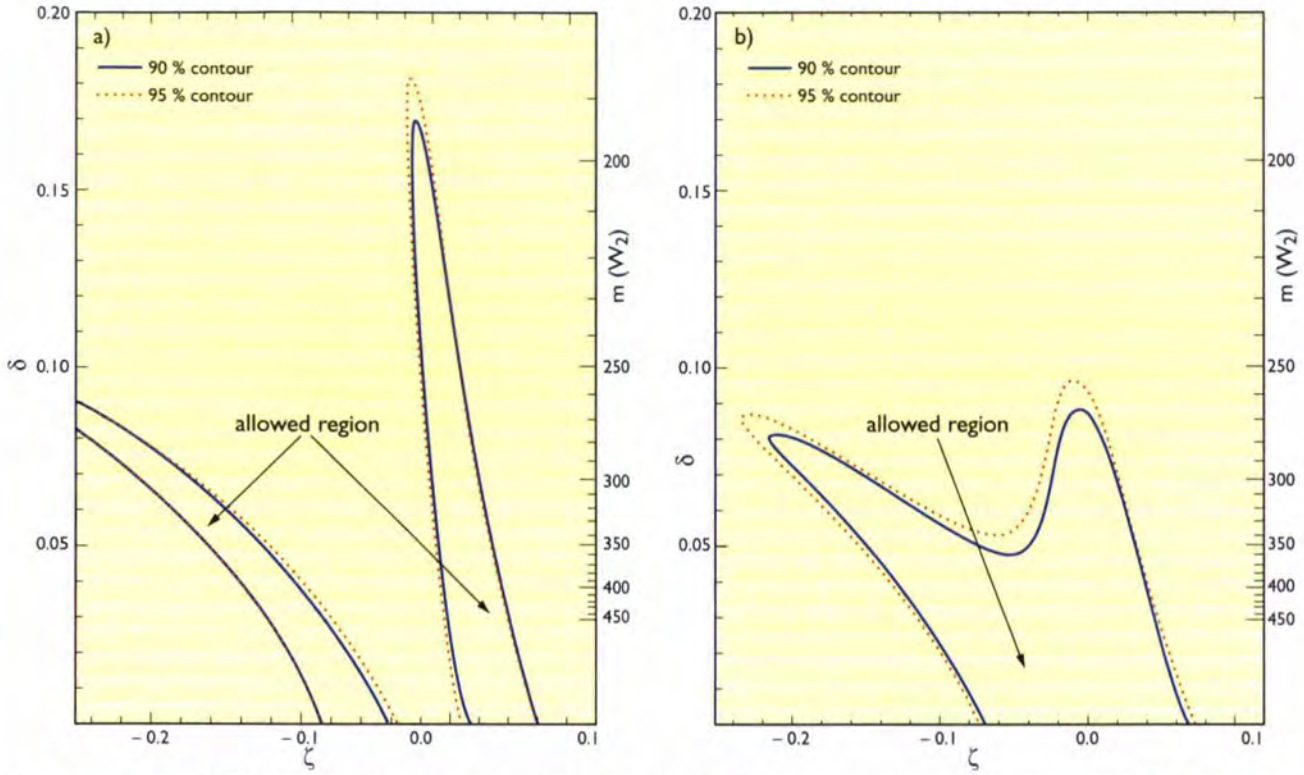

Figure 3: *Limits on right-handed currents (inferred from neutron decay data and nuclear β-decay measurements) are shown as contours in this plot of the mass ratio δ parameter vs. mixing angle ζ. The region outside the contour lines are excluded with 90%, and 95% C.L., respectively.* ***a)*** *Status 1994: the standard model prediction for parameters δ = 0 and z = 0 are excluded by more than two sigma.* ***b)*** *Status 1997: the result is consistent with the standard-model prediction.*

exclusion plot for δ and ζ. The 90% and 95% C.L. contour lines are displayed. Fig. 3a shows the situation in 1994 [16]. The allowed region is not consistent with the standard model prediction δ = 0 and ζ = 0. A fit to the data was consistent with the assumption of a right-handed W. Fig. 3b shows the situation in 1997. We take new direct measurements of the neutron lifetime into account. These measurements were done at the ILL [11,12] and in Gatchina [13]. For the β-asymmetry A we use ref. [7] and our new value additionally. A measurement of A provides the information on mixing ζ. We also use a new value [14] for the neutrino asymmetry coefficient B, which places better restriction on the ratio δ. As can be seen from Fig. 3b the new result is consistent with the standard-model prediction at 90% C.L.

To summarise, we have measured the β-asymmetry in the decay of free polarised neutrons and obtain A = – 0.1189(12). The corrections applied to our raw data are not larger than the quoted error. Our evaluation of all neutron data is consistent with the standard model prediction of the electroweak interaction. No right-handed currents were found.

References

■ [1] R. Feynman et al., Addison-Wesley Publishing Company, Inc., July 1964 ■ [2] D. Dubbers, Prog. Part. Nucl. Phys. 26 (1991) 173 ■ [3] B. G. Erozolimskii et al., Phys. Lett. B 263 (1991) 33 ■ [4] Yu. V. Gaponov et al., Phys. Lett B 253 (1991) 283 ■ [5] A.S. Carnoy et al., J. Phys. G 18 (1992) 823 ■ [6] N.B. Shul'gina, Phys. Rev. Lett. 73 (1994) 2658 ■ [7] Schreckenbach et al., Phys. Lett. B 349 (1995) 427. P. Liaud et al., Nucl. Phys. A 612 (1997) 53 ■ [8] H. Abele et al., Phys. Lett. B 407 (1997) 212 ■ [9] R.M. Barnett et al., Phys. Rev. D 54 (1996) 1 ■ [10] I.K. Towner et al., Proceedings of the ENAM Conference, Arles (1995); D.H. Wilkinson, Z. Phys. A348 (1994) 129; W.E. Ormand et al., Phys. Rev. Lett. 62 (1989) 866 ■ [11] W. Mampe et al., Sov. Phys. JETP Lett. 57 (1993) 82 ■ [12] W. Byrne et al., Europhys. Lett. 33 (1996) 187 ■ [13] V. Nezvishevsky et al., Sov. Phys. JETP 75 (1992) 405 ■ [14] A. Serebrov et al., Proceedings of the ISINN-5 conference, Dubna 1997 ■ [15] I. A. Kuznetsov et al., D. Rein, Birkhäuser Verlag, 1992 ■ [16] L. Montanet et al. Phys. Rev. D 50 (1994) 1173.

Vibrational modes in nuclei

H.G. Börner, Ch. Doll, M. Jentschel (ILL),
R.F. Casten (Yale Univ.).

One of the central challenges in nuclear physics has always been to understand the interplay between the concepts of each nucleon moving in individual quantised orbits and that of coherent excitations (e.g. vibrations or shape oscillations) of the nucleus as a whole. The issue relates to the nature of the nucleus as a many-body quantal object and to the role of the Pauli Principle in this fermionic system. Despite years of studies, both experimental and theoretical, we do not understand these collective excitations. More accurately stated, the understanding we have long thought to be in hand now appears to need a major revision. New techniques and experiments at the ILL have played a very important role, both in this questioning of traditional concepts and in pointing the way to an understanding.

Aside from the "central" potential to which all the nucleons are subject, there are attractive residual interactions that primarily affect the outermost, or valence, nucleons. These interactions lead to correlated motions and, thereby, to collective excitation-modes of the nucleus. Macroscopically, these modes can be viewed as nuclear-shape oscillations. The best studied vibrational modes are those involving quadrupole (ellipsoidal) shapes. In spherical nuclei - that is nuclei with proton and neutron numbers close to magic numbers - these are oscillations of quadrupole shape away from sphericity. In deformed nuclei, they are oscillations around the mean deformed quadrupole shape. These latter can be of two basic types, called β and γ. β-vibrations are oscillations that preserve the axial symmetry of the deformed ellipsoid but increase or decrease the degree of deformation. γ-vibrations are shape excursions perpendicular to this axis in which the nucleus momentarily takes on squashed axially asymmetric shapes. Fig. 1 schematically illustrates these shape oscillations and shows the nuclear level-schemes that result from them. (Note that, on top of each vibrational excitation in a deformed nucleus, there is a band of levels corresponding to an adiabatic rotation of the nucleus as a whole.) For the deformed case, there is a characteristic quantum number, called K, which is the projection of the total angular momentum on the symmetry axis. For β-vibrations, K = 0, for the γ-mode, K = 2.

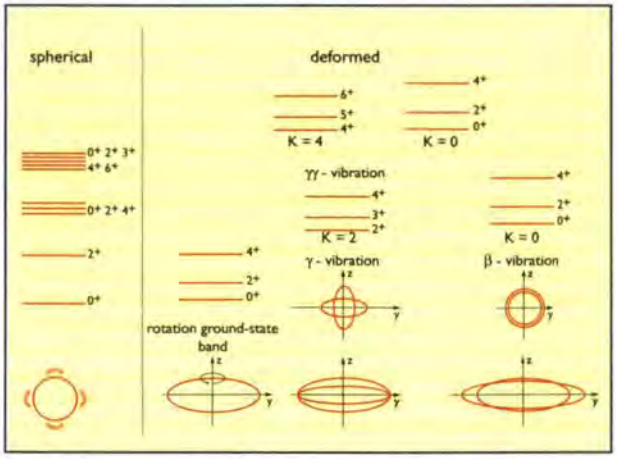

Figure 1: *Phonon and multi-phonon excitations in spherical and deformed nuclei.*

As these vibrational phonons behave as bosons, one can envisage superpositions of them - multi-phonon states. Projection quantum numbers add algebraically. Hence, for the γ-mode there are two 2-phonon excitations, with K = 0 and 4. The most telling experimental signature of these are the observation of deexcitation transitions (γ-rays) to the single phonon band whose strength corresponds to matrix elements that are comparable to or greater than the deexcitation matrix elements from the γ-vibration to the ground-state band.

But there is a problem with this simple picture of multiphonon states. Although the vibrations are boson-like, they are composed of fermions (protons and neutrons). Microscopically, the wave functions of these vibrations correspond to linear combinations of "particle-hole" excitations in which a particle in an occupied orbit is elevated to a vacancy in an unfilled orbit and the fermions out of which these vibrations are constructed occupy single-particle states with, in general, rather low angular momentum j. Due to the Pauli Principle, each orbit, which has 2j + 1 magnetic substates, can only contain at most 2j + 1 identical nucleons. This has long been thought to impede significantly the creation of such modes. Indeed, for thirty years a long-standing issue in the study of the collective behaviour of nuclei has been whether multiphonon vibrational excitations could exist in nuclei that are non spherical.

It was therefore an important fundamental result in 1991, when an experiment at the ILL [1] using the GRID technique (**G**amma **R**ay **I**nduced **D**oppler broadening [2,3]) found a state in ^{168}Er which could be associated with a 2-phonon γ-vibrational mode (γγ-mode). The GRID study deduced the lifetime for this state (here K = 4). The absolute transition matrix elements can be directly obtained from the measured lifetimes.

In the GRID technique the lifetime of a nuclear state is obtained by an analysis of the Doppler broadening of a

deexcitation γ-ray transition (see Fig. 2): highly excited nuclei are produced by thermal neutron-capture, these deexcite to lower energy-states via emission of γ-quanta which induce a recoil to the nuclei. The excited atoms move in the bulk of the target material and are slowed down by collisions with the surrounding atoms. Meanwhile the still excited atomic nuclei deexcite by secondary γ emission. The probability of these emissions depends on the ratios (t/τ) where t is counted from the emission of γ's inducing the recoil and τ is the lifetime of the intermediate state. If the nucleus is in motion when it deexcites ($t \approx \tau$) the γ-ray energy will be Doppler-shifted. If it is stopped, the normal transition energy will be measured. The Doppler effects are on the order of eV. Thus the γ-ray, typically with energy ~ 1 MeV, must be detected with a resolution of $\Delta E/E \approx 10^{-6}$, three orders of magnitude better than obtainable with the usual Ge semi-conductor detectors. Fortunately this is feasible for the GAMS4 and GAMS5 crystal-spectrometers .

The experimental result for ^{168}Er immediately had both far reaching theoretical and experimental consequences. It led to experiments, by others, to confirm this result (which they did [3]), and it led to searches for multi-phonon states

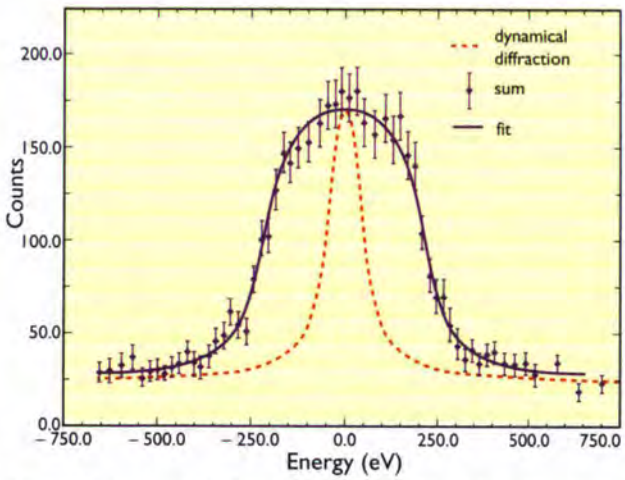

Figure 2: *Broadened GRID lineshape measured for a 2.7 MeV γ-transition with the new GAMS5 spectrometer. Dashed line: instrument response, full line: fitted GRID lineshape.*

in other nuclei (which were successful). Most of these searches took place at the ILL using GRID, but important independent contributions were made at other laboratories. Finally, it led to major revisions and corrections to some of the theoretical models.

Experimental work, triggered by the observation of the 2-phonon state in ^{168}Er, has gone in three general directions. One has been to look for additional γγ modes. Remember: projection quantum numbers add algebraically and the first example found in ^{168}Er was of the γ-vibrational type where the *K*-quantum number (see introduction) added up to 4 (2+2). Such additional γγ modes with good collectivity have been found in ^{164}Dy [4] and ^{166}Er [5]. Secondly, there have been searches for the case where the K-quantum number for the γ-vibration adds up to 0 (2-2). Without going into any detail one may say that the success in finding examples of these has perhaps had an even more profound impact. It turns out that for the lowest K = 0 excitation which was thought to be generally the β-vibration (see Fig. 1) there is evidence that in some cases it is instead this second partner of the γγ mode. This was again deduced from the pattern of the observed transition strengths - in ^{158}Gd for example -, determined via lifetime measurements. The third direction concerns the study of the β-vibration (where we have seen that some of the states at least, which previously were assigned to be β-vibrations, are instead γγ-vibrations). New experiments - on ^{152}Sm and ^{166}Er [5] by others and on ^{178}Hf with GRID - are finding at least a few good candidates for collective β-vibrations and ^{178}Hf reveals the first good candidate for a 2-phonon β-vibration. In other cases like ^{164}Dy [6] and ^{168}Er [6] the situation is more complex as several excitation modes (collective and single particle) seem to compete. Clearly, there is a richness in these vibrational modes heretofore unrealised. Whenever the appropriate, sufficiently sensitive, experiments have been carried out, many of them at ILL, they almost always reveal new examples of multi-phonon states. As a result of all this work most basic concepts of nuclear collective motions are undergoing radical and unexpected revision.

References

■ [1] H.G. Börner, J. Jolie, S.J. Robinson, B. Krusche, R. Piepenbring, R.F. Casten, A. Aprahamian and J.P. Draayer, Phys. Rev. Lett. 66 (1991) 691; 66 (1991) 2837 ■ [2] H.G. Börner and J. Jolie, J. Phys. G 19 (1993) 217 ■ [3] M. Oshima et al., Phys. Rev. C 52 (1995) 3492 ■ [4] F. Corminboeuf, J. Jolie, H. Lehmann, K. Föhl, F. Hoyler, H.G. Börner, C. Doll, and P.E. Garrett, Phys. Rev. C56 (1997) R1201 ■ [5] P.E. Garrett, M. Kadi, MinLi, C.A. McGrath, V. Sorokin Minfang Yeh, and S.W. Yates, Phys. Rev. Lett. 78 (1997) 4545 ■ [6] H. Lehmann, J. Jolie, F. Corminboeuf, H.G. Börner, C. Doll, M. Jentschel, R.F. Casten and N.V. Zamfir, Phys. Rev. C 57 (1998) 569.

Some of ILL's « ladies in science » enjoy the sun during their meeting (from left: Giovanna Fragneto, Teresa Fernandez-Diaz, Emmanuelle Suard).

The man of a thousand theory seminars: Philippe Nozières (centre). Seen here with Massimo Altarelli, ESRF (left) and Pierre Averbusch, CRTBT Grenoble, at the celebration to mark the 1001st seminar.

Bruce and Jane enjoy their workshop: « New Directions in Magnetism » to honour the 65th birthdays of two of our best known neutron scatterers, Jane Brown and Bruce Forsyth. This one-day workshop was held on 12 May (jointly by the ILL and ISIS).

WORKSHOPS

2

Workshops, Conferences and Schools
in which ILL played a major role in the organisation

Inelastic and Quasielastic Scattering with Neutron and Synchrotron Radiation	organised by R. Currat (ILL)	ILL	13-14 Jan. 97
École de Printemps: Diffusion des Neutrons et Sciences des Matériaux	organised by C. Janot (UJF Grenoble, now Univ. Roma) H.G. Büttner (ILL).	Pinsot	21-27 Apr. 97
Workshop on the PIAFE project	organised by U. Köster (Univ. München) and A. Pinston (ISN Grenoble)	ILL	27 June 97
Aperiodic'97, International Conference on Aperiodic Crystals	organised by M. de Boissieu, J-L. Verger-Gaugry, (LTPCM, CNRS and INPG) and H.G. Büttner, R. Currat (ILL)	Alpe d'Huez	27-31 Aug. 97
19th Congress of the Association for the Techniques and Sciences of Radiation Protection (ATSR)	mainly organised by J. Italia (regional representative of the ATSR, ILL), M. Selva (ILL), P. Bory (President of the ATSR, CEA Grenoble) and D. Chatel (CEA Grenoble), and S. Claisse (ILL).	Grenoble	8-10 Oct. 97

WORKSHOPS

Inelastic and Quasielastic Scattering with Neutron and Synchrotron Radiation

A workshop (attended by about 50 people) aiming to review the ILL instrument profile concerning inelastic and quasielastic scattering techniques concluded that x-rays complement rather than compete with neutrons. As a result the ILL's ongoing instrument development programme can stand unchanged. This review was requested by the scientific council to take into account present and short-term capabilities of inelastic x-ray techniques and to increase awareness of potential in this field.

The scientific programme was centred around the presentations of the two ESRF inelastic beamlines: the backscattering spectrometer ID16 (F. Sette) and the nuclear resonance beamline ID18 (R. Rüffer / A. Chumakov). This was followed by presentations from ESRF 'inelastic' users (most of whom turned out to be experienced neutron scatterers as well). An animated discussion, chaired by Bill Stirling the chairman of the scientific council at the time, concluded that synchrotron and neutron techniques are indeed strongly complementary and approved the ILL's instrument development programme.

Fabrizio Barocchi, Univ. Firenze, (centre) explaining his planned Brillouin spectrometer to Peter Verkerk, TU Delft, (left) and Ubaldo Bafile, Univ. Firenze.

Diffusion des Neutrons et Sciences des Matériaux

The aim of this school was to encourage French (materials science) laboratories to use neutrons. Some 40 participants followed the courses given by 13 teachers not only from the neutron centres, but also neutron users from CNRS/university laboratories. Their evaluation questionnaire gave warm feedback for both the scientific programme and the organisation logistics.

This school was mainly financed by the training programme of the CNRS (Centre Nationale de la Recherche Scientifique) with financial contributions from CEA Saclay and ILL. The courses are available on the web (www.ill.fr) under ILL's documentation.

Enjoying the coffee on a lovely spring-day in Pinsot.

Aperiodic'97

Exciting talks and posters on polytypes and incommensurable phases, including phase transitions, were presented at *Aperiodic'97*, the international conference on aperiodic crystals. 150 participants from Europe and abroad enjoyed an extremely interdisciplinary approach to the discussions. It is clear that quasicrystals are catching the interest of a lot of scientists. One of the main subjects was the structure determination of aperiodic systems, which is the base of all further studies on these systems. In addition, there were interesting results on diffuse scattering associated with defects. There is an increase of simulation work comparing results with experiment. The conference was organised jointly by LTPCM (CNRS and INPG) and ILL.

The participants of Aperiodic'97.

Workshop on the PIAFE project

PIAFE is a project for a facility to extract intense radioactive ions from a fission source. 4 g of ^{235}U exposed to an appropriate neutron-flux in the PN1 (Lohengrin) channel would give about 10^{14} fissions per second. The fission products will be ionised, accelerated and mass separated. Further ionisation and post acceleration up to 6 MeV will provide beams for the studies of the dynamical properties of those unstable nuclei. A steering committee under the chairmanship of P. Armbruster was therefore established to guide the new PIAFE project and to seek funds for its implementation.

At the workshop, which gathered some 50 scientists, ILL confirmed its policy: PIAFE is a project to be supported by an autonomous scientific and technical collaboration. PIAFE is not an ILL project, but ILL wants it to be constructed and is therefore ready to take its mandatory share particularly in the domain of source-handling, radioactivity confinement and safety.

The workshop discussed the most important and recent scientific motivations for the project. It was clear that due to the enormous intensities produced by PIAFE, the project is a good candidate to fulfil [1]NuPECC's recommendations to build in Europe one or two high-intensity (second generation) radioactive ion-beam facilities

Recent developments at ISOLDE (CERN, Geneva) on radioactive ion-sources were presented. It was shown that they could be adapted to the PIAFE source, thus improving still more the competitivity of the project. But it requires new research and development which have been undertaken by the members of the collaboration.

A friendly discussion between Claire Tamburella (ISOLDE, CERN), Mitsuo Koizumi (JAERI, Japan) and Matthias Keim (ISOLDE, CERN), from left.

[1] *NuPECC is the "Nuclear Physics Collaboration Committee", an associated committee of the European Science Foundation, which is supported by most of the nuclear-physics laboratories in Europe in order to define a common and collaborative policy on the development of nuclear science.*

Congress of ATSR

ATSR (Association pour les Techniques et les Sciences de Radioprotection) held its 19th conference in Grenoble's ATRIA World Trade Centre under the motto "Half a century of radiation protection in the major nuclear facilities", sponsored by the Grenoble city council and promoted by the CEA Grenoble and the ILL. The array of radiation-protection equipment on display and the quality of the discussions helped to ensure that this 19th ATSR Congress successfully fulfilled its objectives. Its programme covered a broad range of topics:

- radiation protection strategies: developments and challenges
- radiation protection and the environment
- feedback and optimisation
- legal aspects of radiation protection
- metrology and dosimetry instrumentation
- calculation and analysis methods
- incidents and accidents
- management of radioactive waste.

To a successful congress, from left: Jacques Italia, Michel Destot, Constantin Vroussos, Paul Bory.

The progress made in the field of radiation protection over the last 50 years demonstrates that the vast majority of problems have been overcome. The experts have a thorough understanding of the technical aspects of radiation protection, even if the issues of low doses and low-level waste still need to be examined in greater detail. It is nevertheless clear that it would be worthwhile trying to improve communications between decision-makers, operatives and the general public in order to demystify the subject of radiological hazards. It is essential that staff working in and around nuclear facilities be given access to information and training, two elements which form the cornerstone of radiation protection. Two hundred delegates attended the congress, including 39 guest speakers - specialists from the field of radiation protection - who took stock of the developments in radiation protection over the last 50 years. The French Department of Employment and Department of Health were both represented, the latter through OPRI (the Office for Protection against Ionising Radiation), as was the European Union.

Brendan Gibson (left) and Reinhard Kremer (both MPI Stuttgart) uncertain about their D10 results?

Hands on in the workshop to get the sample fitted, John Archer.

Repair work on a cryostat carried out by Jean-Paul Gonzales.

A smile always helps to win the day (lucky local contact): Françoise Ehrburger, CNRS Mulhouse, changing her sample on IN10.

NEW DEVELOPMENTS

3

Continuing development in instrumentation and techniques has always been one of the fundamental pillars of ILL's success and it is essential that this tradition of innovation should continue. In this section we report some selected highlights from the last year. These are given under four headings as listed below. First there are technical developments resulting from ongoing programmes in areas such as cryogenics, neutron optics, detectors etc. Second, a number of new techniques are becoming available to users, particularly in the domain of polarised neutrons. Third, reports are given on progress with instrument upgrades, and finally some early results are given to illustrate the performance of two new instruments now available to users.

Technical Developments

New Techniques

Instrument Upgrades

New Instruments

NEW DEVELOPMENTS

Niels Pyka running a cryomagnet experiment on IN14.

Frédéric Thomas checks D10's cryogenic set-up.

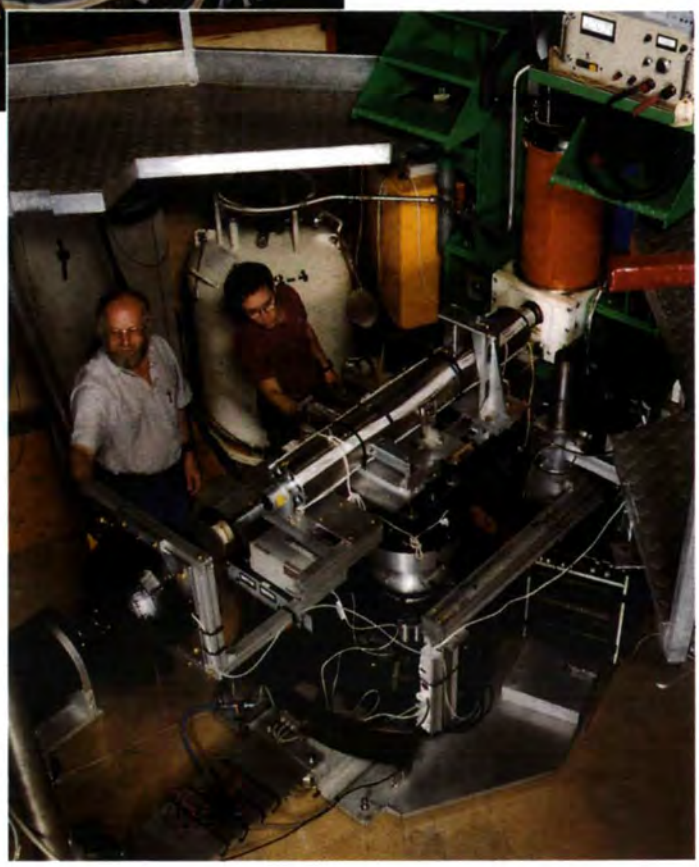

Will it work?
Francis Tasset (left) and Eddy Lelièvre-Berna on D3.

^{3}He insert for standard orange cryostat

M. De Palma, F. Thomas and S. Pujol (ILL).

In 1998, the Sample Environment Laboratory will be making available to experimentalists a simplified version of the ^{3}He insert for orange cryostats. This equipment, which is presently under test, has the following characteristics:
- maximum sample dimensions: diameter: 42 mm, length: 90 mm.
- minimum temperature: 400 mK.
- pure aluminium calorimeter (A5), internal diameter 45 mm, external diameter 48 mm.

Hence, for temperatures down to 400 mK the much more complex dilution systems can be avoided and this system, which is not more difficult to use than a standard orange cryostat, can be operated by the users avoiding the long preparation and cool-down times characteristic of dilution cryostats.

This insert features an extra cooling circuit which uses the same ^{3}He gas to cool the sample from room temperature to 4 K (see Fig. 1). Temperatures between 4 K and 0.4 K are obtained by switching to the Joule-Thomson expansion circuit also shown on the figure.

In this insert no exchange gas is required, not even for fast cool-down. Thermalisation is guaranteed in the insulation vacuum via sample holder conduction. When, for example, electric fields have to be applied to the sample this represents a significant advantage.

Nevertheless it is always possible to use exchange gas in the sample chamber just as in a classical dilution unit.

Cooling time is about 3 hours and the refrigerating power at 0.5 K is 300 μW.

In order to automate the cool-down procedure a Macintosh computer is used to control the various parameters (temperature, cold valve, etc.) of the orange cryostat and to execute the different valve sequences of the gas handling equipment. There is a graphical display of the temperature progress available to the operator.

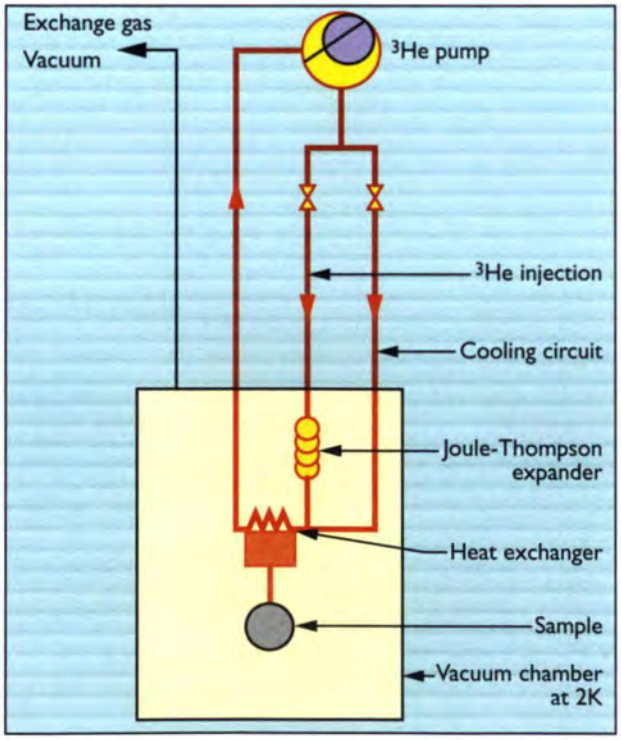

Figure 1: *Schematic view of the ^{3}He insert.*

The real view of the insert, presented by Maurice De Palma.

Neutron spin-echo studies of ultrasonically excited perfect crystals

B. Farago (ILL),
E. Iolin, E. Raitman (FEI Riga),
F. Mezei (HMI Berlin).

Perfect single crystals have relatively low reflectivity for neutrons and x-rays because they are too perfect. Ultrasonically excited crystals can show nearly an order of magnitude increased reflectivity. Here we present a first real energy-analysis of this increased Bragg scattering showing it to be inelastic in origin.

It was observed a long time ago [1] that the scattered intensity of a Bragg peak in perfect crystals (e.g. Si) can be increased by an order of magnitude when it is excited by ultrasound. At first sight this is not that surprising, as ultrasound produces local deformations in the crystal, so it should change the extinction length.

Alternatively it can be argued, that there must be some extra scattering from phonons which are excited by the external sound source. Indeed this was observed by means of x-ray diffraction [2] at extremely small deviation from the Bragg angle corresponding to the wave vector of these low-energy phonons.

With high-resolution neutron spin-echo one can resolve the small energy exchange corresponding to the ultrasound frequency. Si(111) reflection was used with the detector at 120° to choose the longest ($\lambda \approx 5.43$ Å) possible wavelength neutrons (the neutron spin-echo measures directly the correlation function S(Q, t) where the time range is proportional to λ^3). This set-up allowed the time interval up to 8 nsec to be covered. The Si(111) single crystal was placed in Laue (transmission) geometry with a transverse acoustical-wave $LiNbO_3$ transducer glued on the top with the displacement amplitude parallel to the Q-vector of scattering, $Q \approx 2$ Å^{-1}.

In Fig. 1 the scattered intensity is shown as a function of the frequency generator output voltage. (The tension feeds the transducer through a high frequency 10 × amplifier). At 73.5 MHz a 15-fold increase with still a 2-fold increase at 210 MHz of the scattered intensity could be obtained. In Fig. 2 we present the normalised correlation-function S(Q, t) measured by neutron spin-echo at 210 MHz at different excitation levels. This shows well-defined oscillations of S(Q, t) with no sign of damping which means that the sound wave excites phonons at frequency ω = 210 MHz without observable life-time. This observation is in good agreement with the small absorption and scattering of ultrasonic phonons in silicon. S(Q, ω) consists of a delta function corresponding to the elastic scattering and two additional sharp excitations at ± 210 MHz.

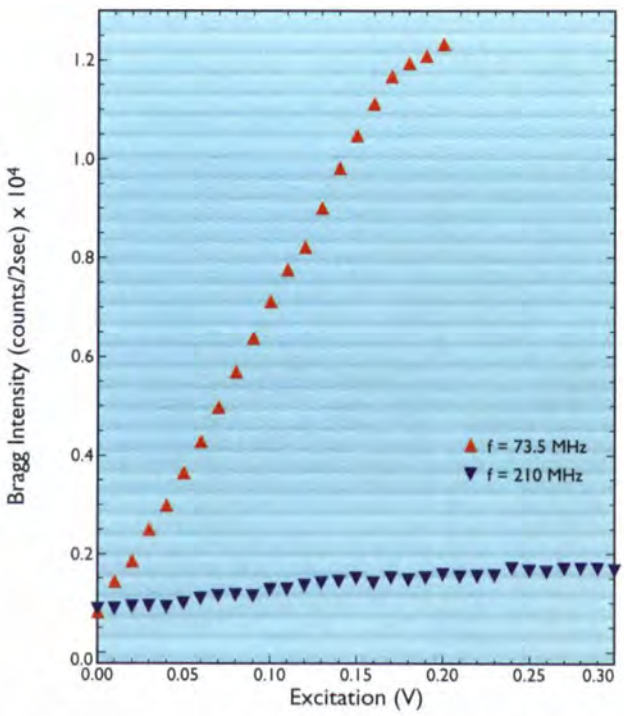

Figure 1: *Scattered intensity of the Si(111) reflection as a function of the output voltage of the frequency generator at f = 73.5 MHz and 210 MHz.*

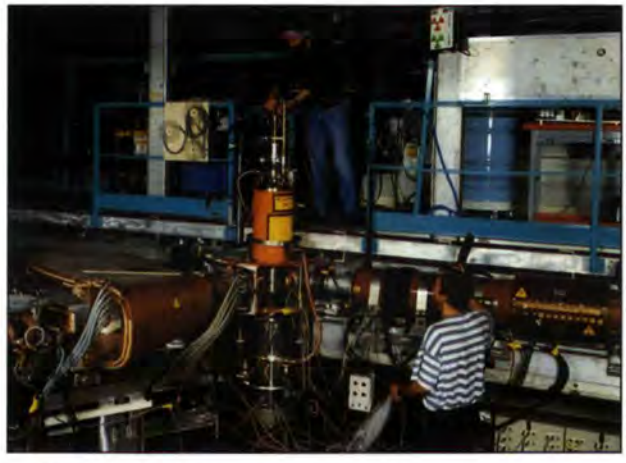

Bela Farago (right) and György Kali set up IN11C.

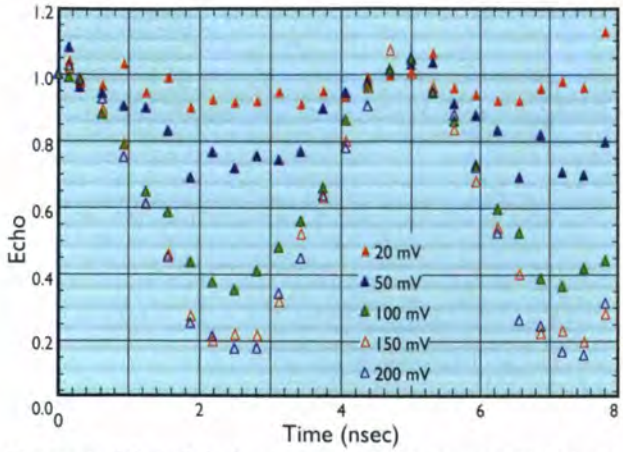

Figure 2: *S(Q, t) / S(Q, 0) as measured with neutron spin-echo at f = 210 MHz with different excitation levels. No higher harmonics are apparent, and there is no detectable damping.*

Decomposing the signal S(Q, t) into a form of const. + (1-const.)·cos(ωt) and comparing to the increased total intensity we find that in fact **almost all the additional scattered intensity is coming from the inelastic phonon scattering!**

We have to note here that although the incoming beam on IN11 is monochromatised only roughly (about 18% FWHM) the Si crystal acts as a monochromator, so no smearing in the Fourier time happens.

In Fig. 3 the 73.5 MHz data are shown. Clearly at stronger excitations the curve cannot be described any more with one single cosine function. In fact above 60 mV up to 6th harmonics at least had to be included to get a good fit to the data (solid lines). Nevertheless the amazing fact is that again the elastic intensity stays almost constant and all additional scattering is inelastic. This amounts to 87% of the total at 150 mV!

It is also well known that deformation of a single crystal increases its reflectivity by increasing the effective penetration-length as the d-spacing slightly changes through the thickness of the crystal. It might be less known [3] that the ultrasound applied to a deformed crystal first sharply decreases and then increases the reflectivity with increasing amplitude (Fig. 4).

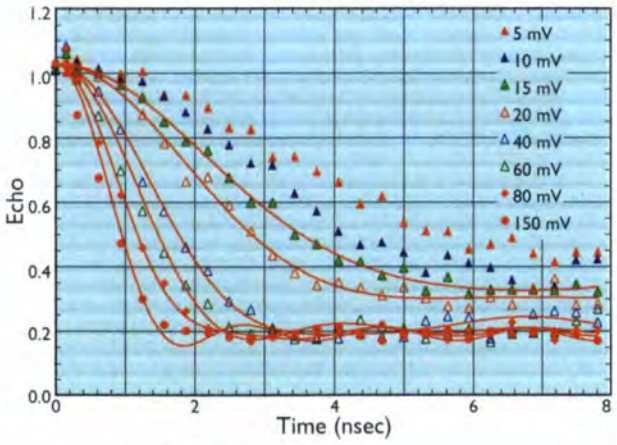

Figure 3: *S(Q, t) / S(Q, 0) at f = 73.5 MHz. The addition of higher harmonics is evident with increasing excitation voltage.*

Using neutron spin-echo we find that in fact where the total intensity decreases, the elastic intensity decreases even faster, and furthermore the phonon contribution is higher than in the case of a non-deformed crystal. There is no elementary explanation for this, one has to consider the full dynamical diffraction theory [4].

This is the first time [5] that such clear oscillatory behaviour could be observed by neutron spin-echo and we are looking forward to extend these studies to less-ordered materials.

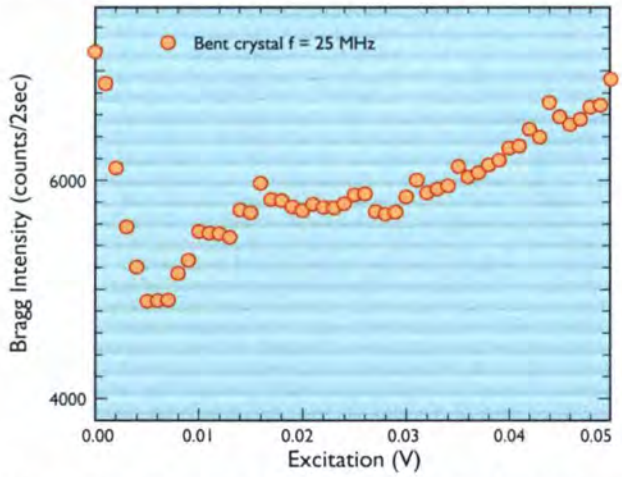

Figure 4: *Scattered intensity of the Si (111) reflection as a function of the output voltage at f = 25 MHz in the case of a bent crystal. First there is a sharp drop and then a gradual increase. Compare with Fig. 1 !*

References

■ [1] W.J. Spencer, G.T. Pearman, Adv.: X-ray Anal. 13 (1970) 507 ■ [2] S.D. LeRoux et al., Phys. Rev. Lett 35 (1975) 230 ■ [3] E.M. Iolin, E.A. Raitman, B.V. Kuvaldin, E.V. Zolotoyabko, Zh. Eksp. Teor. Fiz., 94 (1988) 218 [Sov.Phys.JETP 67 (1988) 989] ■ [4] see e.g.: V.F. Sears, Neutron Optics Oxford University Press (1989) ■ [5] E. Iolin, B. Farago, F. Mezei, E. Raitman, and L. Rusevich, Proc. ICNS'97, Physica B (1998) in press.

Spherical neutron-polarimetry with Cryopad-II

F. Tasset, J. Brown, E. Lelièvre-Berna, T. Roberts, S. Pujol and E. Bourgeat-Lami (ILL).

Spherical neutron polarimetry, the ultimate step in polarised neutron methods, allows a new approach to the study of magnetism by neutron-scattering. It is made possible by replacing the adiabatic coil arrangement used on IN20 for classical uniaxial polarisation-analysis with the zero-field polarimeter Cryopad. We give here a short description of this arrangement and two examples of magnetic studies which could not be done or were not successful using simpler methods.

Investigating the final spin state of a scattered neutron gives valuable information on what it has seen in the sample. A complete theoretical description of elastic magnetic neutron-scattering therefore includes the effect on neutron beam polarisation as well as the usual cross section. It requires two equations which are called Blume's equations and where first derived in the early 60's [1,2]. At a position $\vec{k}$ in reciprocal space, the magnetic interaction vector being $\vec{Q}(\vec{k}) = p\vec{M}_{\perp}(\vec{k})$, with $p = 0.2695\ 10^{-12}$ [cm/μ_B], the scalar equation (1) describes how the neutron cross-section depends on the initial polarisation vector $\vec{P}_i$:

$$\frac{\partial\sigma}{\partial\Omega} = NN^* + \vec{P}_i\cdot\vec{Q}N^* + \vec{P}_i\cdot\vec{Q}^*N + \vec{Q}\cdot\vec{Q}^* + i\,\vec{P}_i\cdot(\vec{Q}^*\wedge\vec{Q}) \quad (1),$$

and the vector equation (2) for final polarisation $\vec{P}_f$ is necessary to describe how the neutron polarisation is rotated and/or created during the scattering process

$$\vec{P}_f\,\frac{\partial\sigma}{\partial\Omega} = \vec{P}_i NN^* + \vec{Q}N^* + \vec{Q}^*N - i(\vec{P}_i\wedge\vec{Q}N^* - \vec{P}_i\wedge\vec{Q}^*N) + \vec{Q}(\vec{P}_i\cdot\vec{Q}^*) + \vec{Q}^*(\vec{P}_i\cdot\vec{Q}) - \vec{P}_i(\vec{Q}\cdot\vec{Q}^*) - i(\vec{Q}^*\wedge\vec{Q}) \quad (2).$$

The measurement of (1) being known as polarised neutron-diffraction, we call the measurement of (2) neutron polarimetry. Because full neutron polarimetry necessitates the simultaneous and independent control of the three components of the two polarisation vectors, we call it spherical neutron-polarimetry.

Spherical neutron-polarimetry is difficult to accomplish because the magnetic moment of the neutron interacts with small magnetic fields (like the earth's field). This results in parasitic precessions of the polarisation and spherical neutron-polarimetry is only possible using some sort of zero-field neutron polarimeter in which the initial and final neutron polarisation vectors propagate in a well-defined manner. Cryopad is, to our knowledge, the only zero-field polarimeter which is able to accomplish such a difficult task up to large scattering angles. Invented and developed at ILL [3,4], it comprises two cylindrical low-temperature Niobium Meissner shields transparent to neutrons and to their polarisation. They are key ingredients for a precise control of the magnetic field and hence of the polarisation direction along the neutron trajectory.

Cryopad-II represents the current state of this unique facility [5] (Fig. 1). It features numerous practical improvements relative to the prototype Cryopad-I:

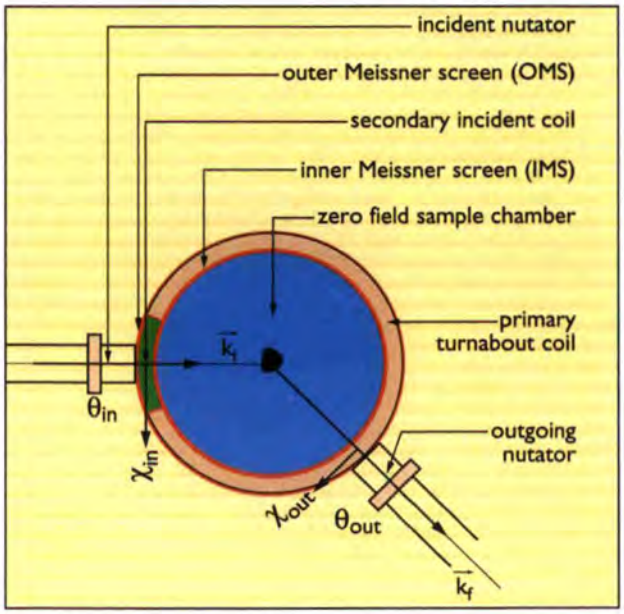

Figure 1: Schematic top view of Cryopad-II.

1. A monolithic magnetic design: higher reliability and ease of use.

2. A large diameter size for the cylindrical Meissner shields:
   - better geometrical and magnetic field precision
   - possibility to use larger beam size and samples
   - larger scattering angle (in conjunction with redesigned nutators)

3. Room temperature zero-field chamber
   - open to any non-magnetic sample environment
   - possibility to field-cool the sample outside Cryopad-II

4. Long liquid He autonomy (1 week), cheap and very easy operation

Magneto-electric domain formation in Cr_2O_3 [6]

For an anti-centrosymmetric magnetic crystal, one cannot obtain information about 180° antiferromagnetic domains by measuring the cross section or by only analysing the polarisation in the direction $\vec{P}_i$ [7]. Therefore, spherical neutron-polarimetry is the only neutron measurement able to determine such magneto-electric domain populations.

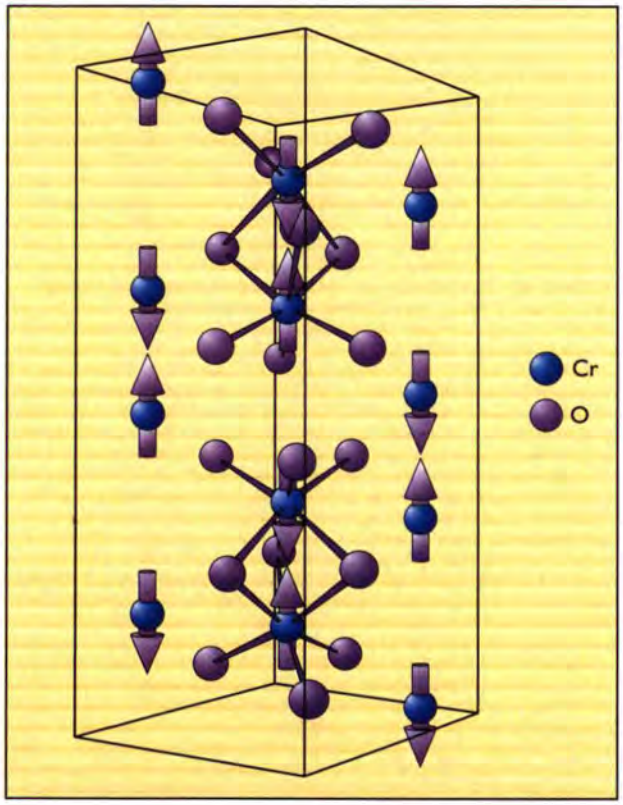

Figure 2: *The magnetic structure of Cr_2O_3. The domain which is illustrated is that which is stabilised when the crystal is cooled in electric and magnetic fields applied in the same sense parallel to $\vec{c}$.*

Spherical neutron-polarimetry was used to determine the imbalance in the population of 180° domains in antiferromagnetic Cr_2O_3 produced by cooling through the Néel temperature under different conditions. We could show that cooling with combined electric and magnetic fields along the trigonal axis leads to single domain crystals. The type of domain produced depends on whether the fields are parallel or antiparallel. The domain shown in Fig. 2 is obtained by cooling in parallel fields. The magnetic moments on the Cr^{3+} ions point towards the centre of the smaller triangle of ligand oxygens. The magneto-electric mechanism which is most effective in stabilising a particular magnetic domain during the magnetic annealing process is probably the g-factor effect.

It is to be noted that, although the spherical neutron-polarimetry measurement had to be done with zero-field in Cryopad, the prior cooling of the sample in an applied field was done outside and the sample environment device finally inserted in the large ambient-temperature chamber of Cryopad-II.

Triangular magnetic structure in $U_{14}Au_{51}$ [8]

The determination of magnetic arrangement in structures with zero propagation vector is difficult because of the coincidence of the magnetic and nuclear reflections. By looking at nuclear-magnetic interference terms which arise in such reflections, spherical neutron-polarimetry is particularly applicable to the determination of such arrangements. Contrary to a prior determination using powder neutron-scattering data which led to a collinear structure with moments parallel to the $\vec{c}$ axis, spherical neutron-polarimetry measurements on a single crystal of $U_{14}Au_{51}$ have shown that the structure is non-collinear with the U moments confined to the $\vec{a} - \vec{b}$ plane (Fig. 3).

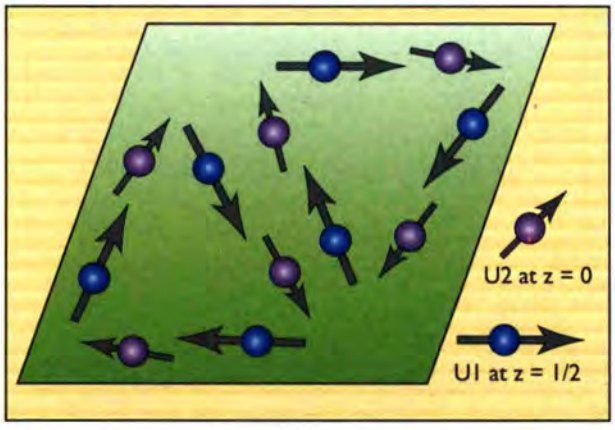

Figure 3: *Projection on (001) of the magnetic structure of $U_{14}Au_{51}$ showing the relative directions of the moments on the U1 and U2 atoms.*

References

■ [1] S.V. Maleev, V.G. Bar'yakhtar and R.A. Suris, Sov. Phys. -Solid State, 4 (12) (1963) 2533 ■ [2] M. Blume, Phys. Rev., 130 (1963) 1670 ■ [3] F. Tasset, Physica B, 156-157 (1989) 627 ■ [4] P.J. Brown, J.B. Forsyth and F. Tasset, Proc. R. Soc. Lond. A, 442 (1993) 147 ■ [5] F. Tasset, E. Lelièvre-Berna, T. Roberts, E. Bourgeat-Lami, S. Pujol, M. Thomas Proc. ICNS'97, Physica B (1998) in press ■ [6] P.J. Brown, J.B. Forsyth and F. Tasset, Journal of Physics: Condensed Matter, 10 (1998) 663 ■ [7] H. Alperin, in Int. Conf. Magnetism. 1973. Moscow: Proc. ICM-73 ■ [8] P.J. Brown, J. Crangle, K.-U. Neumann, J.G. Smith and K.R.A. Ziebeck, Journal of Physics: Condensed Matter 9 (1997) 4729.

^{3}He neutron-spin filter at ILL: first experiments

K. Andersen, W. Heil, D. Hofmann, H. Humblot, J. Kulda, E. Lelièvre-Berna, F. Tasset (ILL), O. Schärpf (TU München).

The strongly spin-dependent absorption of neutrons in nuclear spin polarised ^{3}He opens the possibility for polarising neutrons over the full spectrum of cold, thermal and hot neutrons. Optical pumping of metastable ^{3}He atoms in a plasma at 1 mbar is a very efficient method for producing large quantities of spin-polarised ^{3}He gas. Subsequent polarisation-preserving compression by a two stage compressor system allows the preparation of neutron-spin filter cells of about 300 cm^3 volume with 4 bar of polarised ^{3}He (P_{He} = 50-55%) within 4 hours. The neutron-spin filter is closed off by a valve and moved for remote operation. Relaxation times around 100 hours can be achieved in cesium-coated neutron-spin filter cells. This makes it sufficient to refill the cells with fresh gas only once a day keeping an average P_{He} close to 50%. We report results of two recent experiments performed at ILL which demonstrate the high potentiality of ^{3}He neutron-spin filter for polarised neutron applications.

The principles and method for the production of ^{3}He spin-filter cells was described in last year's annual report. Here we give two examples of the use of these filters on existing ILL instruments. The most striking example of the parity non-conservation effect in neutron optics is the discovery of the large parity non-conservation dichroism in the p-wave resonance in ^{139}La at $\lambda \approx 0.33$ Å [1]. Briefly stated, the coherent forward scattering amplitude f(0) of a neutron wave propagating through a target material in the presence of a parity non-conservation interaction will acquire a parity non-conservation component which can be written $f_{PNC} = C \cdot < \vec{\sigma} \cdot \vec{k} >$ [2], where $\vec{\sigma}$ is the Pauli spin and $\vec{k}$ the neutron wave-vector, and where C, which can be complex, is the parity non-conservation amplitude. The imaginary part of f_{PNC} describes the helicity-dependent neutron absorption (dichroism) [3], while the real part indicates a different phase-velocity for the two neutron helicity states which is equivalent to a rotation of the neutron spin about its momentum vector. At the D3 neutron diffractometer, the incident neutrons from the hot source were polarised and monochromatised using the 200 reflection of a CoFe crystal. Both parity non-conservation dichroism and parity non-conservation spin-rotation were measured, using a zero-field polarimeter constructed at Gatchina (A. Serebrov, A. Petukhov et al.). Finally, the unit of crossed polariser and analyser with a 5 cm thick ^{139}La-target in between were added to the set-up (expected spin-rotation: $d\Phi_{PNC}/dl \approx 4$ mrad/cm). The ^{3}He-neutron-spin filter in this case was used as an analyser. Preliminary results on parity non-conservation spin-rotation are presented in Fig. 1 and show the statistical accuracy achieved in a 12 hours of counting time. In total the measurement lasted 3 weeks, in the course of which two cylindrical ^{3}He cells optimised for short wavelengths were used in a sequence of daily interchange. Their relaxation times were 60 and 90 hours, respectively. Fig. 2 shows the wavelength dependence of both the analysing power A deduced from the measured flipping ratio and the total

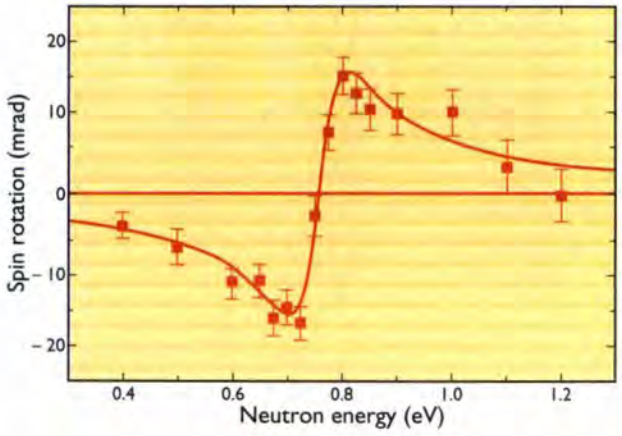

Figure 1: *Parity non-conservation neutron spin-rotation Φ_{PNC} observed in the vicinity of the p-wave resonance in ^{139}La. The error bars on the data points give the statistical error achieved after 12 hours of data-taking. The solid line shows the theoretical prediction.*

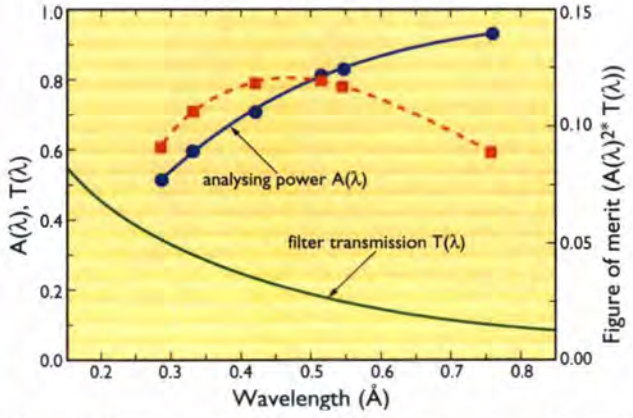

Figure 2: *Wavelength dependence of both the analysing power A deduced from the measured flipping ratio and the total transmission T_n for a cylindrical neutron-spin filter cell with l = 20 cm, Φ = 5 cm, P_{He} = 3.02 bar and P_{He} = 52%. Dashed line: wavelength dependence of the figure of merit for the ^{3}He filter.*

transmission T_n of the neutron-spin filter cell.

Projected experiments along these lines try to increase the experimental accuracy by at least three orders of magnitude in order to reach the predicted sensitivity needed to investigate P, T-violating effects [4]. In particular, it has been shown that the P, T-violating interaction is enhanced near a p-wave resonance by the same factors as in the case of P violation [5].

The second experiment demonstrated the possibility of large solid-angle polarisation analysis. In order to exploit the rich spectrum of possibilities of polarisation analysis a large solid-angle instrument can gain a significant advantage in counting rate over a single detector system. At ILL the diffuse scattering instrument D7 is equipped with 32 analysers incorporating a total of 6 000 supermirrors which are distributed over an angular range of 180° in the equatorial plane [6]. The mirror reflectivity drops off rapidly for neutron wavelengths shorter than 3 Å which prevents their use for thermal neutrons. ^{3}He-neutron-spin filter however, can be used for both cold and thermal neutrons. Positioned close to the sample a large fraction of 4π can be covered making its use feasible on existing multidetector instruments. The neutron-spin filters were placed to the left and right of the sample (silica glass) on D7 and fixed on a turn-table with the sample centred on the axis of rotation. Each cell covered 90° in the equatorial plane. The two banana-shaped cells were made out of ordinary silica glass internally coated with cesium which showed a relaxation time of 15 hours only, resulting in an average ^{3}He polarisation during the measurement of $\overline{P}_{He} = 30\%$ at p = 2.2 bar.

The monochromatic beam ($\lambda = 4.8$ Å) on D7 is polarised by a supermirror bender polariser which is followed by a flipper placed between the polariser and the sample. Helmholtz coils provided a homogeneous guiding field in the vertical direction for both neutrons and the ^{3}He spin. Fig. 3 shows the measured flipping ratios for both cells by scanning them through the direct beam. They were monitored using a ^{3}He detector unit positioned downstream from the sample table. As expected, a constant flipping ratio can be observed which reaches 6 and 8.5 respectively. With the ^{3}He neutron-spin filter cells in the scattered beam, however, the flipping ratio is reduced and strongly correlated to the measured counting rates in the individual detector units. The reason for this can be traced back to the poor transmission T of neutrons through the walls of the ^{3}He container (T ≈ 60%) at this wavelength.

The cell itself acts as a second scatterer and background cannot be subtracted in the usual way. In particular neutrons scattered from the cell edges which do not pass through the full filter-length dilute the effective analysing power. A mark II version of a banana-shaped cell is now under construction and will be made out of pure silicon which is highly transparent for neutrons, and in this way we hope to get a uniform distribution of flipping ratios in the scattered beam. Using silicon single crystals as a container material or at least for certain parts such as entrance and exit windows will have several advantages. It will for instance allow polarisation analysis on small-angle neutron scattering instrumentations without lowering the high angular resolution of such devices.

In conclusion, the availability of the ^{3}He filter and its use on a variety of existing instruments at ILL has been shown. It is a realistic perspective that further improvements of the present technology will provide neutron-spin filter cells with a ^{3}He polarisation of about 70%. This was the declared aim from the early stage of this project.

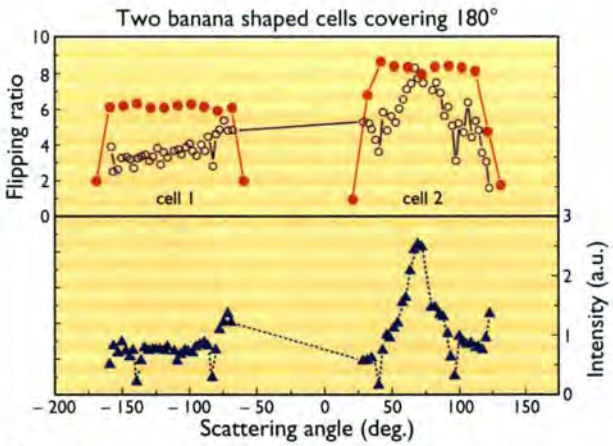

Figure 3: *Large solid-angle polarisation-analysis. Full circles: measured flipping ratios by scanning the neutron-spin filter cells (No.1, No.2) through the direct beam. To facilitate a direct comparison the data points are shifted to the actual angular positions of the cells in the scattered beam arrangement. Open circles: measured flipping ratios in the scattered beam (silica glass scatterer) in the angular range of the D7 detectors of [– 70°, – 160°] and [30°, 120°], respectively. Triangles: intensity measured in the individual detector units.*

References

■ [1] V.P. Alfimenkov, S.B. Borzakov, Vo Van Than et al., Nucl. Phys. A398 (1983) 93 ■ [2] V.E. Bunakov and V.P. Gudov, Nucl. Phys. A401 (1983) 93 ■ [3] B.R. Heckel, Nucl. Instr. Meth. A284 (1996) 66 ■ [4] S.K. Lamoreaux and R. Golub, Phys. Rev. D50 (1994) 5632 ■ [5] V.E. Bunakov and V.P. Gudov, J. Phys. (Paris) Colloq. 45 (1984) C3-77; JETP Lett. 36 (1982) 329; Z. Phys. A 308 (1982) 308 ■ [6] O. Schärpf, Physica B 156-157 (1989) 681; Physica B 156-157 (1989) 639.

INSTRUMENT UPGRADES

Continuous efforts are made to upgrade the performance of all instruments but progress is limited by money and manpower rather than by ideas. Nevertheless, progress has been made, e.g. the extension of the Q-range of the spin-echo spectrometer IN11. News on this spectrometer and a continuous update on instrument improvements can be found in the « ILL News for Reactor Users » which appears twice a year. One example is given here, the improvements to the diffractometer D1A for its use in stress measurements.

In addition, ILL has launched a major upgrade programme of 5 instruments planned for the period 1996 – 2000. This involves the straightening of two neutron guides and the re-siting of two instruments to view the full guide apertures: D17 which is being rebuilt as a dedicated reflectometer and the low-Q diffractometer D16 which will have a new focusing monochromator and new detector.

The work on the guides is currently in progress and the old instruments D16 and D17 have been dismantled – the upgraded instruments are scheduled to begin commissioning before the end of 1998. These changes will also permit the time-of-flight spectrometer IN5 to receive all the neutrons from its guide (previously shared) and it will be equipped with a focusing guide and a new chopper system, the specification for which is now finalised.

There are two remaining upgrades in progress. One is the rebuild of the primary spectrometer of the three-axis instrument IN8, which is being carried out in collaboration with Spain and for which design work is currently in progress. The final project is the replacement of the detector system on the diffractometer D4 by a new system based on nine microstrip detectors which will increase the count rate by a factor of ten. A separate report is given below on the first, very successful test of the prototype detector.

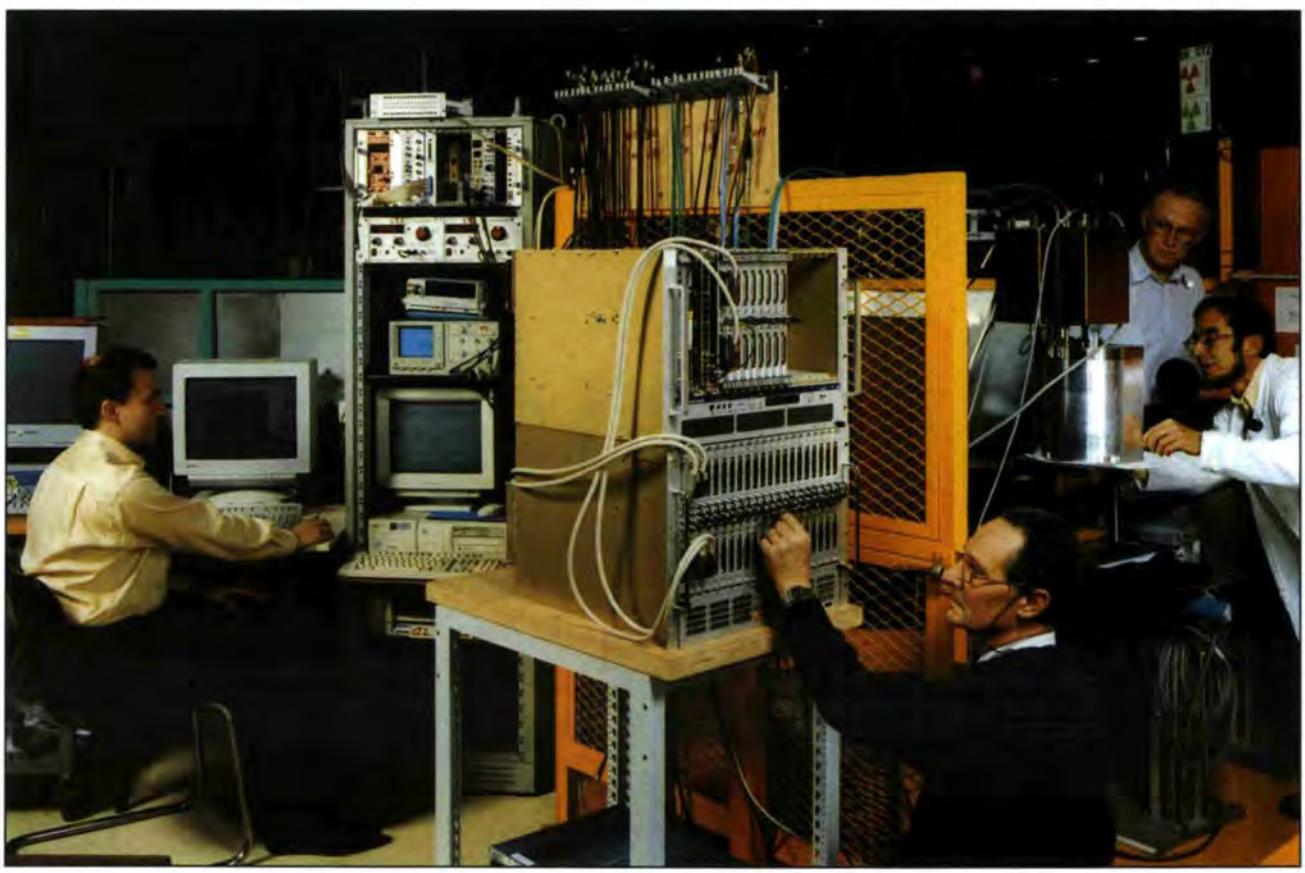

Tests on D4C (from left: Henry Fischer, André Rambaud, Dominique Feltin, Pierre Palleau).

Recent developments in the D4C diffractometer project

H. Fischer (ILL).

The D4C project involves replacing the 2 existing multiwire detectors of the D4B liquids diffractometer with 9 microstrip detectors, thereby greatly increasing both the counting rate and detector stability. These two criteria are essential to extending the range of feasible isotopic-substitution experiments. The D4C prototype detector was successfully tested in Nov. 1997 along with the new instrument control and data-acquistion system. Further tests will be conducted in early 1998 in order to finalise the designs for neutron shielding and collimation.

The D4 instrument in its present configuration, D4B, is optimised for diffraction experiments on liquids and amorphous solids, having a relatively high incident flux at short neutron wavelengths. The 9 microstrip detectors of D4C will increase the solid angle of detection and hence the counting rate by a factor of 10 compared to the average configuration for D4B's 2 multiwire detectors, in addition to improving the stability of detector cell efficiencies. High counting rate, good detector stability and low background counts are crucial features for accurate measurements of static structure-factors, especially in the context of sensitive isotopic substitution experiments used for determining partial structure-factors.

The D4C prototype detector was tested in Nov. at the test beamline of ILL's detector group. The 1-dimensional 64-cell detector, which is the world's first microstrip detector to function at 15 bar ^{3}He, performed to expectations on the very first day of tests. Fig. 1 shows a close-up of the frontside of the D4C prototype which has a detection height of 100 mm and width of 64 × 2.5 = 160 mm. The experiments also successfully tested the new VME + UNIX instrument control and data-acquisition system, whose software permitted storage, retrieval and analysis of data sets from the prototype detector.

The microstrip technology for D4C is the same as that already in service for the newly operational D20 detector. In a microstrip detector, the ionisation electrons resulting from the ^{3}He(n, p)^{3}H + 764 keV nuclear reaction are attracted to a substrate of electrically conducting glass which supports the high voltage anodes and cathodes in the form of an array of closely spaced (~ 1 mm period) metallic strips. The strong electric field near the very narrow (10 µm) anodes precipitates an avalanche cascade of secondary ionisation, resulting in a very large gas gain for a given applied potential. The proximity of the cathodes ensures a rapid evacuation of positive ions and therefore a very small intrinsic deadtime that is, however, convoluted with the collection time of the total charge produced along the particle traces, being on average about 1 µs for D4C.

The choice of a comparable electronic integration time-constant leads to an optimised trade-off between energy resolution and maximum counting rate, the latter being about 200 kHz per detector cell for D4C after accounting for coincidence logic and Poisson statistics corrections. Other than the stable fixed nature of the substrate-supported electrodes, the superior energy-resolution as compared to conventional multiwire detectors leads to an improved stability in detector-cell efficiencies. The goal for D4C is to have cell efficiencies stable to 10^{-4} over several days.

The spatial resolution is determined fundamentally by the mean path-length of the nuclear reaction particles (proton and triton) in the gas mixture; in our case the choice of 0.3 bar CF_4 quench gas and 15 bar ^{3}He gives about

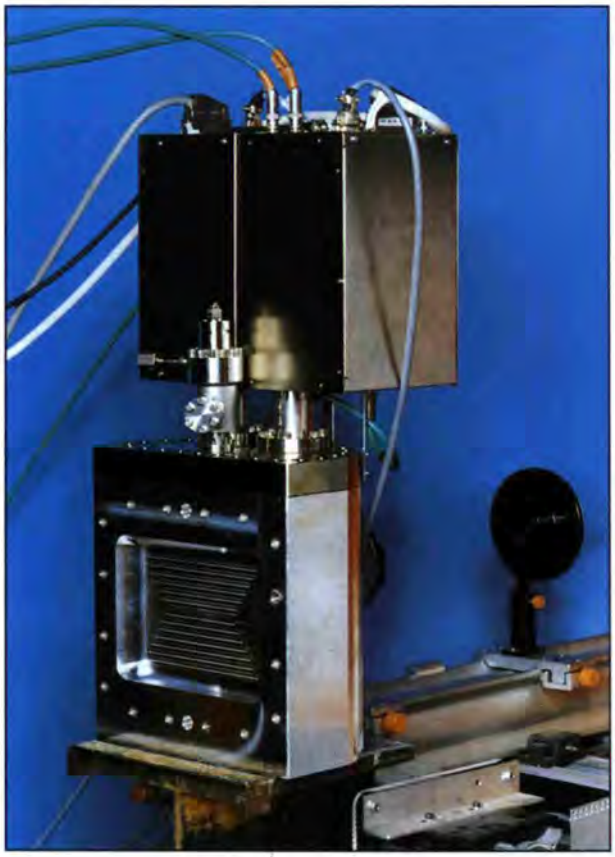

Figure 1: *Close-up of the D4C prototype detector (front face).*

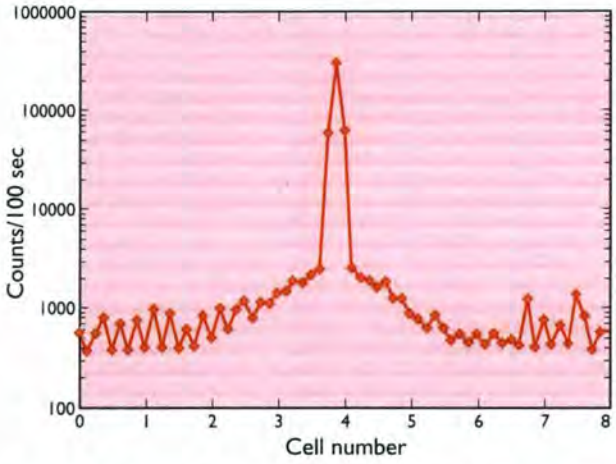

Figure 2: *D4C detector response for an incident beam width of 1 mm. The cell spacing is 2.5 mm.*

2.3 mm, which is slightly smaller than the cell spacing of 2.5 mm (each cell consisting of 2 anodes + 2 cathodes). Fig. 2 shows the response of the D4C prototype detector to an incident beam ($\lambda = 2.5$ Å) of 1 mm width and 25 mm height centred on the 32nd cell. The diffuse tails, resulting from diffraction by the 10 mm thick aluminium entrance windows, are at the 1% level and are not problematic for diffraction from liquid or amorphous samples. Fig. 3 shows a diffraction diagram from a sample of polycrystalline sapphire (Al_2O_3).

In order to insure low background neutron counts for the D4C detector system, whether ambient or due to secondary diffusion from the sample, several materials have been tested for the D4C collimation and shielding design. For example, the lowest-angle detector's beam-stop and collimation will be made of high-density $^{10}B_4C$, having an absorption constant of about 160 cm^{-1} for neutrons of $\lambda = 0.7$ Å (80 cm^{-1} for $\lambda = 0.35$ Å). The ambient neutron shielding will consist of several centimetres of thermalising material (e.g. polyethylene) followed by borated polymer and finally cadmium. The precise design of the D4C shielding and collimation will be finalised following the results of tests with the prototype detector at the D4 experimental zone in early 1998. The final 9-detector assembly should be tested in early 1999. The D4C project is expected to engender a total downtime for the D4 instrument of only about 1 month.

Acknowledgement

The participation of the following individuals in the D4C project is greatly appreciated (listed in no particular order): P. Palleau as technical coordinator; D. Feltin and the other members of the detector group; F. Cecillon, J. Munnier and others in the Service Contrôle des Instruments; G. Viande, S. Rowe, and Ph. Malbert of the Bureau d'Etudes; and finally P. Chieux, Ph. Leconte and others having a consultative or administrative role.

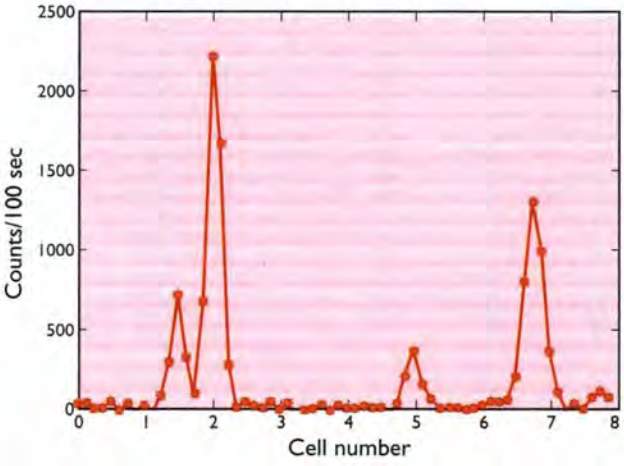

Figure 3: *Diffraction diagram for a sample of sapphire (3 mm diameter cylinder) as measured by the D4C prototype detector.*

Stress measurements on D1A: a new high precision strain-scanner

T. Pirling and R. Wimpory (ILL).

A number of big improvements for strain-scanning has been carried out on the 2-axis high-resolution diffractometer D1A. Alignment has become easier with the addition of laser, TV-camera and theodolites. The recent addition of a highly efficient two-dimensional position-sensitive detector has reduced data-acquisition time considerably. A Eulerian-cradle and a smart stress-rig for 15kN load extend the applications of the instrument. An important development is the addition of a radial collimator instead of slits, that are normally used for strain-scanning experiments. Computer simulation and first measurements have shown that a collimator is essential for the performance of precise measurements.

The neutron strain-scanning method has become more and more important as a non-destructive method for measuring stresses in all kinds of materials with crystalline phases, such as metals, alloys, ceramics and composite materials. These materials are of industrial relevance as well as of interest for the materials scientist. As neutrons can penetrate materials up to several centimetres the method is applicable to real components as well as to small mock-ups or just samples of a material. The applications range from analysing stresses during manufacturing at different stages of production - extrusion, rolling, machining, welding, heat-treatment - and causes of failure of used components to the development of new materials and the verification of computer models. It is also a good method to calibrate other measuring techniques and determine elastic constants of materials.

The high penetrating power of neutrons means that this is the only non-destructive method that gives space-resolved information about stress deep within materials. The probe for stress is the d-spacing of the crystalline phases in the sample. Their variation must be measured with high accuracy, typically $\Delta d/d = 10^{-4}$. From the shift of the corresponding Bragg-peak one gets information about the (elastic) stress state whereas analysis of the peak shape can give information about plastic deformation.

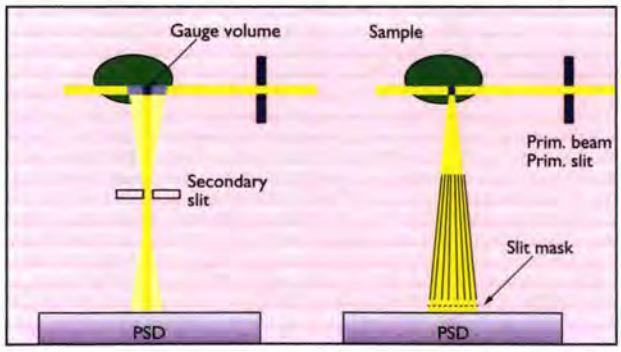

Figure 1: *Different set-ups for strain scanning: on the left side the common set-up with slits. On the right side the radial collimator now installed at ILL. (PSD = position-sensitive detector)*

The common set-up of a strain scanner is shown in Fig. 1 (left). It consists of a high-resolution (neutron) diffractometer with an xyz-translation table for sample positioning and a pair of slits that defines the measuring or gauge volume. The gauge volume is at a fixed position in the centre of the diffractometer and the sample is moved to scan its properties.

The size and shape of the primary beam is defined by an aperture close to the sample. A vertical slit is positioned in front of the detector and as close to the sample as possible. (Fig. 1, left). These two apertures define the gauge volume. But this is an oversimplification and it is not only the divergence of the neutron beam that leads to inaccuracies as we will see later. What are the requirements on a high-precision strain scanner?

There are two types of resolution to be considered: lateral and angular resolution. The latter means the accuracy with which the peak positions can be determined. As the peak-shifts are much smaller than the peak width this is a question of how well the peaks can be fitted. High counting rates and many measuring points in the peak are needed. The strain scanning set-up at D1A includes a highly efficient two-dimensional position-sensitive detector, developed at the ILL. With this detector high counting-rates in a reasonable time with angular resolution of better than 0.05° in 2 θ are possible. Measuring the true peak-shape is also important for a good fit and, of course, for the analysis of plastic deformation. This is a question of the performance of the optical components. They are also responsible for the lateral resolution because they define the gauge volume.

We have developed a computer simulation program to determine the accuracy of the experiment. The program calculates the image of the peak on the detector while scanning the sample through the gauge volume, performs

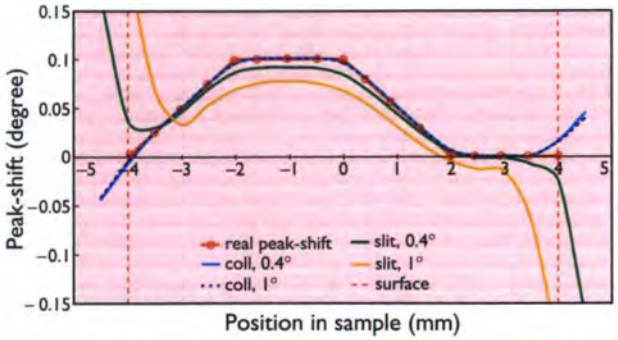

Figure 2: *Simulations of a scan along a linear stress gradient and through a surface (red curve) in an iron like sample. The diagram shows a comparison between the use of a secondary slit and a collimator for two different peak-widths: 0.4° and 1°. The measured peak-shifts are the same for the collimator (blue curves, almost superimposed) but depend a lot on peak width for the slit (yellow and green curves). The surface effect is much smaller for the collimator extending to less than 0.5 mm below the surface. This shows the good definition of the gauge volume which is nominally 1 × 1 × 1 mm³ in both set-ups. Note that there are errors along the gradient even with the gauge volume totally in the sample when using the slit set-up.*

a fit and plots the resultant peak parameters. This leads to some surprising results concerning the slit set-up.

The computer model of the slit set-up shows that the size of the gauge volume is not well defined. Apart from beam divergence it is not sharp edged, its size depends strongly on the peak width, the detected peak shape becomes asymmetric at interfaces and along stress gradients which leads to misinterpretation of the peak position and makes peak-shape analysis impossible. Fig. 2 shows the result of the simulation of a scan through an artificial sample that contains a stress gradient as well as an unstressed surface region to see the consequences of the surface effect itself. The surface effect occurs at interfaces and surfaces and means that the centre of gravity of the emitted radiation is shifted when the gauge volume is only partially filled. This leads to a shift of the peak position on the detector. In case of a slit system the peak also becomes asymmetric which complicates peak fitting.

The yellow and green curves show the result using a conventional slit for peak widths of 1° and 0.4° respectively: there is a strong dependence of the measured position on the peak width. As these errors depend on the sample it is impossible or at least very difficult to correct them properly. But simulations show also that there are conditions under which precise measurements can be performed with the slit set-up. These are roughly: the peak-width should be smaller than 0.3° and the distance of the secondary slit to the gauge volume should be less than 20 mm. This allows only measurements near the surface or in small samples. But it is the big advantage of the neutron method to penetrate right through thick samples. So the slit does not then meet the requirements for accuracy.

The solution to these problems is to use a radial collimator positioned between sample and detector (Fig. 1 right). The results of the simulation for this set-up are also shown in Fig. 2 (blue curves). The collimator defines the secondary component of the gauge volume as nearly ideally sharp and independent of the properties of the sample. There is no additional peak-shift near stress gradients nor any dependence on the peak width. Only the surface effect remains but it is much smaller because of the good definition of the volume, and, more importantly, it is an instrumental constant which can be corrected. In all measuring conditions, including the surface, the detector sees the true peak shape of the reflection so that peak-shape analysis is now possible.

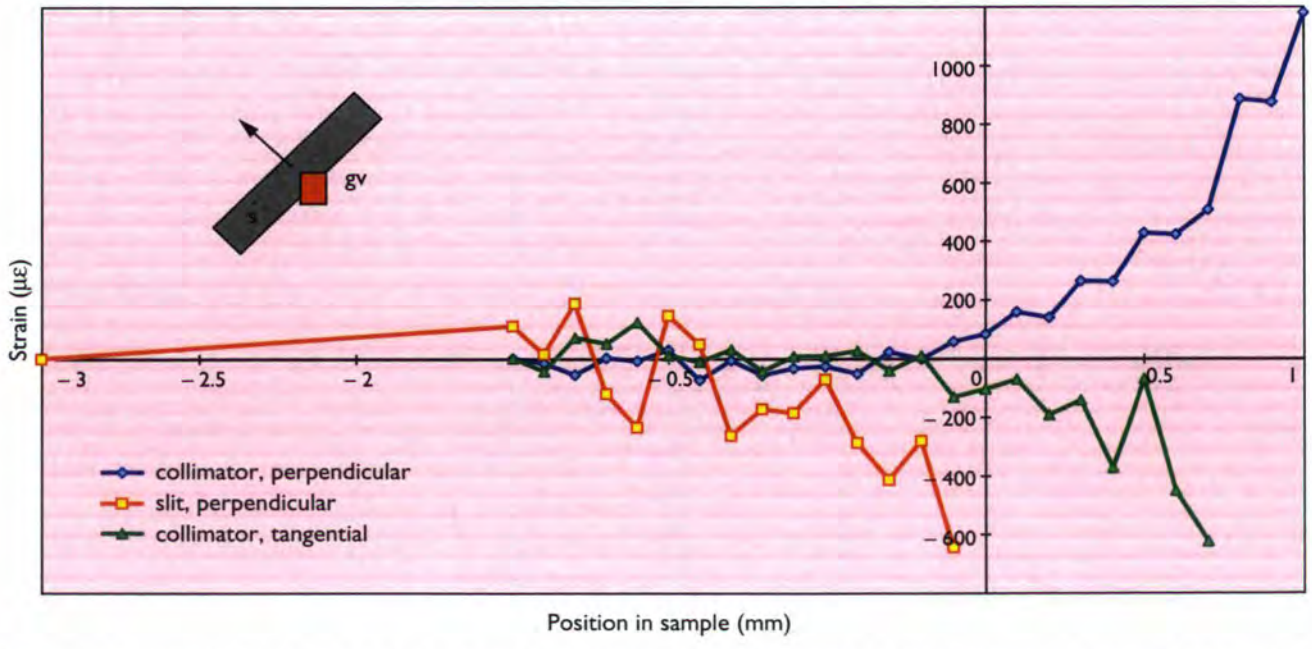

Figure 3: *Measurement of pseudo-strain near the surface of a powder sample. The* ***inset*** *demonstrates how the gauge volume (gv) penetrates the sample (s) in reflecting geometry. Transmission geometry means the sample is turned by 90° so that the scattering vector is parallel to the surface. « Position in the sample » means the position of the centre of gravity of the gauge volume. 0 is the position at the surface, negative positions are in the sample, positive positions outside.*

In August 1997 the strain scanner at the D1A high-resolution powder diffractometer, was equipped with a radial collimator and a 2-dimensional position-sensitive detector. The collimator is 450 mm long and has 22 channels each with an input aperture of only 0.42 mm and a divergence of 0.19°! It was specially made by Euro-Collimators (U.K.) and shows excellent performance. The focal length of the collimator is 150 mm and it leaves enough space for many applications. By installing different slit masks at the end of the collimator - next to the detector - the gauge volume can be defined between 0.5 and 1.1 mm.

The angular resolution of the detector depends on its distance from the gauge volume and is typically 0.05° per channel.

A first experiment to verify the performance of the collimator is shown in Fig. 3. It focuses on the problem of the surface effect that results in what are called pseudo-strains when analysing data, because measured peak-shifts are caused by instrumental errors and not by the sample. To be able to measure the surface effect without additional complications we used for the measurements a rectangular shaped thin-walled aluminium container filled with Ni-powder, so that the sample has no strain gradient. The reflection measured was the (111) which occurs at 94.7° in 2 θ at a wavelength of 2.99 Å. Two scans were performed: one with the scattering vector perpendicular to the surface (arrow in Fig. 3) and the other with the scattering vector parallel to it. The sample was scanned perpendicular to the surface. From the fitted peak positions the strain was calculated and is plotted in Fig. 3. One can see that using the collimator the surface effect starts at less than 0.5 mm in the sample, whereas it starts already more than 1 mm below the surface for the slit geometry, which is in good agreement with the simulations.

The simulations and measurements described above show that the diffraction peak-shape is not distorted when using the collimator which is therefore important for the accurate determination of peak shapes. Fig. 4 shows an example: the results of a measurement of the 110 reflection of an iron tube, bent so as to have 10% plastic deformation in the tensile and compressed regions. The object of the experiments is to relate the microscopic behaviour as revealed in the diffraction peak-positions and widths to the macroscopic properties important to the engineer.

Data were obtained for both the radial and axial direction for which the results for the broadening were almost identical. The peak broadening is related to the plastic deformation and this relation has to be established by calibration experiments specific to the sample material being measured.

By comparing peak shapes with known deformations (tensile, compressive and a combination of the two) as well as microscopic modelling of plastic deformation, the information obtained in a diffraction peak can be interpreted with more accuracy.

Conclusion

The ILL now has available a high-precision strain scanner equipped with a radial collimator which has been shown to be essential for accurate measurements. Examples of experiments already performed are plastic strain in metals and residual stress in wear-resistant new generation coatings in synchronisers for automotive gears.

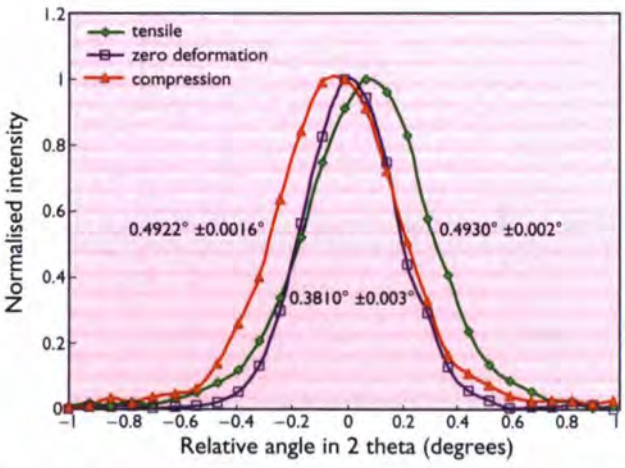

Figure 4: *The (110) iron reflection using a wavelength of 2.99 Å for a gauge volume of 1.1 mm³ in the tensile, undeformed and compressive regions of a bent iron tube. The full peak widths at half maximum in 2 θ are inserted in the graph.*

Thilo Pirling (left) and Robert Wimpory show the previous D1A set-up with slits and the position-sensitive detector. The stress rig is on the sample table.

NEW INSTRUMENTS

In the last year the ultra-high-resolution spin-echo spectrometer **IN15**, a joint project between **ILL**, **HMI** Berlin and Forschungszentrum Jülich, has been scheduled for users. **ILL** users have access to about 50% of the available beam time and the instrument is opening up to neutron studies a new range of Fourier time approaching half a microsecond. Further options (time-of-flight and very low **Q**) will become available during the next year.

The 2π image-plate detector optimised for **LAUE** studies of biological crystals (**LADI**) has seen its development phase reach fruition and it will be scheduled for users on a half-time basis in 1998 with the low-resolution diffractometer **DB21** being reduced from full to half time. Both these instruments will be operated jointly with **EMBL**.

An example of the performance of **LADI** for biology is given here together with two examples demonstrating its power for small molecule and magnetic problems when mounted on a thermal beam.

The construction of the new **ILL** thermal time-of-flight spectrometer **IN4** is now completed, but problems related to the necessary protection of the reactor against the risk of explosion of the background chopper have delayed the commissioning. However, testing of the choppers with neutrons, using an aluminium shield between the first chopper and the reactor, started at the end of 1997. The shield is transparent to a large fraction of the neutron flux. First tests will be made with a fixed vertical curvature, horizontally flat monochromator because of difficulties with the curvature mechanism for the variable focusing monochromator. Although full performance of the instrument will not be available initially we look forward to carrying out the first commissioning experiments in the first half of 1998.

Two new instruments constructed by collaborating research groups (**CRG**s) have come into operation in 1997: the reflectometer **ADAM**, described below on which **ILL** users will have 30% of the beam time, and **AVOGADRO**, a dedicated experiment (**CRG-C**) which has no user access. **AVOGADRO** is an experiment from the **PTB** Braunschweig which uses prompt (n,γ) spectrometry to determine impurity levels and their spatial distribution in high-purity silicon monocrystals in connection with a long-term project to improve the accuracy of the Avogadro constant.

The reflectometer ADAM is operational

R. Siebrecht, A. Schreyer, F. Adams, H. Zabel (Ruhr-Universität Bochum).

Since summer 1997 the reflectometer ADAM (Advanced Diffractometer for the Analysis of Materials) is available to the neutron community. Outstanding features like high intensity, large dynamic-range and high resolution make ADAM an excellent tool to probe density profiles. Furthermore, the availability of polarised neutrons with spin analysis offers extended possibilities in the field of magnetic reflectivity at ILL. A variety of sample environments like a cryo-furnace, a magnet and a gas-loading chamber are offered for this new instrument. As a collaborating research group instrument ADAM was conceived and is operated by the University of Bochum/Germany. It is available for users via ILL proposals and the Deutsche Verbundforschung.

After a construction and test phase of about one year the new reflectometer ADAM is now open to users. Since 1996 a variety of tests have shown the instruments high performance [1]. Fed by a cold source (neutron guide H53) the (002) graphite monochromator selects a wavelength of $\lambda = 4.4$ Å at the peak-flux position of the neutron guide. The monochromator focuses the beam vertically down to a height of 50 mm (FWHM) at the sample position. The scattering plane is horizontal and thus suitable for the study of any non-liquid sample. In Fig. 1 we show the reflectivity of a sputtered iron isotope superlattice of the following composition:

50Å Pd / 90Å ^{56}Fe / [10Å ^{57}Fe / 90Å ^{56}Fe]$_{15}$ / MgO.

Since neutrons are sensitive to isotopes and due to ADAM's high dynamic range we measured superlattice peaks up to the 6th order. Additionally, we were able to easily resolve thickness oscillations of a total sample thickness of 1650 Å (see inset of Fig. 1). This clearly demonstrates the instrument's high resolution. The option of polarised neutrons with spin analysis offers the possibility to study vectorised magnetic-density profiles. The polarisation analysis set-up is characterised by a high efficiency with flipping ratios of 35 under ordinary experimental conditions. The high flux (e.g. $2 \cdot 10^6$ n·cm^{-2}·s^{-1} For a collimation of 1 mrad) at the sample position and the low background yield a dynamic range up to eight orders of magnitude as demonstrated by the reflectivity of a Si wafer in Fig. 2. In Fig. 3 we show different reflectivity curves for a sputtered [15Å Cu / 34Å Co]$_7$ / Al_2O_3 superlattice with a strong uniaxial magnetic anisotropy. The measurements reveal the orientation and the magnitude of the magnetic in-plane Co moments for two distinct sample orientations. In 3a) the ferromagnetically coupled moments are aligned

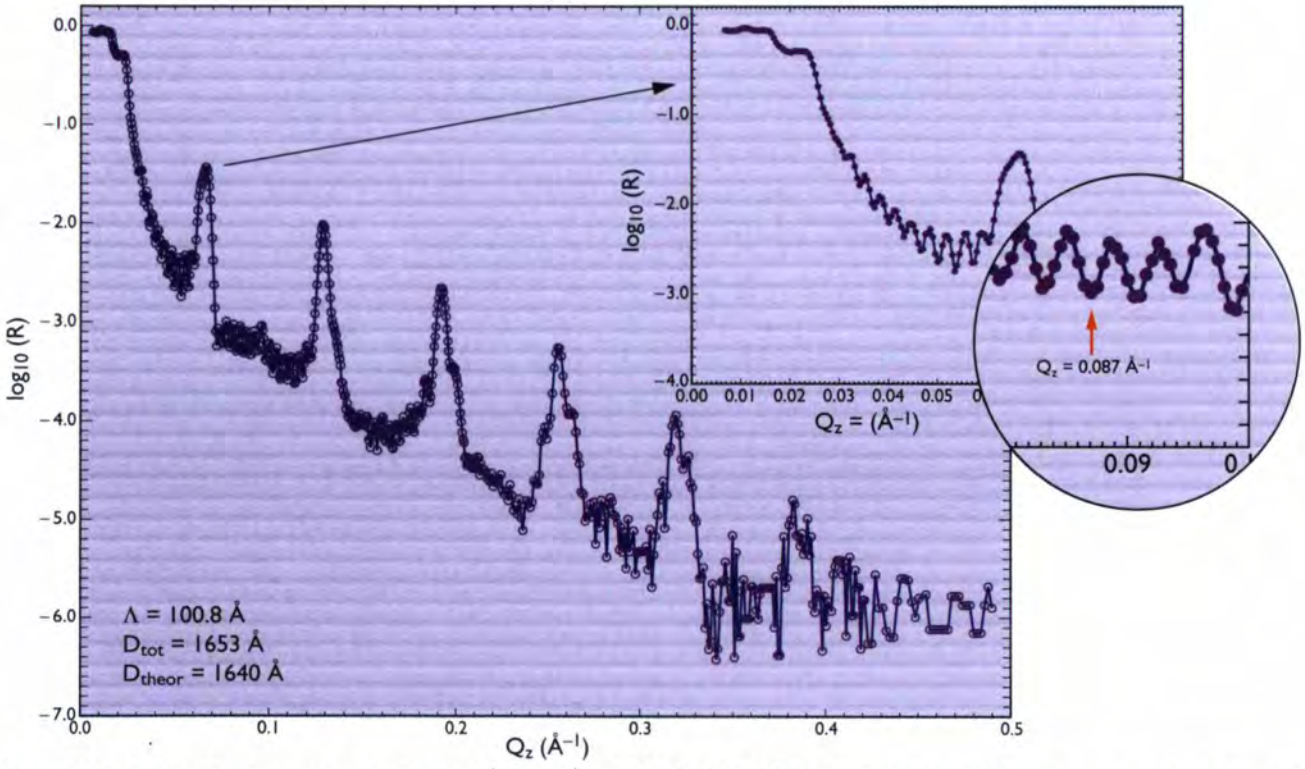

Figure 1: *Reflectivity of an iron isotope superlattice (50Å Pd / 90Å ^{56}Fe / [10Å ^{57}Fe / 90Å ^{56}Fe]$_{15}$ / MgO). A wide dynamic range combined with a high resolution made it possible to measure 6 superlattice oscillations and thickness oscillations for a total sample thickness of 1653 Å.*

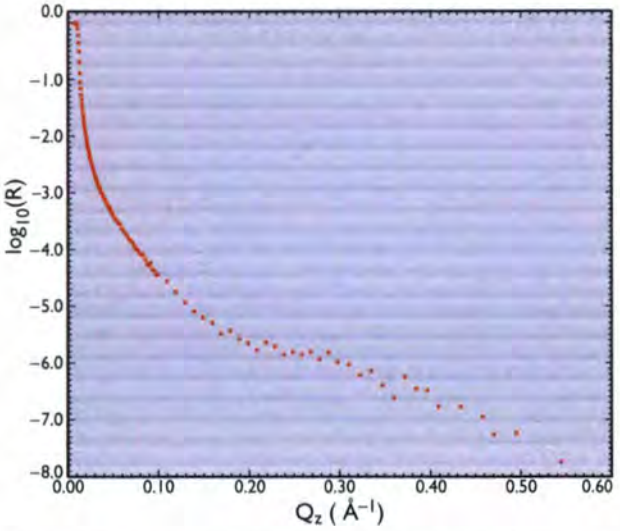

Figure 2: *Reflectivity of a Si wafer over nearly 8 orders of magnitude measured with ADAM.*

along the polarisation axis of the neutrons which yields a large splitting between the + + and the – – reflectivity.

In 3b) the magnetisation vector is rotated by 90° to be parallel to the spin-flip axis as shown on the right-hand side. Now the orientation of the magnetic moments gives rise to a purely magnetic signal in the – + and + – channel. This experiment is just one example for the possibilities in the regime of neutron reflectivity with polarisation analysis. Besides the systems presented here organic samples have also been studied [2]. Especially in the field of biology the interest in neutron reflectivity is growing considerably and ADAM will also be an ideal instrument for the investigation of Langmuir-Blodget films, biological membranes or polymers. Independent of the research field we already have a high demand of beam time and further instrumental improvements will make ADAM even more interesting. At the end of 1998 a 2-dimensional

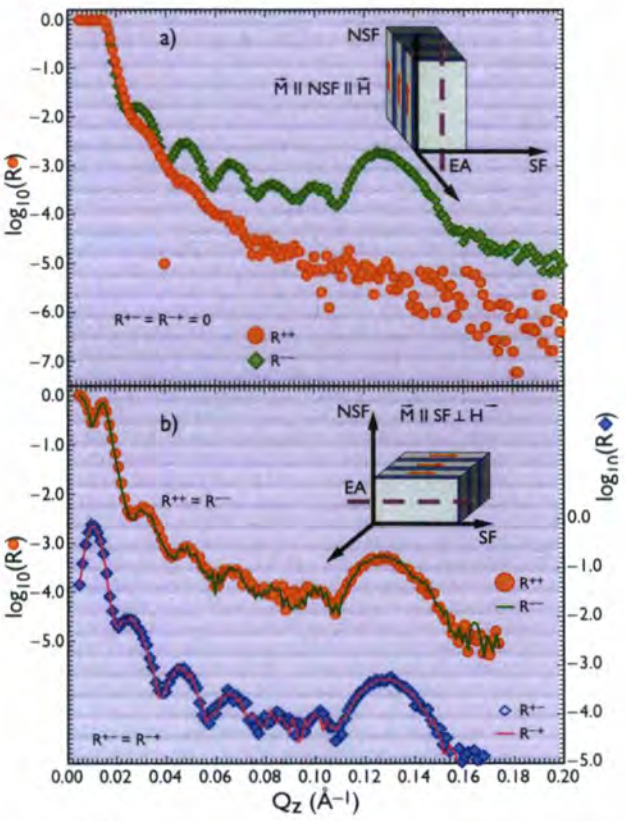

Figure 3: *Reflectivity of a (15Å Cu / 34Å Co)$_7$/Al$_2$O$_3$ superlattice with a strong uniaxial magnetic anisotropy. In* ***a)*** *the ferromagnetically coupled Co moments are aligned along the non-spin-flip axis (NSF) causing a maximum splitting between the ++ and – reflectivity and no spin-flip intensity. With the magnetisation vector aligned along the spin-flip axis (SF) in* ***b)*** *the magnetic splitting in the ++ and – – channels vanishes. At the same time due to pure spin-flip scattering the superlattice structure is reproduced in R– + and R+–.*

position-sensitive detector will be available. By removing the nitrogen-cooled Be-filter a wavelength of $\lambda = 2.2$ Å is accessible extending the Q-range up to 5.4 Å^{-1}. This will open the possibility of high and small-angle scattering within the same experimental set-up.

References

- [1] A. Schreyer, R. Siebrecht, U. Englisch, U. Pietsch and H. Zabel, 5SXNS Proceedings, Physica B (1998) in press
- [2] U. Englisch, F. Penacorada, I. Samolenko and U. Pietsch, 5SXNS Proceedings, Physica B (1998) in press.

The 2π image-plate detector LADI

The development by ILL and EMBL of the large area image-plate detector, aimed primarily at the study by the Laue technique of the structure of biological molecules at medium resolution, has now reached the stage where the advanced prototype can be made available to users. The performance is illustrated below by a comparison of LADI data on the solvent regions of coenzyme B12r with results obtained using other techniques.

In addition, test experiments have been carried out to demonstrate the potential of the Laue technique using this detector not only for large-scale structures using cold neutrons, but also for small unit-cell crystals using a thermal neutron beam. Two such experiments are outlined below; they were carried out at the end of a thermal neutron guide and concern a disordered molecular crystal and a magnetic phase-transition.

Crystallographic analysis of solvent regions in biomolecular crystals: coenzyme B12r as a test case

P. Langan, M. Lehmann, S. Mason (ILL),
C. Wilkinson (EMBL), G. Jogl, C. Kratky (Univ. Graz).

In spite of its tremendous potential biological significance, high-resolution single-crystal neutron studies of biological macromolecules have been rare, due to the prohibitive crystal size needed (> 5 mm^3) and the long data collection time (weeks to months). The LADI detector on a cold neutron beam allows the data collection time and/or required crystal volume to be decreased by up to 2 orders of magnitude for medium-resolution studies. We have collected neutron diffraction data on LADI and high-resolution single-crystal diffractometer D19 using the same crystal specimen of B12r grown from D_2O/D_6-acetone. Moreover, we also collected synchrotron x-ray data from B12r crystals grown from water/acetone under otherwise identical conditions (EMBL station X31 at DESY, Hamburg). The LADI data extend to a medium resolution of 1.43 Å while both D19 and synchrotron data extend to high resolution of less than 1 Å. The comparison of the LADI results with results from D19 the world-wide best biological high-resolution neutron diffractometer as well as with synchrotron x-ray diffraction results constitutes a unique and extremely challenging test for the performance of this new instrument.

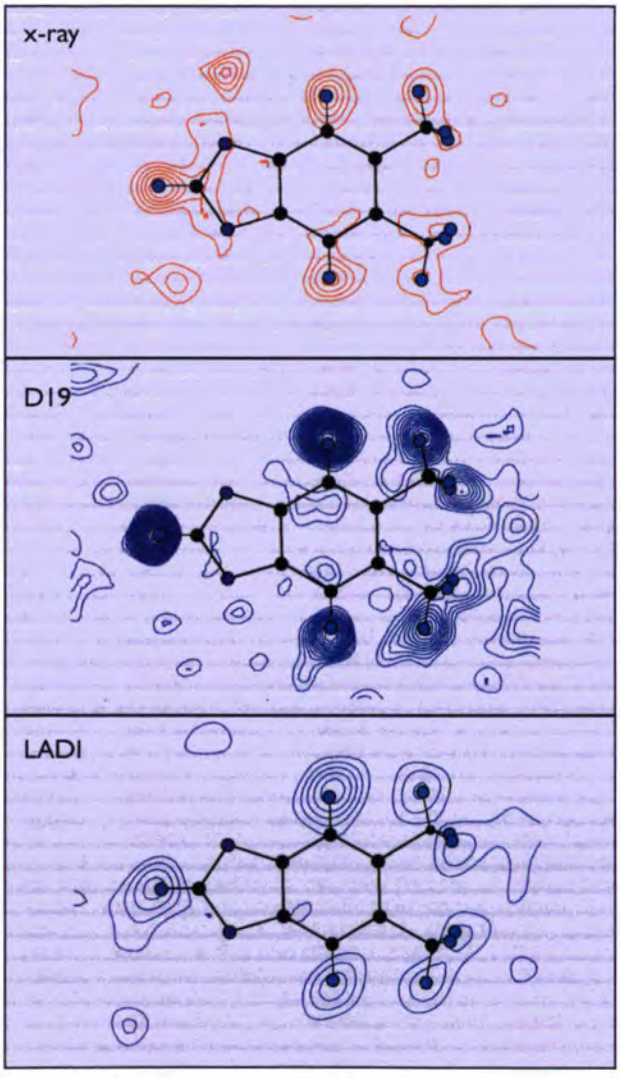

Figure 1: *Difference density omit maps for the crystal structure of B12r, computed from synchrotron x-ray data (0.9 Å resolution, top), D19-data (1.0 Å, middle) and LADI-data (1.43 Å, bottom). The map passes through the atoms of the dimethyl-benzimidazole base, whose hydrogen atoms have been omitted for the calculation of phases. Note that all three maps are contoured at the same level of significance. Positive contours are drawn in red, negative ones in blue.*

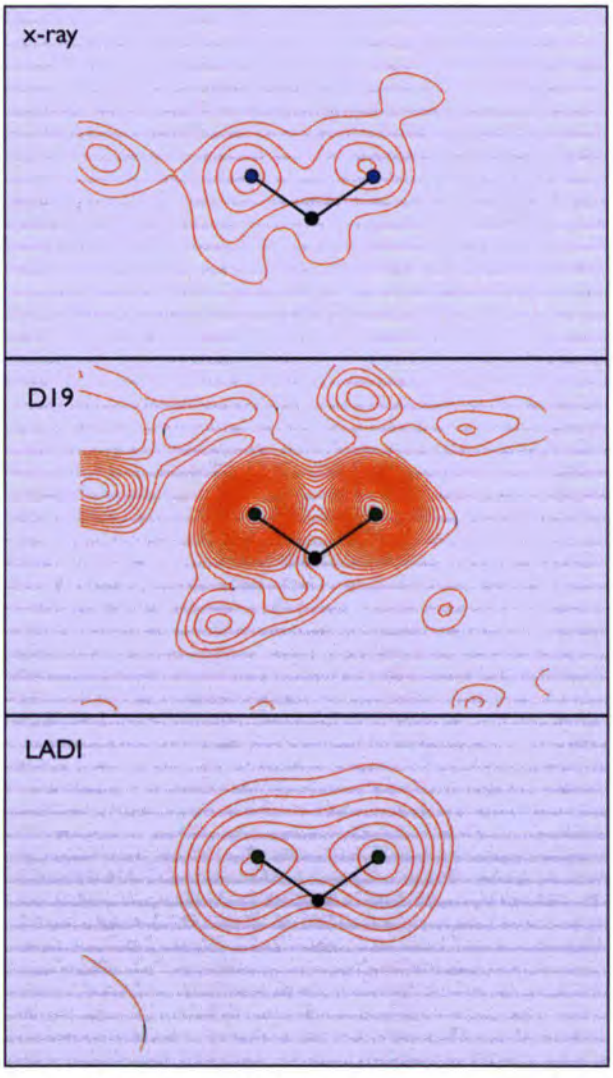

Figure 2: *Omit maps through the atoms of a solvent water molecule, whose hydrogen (top) or deuterium (middle and bottom) atoms have been omitted for the phase calculation.*

A comparison of the results of the three experiments is shown in the form of so-called "omit" maps, Fig. 1 and 2. These maps consist of density sections through corresponding parts of three crystal structures, and they were computed by omitting hydrogen/deuterium atoms in the corresponding phase calculations. The height of peaks (or depths of minima) indicate the power of the corresponding data set to determine hydrogen or deuterium atom positions. Fig. 1 is a section through the dimethyl-benzimidazole part of the B12r moiety. Clearly, the high-resolution monochromatic neutron data (D19) are outstanding in revealing hydrogen positions, which appear as negative peaks in neutron density maps. Surprisingly, the medium resolution LADI data are at least as good in revealing these positions as the high-resolution x-ray data, in spite of the much better statistical significance of the latter. This view is corroborated in Fig. 2, which shows a section through three atoms constituting a solvent water molecule. Again D19 wins but LADI comes second with regard to revealing the deuterium positions. Since we know from experience that proton positions are invisible in x-ray electron density maps of proteins diffracting to 1.5 Å or less, the power of the LADI data is impressive. **LADI is therefore a novel powerful tool for locating H or D positions in biological macromolecules, and it will tremendously enhance the use of neutron diffraction as a complement to x-ray crystallography in many areas of structural biology.**

Nickel hexammine salts

- P. Schiebel (ILL and Univ. Tübingen),
- H.G. Büttner, G.J. Kearley, M.S. Lehmann (ILL),
- K. Burger, W. Prandl (Univ. Tübingen).

Nickel hexammine salts $Ni(NH_3)_6Y_2$ (Y = Br, Cl, I, NO_3, PF_6) form face-centred cubic lattices in their high-temperature phase (space group Fm3m). The incompatibility of the molecular symmetry 3m of NH_3 with the symmetry 4mm of the lattice site gives rise to the orientational disorder found in these compounds. Although the nickel hexammine salts and their order-disorder phase-transitions have been investigated with several different techniques, there is still considerable lack of structural data.

In the test experiment, a deuterated nickel-hexammine-chloride crystal ($Ni(ND_3)_6Cl_2$) of 1.5 mm^3 volume was used, being measured at 4 different crystal settings ($\phi = 0°, 20°, 40°, 60°$) each for 50 min. After indexing and integrating the measured data 105 symmetry-independent Bragg reflections were obtained. The nuclear-density distribution is derived from a combination of conventional crystallographic split-atom density interpolation and maximum-entropy density reconstruction. Fig. 3 shows how the deuteron density obtained in $Ni(ND_3)_6Cl_2$ is concentrated on a plane perpendicular to the 4-fold axis.

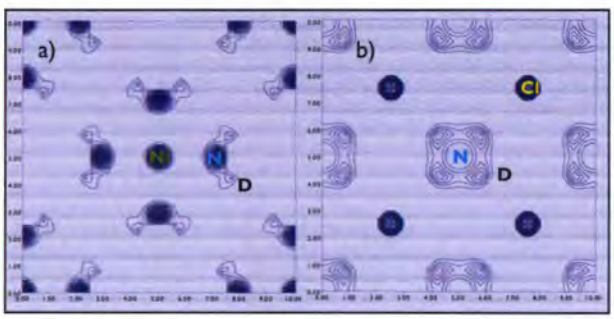

Figure 3: a) *Cut through the $Ni(ND_3)_6Cl_2$ unit-cell parallel to the face of the unit cell at z = 0.* ***b)*** *Cut parallel to the face of the unit cell at z = 1/4 where the maximum deuteron-density occurs.*

This finding can only be explained by a movement of the ammonia centre of mass combined to the rotational motion of the ammonia molecule and is due to the rotational-translational coupling found in these compounds [1,2].

Recent studies on a series of nickel and cobalt hexammine salts showed a similar density distribution which can consistently be explained as a consequence of rotational-translational coupling in an anharmonic crystal-potential. However, all these previous data were collected on a four-circle diffractometer requiring a single crystal of 30 mm^3 volume with an average measuring-time of 6 days to collect the data, whereas on LADI we measured 4 sets of different orientations, 50 min. each, on a 2 mm^3 crystal. This gives a gain of a factor 100.

Neutron Laue-diffraction combined with maximum-entropy methods provides a powerful tool for a direct observation of the density distribution of dynamically disordered molecules. It offers a new and unique method to study the freezing of molecules in crystals and the associated order-disorder phase-transition.

The magnetic structure of 4%Ga doped $FeGe_2$

C. Wilkinson (EMBL Grenoble),
J.B. Forsyth (RAL),
P.J. Brown, D. Myles (ILL),
A.Z. Men'shikov (Inst. Metal Physics, Ekaterinburg).

It is known [3] that the tetragonal antiferromagnet $FeGe_2$ has a paramagnetic to antiferromagnetic spiral transition at 289 K (propagation vector $1+\delta\ 0\ 0$) with δ varying from ~ 0.053 at the transition to 0.0 at a second transition to a simple colinear antiferromagnetic commensurate phase at 263 K. Adding 4% of Ga to $FeGe_2$ extends the range of stability of the incommensurate phase. Typically, such magnetic structures have been studied in monochromatic powder or single-crystal neutron-diffraction experiments.

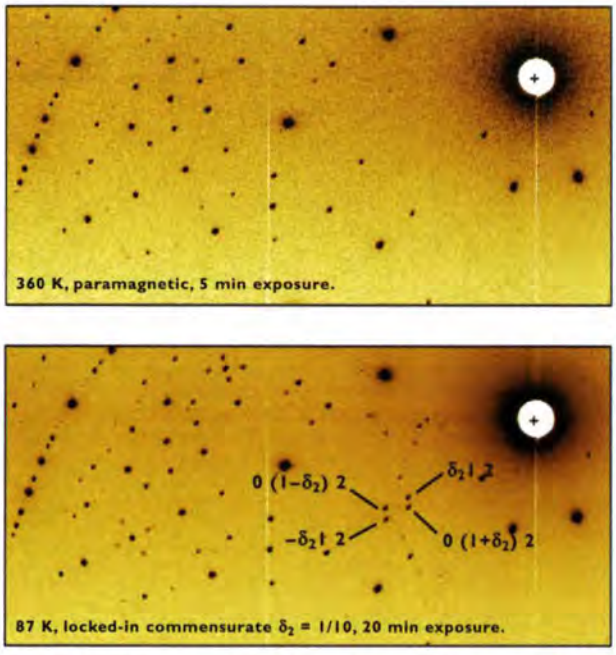

Figure 4: *Laue diagrams of 4%Ga doped $FeGe_2$ at 306 K and 87 K.*

Powder diffraction works well in the case where the magnetic structure is relatively simple and whilst monochromatic single-crystal methods provide the most precise way of following the development of individual reflections in complex structures like that of $FeGe_2$, they are relatively slow. One way to speed up the survey of reciprocal space is to use a white-beam (Laue) technique, which for its efficiency relies on the use of a large detector [4]. The text experiments used a crystal of 36 mm^3. At 306 K, above the paramagnetic transition temperature, exposure times of 5 min. were sufficient to give Laue diagrams in which the strongest (nuclear) reflections saturated the detector (upper part of Fig. 4). The main beam passes through the centre of the hole seen in the top right corner of the image. Exposures were taken at 10 K temperature intervals down to the lowest achievable specimen temperature of 87 K and in order to see clearly the magnetic reflections which developed over this range the exposure times were raised to 20 min.

The 87 K image is shown in the lower part of Fig. 4. The most prominent extra reflections correspond to a propagation vector $(1+\delta\ 0\ 0)$, with three other equivalent domains giving vectors $(1-\delta\ 0\ 0)$, $(0\ 1+\delta\ 0)$ and $(0\ 1-\delta\ 0)$ with $\delta \sim 0.1$. This gives a characteristic pattern of four magnetic satellite-reflections in the « star » around nuclear-reflection positions; the cluster around the (012) nuclear position is marked. The groups of four first-order satellites are the prominent feature of the diagrams but reflections which can be indexed as higher-order satellites are also present; the most significant have indices of the type $(h + n\delta\ k + n\delta\ l)$ with l even.

It is clear that this technique offers a rapid and quantitative method for the study of magnetic structures, particularly when the magnetic and nuclear Bragg reflections are resolved on the Laue diagram.

References

[1] P. Schiebel et al., J. Phys. Condens. Matter 6 (1995) 10989 ■ [2] P. Schiebel et al., Acta Cryst. A52 (1996) 189 ■ [3] L.M.Corliss, J.M.Hastings, W. Kunnmann, R.Thomas, J. Zhuang , R. Butera and D. Mukamel, Phys. Rev. B 31 (1985) 4377. ■ [4] F. Cipriani, J-C. Castagna, C. Wilkinson, P. Oleinek and M.S. Lehmann, J. Neutron Research 4 (1996) 79.

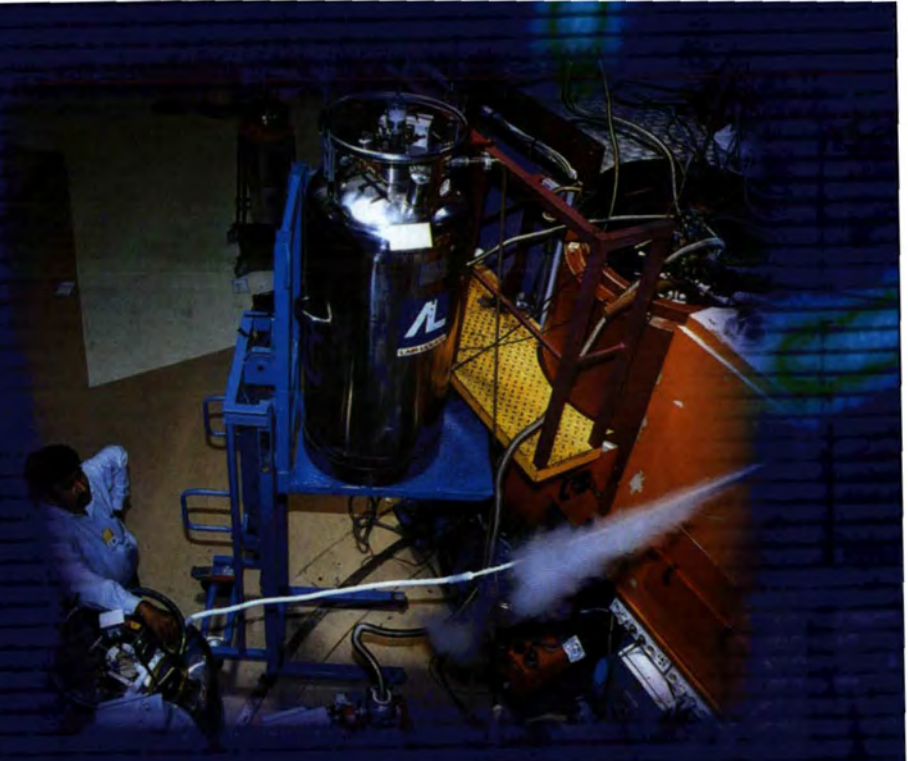

Neville Adroja, Univ. Southampton, fills IN6's cryostat with liquid nitrogen.

Christina Line experimenting on IN5.

Can you see the crystal? Petra Schiebel aligns one for the LADI experiment.

EXPERIMENTAL PROGRAMME

4

Instruments

Beam-time allocation

Reactor operation

Instrument performance

EXPERIMENTAL PROGRAMME

List of instruments

ILL instruments

D1A (1/2)	powder diffractometer	operational
D2B	powder diffractometer	operational
D3	single-crystal diffractometer	operational
D4 (1/2 with IN1)	liquids diffractometer	operational
D7	diffuse-scattering spectrometer	operational
D9	single-crystal diffractometer	operational
D10	single-crystal diffractometer	operational
D11	small-angle scattering diffractometer	operational
D16	small momentum-transfer diffractometer	under reconstruction
D17	reflectometer	under reconstruction
D19	single-crystal diffractometer	operational
D20	powder diffractometer	operational
D22	small-angle scattering diffractometer	operational
IN1 (1/2 with D4)	three-axis spectrometer	operational
IN4	time-of-flight spectrometer	commissioning
IN5	time-of-flight spectrometer	operational
IN6	time-of-flight spectrometer	operational
IN8	three-axis spectrometer	operational
IN10	backscattering spectrometer	operational
IN11	spin-echo spectrometer	operational
IN14	three-axis spectrometer	operational
IN16	backscattering spectrometer	operational
IN20	three-axis spectrometer	operational
PF1	neutron beam for fundamental physics	operational
PF2	ultracold neutron source for fundamental physics	operational
PN1	fission product mass-spectrometer	operational
PN3	gamma-ray spectrometer	operational

Jointly funded instruments

DB21 (1/2)	single-crystal diffractometer	operational, with EMBL
LADI (1/2)	LAUE diffractometer	commissioning, with EMBL
IN15	spin-echo spectrometer	operational, with FZ Jülich and HMI Berlin

CRG instruments

ADAM	reflectometer	CRG-B operational
D1A (1/2)	powder diffractometer	CRG-A operational
D1B	powder diffractometer	CRG-A operational
D15	single-crystal diffractometer	CRG-B operational
D23	single-crystal diffractometer	CRG-B under construction
EVA	reflectometer	CRG-B operational
IN3	three-axis spectrometer	CRG-A operational
IN12	three-axis spectrometer	CRG-B operational
IN13	backscattering spectrometer	potential CRG (currently unused)
IN22	three-axis spectrometer	CRG-B under construction
S18	interferometer	CRG-C commissioning
S20	topography	CRG-B operational (closed end of 1997)
S51	Avogadro	CRG-C operational

Test beams

CT1, CT2	detector test-facility
S42	Laue crystal alignment facility
T3	neutron optic test-facility
T13A,C	monochromator test-facility
T17 test	cold neutron-beam test-facility
S10, S34,	uninstrumented beam-positions

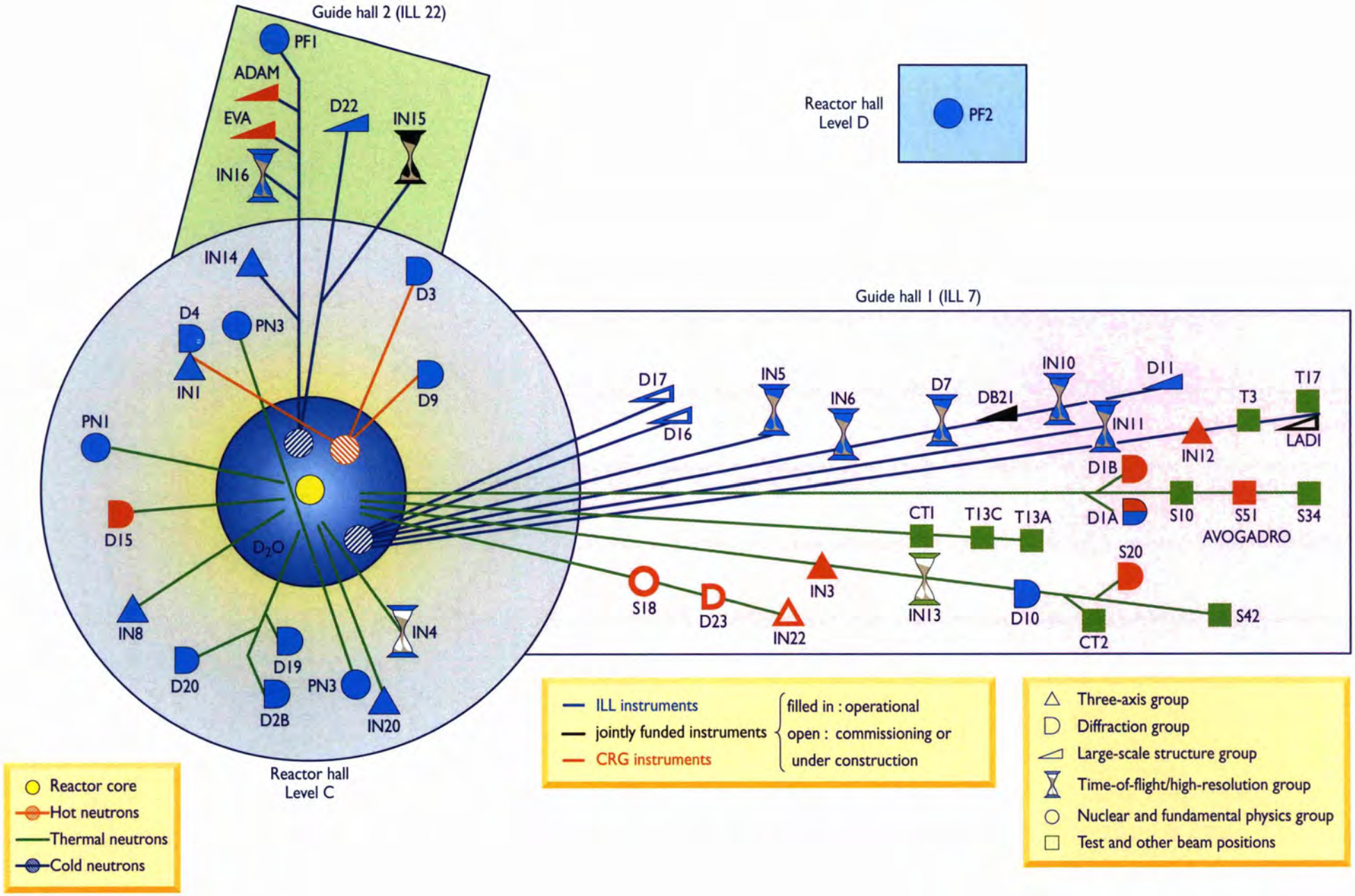
Guide hall 2 (ILL 22)
PF1
ADAM
EVA
IN16
D22
IN15
Reactor hall
Level D
PF2
IN14
D3
D4
PN3
IN1
D9
PN1
D15
D2O
IN8
D20
D19
PN3
D2B
IN4
IN20
Reactor hall
Level C
Guide hall 1 (ILL 7)
D17
D16
IN5
IN6
D7
DB21
IN10
D11
IN11
T3
T17
LADI
IN12
D1B
D1A
S10
S51
S34
AVOGADRO
CT1
T13C
T13A
S18
D23
IN22
IN3
IN13
D10
S20
CT2
S42
Reactor core
Hot neutrons
Thermal neutrons
Cold neutrons
ILL instruments
jointly funded instruments
CRG instruments
filled in : operational
open : commissioning or
under construction
Three-axis group
Diffraction group
Large-scale structure group
Time-of-flight/high-resolution group
Nuclear and fundamental physics group
Test and other beam positions

Beam-time allocation

instrument	beam-time requested (in days)	beam-time allocated (in days)	number of experiments
*ADAM**	*51*	*27*	*3*
*D1A**	*163*	*124*	*29*
*D1B**	*218*	*110*	*45*
D2B	348	188	81
D3	275	150	14
D4	194	92	22
D7	261	167	14
D9	377	185	23
D10	319	183	20
D11	267	155	58
*D15**	*85*	*49*	*5*
D16	241	150	16
D17	246	143	27
D19	159	168	12
D20	108	95	31
DB21	164	163	6
D22	287	155	65
*EVA**	*99*	*55*	*6*
IN1	139	80	12
*IN3**	*79*	*89*	*6*
IN4	72	0	0
IN5	382	167	37
IN6	418	169	47
IN8	349	190	23
IN10	269	142	22
IN11	485	157	16
*IN12**	*43*	*54*	*6*
IN14	421	171	21
IN15	64	26	4
IN16	314	177	31
IN20	188	119	14
PF1	670	158	3
PF2	406	186	11
PN1	348	186	14
PN3	458	201	13
*S20**	*0*	*24*	*3*
TOTAL	**8967+**	**4655**	**760**

** CRG instruments.*

+ A purely Russian proposal was not included in the beam-time request because the meetings took place before Russia became a scientific member. However, the statistics by country were recalculated including Russia after the signature of the contract (table 2) and therefore in table 2 the total beam-time request is higher than in table 1.

Overall the subcommittees of the scientific council (meetings in Oct. '96 and Apr. '97) scrutinised over 1000 proposals, out of which over 700 proposals received beam time, allocating over 4600 instrument days of beam time on the different instruments; 760 experiments were carried out. The table above shows the request and allocation of beam time per instrument.

Note that D4 and IN1 share a beam and that the CRG instruments offer a reduced number of days for ILL users. D1B gave a reduced number of days, because it became a CRG instrument in May, when D20 came into operation. D16 and D17 are slightly down in their allocation, because they stopped operation earlier, i.e. in the middle of the last cycle, so that the reconstruction work on these two instruments could start. Both instruments will be shut down in 1998. For PF2 several experiments share the beam taking neutrons alternately, so the table contains the beam-days allocated but gives the total number of experiments running simultaneously.

The table below shows the distribution of beam-time request and allocation amongst the member and scientific-member countries:

country	requested days	requested in %	allocated days	allocated in %
AUT	116.4	1.3%	76.1	1.6%
CH	417.5	4.6%	202.1	4.3%
D	**2489.9**	**27.7%**	**1399.3**	**30.1%**
E	309.4	3.4%	170.7	3.7%
F	**2410.0**	**26.8%**	**1358.1**	**29.2%**
GB	**2377.9**	**26.5%**	**1140.7**	**24.5%**
I	282.8	3.1%	134.9	2.9%
RUS	582.8	6.5%	172.3	3.7%
total	8986.7	100.0%	4654.2	100.0%

In 1997 the number of members increased from six to eight; they were France, Germany, UK, Spain, Switzerland, Austria, Russia and Italy. In calculating the above statistics of beam time per country the attribution is based on the location of the laboratory of the proposers, not their individual nationality. For a proposal involving laboratories from more than one member country, the total number of days is divided equally among the collaborating countries. When a proposal involves a collaboration with a non-member country, the allocated time is attributed entirely to the collaborating member country (or countries). When ILL scientists are proposers or co-proposers, the allocated « ILL time » is attributed among the member countries according to their financial contributions to ILL. Local contacts are not counted as proposers.

In 1997, three-quarters of ILL's annual 1350 visitors came from the member countries including 372 from France, 303 from Germany and 237 from the UK and many of them were welcomed more than once. There were thus almost 2500 visits and over 750 experiments. The distribution of beam time for these experiments amongst the different 'colleges' was as follows: 14% of the days were allocated to nuclear and fundamental physics (college 3), 15% to structural and magnetic excitations (college 4), 35% to crystal and magnetic structures (college 5), 9% to structure and dynamics of liquids and glasses (college 6), 8% to materials science, surfaces and spectroscopy (college 7), 10% to biology (college 8) and 9% to structure and dynamics of soft-condensed matter (college 9).

Reactor operation

cycle n°	start date	finish date	number of days scheduled	number of days operation	number of unscheduled shutdowns	observations
108/2*	4/2/97	01/3/97	25	25	0	
109	11/3/97	02/5/97	50	50	2	Beam-line flux measurement on 10/3/97
110	21/5/97	10/7/97	50	50	0	
111	7/8/97	26/9/97	50	50	0	Cold source flux measurement on 6/8/97
112	13/10/97	2/12/97	50	50	0	Cold source flux measurement on 13/10/97

* *The fuel element used for cycle 108/2 was already partially used for cycle 108/1 in 1996.*

The 1997 operating schedule was based on 225 days spread over 4.5 cycles. The major shutdown needed to carry out lengthy maintenance work now takes place between December and January in order to reduce electricity costs. The inter-cycle shutdowns needed to replace the fuel element last around two to three weeks. These shorter shutdowns are also used to carry out minor maintenance work, as well as the periodic checks which must be performed before each start-up.

There was one significant incident to report in 1997. During the night of 1 to 2 January, the operation of the general compressed air system was disrupted due to a power failure on an air dryer. Venting operations carried out on the system on 2 January revealed the presence of slightly contaminated water in the pipework. Investigations to establish the origin of the water revealed it to be from a tank containing slightly radioactive effluents. These effluents are kept in continuous circulation by a flow of compressed air, which enters the lower part of the tank and is evacuated through a vent connected to the gaseous effluents system. The disruptions to the compressed air system triggered the automatic closure of this vent causing a momentary increase of pressure inside the tank. Part of the tank's contents was forced back into the compressed air pipework. As a result of this incident, the contaminated sections of the compressed air system had to be isolated immediately and a temporary system set up. Although this was without consequence to the safety of staff or the general public, the reactor start-up was delayed by a week. To date, all the contaminated pipes have been dismantled and disposed of as radioactive waste. New equipment has been installed and the compressed air system is once again operating at its original capacity. In the second cycle, two unforeseen reactor shutdowns occurred, but in both cases the beam time was recuperated by extension of the reactor operating cycle. The table above sets out the operating and shutdown periods in 1997.

In 1997, a number of pieces of equipment were replaced, including the converter sets used to power two heavy water shutdown coolant pumps and the computerised system for monitoring the reactor's thermodynamic characteristics. As far as new projects are concerned, efforts have been focused for the most part on installing the new guide tubes H17-H18. Within the framework of this project, the reactor division has, among other things, made modifications to the water-tight panel of the swimming pool of guide tubes H1-H2.

1997 brought a satisfactory conclusion to the fuel cycle question, with the signing of a commercial contract bet-

Jacques Corréard (left) and Christian Barbe supervise the transport of the first flask containing two burnt fuel-elements.

ween ILL and COGEMA for the removal and reprocessing of ILL's spent fuel-elements. The first flask containing two elements left ILL on 15 December 1997, with other shipments from ILL planned for the beginning of 1998. The campaign will then continue with the transfer of fuel elements currently held in interim storage at the CEA Cadarache facility.

Problems have been encountered regarding the supply of fresh uranium for the reactor, due to delays in deliveries from Russia. Every effort is being made to obtain supplies of uranium as soon as possible, so that the regular production of fuel elements and hence normal reactor-operation can continue in the future.

An extensive programme of maintenance work on the detritiation facility was completed at the beginning of the year. The facility was restarted at the beginning of April for the treatment of the reactor's heavy water. Once this process was completed, the facility was shut down again at the beginning of November. It was decided to operate the detritiation facility during the summer months in order to reduce electricity costs. No particular problems were encountered during the treatment process and as a result of this campaign it was possible to reduce considerably the level of activity of the reactor's heavy water. The detritiation facility's operational characteristics once again resemble those observed prior to the 1991 shutdown.

Instruments

The instrumental facilities at the ILL are shown in the schematic diagram on page 99. Besides the ILL instruments there are CRG-instruments, which are operated by external **C**ollaborating **R**esearch **G**roups. There are currently three different categories of CRG instruments: CRG-A in which the external group leases an instrument owned by ILL. They have 50% of the beam time at their disposal and for the other 50% they support ILL's scientific user programme. The CRG-B category owns their instrument and have 70% of the beam time, supporting the ILL programme for the other 30%. Finally, CRG-C instruments are used full time for specific research programmes by the external group which has exclusive use of the beam.

DB21, LADI and IN15 have a special status, since they are a joint venture of ILL with other laboratories: in the case of DB21/LADI with EMBL and for IN15 with FZ Jülich and HMI Berlin. The list of instruments by type as at December 1997 is summarised below (CRG instruments are marked with an asterisk *)

- powder diffractometers: D1A*(note that D1A is only half a CRG instrument), D1B*, D2B, D20
- liquids diffractometer: D4
- single-crystal diffractometers: D3, D9, D10, D15*, D19, DB21, (D23* under construction), (LADI in commissioning)
- small-angle scattering: D11, D22
- small momentum-transfer diffractometer: (D16 in reconstruction)
- reflectometers: ADAM*, (D17 in reconstruction), EVA*
- diffuse-scattering spectrometer: D7
- three-axis spectrometers: IN1, IN3*, IN8, IN12*, IN14, IN20 (spin-echo option in commissioning), (IN22* under construction)
- time-of-flight spectrometers: IN5, IN6, (IN4 in commissioning)
- backscattering and spin-echo spectrometers: IN10, IN11, IN16, IN15
- topography: S20* (being dismantled after 1997)
- nuclear-physics instruments: PN1, PN3
- fundamental-physics instruments: PF1, PF2

Details of the instruments can be found on the web under http://www.ill.fr.

AVOGADRO* and S18*, an interferometer, are CRG-C instruments and are not available as 'user' instruments.

Subcommittee 7 hard at it (from left: Hervé Jobic, Inst. Catalyse Villeurbanne, Andreas Magerl, Univ. Erlangen, John Tomkinson, ISIS Didcot, Bernd Asmussen, Univ. Kiel, Winfried Petry, TU München, Mark Johnson, Jürgen Schreiber, Frauenhofer Inst. Dresden, Gernot Kostorz, ETH Zürich, Robert Richardson, Univ. Bristol, Christian Janot, Univ. Roma).

Instrument performance

The table below gives a summary of instrument performance for 1997 (for ILL-funded instruments). For each cycle a record is kept of any time lost from the total available beam-time, and the reasons for the lost time are analysed for all the instruments. The table gives a global summary for the year:

Overall about 300 days of the total available beam-time were lost due to various malfunctions (compared to 1996 the loss of beam time decreased by 100 days). However, most of this time was not lost to users because time for minor breakdowns, tests, calibrations and scheduling difficulties is allowed for by initially scheduling about 80% of the total available beam-time. Thus the total number of days delivered to users was higher than the number of days originally scheduled: 4648 compared with 4530 originally scheduled. Please note that CRG instruments are not included, because they are not operated by ILL. The record for D1B gives only the figures for the one and a half cycles when it was operated by ILL at the beginning of the year. D1B was replaced by D20 which became operational in May; D20's performance is indicated for 3 cycles, but it still had some commissioning experiments in this period. Moreover, IN15, the high-resolution spin-echo spectrometer, was only performing for 1 cycle, in autumn, as a fully scheduled instrument.

Detailed comments on the larger beam-time losses (10% or more) are as follows:

- D22's loss is mainly due to breakdowns of the velocity selector.
- IN1 experienced some time loss due to a breakdown of the monochromator's motor. Because of the high activity of the monochromator the intervention could not be undertaken immediately and delayed the repair.
- IN6's lost time was mainly due to the breakdown of the ageing Fermi chopper. A replacement has now been ordered.
- PN1's time loss was caused by breakdowns in high-tension equipment; the equipment is now replaced.

instrument	days lost	% lost	sched. days	days used	instrument
D1A	10.8	6.1%	184.0	188.5	D1A
D1B	0.0	0.0	62.0	63.0	D1B
D2B	6.5	2.9%	190.0	196.0	D2B
D3	9.5	4.2%	182.0	181.0	D3
D4	3.4	2.7%	83.0	97.5	D4
D7	10.5	4.7%	191.0	192.0	D7
D9	4.0	1.8%	186.0	208.0	D9
D10	9.8	4.4%	182.0	184.3	D10
D11	16.0	7.1%	163.0	154.0	D11
D16	12.0	5.3%	169.0	162.0	D16
D17	16.2	7.9%	158.0	170.5	D17
D19	7.5	3.3%	181.0	185.5	D19
D20	2.8	2.1%	93.0	107.5	D20
DB21	11.0	4.9%	164.0	196.0	DB21
D22	33.5	14.9%	167.0	165.3	D22
IN1	16.0	13.1%	101.0	93.0	IN1
IN5	6.2	2.7%	167.0	193.0	IN5
IN6	22.5	10.0%	214.0	200.0	IN6
IN8	11.5	5.1%	189.0	195.0	IN8
IN10	18.3	8.1%	170.0	187.5	IN10
IN11	19.5	8.7%	157.0	154.0	IN11
IN14	10.5	4.7%	176.0	175.5	IN14
IN15	0.0	0.0%	26.0	26.0	IN15
IN16	13.1	5.8%	177.0	187.0	IN16
IN20	9.0	4.0%	182.0	186.0	IN20
PF1	0.1	0.0%	217.0	216.9	PF1
PF2	2.0	0.9%	*	*	PF2
PN1	32.0	14.2%	198.0	166.0	PN1
PN3	2.5	1.1%	201.0	217.5	PN3
Total	**316.5**		**4530.0**	**4648.4**	**Total**

** PF2 consists of several long-term experiments so comparison of days scheduled and used is not meaningful.*

Seen here the sitting at the stand-up buffet of the subcommittee meetings; from left: Christian Bärlocher, ETH Zürich, Hans Boysen, Univ. München, Werner Kuhs, Univ. Göttingen, Thomas Brückel, FZ Jülich.

Happy user on D1A: Andrei Podlesnyak, Metal Physics Inst. Ekaterinburg, helped by François Fauth, LNS Villigen & ILL.

Another shot of our famous stand-up buffet; from left: Christoph Kratky, Univ. Graz, Sax Mason, Amir Murani, Ken Andersen, Barbara Gabrys, Brunel Univ.

FACTS AND FIGURES

5

for 1997

30 years of ILL

FACTS AND FIGURES

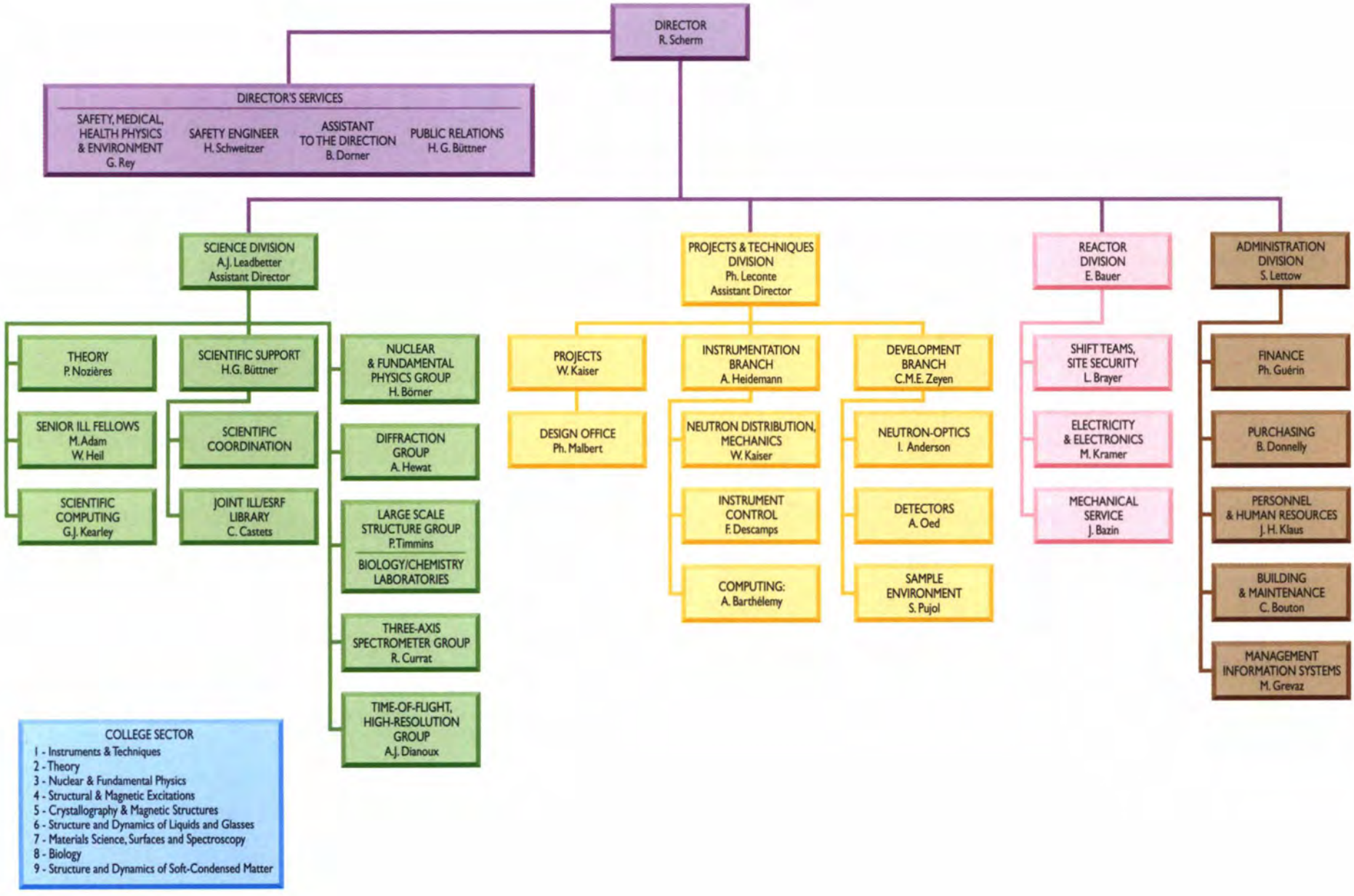
DIRECTOR
R. Scherm
DIRECTOR'S SERVICES
SAFETY, MEDICAL, HEALTH PHYSICS & ENVIRONMENT
G. Rey
SAFETY ENGINEER
H. Schweitzer
ASSISTANT TO THE DIRECTION
B. Dorner
PUBLIC RELATIONS
H. G. Büttner
SCIENCE DIVISION
A.J. Leadbetter
Assistant Director
THEORY
P. Nozières
SENIOR ILL FELLOWS
M. Adam
W. Heil
SCIENTIFIC COMPUTING
G.J. Kearley
SCIENTIFIC SUPPORT
H.G. Büttner
SCIENTIFIC COORDINATION
JOINT ILL/ESRF LIBRARY
C. Castets
NUCLEAR & FUNDAMENTAL PHYSICS GROUP
H. Börner
DIFFRACTION GROUP
A. Hewat
LARGE SCALE STRUCTURE GROUP
P. Timmins
BIOLOGY/CHEMISTRY LABORATORIES
THREE-AXIS SPECTROMETER GROUP
R. Currat
TIME-OF-FLIGHT, HIGH-RESOLUTION GROUP
A.J. Dianoux
PROJECTS & TECHNIQUES DIVISION
Ph. Leconte
Assistant Director
PROJECTS
W. Kaiser
DESIGN OFFICE
Ph. Malbert
INSTRUMENTATION BRANCH
A. Heidemann
NEUTRON DISTRIBUTION, MECHANICS
W. Kaiser
INSTRUMENT CONTROL
F. Descamps
COMPUTING:
A. Barthélemy
DEVELOPMENT BRANCH
C.M.E. Zeyen
NEUTRON-OPTICS
I. Anderson
DETECTORS
A. Oed
SAMPLE ENVIRONMENT
S. Pujol
REACTOR DIVISION
E. Bauer
SHIFT TEAMS, SITE SECURITY
L. Brayer
ELECTRICITY & ELECTRONICS
M. Kramer
MECHANICAL SERVICE
J. Bazin
ADMINISTRATION DIVISION
S. Lettow
FINANCE
Ph. Guérin
PURCHASING
B. Donnelly
PERSONNEL & HUMAN RESOURCES
J.H. Klaus
BUILDING & MAINTENANCE
C. Bouton
MANAGEMENT INFORMATION SYSTEMS
M. Grevaz
COLLEGE SECTOR
1 - Instruments & Techniques
2 - Theory
3 - Nuclear & Fundamental Physics
4 - Structural & Magnetic Excitations
5 - Crystallography & Magnetic Structures
6 - Structure and Dynamics of Liquids and Glasses
7 - Materials Science, Surfaces and Spectroscopy
8 - Biology
9 - Structure and Dynamics of Soft-Condensed Matter

Facts and Figures for 1997

Name: **Institut** Max von **Laue** - Paul **Langevin (ILL)**

Founded: 1967

Associates: France: Commissariat à l'Energie Atomique (CEA)
Centre National de la Recherche Scientifique (CNRS)
Federal Republic of Germany: Forschungszentrum Jülich (FZJ)
United Kingdom: Engineering and Physical Sciences Research Council (EPSRC)

Countries with Scientific Membership:
Spain: Comisión Interministerial de Ciencia y Tecnología (CICT)
Switzerland: Schweizer Bundesamt für Bildung und Wissenschaft (SBBW)
Austria: Österreichische Akademie der Wissenschaften (ÖAW)
Russia: Russian Ministry of Atomic Energy (Minatom)
Italy: Istituto Nazionale per la Fisica della Materia (INFM)

Staff: 402 people including 52 experimentalists in the scientific sector
243 French, 70 German, 56 British, 33 others

Budget: 372.042 MF (excluding taxes)

Income in MF

306.962	- 82.51%	from associates, (divided: F 37.87%; D 37.13%; UK 25.00%)
26.358	- 7.08%	from scientific members,
31.960	- 8.59%	carry-forward from 1996
4.462	- 1.20%	own income
2.300	- 0.62%	income from CRGs

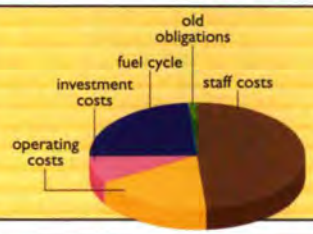

Expenditure in MF (including expenditure on CRGs)

181.520	- 48.79%	staff costs
65.989	- 17.74%	operating costs
31.305	- 8.41%	investment costs
88.143	- 23.69%	fuel cycle
5.085	- 1.37%	old obligations

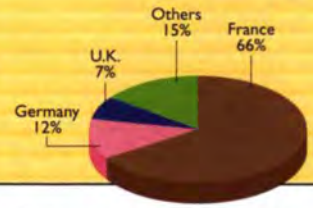

Purchases in MF (total 59.3 MF)

39.1 MF	- 66%	France
7.3 MF	- 12%	Germany
4.1 MF	- 7%	UK
8.8 MF	- 15%	Others

Bodies: Steering Committee, meeting twice a year
Scientific Council with 8 Subcommittees, meeting twice a year
Management Board, meeting weekly

Reactor: 58 MW, running 4.5 reactor cycles per year (with cycles of 50 days)

Experimental Programme:
about 760 experiments (allocated by subcommittees) on 25 ILL-funded and 9 CRG instruments
about 1350 visitors coming from 33 countries
about 1000 proposals submitted and 700 accepted

Experiment Selection by the Scientific Council via its 8 Subcommittees:
nuclear and fundamental physics (college 3)
structural and magnetic excitations (college 4)
crystallographic structures (college 5a)
magnetic structures (college 5b)
structure and dynamics of liquids and glasses (college 6)
materials science, surfaces and spectroscopy (college 7)
biology (college 8)
structure and dynamics of soft-condensed matter (college 9)

Scientific Life: based on 10 colleges
8 of which map on to the subcommittees plus two others:
instruments and techniques (college 1); theory (college 2)

LE DAUPHINÉ Libéré

Téléphone
44-69-20 (8 lignes groupées)
44-85-40 (3 lignes groupées)
87-23-11 (8 lignes groupées)
Télex : 32.822

Mercredi 1er septembre 1971
27ème année - N° 8311

0,50

Le Grand Quotidien d'Information des Alpes et de la Vallée du Rhône

H 38

'67 Foundation of the ILL: French/German venture
First ever heart transplant in South Africa

'68 Start of the construction
Olympic winter games in Grenoble

'71 The reactor goes critical on the 31st August and reaches full power in December
'Imagine', solo album by John Lennon

'72 Start of routine operation of the following instruments:
IN2, three-axis spectrometer,
D2, two-axis diffractometer,
D10, 4-circle diffractometer,
D11, small-angle diffractometer and
PN4, anti-compton spectrometer
Richard Nixon meets Mao, is re-elected President and Watergate breaks out

'73 UK membership of the ILL
Denmark, Ireland and UK join the EEC
Pablo Picasso dies

'79 Start of modernisation programme - 'deuxième souffle'
Islamic revolution in Iran, Ayatollah Khomeiny overthrows the Shah

'81 Extension of the intergovernmental agreement until 31 Dec. 92
François Mitterand becomes President

'84 Shutdown of the reactor for general overhaul
Indira Ghandi is assassinated

'85 Restart with a new vertical cold source
Mikhail Gorbatchev becomes General Secretary of the CPSU

Nouveau record scientifique mondial à Grenoble

La plus puissante "sonde de la matière" a commencé à fonctionner hier soir

Evénement scientifique de portée mondiale hier soir, à Grenoble : le réacteur nucléaire à haut-flux construit conjointement par la France et l'Allemagne, pour quelque 35 milliards anciens, a commencé à diverger. Cette installation constitue la sonde de la matière la plus puissante du monde. Elle permettra des observations sans précédent sur le comportement des atomes. L'énorme cloche métallique blanche sous laquelle elle se trouve (notre photo) est désormais la pièce la plus en vue de l'immense faubourg grenoblois entièrement voué à la recherche scientifique. (Photo Pierre Guyot)

'87 Spanish scienti
Second cold sour
First flight of the Airbus A320

'88 Swiss scient
George Bush be
Benazir Bhutto becomes

'90 Austri
Nelson
Lech Walesa beco

'9
Mad
Gulf

30 years of ILL - some landmarks

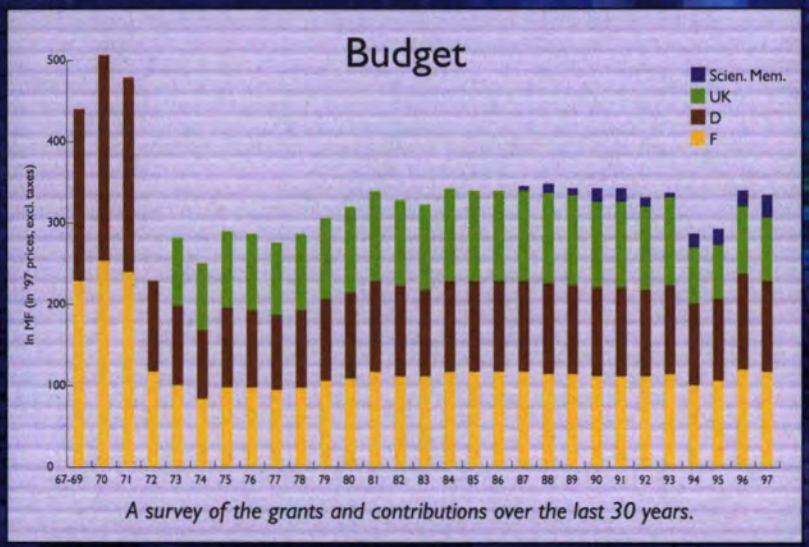

A survey of the grants and contributions over the last 30 years.

The budget plot highlights well the historical dates: the UK membership in 1973, the first scientific membership in 1987 and the budget reduction 1994 because of the changed UK participation (intergovernmental agreement of 1993).

The budget reduction in 1994 had several consequences for ILL's operation:

- Reactor cycles: the number of cycles per year was reduced from 6 to 5 cycles, i.e. from 276 to 230 days.
- Instruments: the scheduled instruments were reduced from 30 to 25, but there are now a number of CRG-instruments operated by external Collaborating Research Groups (see also page 98).
- Beam-time allocation: the allocation of time on scheduled instruments should reflect the relative contribution of the member countries to the annual budget (for details see page 100).
- Staff: the number of staff was reduced by about 100, from 483 in 1990 to 382 in 1993. The level is now settled at around 400 people.

'93 Extension of the intergovernmental agreement until 31 Dec. 2003
Partition of Czechoslovakia into the republics Czech and Slovakia

'95 January, restart of the reactor
Jacques Chirac becomes President

'96 Russian scientific membership
François Mitterand dies
Germany wins European Football Championship
Marcello Mastroiani dies

'97 Italian scientific membership
Deng Xiaoping dies
Tony Blair becomes Prime Minister

embership
rizontal)

mbership
resident
nt

ntific membership
liberated
ident

tdown of the reactor,
lacement of reactor vessel
summit

In 1973 the reactor level D (with the swimming pool) had no instrumental installations (left). Compare this with a recent photo of level D with PF2 (right).

Reactor

The high-flux reactor has operated very reliably. However, there were two major shutdowns: Oct. 84 - Aug. 85 and Apr. 91 - Jan. 95. Altogether up to the end of 1997 the reactor has run for 5202 days in 112 reactor cycles with a reliability per year of around 98% (one year, in 1996, there was no unforeseen shutdown at all). The length of cycles increased over the years. It started with 44 days and now we have reached 50 days of continuous reactor operation per cycle.

The 'hedgehog', D6, an instrument ahead of its time.

Instruments

It is quite remarkable that the instruments came into user operation about 6 months after the reactor was up to full power; the development of reactor and instrumentation went hand-in-hand. Over the years there was a continuous evolution of the instrument profile: instruments were upgraded, replaced, shut down, taken over by CRGs and new ones constructed. This is at least partially illustrated by the following list of existing and previous ILL- and CRG-instruments (excluding special-beam instruments):

Diffractometers

in operation (or in construction): **ADAM, D1A, D1B, D2B, D3, D4, D7, D9, D10, D11, D16, D17, D19, D20, DB21, D22, D23, EVA, LADI, S20**
closed: **D5, D6, D8, D12**

Inelastic spectrometers

in operation (or in construction): **IN1, IN3, IN4, IN5, IN6, IN8, IN10, IN11, IN12, IN13, IN14, IN15, IN16, IN20, IN22**
closed: **IN2, IN7, IN9**

Nuclear and fundamental-physics instruments

in operation (or in construction): **PF1, PF2, PN1, PN3**
closed: **PN2, PN4, PN5, PN6, PN7, PN8.**

PUBLICATIONS

6

In 1997, the ILL received notice of 534 publications by ILL staff and users of which 319 were published as journal articles, and 212 as conference proceedings[1] in journals, books or reports. The distribution by subject is as follows: 57 in instruments and techniques, 24 in theory, 33 in fundamental and nuclear physics, 88 in structural and magnetic excitations, 58 in crystallographic structures, 101 in magnetic structures, 35 in structure and dynamics of liquids and glasses, 72 in materials science, surfaces and spectroscopy, 25 in biology, 33 in structure and dynamics of soft-condensed matter.

« Experimental Reports & Theory College Activities »
Please note that the above ILL document will no longer be published in paper form. In future you will be able to access and print the ILL experimental reports via the web (http://www.ill.fr). This new system will be available from summer 1998.

[1]For example 130 publications related to ILL experiments were published in the Proceedings of ECNS'96 in Physica B.

PUBLICATIONS

This list gives publications received during 1997 resulting from research carried out at the ILL.
It was generated from the library database LORIS-DORIS and can be consulted on the Web at http://www.ill.fr.

PAPERS PUBLISHED IN SCIENTIFIC PERIODICALS, BOOKS AND CONFERENCE PROCEEDINGS

ABELE H., BAESSLER S., DUBBERS D., LAST J., MAYERHOFER U., METZ C., MÜLLER T.M., NESVIZHEVSKY V.V., RAVEN C., SCHÄRPF O., ZIMMER O. A measurement of the beta asymmetry *A* in the decay of free neutrons.
Physics Letters B **407**, 212-218 (1997)

ACET M., WASSERMANN E.F., ANDERSEN K.H., MURANI A.P., SCHÄRPF O. Large moment fluctuations in Fe-Ni anti-Invar (abstract).
Journal of Applied Physics **81**, 3876 (1997)

ACET M., WASSERMANN E.F., ANDERSEN K.H., MURANI A.P., SCHÄRPF O. The anomalous temperature dependence of the paramagnetic response of Fe-rich fcc Fe-Ni.
Europhysics Letters **40**, 93-98 (1997)

ADAM M., LAIREZ D., KARPASAS M., GOTTLIEB M. Static and dynamic properties of cross-linked poly(dimethylsiloxane) pregel clusters.
Macromolecules **30**, 5920-5929 (1997)

ADAM M., LAIREZ D., RASPAUD E., FARAGO B. Dynamic properties of semidilute solutions at the theta point [Phys. Rev. Lett. 77, 3673 (1996)]. Errata.
Physical Review Letters **78**, 1197 (1997)

AEBERSOLD M.A., ANDRES H., BÜTTNER H.G., BORRAS-ALMENAR J.J., CLEMENTE J.M., CORONADO E., GÜDEL H.U., KEARLEY G.J. Magnetic excitations in polyoxometalate tetrameric clusters.
Physica B **234-236**, 764-765 (1997)

AEPPLI G., MASON T.E., HAYDEN S.M., MOOK H.A., KULDA J. Nearly singular magnetic fluctuations in the normal state of a high-Tc cuprate superconductor.
Science **278**, 1432-1435 (1997)

AIN M., LORENZO J.E., REGNAULT L.P., DHALENNE G., REVCOLEVSCHI A., HENNION B., JOLICOEUR T. Double gap and solitonic excitations in the spin-Peierls chain $CuGeO_3$.
Physical Review Letters **78**, 1560-1563 (1997)

AÏN M., REGNAULT L.P., DHALENNE G., REVCOLEVSCHI A., LORENZO J.E., JOLICOEUR T. Double gap in the spin-Peierls compound $CuGeO_3$.
Journal of Applied Physics **81**, 4393-4395 (1997)

ALBA-SIMIONESCO C., FUJIMORI H., MORINEAU D., FRICK B. A study of the glass transition of molecular liquids as a function of pressure and temperature.
Progress of the Theoretical Physics. Supplement **126**, 229-233 (1997)

ALBINATI A., KLOOSTER W.T., KOETZLE T., FORTIN J.B., RICCI J.S., ECKERT J., FONG T.P., LOUGH A.J., MORRIS R.H., GOLOMBEK A.P. Single-crystal x-ray and neutron diffraction structure determination and inelastic neutron scattering study of the dihydrogen complex *trans*-$[Ru(H_2)(H)(dppe)_2][BPh_4]$.
Inorganica Chimica Acta **259**, 351-357 (1997)

ALEFELD B., HAYES C., MEZEI F., RICHTER D., SPRINGER T. High-resolution focusing SANS with a toroidal neutron mirror.
Physica B **234-236**, 1052-1054 (1997)

ALEGRIA A., CENDOYA I., COLMENERO J., ALBERDI J.M., FRICK B. QENS investigation of the segmental dynamics of a PVME/dPS miscible polymer blend.
Physica B **234-236**, 442-444 (1997)

ALLEN F.H., HOY V.J., HOWARD J.A.K., THALLADI V.R., DESIRAJU G.R., WILSON C.C., MCINTYRE G.J. Crystal engineering and correspondence between molecular and crystal structures. Are 2- and 3-aminophenols anomalous ?
Journal of the American Chemical Society **119**, 3477-3480 (1997)

ALLENSPACH P., FURRER A., GÜDEL H.U., FURER N., BÜTTNER H.G. Crystal electric field and dimer splitting in $Cs_3Er_2X_9$ (X= Cl, Br).
Physica B **234-236**, 744-745 (1997)

ALMAIRAC R., BORDALLO H.N., BULOU A., NOUET J., CURRAT R. Slow dynamics and instability in $BaZnF_4$.
Physical Review B **55**, 8249-8256 (1997)

ALONSO J.A., CASAIS M.T., MARTINEZ-LOPE M.J., MARTINEZ J.L., FERNANDEZ-DIAZ M.T. A structural study from neutron diffraction data and magnetic properties of RMn_2O_5 (R=La, rare earth).
Journal of Physics Condensed Matter **9**, 8515-8526 (1997)

ALONSO J.A., MARTINEZ-LOPE M.J., CASAIS M.T., MACMANUS-DRISCOLL J.L., DE SILVA P.S.I.P.N., COHEN L.F., FERNANDEZ-DIAZ M.T. Non-stoichiometry, structural defects and properties of $LaMnO_{3+\delta}$ with high δ values ($0.11 \leq \delta \leq 0.29$).
Journal of Materials Chemistry **7**, 2139-2144 (1997)

ALONSO J.A., MARTINEZ-LOPE M.J., GARCIA-MUNOZ J.L., FERNANDEZ M.T. Crystal structure and magnetism in the defect perovskite $LaNiO_{2.5}$.
Physica B **234-236**, 18-19 (1997)

ALONSO J.A., MARTINEZ-LOPE M.J., GARCIA-MUNOZ J.L., FERNANDEZ-DIAZ M.T. A structural and magnetic study of the defect perovskite $LaNiO_{2.5}$ from high-resolution neutron diffraction data.
Journal of Physics Condensed Matter **9**, 6417-6426 (1997)

AMARA M., MORIN P., BOURDAROT F. Experimental study of the magnetic phase diagrams of DyCu.
Journal of Physics Condensed Matter **9**, 7441-7454 (1997)

ANDERSEN K.H., STIRLING W.G., GLYDE H.R. Momentum distribution and final-state effects in liquid ^{4}He.
Physical Review B **56**, 8978-8987 (1997)

ANTORRENA G., LE CAËR G., MALAMAN B., PALACIO F., RESSOUCHE E., SCHWEIZER J. Magnetic structure of the molecular compound $Fe(dtc)_2Cl$.
Physica B **234-236**, 780-782 (1997)

ARBE A., RICHTER D., COLMENERO J., FARAGO B. Coherent quasielastic scattering from internal relaxations in polymers.
Physica B **234-236**, 437-441 (1997)

ARRIGHI V., HIGGINS J.S. Molecular dynamics of a main-chain liquid crystalline polyester below the crystalline to nematic phase transition.
Journal of the Chemical Society Faraday Transactions **93**, 1605-1612 (1997)

ARTIGAS M., BACMANN M., FRUCHART D., MORALES M.F., TOMEY E. Transition metal distribution in the $ErMn_{12-x}Fe_x$ ($0 \leq x \leq 8$) compounds.
Physica B **234-236**, 155-156 (1997)

ARZUMANOV S.S., BONDARENKO L.N., KOROBKINA E.I., MOROZOV V.I., PANIN Y.N., FOMIN A.I., CHERNYAVSKII S.M., SHILKIN S.V., GELTENBORT P., DREXEL W., PENDLEBURY J.M., SCHRECKENBACH K. Observation of selective enhancement of the capture of ultracold neutrons by nuclei.
JETP Letters **65**, 1-6 (1997)

BAFILE U., BENMORE C.J., EGELSTAFF P.A., MOS B., SUCK J.B., VERKERK P., ANDERSEN K.H., BAROCCHI F., COOK J.C. Heavily damped sound modes in dense krypton gas studied by neutron Brillouin scattering.
Physica B **234-236**, 311-312 (1997)

BARNES A.C., LAGUE S.B., SALMON P.S., FISCHER H.E. A determination of the structure of liquid Ag_2Se using neutron diffraction and isotopic substitution.
Journal of Physics Condensed Matter **9**, 6159-6173 (1997)

BAROCCHI F., BAFILE U., MAGLI R. Recent experiments in neutron scattering by simple fluids.
Journal of Physics Condensed Matter **8**, 9111-9126 (1996)

BAROCCHI F., CHIEUX P., FONTANA R., MAGLI R., MERONI A., PAROLA A., REATTO L., TAU M. The pair correlation function of krypton in the critical region: theory and experiment.
Journal of Physics Condensed Matter **9**, 8849-8871 (1997)

BARUCHEL J., SCHLENKER M. Application of diffraction topography to the study of magnetic domains and phase transitions.
In: 'X-ray and Neutron Dynamical Diffraction - Theory and Applications', AUTHIER A. et al. (Eds.) (Plenum Press, 1996) pp. 187-197

BATTLE P.D., COX D.E., GREEN M.A., MILLBURN J.E., SPRING L.E., RADAELLI P.G., ROSSEINSKY M.J., VENTE J.F. Antiferromagnetism, ferromagnetism, and phase separation in the GMR system $Sr_{2-x}La_{1+x}Mn_2O_7$.
Chemistry of Materials **9**, 1042-1049 (1997)

BATTLE P.D., HEPBURN J.A., MILLBURN J.E., RADAELLI P.G., ROSSEINSKY M.J., SPRING L.E., VENTE J.F. $Sr_{1.8}Nd_{1.2}Mn_2O_7$: synthesis, crystal structure, and physical properties.
Chemistry of Materials **9**, 3215-3221 (1997)

BATTLE P.D., MILLBURN J.E., ROSSEINSKY M.J., SPRING L.E., VENTE J.F., RADAELLI P.G. Neutron diffraction study of the structural and electronic properties of $Sr_2HoMn_2O_7$ and $Sr_2YMn_2O_7$.
Chemistry of Materials **9**, 3136-3143 (1997)

BAUER E., FISCHER P., MARABELLI F., ELLERBY M., MCEWEN K.A., ROESSLI B., FERNANDEZ-DIAZ M.T. Magnetic structures and bulk magnetic properties of $YbCu_4M$, M=Au, Pd.
Physica B **234-236**, 676-678 (1997)

BAUER E., LIENDL M., NABER L., WERNER D., MICHOR H., HILSCHER G., DÖNNI A., FISCHER P., FAUTH F., ZOLLIKER M. Transport, magnetic and thermodynamic properties of $REPd_2Ga_3$, RE=Pr, Nd, Sm.
Zeitschrift für Physik B **102**, 291-298 (1997)

BECKER J., EBERT M., GROSSMANN T., HEIL W., HOFMANN D., HUMBLOT H., LEDUC M., OTTEN E.W., ROHE D., SIEMENSMEYER K., SURKAU R., STEINER M., TASSET F., TRAUTMANN N. Realization of a broad-band neutron spin filter with compressed, polarized ^{3}He gas.
Physica B **234-236**, 1078-1079 (1997)

BEE M., COMBET J., DJURADO D., CURTET J.P., DIANOUX A.J. Structural and dynamical aspects of solid sulpholan in the temperature range 160-300 K. II.- Incoherent quasielastic neutron scattering study.
Physica B **233**, 102-110 (1997)

BEE M., COMBET J., DJURADO D., FERRAND M., DIANOUX A.J. Dynamics of bromohexadecane and bromodecane chains included in an organic matrix: an incoherent quasielastic neutron scattering study.
Molecular Physics **91**, 681-688 (1997)

BEE M., COMBET J., MORELON N.D., FERRAND M., DJURADO D., DIANOUX A.J., FRICK B. Dynamics of channel-type inclusion compounds with guest linear alkyl chains.
Physica B **234-236**, 109-111 (1997)

BELLISSENT-FUNEL M.C., FILABOZZI A., CHEN S.H. Dynamics of a deuterated C-phycocyanin protein as studied by coherent inelastic neutron scattering.
In: 'Biological Macromolecular Dynamics', CUSACK S. et al. (Eds.) (Adenine Press, 1997) pp. 143-146

BERMEJO F.J., CRIADO A., FAYOS R., FERNANDEZ-PEREA R., FISCHER H.E., SUARD E., GUELYLAH A., ZUNIGA J. Structural correlations in disordered matter: an experimental separation of orientational and positional contributions.
Physical Review B **56**, 11536-11545 (1997)

BERMEJO F.J., FERNANDEZ-PEREA R., ALVAREZ M., ROESSLI B., FISCHER H.E., BOSSY J. Collective, short-wavelength excitations in liquid gallium.
Physical Review E **56**, 3358-3369 (1997)

BERMEJO F.J., FISCHER H.E., RAMOS M.A., DE ANDRES A., DAWIDOWSKI J., FAYOS R. Microscopic dynamics in glasses in relation to that shown by other complex systems.
In: 'Complex Behaviour of Glassy Systems', RUBI M. et al. (Eds.) (Springer Verlag, 1997) pp. 45-61

BEWLEY R.I., STEWART J.R., RITTER C., SCHLEGER P., CYWINSKI R. Neutron spin echo study of a random anisotropy magnet.
Physica B **234-236**, 762-763 (1997)

BIANCONI A., SAINI N.L., LANZARA A., LUSIGNOLI M., ROSSETTI T., RADAELLI P.G., BORDET P., KVICK Å., OYANAGI H. Stripe structure and non-homogeneity of the CuO_2 plane by joint EXAFS and diffraction.
Journal de Physique IV **7**, C2/735-C2/740 (1997)

BIENFAIT M., ZEPPENFELD P., BOVIE L.J., VILCHES O.E., LAUTER H.J. Structure of monolayer films of hydrogen isotope mixtures.
Physica B **234-236**, 159-163 (1997)

BIENFAIT M., ZEPPENFELD P., VILCHES O.E., PALMARI J.P., LAUTER H.J. Structure and phase transitions of D_2+Ar mixtures adsorbed on graphite.
Surface Science **377-379**, 504-508 (1997)

BLANCO J.A., FÅK B., NICKLOW R.M., ROESSLI B., SCHMITT D. Dynamics of $PrNi_2Si_2$ in its modulated magnetic phase.
Physica B **234-236**, 756-757 (1997)

BLAND J.A.C. Magnetic multilayers studied by polarised neutron reflection.
Physica B **234-236**, 458-463 (1997)

BLASCO J., GARCIA J., DE TERESA J.M., IBARRA M.R., PEREZ J., ALGARABEL P.A., MARQUINA C., RITTER C. Structural, magnetic, and transport properties of the giant magnetoresistive perovskites $La_{2/3}Ca_{1/3}Mn_{1-x}Al_xO_{3-\delta}$.
Physical Review B **55**, 8905-8910 (1997)

BLASCO J., GARCIA J., DE TERESA J.M., IBARRA M.R., PEREZ J., ALGARABEL P.A., MARQUINA C., RITTER C. Charge ordering at room temperature in $Tb_{0.5}Ca_{0.5}MnO_3$.
Journal of Physics Condensed Matter **9**, 10321-10331 (1997)

BOBROVSKII V.I., MIRMELSTEIN A., PODLESNYAK A., ZHDAKHIN I., GOSHCHITSKII B.N., MITBERG E., ZUBKOV V., D'YACHKOVA T., KADYROVA N., KHLYBOV E., FAUTH F., FURRER A. Neutron powder diffraction study of the infinite-layer compounds $Sr_{1-x}Nd_xCuO_2$.
Physica B **234-236**, 818-820 (1997)

BÖRJESSON L., BUCHENAU U., DIANOUX A.J., ENGBERG D., SOKOLOV A.P., WISCHNEWSKI A. Sound waves and other modes in the strong glassformer B_2O_3.
Physica B **234-236**, 383-385 (1997)

BONDARENKO L.N., CHERNYAVSKII S.M., FOMIN A.I., GELTENBORT P., MOROZOV V.I., SHILKIN S.V. The investigation of UCN interaction with the surface of beryllium and stainless steel by the new method based on the neutron induced γ-radiation analysis.
Physica B **234-236**, 1189-1191 (1997)

BOOTHROYD A.T. Neutron crystal field relaxation spectroscopy in superconductors.
Neutron News **8**, 28-33 (1997)

BORDET P., DUC F., RADAELLI P.G., LANZARA A., SAINI N.L., BIANCONI A., ANTIPOV E.V. Structural instability around T_c observed in Hg-1201 by neutron powder diffraction and EXAFS.
Physica C **282-287**, 1081-1082 (1997)

BORDET P., LOUREIRO S.M., LE FLOCH S., CAPPONI J.J., CHAILLOUT C., CHENEVAS J., THOLENCE J.L., ANTIPOV E.V., RADAELLI P.G., MAREZIO M. High pressure synthesis and structure of the superconducting mercury cuprates $(Hg_{1-x}M_x)$ $Ba_2Ca_{n-1}Cu_nO_{2+2n+\delta}$ with M=C,S.
Physica C **282-287**, 65-68 (1997)

BORTZ M., HEWAT A.W., YVON K. Synthesis and structure determination of complex zinc hydrides. Part 3: Dirubidium- and dicaesiumtetrahydridozincate (II), Rb_2ZnH_4 and Cs_2ZnH_4.
Journal of Alloys and Compounds **248**, L1-L4 (1997)

BORTZ M., HEWAT A.W., YVON K. Synthesis and structure determination of complex zinc hydrides. Part 4: Trirubidium and tricaesium tetrahydridozincate(II) hydride, Rb_3ZnH_5 and Cs_3ZnH_5.
Journal of Alloys and Compounds **253-254**, 13-16 (1997)

BÖTTGER G., ALLENSPACH P., DÖNNI A., AOKI Y., SATO H. Low-temperature specific heat of $Er_2Ba_4Cu_7O_{15-\delta}$.
Zeitschrift für Physik B **104**, 195-198 (1997)

BÖTTGER G., FISCHER P., DÖNNI A., BERASTEGUI P., AOKI Y., SATO H., FAUTH F. Long-range magnetic order of the Er ions in $Er_2Ba_4Cu_7O_{14.92}$.
Physical Review B **55**, R12005-R12007 (1997)

BÖTTGER G., MESOT J., FISCHER P., FURRER A. Ca substitution in $RBa_2Cu_3O_{7-\delta}$ (R= Y, Er; δ<0.15): the influence on structure and superconductivity.
Physica B **234-236**, 843-845 (1997)

BOUCHERLE J.X., GIVORD F., LAPERTOT G., SCHWEIZER J., PUJOL S., OULADDIAF B. Very low-temperature magnetic structure in Ce_3Al_{11}.
Physica B **234-236**, 687-688 (1997)

BOUCHERLE J.X., GIVORD F., SCHWEIZER J., ISIKAWA Y. Crystal electric field effects on the magnetic form factor of the Kondo compound $CeNi_2Al_5$.
Physica B **234-236**, 875-876 (1997)

BOURDAROT F., BOSSY J., BURLET P., FÅK B., MONACHESI P., REBIZANT J., REGNAULT L.P., SPIRLET J.C., VOGT O. Magnetic excitations in NpBi.
Physical Review B **56**, 14029-14035 (1997)

BOURDAROT F., BURLET P., BOSSY J., FÅK B., LANDER G.H., REBIZANT J., REGNAULT L.P., SPIRLET J.C. Magnetic excitations in NpBi.
Physica B **234-236**, 754-755 (1997)

BOURGES P., CASALTA H., IVANOV A.S., PETITGRAND D. Superexchange coupling and spin susceptibility spectral weight in undoped monolayer cuprates.
Physical Review Letters **79**, 4906-4909 (1997)

BOURGES P., CASALTA H., REGNAULT L.P., BOSSY J., BURLET P., VETTIER C., BEAUGNON E., GAUTIER-PICARD P., TOURNIER R. High magnetic field dependence of spin fluctuations in $YBa_2Cu_3O_7$.
Physica B **234-236**, 830-831 (1997)

BOURGES P., FONG H.F., REGNAULT L.P., BOSSY J., VETTIER C., MILIUS D.L., AKSAY I.A., KEIMER B. High-energy spin excitations in $YBa_2Cu_3O_{6.5}$.
Physical Review B **56**, R11439-R11442 (1997)

BOURGES P., REGNAULT L.P., SIDIS Y., BOSSY J., BURLET P., VETTIER C., HENRY J.Y., COUACH M. Shifting of the magnetic-resonance peak to lower energy in the superconducting state of underdoped $YBa_2Cu_3O_{6.8}$.
Europhysics Letters **38**, 313-318 (1997)

BOUVET A., FILHOL A., KULDA J. PkFit - a tool to fit the data from neutron three-axis spectrometers.
Nuclear Instruments and Methods in Physics Research A **390**, 359-365 (1997)

BRADEN M., WILKENDORF G., LORENZANA J., AÏN M., MCINTYRE G.J., BEHRUZI M., HEGER G., DHALENNE G., REVCOLEVSCHI A. Beziehung zwischen Kristallstruktur und magnetischer Wechselwirkung in $CuGeO_3$.
Zeitschrift für Kristallographie Supplement **11**, 154 (1996)

BRANDSTÄTTER G., VOSTNER A., WEBER H.W., CHATTOPADHYAY T., CUBITT R., FISCHER H.E., EMEL'CHENKO G.A. Neutron diffraction by the flux line lattice in $YBa_2Cu_3O_{7-\delta}$ single crystals.
Physica C **282-287**, 2089-2090 (1997)

BRANDSTÄTTER G., WEBER H.W., CHATTOPADHYAY T., CUBITT R., FISCHER H., WYLIE M., EMEL'CHENKO G.A., WIEDENMANN A. Neutron diffraction by the flux line lattice in $YBa_2Cu_3O_{7-\delta}$ single crystals.
Journal of Applied Crystallography **30**, 571-574 (1997)

BRISON J.P., BUZDIN A., GLEMOT L., THOMAS F., FLOUQUET J. Upper critical field of heavy fermion superconductors.
Physica B **230-232**, 406-408 (1997)

BROWN C.M., PRASSIDES K., IWASA Y., SHIMODA H. Magnetism and dynamics of ammoniated K_3C_{60}.
In: 'Recent Advances in the Chemistry and Physics of Fullerenes and Related Materials', KADISH K.M. et al. (Eds.) (Electrochemical Society, 1997) pp. 1224-1231

BROWN P.J., CHATTOPADHYAY T. The helimagnetic structure of $Eu(As_{0.20}P_{0.80})_3$ determined by zero-field neutron polarimetry.
Journal of Physics Condensed Matter **9**, 9167-9173 (1997)

BROWN P.J., CRANGLE J., NEUMANN K.U., SMITH J.G., ZIEBECK K.R.A. The structure and magnetic moment distribution in the antiferromagnetic phase of $U_{14}Au_{51}$.
Journal of Physics Condensed Matter **9**, 4729-4742 (1997)

BUCHENAU U. Dynamics of polymers.
In: 'New Instruments and Science around SINQ. Lecture Notes of the '4th Summer School on Neutron Scattering' PSI Proceedings 96-02 (PAUL SCHERRER INSTITUTE, 1996) pp. 379-395

BÜNEMANN J., GEBHARD F., WEBER W. Gutzwiller-correlated wave functions for degenerate bands: exact results in infinite dimensions.
Journal of Physics Condensed Matter **9**, 7343-7358 (1997)

BÜTTNER H.G. New ILL instrumentation.
Neutron News **8**, 21-26 (1997)

BÜTTNER H.G., KEARLEY G.J., FRICK B. Tunnelling of the one-dimensionnal rotor NH_3D^+ in the NH_4ClO_4 and NH_4PF_6 lattices.
Chemical Physics **214**, 425-429 (1997)

CABANE B., WONG K., LINDNER P., LAFUMA F. Shear induced gelation of colloidal dispersions.
Journal of Rheology **41**, 531-547 (1997)

CACIUFFO R., AMORETTI G., CARLILE C.J., FERRERO C., GEREMIA S., PACI B., PRAGER M., UGOZZOLI F. Molecular dynamics and tunnelling in supramolecular complexes.
Physica B **234-236**, 115-120 (1997)

CAMPBELL A.J., BALAKRISHNAN G., LEES M.R., PAUL D. MCK., MCINTYRE G.J. Single-crystal neutron-diffraction study of a structural phase transition induced by a magnetic field in $La_{1-x}Sr_xMnO_3$.
Physical Review B **55**, R8622-R8625 (1997)

CAMPO J., PALACIO F., PADUAN-FILHO A., BECERRA C.C., FERNANDEZ-DIAZ M.T., RODRIGUEZ CARVAJAL J. Anomalous AF-SF line boundary in the phase diagram of $Rb_2Fe_{1-x}In_xCl_5.H_2O$ solid solutions.
Physica B **234-236**, 622-624 (1997)

CAPPELAERE E., BERRET J.F., DECRUPPE J.P., CRESSELY R., LINDNER P. Rheology, birefringence, and small-angle neutron scattering in a charged micellar system: evidence of a shear-induced phase transition.
Physical Review E **56**, 1869-1878 (1997)

CASALTA H., BOURGES P., PETITGRAND D., D'ASTUTO M., IVANOV A.S. 2D magnetic behaviour of Nd in Nd_2CuO_4 below T_N.
Physica B **234-236**, 803-805 (1997)

CASALTA H., BOURGES P., PETITGRAND D., IVANOV A.S. Low temperature magnetic excitations in Nd_2CuO_4 single crystals studied by neutron scattering.
Solid State Communications **100**, 683-686 (1996)

CASTELLANI C., DI CASTRO C., PISTOLESI F., STRINATI G.C. Exact infrared behavior of superfluid interacting bosons at zero temperature.
Physica C **282-287**, 1821-1822 (1997)

CASTELLANI C., DI CASTRO C., PISTOLESI F., STRINATI G.C. Infrared behavior of interacting bosons at zero temperature.
Physical Review Letters **78**, 1612-1615 (1997)

CASTELLANI C., DI CASTRO C., PISTOLESI F., STRINATI G.C.Symmetry properties and renormalization group in the stable superfluid phase of bosons at zero temperature.
Zeitschrift für Physik B **103**, 331-333 (1997)

CELLI M., BAROCCHI F., FISCHER H.E., MAGLI R. The structure of low-density ortho-deuterium investigated through neutron diffraction.
Physica B **234-236**, 331-333 (1997)

CHAMBERLAIN D., O'HARA B.P., WILSON S.A., PEARL L.H., PERKINS S.J. Oligomerization of the amide sensor protein AmiC by x-ray and neutron scattering and molecular modeling.
Biochemistry **36**, 8020-8029 (1997)

CHAPUIS G., FARKAS-JAHNKE M., PEREZ-MATO J.M., SENECHAL M., STEURER W., JANOT C., PANDEY D., YAMAMOTO A. Checklist for the description of incommensurate modulated crystal structures. Report of the International Union of Crystallography Commission on Aperiodic Crystals.
Acta Crystallographica A **53**, 95-100 (1997)

CHARITAT T., FOURCADE B. Lattice of passages connecting membranes.
Journal de Physique II **7**, 15-35 (1997)

CHARRIER B., OULADDIAF B., SCHMITT D. Observation of quasimagnetic structures in rare-earth-based icosahedral quasicrystals.
Physical Review Letters **78**, 4637-4640 (1997)

CHATTOPADHYAY T., MCINTYRE G.J. Existence of two length scales in critical scattering in $CeAl_2$.
Physica B **234-236**, 682-684 (1997)

CHATTOPADHYAY T., SIEMENSMEYER K., SCHNEIDER H. Field-induced double-*k* to single-*k* phase transition in Nd_2CuO_4 at millikelvin temperatures.
Physica B **234-236**, 715-716 (1997)

CHIEUX P., DUPUY-PHILON J., JAL J.F., SUCK J.B. Temperature dependence of the collective atomic dynamics of liquid rubidium.
Journal of Non-Crystalline Solids **205-207**, 370-374 (1996)

CHRISTENSEN A.N., HAZELL R.G., HEWAT A.W. Synthesis, crystal growth and structure investigations of rare-earth disilicates and rare-earth oxyapatites.
Acta Chemica Scandinavica **51**, 37-43 (1997)

CICOGNANI G., GUERARD B.V., OED A. Performance of MSGC on diamond-coated glass.
Nuclear Instruments and Methods in Physics Research A **392**, 115-119 (1997)

CIPRIANI F., CASTAGNA J.C., CLAUSTRE L., WILKINSON C., LEHMANN M.S. Large area neutron and x-ray image-plate detectors for macromolecular biology.
Nuclear Instruments and Methods in Physics Research A **392**, 471-474 (1997)

CIPRIANI F., CASTAGNA J.C., WILKINSON C., LEHMANN M.S., BÜLDT G. A neutron image plate quasi-Laue diffractometer for protein crystallography.
In: 'Neutrons in Biology', SCHOENBORN B.P., KNOTT R.B. (Eds.) (Plenum Press, 1996) pp. 423-431

CLARKE S.M., RENNIE A.R., OTTEWILL R.H. Stacking of hexagonal layers of colloidal particles: study by small-angle neutron diffraction.
Langmuir **13**, 1964-1969 (1997)

CLEMENTE J.M., ANDRES H., AEBERSOLD M.A., BORRAS-ALMENAR J.J., CORONADO E., GÜDEL H.U., BÜTTNER H.G., KEARLEY G.J. Magnetic excitations in tetrameric clusters of polyoxometalates observed by inelastic neutron scattering. Evidence for anisotropic exchange interactions in cobalt(II) clusters.
Inorganic Chemistry **36**, 2244-2245 (1997)

CLERC M., HENDRIKX Y., FARAGO B. Dynamics of a lyotropic cubic phase.
Journal de Physique II **7**, 1205-1214 (1997)

COAD S., PETRENKO O., PAUL D. MCK., FÅK B., LUSSIER J.G., MCMORROW D.F. Magnetic excitations in single crystals of $Cu_{1-x}Ni_xGeO_3$.
Physica B **239**, 350-357 (1997)

COLDEA R., TENNANT D.A., COWLEY R.A., MCMORROW D.F., DORNER B., TYLCZYNSKI Z. Quasi-1D S=1/2 antiferromagnet Cs_2CuCl_4 in a magnetic field.
Physical Review Letters **79**, 151-154 (1997)

COLE J.M., DORNER B., HOWARD J.A.K., MCINTYRE G.J. The use of neutrons in the analysis of the non-linear optical phenomenon.
Physica B **234-236**, 922-924 (1997)

COLMENERO J., ARBE A., CODDENS G., FRICK B., MIJANGOS C., REINECKE H. Crossover from independent to cooperative segmental dynamics in polymers: Experimental realization in poly(vinyl chloride).
Physical Review Letters **78**, 1928-1931 (1997)

COMBET J., MORELON N.D., FERRAND M., BEE M., DJURADO D., COMMANDEUR G., CASTEJON J.M. Pressure dependence of the dynamics of an organic inclusion compound investigated by incoherent quasielastic neutron scattering.
Journal of Physics Condensed Matter **9**, L403-L409 (1997)

CONVERT P., BERNERON M., GANDELLI R., HANSEN T., OED A., RAMBAUD A., RATEL J., TORREGROSSA J. A large high counting rate one-dimensional position sensitive detector: the D20 banana.
Physica B **234-236**, 1082-1083 (1997)

COOPER N.R. Skyrmions in quantum Hall systems with realistic force laws.
Physical Review B **55**, R1934-R1937 (1997)

COOPER N.R., CHKLOVSKII D.B. Theory of photoluminescence at ν=1 quantum Hall state: excitons, spin waves, and spin textures.
Physical Review B **55**, 2436-2455 (1997)

COOPER N.R., HALPERIN B.I., CHIN-KUN HU, RUZIN I.M. Statistical properties of the low-temperature conductance peak-heights for Corbino disks in the quantum Hall regime.
Physical Review B **55**, 4551-4557 (1997)

COOPER N.R., HALPERIN B.I., RUZIN I.M. Thermoelectric response of an interacting two-dimensional electron gas in a quantizing magnetic field.
Physical Review B **55**, 2344-2359 (1997)

CORMINBOEUF F., JOLIE J., LEHMANN H., FÖHL K., HOYLER F., BÖRNER H.G., DOLL C., GARRETT P.E. $K\pi=4^+$ double-γ vibration in ^{164}Dy.
Physical Review C **56**, R1201-R1205 (1997)

CORNELL K., WIPF H., ANTONOV V.E., ANTONOVA T.E., KOLESNIKOV A.I., PONYATOVSKY E.G., DORNER B. The inelastic neutron scattering spectrum of dhcp iron hydride.
Polish Journal of Chemistry **71**, 1792-1796 (1997)

COSTI T.A. Renormalization-group approach to nonequilibrium Green functions in correlated impurity systems.
Physical Review B **55**, 3003-3009 (1997)

COSTI T.A. Spectral density of the local Cu-O model.
Physical Review B **55**, 6670-6673 (1997)

CURRAT R. Inelastic and quasielastic scattering workshop held at ILL.
Neutron News **8**, 2-4 (1997)

CYWINSKI R., KILCOYNE S.H. Magnetic correlations in $Y(CoMn)_2$ and $Y(CoFe)_2$.
Physica B **234-236**, 592-593 (1997)

DAVI M., DENSCHLAG J.O., TSEKHANOVITCH I., WÖSTHEINRICH M., FAUST H.R., OBERSTEDT S. Gerade-Ungerade-Effekte in der Spaltungsreaktion $^{237}Np(2n_{th},f)$.
Physik der Hadronen und Kerne, 1997-02-24 / 28, Göttingen, Germany (Abstract)

DE TERESA J.M., IBARRA M.R., ALGARABEL P.A., RITTER C., MARQUINA C., BLASCO J., GARCIA J., DEL MORAL A., ARNOLD Z. Evidence for magnetic polarons in the magnetoresistive perovskites
Nature **386**, 256-259 (1997)

DE TERESA J.M., RITTER C., IBARRA M.R., ALGARABEL P.A., GARCIA-MUNOZ J.L., BLASCO J., GARCIA J., MARQUINA C. Charge localization, magnetic order, structural behavior, and spin dynamics of $(La\text{-}Tb)_{2/3}Ca_{1/3}MnO_3$ manganese perovskites probed by neutron diffraction and muon spin relaxation.
Physical Review B **56**, 3317-3323 (1997)

DE VISSER A., KEIZER R.J., MENOVSKY A.A., MIHALIK M., TAUTZ F.S., FRANSE J.J.M., FÅK B., VAN DIJK N.H., FLOUQUET J., BOSSY J., PUJOL S. Neutron-diffraction study of antiferromagnetic order in $U(Pt,Pd)_3$.
Physica B **230-232**, 49-52 (1997)

DEBERNARDI A., PYKA N.M., GÖBEL A., RUF T., LAUCK R., KRAMP S., CARDONA M. Lattice dynamics of wurtzite CdS: neutron scattering and *ab-initio* calculations.
Solid State Communications **103**, 297-301 (1997)

DERIU A., CAVATORTA F., DE MICHELI T., RUPPRECHT A., LANGAN P. The distribution of water in highly ordered fibres of hyaluronic acid.
Physica B **234-236**, 215-216 (1997)

DIEHL M., DOSTER W., PETRY W., SCHOBER H. Water-coupled low-frequency modes of myoglobin and lysozyme observed by inelastic neutron scattering.
Biophysical Journal **73**, 2726-2732 (1997)

DOBRZYNSKI L., PAPOULAR R.J., SAKATA M. Internal magnetization density distribution of iron and nickel by the maximum entropy method.
Journal of the Physical Society of Japan **65**, 255-263 (1996)

DÖNNI A., FURRER A., BAUER E., KITAZAWA H., ZOLLIKER M. Crystalline-electric field excitations in RPd_2Ga_3 (R=Ce, Pr, Nd) studied by powder neutron scattering.
Zeitschrift für Physik B **104**, 403-409 (1997)

DÖNNI A., FURRER A., KITAZAWA H., ZOLLIKER M. Neutron crystalline-electric-field spectroscopy of RPd_2Al_3 (R= Ce, Pr, Nd).
Journal of Physics Condensed Matter **9**, 5921-5933 (1997)

DÖNNI A., KITAZAWA H., FISCHER P., VOGT T., MATSUSHITA A., IIMURA Y., ZOLLIKER M. Sample dependence of magnetic properties and determination of antiferromagnetic structure of $NdPd_2Al_3$.
Journal of Solid State Chemistry **127**, 169-177 (1996)

DORNER B. Polarised neutrons replace high resolution in particular cases.
In: 'Cold Neutrons: Large Scales - High Resolution. Lecture Notes of the '5th Summer School on Neutrons' PSI Proceedings 97-01 (Paul Scherrer Institute, 1997) pp. 261-273

DORNER B., TOPERVERG B.P., BAEHR M., PETITGRAND D. Identification of different magnetic modes in $CsFeCl_3$ by polarisation analysis.
Physica B **234-236**, 549-551 (1997)

DUGAIN F., MIHALKOVIC M., SUCK J.B. Temperature dependence of the generalized vibrational density of states of $Al_{70}Co_{15}Ni_{15}$ and $Al_{62}Co_{15}Cu_{20}Si_3$.
Materials Science and Engineering A **226-228**, 967-971 (1997)

EASTOE J., SHARPE D., HEENAN R.K. Bending elasticities of Di-chained surfactant films in microemulsions.
Progress in Colloid and Polymer Science **105**, 340-345 (1997)

EASTOE J., SHARPE D., HEENAN R.K., EGELHAAF S.U. Rigidities of cationic surfactant films in microemulsions.
Journal of Physical Chemistry B **101**, 944-948 (1997)

ECCLESTON R.S., MUTKA H., PAYEN C. Low-energy response in the spin-ladder compound $(VO)_2P_2O_7$.
Physica B **234-236**, 895-896 (1997)

EGELHAAF S.U., SCHURTENBERGER P. A time-resolved small angle neutron scattering study of the micelle-to-vesicle transition.
Physica B **234-236**, 276-278 (1997)

EHLERS G., AHLERT D., RITTER C., MIEKELEY W., MALETTA H. Anomalous transition from antiferromagnetic to ferromagnetic order in the pseudoternary series $TbNi_{1-x}Cu_xAl$.
Europhysics Letters **37**, 269-274 (1997)

ENCISO E., ALMARZA N.G., CALZAS D.S., GONZALEZ M.A. Low density equation of state of asymmetric hard sphere mixtures (Preliminary communication).
Molecular Physics **92**, 173-176 (1997)

ENSS C., GAUKLER M., NULLMEIER M., WEIS R., WÜRGER A. Novel dielectric relaxation in Li^+ doped KCl.
Physical Review Letters **78**, 370-373 (1997)

EWEN B., RICHTER D. Neutron spin echo investigations on the segmental dynamics of polymers in melts, networks and solutions.
Advances in Polymer Science **134**, 1-129 (1997)

FÅK B., DORNER B. Phonon line shapes and excitation energies.
Physica B **234-236**, 1107-1108 (1997)

FÅK B., GLYDE H.R. Density and spin-density excitations in normal-liquid ^3He.
Physical Review B **55**, 5651-5654 (1997)

FÅK B., VETTIER C., FLOUQUET J., BOURDAROT F., RAYMOND S., VERNIERE A., LEJAY P., BOUTROUILLE P., BERNHOEFT N.R., BRAMWELL S.T., FISHER R.A., PHILLIPS N.E. Influence of sample quality on the magnetic properties of URu_2Si_2.
Journal of Magnetism and Magnetic Materials **154**, 339-350 (1996)

FAYOS R., BERMEJO F.J., DAWIDOWSKI J., FISCHER H.E., GONZALEZ M.A. The relationship between intermediate-range order in glasses and discernible features in the static structure factor.
Physica B **234-236**, 448-449 (1997)

FERNANDEZ J.F., KEMALI M., JOHNSON M.R., ROSS D.K. Quasi-elastic neutron-scattering measurements on the $ZrTi_2H_{3.6}$ C-15 Laves phase compound.
Physica B **234-236**, 903-905 (1997)

FERNANDEZ-PEREA R., BERMEJO F.J., DAWIDOWSKI J., SCHOBER H. On the origin of the anomalous temperature dependence of the first diffraction peak in v-B_2O_3.
Physica B **234-236**, 380-382 (1997)

FERRAND M. Neutron instrumentation in studying dynamics of biomolecules.
In: 'Biological Macromolecular Dynamics', CUSACK S. et al. (Eds.) (Adenine Press, 1997) pp. 9-19

FILLAUX F., BARON M.H., NICOLAI B., TOMKINSON J., KEARLEY G.J. A new view of proton dynamics in amides and peptides: vibrational spectroscopy with neutrons.
In: 'Biological Macromolecular Dynamics', CUSACK S. et al. (Eds.) (Adenine Press, 1997) pp. 69-72

FISCHER H.E., BERMEJO F.J., FAYOS R., DAWIDOWSKI J., RAMOS M.A., VIEIRA S., SCHOBER H., GONZALEZ M.A. Polymorphic ethyl alcohol as a model system for the quantitative study of glassy behavior.
Physica B **234-236**, 433-434 (1997)

FISCHER P., DÖNNI A., STAUB U., ZOLLIKER M. Powder neutron diffractometers HRPT and DMCG.
In: 'New Instruments and Science Around SINQ. Lecture Notes of the '4th Summer School on Neutron Scattering' PSI Proceedings 96-02 (PAUL SCHERRER INSTITUTE, 1996) pp. 15-21

FISCHER P., FAUTH F., SKRIPOV A.V., PODLESNYAK A., PADURETS L.N., SHILOV A.L., OULADDIAF B. Neutron diffraction study of deuterium ordering in C15 type TaV_2D_x (x>1) in the temperature range of 1.5-295 K.
Journal of Alloys and Compounds **253-254**, 282-285 (1997)

FISCHER P., MESOT J., LUCAS B., LUDI A., PATTERSON H., HEWAT A.W. Pressure dependence investigation of the low-temperature structure of $TlAu(CN)_2$ by high-resolution neutron powder diffraction and optical studies.
Inorganic Chemistry **36**, 2791-2794 (1997)

FORET M., COURTENS E., VACHER R., SUCK J.B. Comment on "Evidence of high frequency propagating modes in vitreous silica".
Physical Review Letters **78**, 4669-4670 (1997)

FORMISANO F., DAMAY P., JAL J.F., LECLERCQ F., MAGLI R. The critical scattering universal function measured through sans: an experimental test of the scaling laws.
Physica B **234-236**, 319-320 (1997)

FORSYTH V.T., LANGAN P., WHALLEY M.A., MAHENDRASINGAM A., WILSON C.C., GIESEN U., DAUVERGNE M.T., MASON S.A., FULLER W. Time-of-flight Laue fiber diffraction studies of perdeuterated DNA.
In: 'Neutrons in Biology', SCHOENBORN B.P., KNOTT R.B. (Eds.) (Plenum Press, 1996) pp. 359-367

FRANZ H., MATHE G., CIUCHI F., MARIANI P., PETRY W., SCHMIDT W. Dynamics of guanosine self-assembled aggregates in the hexagonal columnar phase by quasielastic neutron scattering.
Molecular Crystals and Liquid Crystals **290**, 155-162 (1996)

FRANZETTI B., SOHLBERG B., ZACCAI G., VON GABAIN A. Biochemical and serological evidence for a RNase E-like activity in halophilic *Archaea*.
Journal of Bacteriology **179**, 1180-1185 (1997)

FRICK B. Methyl group dynamics in poly(dimethylsiloxane).
In: 'Proceedings of the Workshop on Non Equilibrium Phenomena in Supercooled Fluids, Glasses and Amorphous Materials. A Euroconference', GIORDANO M. et al. (Eds.) (World Scientific, 1996) pp. 255-256

FRICK B., ALBA-SIMIONESCO C., HENDRICKS J., WILLNER L. Incoherent inelastic neutron scattering on polybutadiene under pressure.
Progress of the Theoretical Physics. Supplement **126**, 213-218 (1997)

FRICK B., MAGERL A., BLANC Y., REBESCO R. The new backscattering spectrometer IN16 at the ILL.
Physica B **234-236**, 1177-1179 (1997)

FRIES T., SHAPIRA Y., PALACIO F., MORON M.C., MCINTYRE G.J., KERSHAW R., WOLD A., MCNIFF E.J.Jr. Magnetic ordering of the antiferromagnet Cu_2MnSnS_4 from magnetization and neutron-scattering measurements.
Physical Review B **56**, 5424-5431 (1997)

FULLER W., FORSYTH V.T., MAHENDRASINGAM A., LANGAN P., PIGRAM W.J., MASON S.A., WILSON C.C. DNA hydration studied by neutron fiber diffraction.
In: 'Neutrons in Biology', SCHOENBORN B.P., KNOTT R.B. (Eds.) (Plenum Press, 1996) pp. 345-358

FURRER A., MESOT J., HENGGELER W. Inelastic neutron scattering in cuprate superconductors: evidence for inhomogeneous materials properties.
Journal of Superconductivity **9**, 349-355 (1996)

GABRYS B., ANDERSEN K.H. D7: the polarization analysis multidetector instrument.
Neutron News **8**, 15-20 (1997)

GARCIA SOLDEVILLA J., ESPESO J.I., BLANCO J.A., GOMEZ SAL J.C., GALEZ P., PACCARD D., RODRIGUEZ CARVAJAL J., OULADDIAF B. Elastic and inelastic neutron scattering on $NdNi_{1-x}Cu_x$.
Physica B **234-236**, 758-759 (1997)

GARCIA-MATRES E., MARTINEZ J.L., RODRIGUEZ CARVAJAL J. Temperature evolution of the magnetic structures in R_2BaNiO_5 oxides.
Physica B **234-236**, 567-568 (1997)

GARCIA-MUNOZ J.L., SUAAIDI M., RITTER C. Magnetostructural effects in insulating and metallic $La_{0.85-x}Y_{0.15}Ca_xMnO_3$ (x<0.50).
Physica B **234-236**, 854-855 (1997)

GASSER U., ALLENSPACH P., BUCHGEISTER M., FAUTH F., HENGGELER W., MESOT J., ROSENKRANZ S., VORDERWISCH P., FURRER A. Neutron crystal-field spectroscopy of $RNi_2{}^{11}B_2C$ (R= Ho, Er, Tm).
Czechoslovak Journal of Physics **46 Suppl. S2**, 821-822 (1996)

GASSER U., ALLENSPACH P., FAUTH F., HENGGELER W., MESOT J., FURRER A., ROSENKRANZ S., VORDERWISCH P., BUCHGEISTER M. Neutron crystal-field spectroscopy of $RN_2{}^{11}B_2C$ (R= Ho, Er, Tm).
Zeitschrift für Physik B **101**, 345-352 (1996)

GAWRONSKI M., CONRAD H., SPRINGER T., STAHMANN K.P. Conformational changes of the polysaccharide cinerean in different solvents from scattering methods.
Macromolecules **29**, 7820-7825 (1996)

GAZZANO M., KAGUNYA W.W., MATTEUZZI D., VACCARI A. Neutron diffraction studies of polycrystalline Ni/Mg/Al mixed oxides obtained from hydrotalcite-like precursors.
Journal of Physical Chemistry B **101**, 4514-4519 (1997)

GEBHARD F., BOTT K., SCHEIDLER M., THOMAS P., KOCH S.W. Exact results for the optical absorption of strongly correlated electrons in a half-filled Peierls-distorted chain.
Philosophical Magazine B **75**, 13-46 (1997)

GEBHARD F., BOTT K., SCHEIDLER M., THOMAS P., KOCH S.W. Optical absorption of strongly correlated half-filled Mott-Hubbard chains.
Philosophical Magazine B **75**, 47-65 (1997)

GEBHARD F., BOTT K., SCHEIDLER M., THOMAS P., KOCH S.W. Optical absorption of non-interacting tight-binding electrons in a Peierls-distorted chain at half band-filling.
Philosophical Magazine B **75**, 1-12 (1997)

GEISSLER E., HORKAY F., HECHT A.M., ROCHAS C., LINDNER P., BOURGAUX C., COUARRAZE G. Investigation of PDMS gels and solutions by small angle scattering.
Polymer **38**, 15-20 (1997)

GERNDT E.K.E., KNAPP B.A., SHIPSEY I.P.J., GELTENBORT P. Properties of a Moscow glass micro strip gas chamber.
Nuclear Instruments and Methods in Physics Research A **388**, 42-54 (1997)

GHOMI M., AAMOUCHE A., JOBIC H., COULOMBEAU C., BOULOUSSA O. Neutron inelastic scattering spectra of pyrimidine nucleic acid bases, ribonucleosides and ribonucleotides.
In: 'Biological Macromolecular Dynamics', CUSACK S. et al. (Eds.) (Adenine Press, 1997) pp. 73-78

GINGL F., HEWAT A.W., YVON K. Orthorhombic $Ba_6Mg_7H_{26}$: a new fluoride-related ternary alkaline earth hydride.
Journal of Alloys and Compounds **253-254**, 17-20 (1997)

GINGL F., YVON K., VOGT T., HEWAT A.W. Synthesis and crystal structure of tetragonal $LnMg_2H_7$ (Ln= La, Ce), two Laves phase hydride derivatives having ordered hydrogen distribution.
Journal of Alloys and Compounds **253-254**, 313-317 (1997)

GIRARD P., ALIEV A.E., GUILLAUME F., HARRIS K.D.M., HOLLINGSWORTH M.D., DIANOUX A.J., JONSEN P. Reorientational motions of dioctanoyl peroxide guest molecules within the urea tunnel structure: assessment of two-site jump models.
Physica B **234-236**, 112-114 (1997)

GIVORD F., SCHWEIZER J., TASSET F. On the magnetic structure of $CeAl_2$: a 3-d neutron polarization analysis investigation.
Physica B **234-236**, 685-686 (1997)

GLADYSHEVSKII R.E., GALEZ P., LEBBOU K., BELLINGERI E., COUACH M., FLÜKIGER R., JORDA J.L., COHEN-ADAD M.T. Structural refinements on high-T_c superconductor $Tl_{0.5}Pb_{0.5}Sr_{2-x}Ba_xCa_2Cu_3O_{9-\delta}$.
Czechoslovak Journal of Physics **46 Suppl. S3**, 1415-1416 (1996)

GOMEZ SAL J.C., GARCIA SOLDEVILLA J., BLANCO J.A., ESPESO J.I., RODRIGUEZ FERNANDEZ J., LUIS F., BARTOLOME F., BARTOLOME J. Spin-glass freezing above the ordering temperature for the Kondo ferromagnet $CeNi_{0.4}Cu_{0.6}$.
Physical Review B **56**, 11741-11748 (1997)

GOMPF F., REICHARDT W., SCHOBER H., RENKER B., BUCHGEISTER M. Lattice vibrations and electron-phonon coupling in superconducting quaternary borocarbides: an inelastic neutron-scattering investigation.
Physical Review B **55**, 9058-9066 (1997)

GONCHARENKO I.N., MIREBEAU I., IRODOVA A.V., SUARD E. Interplay of magnetic and hydrogen orders in the laves hydride $YMn_2H_{4.3}$.
Physical Review B **56**, 2580-2584 (1997)

GONZALEZ MAC DOWELL L., GUILLAUME F., RYCKAERT J.P., GIRARD P., RODRIGUEZ V., DIANOUX A.J. Rotational molecular dynamics in the R_I phase of n-nonadecane.
Physica B **234-236**, 106-108 (1997)

GRAETSCH H., IBEL K. Small angle neutron scattering by opals.
Physics and Chemistry of Minerals **24**, 102-108 (1997)

GREMPEL D.R., ROZENBERG M.J. Fluctuations in a quantum random Heisenberg paramagnet.
Physical Review Letters **80**, 389-392 (1997)

GRENIER B., REGNAULT L.P., LORENZO J.E., BOSSY J., RENARD J.P., DHALENNE G., REVCOLEVSCHI A. Effect of magnetic field and Si-doping on the spin-Peierls phase of $CuGeO_3$.
Physica B **234-236**, 534-535 (1997)

GROSS M., FRIEDRICHS T., FAUST H.R., MÜNNICH F., KEYSER U. A first measurement of the β-decay energy of ^{94}Kr.
In: 'International Workshop on Research with Fission Fragments', VON EGIDY T. et al. (Eds.) (World Scientific, 1997) pp. 247-251

GÜDEL H.U. Inelastic neutron scattering.
In: 'Molecular Magnetism: from Molecular Assemblies to the Devices', CORONADO E. et al. (Eds.) (Kluwer Academic Publishers, 1996) pp. 229-242

GÜNTHER R., ODENBACH S., SCHÄRPF O., DOSCH H. Reflectivity and evanescent diffraction of polarized neutrons from Ni(110).
Physica B **234-236**, 508-509 (1997)

GUSMAO M., ZIMAN T. Spin-density-wave instabilities for imperfectly nested Fermi surfaces: application to BEDT-TTF salts.
Physical Review B **54**, 16663-16669 (1997)

GUTMANN M., ALLENSPACH P., FAUTH F., FURRER A., ZOLLIKER M., ROSENKRANZ S., ECCLESTON R.S. Neutron investigation of $Nd_{2-x-y}Ce_xLa_yCuO_4$ ($0 \le x \le 0.2$; $y = 0.5, 1$).
Physica B **234-236**, 812-814 (1997)

GYGAX F.N., AMATO A., PINKPANK M., SCHENCK A., ANDERSON I.S., SOLT G., UDOVIC T.J. Electric field gradients probed by μ⁺SR in Sc and α-ScH_x solid solutions.
Hyperfine Interactions **106**, 91-95 (1997)

HABASH J., RAFTERY J., WEISGERBER S., CASSETTA A., LEHMANN M.S., HØGHØJ P., WILKINSON C., CAMPBELL J.W., HELLIWELL J.R. Neutron Laue diffraction study of concanavalin A: the proton of ASP28.
Journal of the Chemical Society Faraday Transactions **93**, 4313-4317 (1997)

HABS D., KESTER O., THIROLF P., LÖBNER K.E.G., MAIER H.J., RUDOLPH D., RUDOLPH K., SCHRAMM U., FAESTERMANN T., HINDERER G., KIENLE P., KÖSTER U., KÖRNER H.J., STEICHELE E., ULRICH A., VON EGIDY T., FAUST H.R., GROSS M. The Munich fission fragment accelerator.
Nuclear Physics A **616**, 39c-44c (1997)

HAMBSCH F.J., OBERSTEDT S. Investigation of the far asymmetric region in $^{252}Cf(sf)$.
Nuclear Physics A **617**, 347-355 (1997)

HAMBSCH F.J., VIVES F., OBERSTEDT S., BARREAU G. Neutron induced fission of ^{238}U.
Physik der Hadronen und Kerne, 1997-02-24 / 28, Göttingen, Germany (Abstract)

HAVERMEYER F., RUPP R.A., SCHELLHORN U., MAY R.P. Electrooptic effect for neutrons in $^7LiNbO_3$:Fe.
Waseda International Symposium on Phase Conjugation and Wave Mixing, 1997-06-09 / 10, Tokyo, Japan / 1997 Topical Meeting on Photorefractive Materials, Effects and Devices, PR'97, 1997-06-11 / 13, Chiba, Japan, pp. 281-283

HAYES C., ALEFELD B., COPLEY J.R.D., LARTIGUE C., MEZEI F. On the use of a toroidal mirror to focus neutrons at the ILL neutron spin echo spectrometer IN15.
In: 'Proceedings of a Workshop on Methods for Neutron Scattering Instrumentation Design', HJELM R.P. (Ed.) (1997) pp. 101-111

HAYES C., LARTIGUE C., KOLLMAR A., COPLEY J.R.D., ALEFELD B., MEZEI F., RICHTER D., SPRINGER T. The focusing mirror at the ILL spin-echo spectrometer IN15: experimental results.
Journal of the Physical Society of Japan **65 Suppl. A**, 312-315 (1996)

HEIL W. Helium läßt die Lunge "leuchten".
Physik in unserer Zeit **4**, 168-174 (1997)

HELLIWELL J.R. Neutron Laue diffraction does it faster.
Nature Structural Biology **4**, 874-876 (1997)

HENGGELER W., CHATTOPADHYAY T., ROESSLI B., VORDERWISCH P., THALMEIER P., ZHIGUNOV D.I., BARILO S.N., FURRER A. Neutron spectroscopy of 4*f* collective magnetic excitations in $R_{2-x}Ce_xCuO_4$ (R=Nd, Pr).
Physical Review B **55**, 1269-1279 (1997)

HENGGELER W., CHATTOPADHYAY T., THALMEIER P., ROESSLI B., VORDERWISCH P., FURRER A. Magnetic excitations of Nd in $Nd_{2-x}Ce_xCuO_4$ (x=0 and 0.13).
Physica B **234-236**, 703-707 (1997)

HENNION M., PARDI L., MIREBEAU I., SUARD E., SESSOLI R., CANESCHI A. Neutron study of mesoscopic magnetic clusters: $Mn_{12}O_{12}$.
Physical Review B **56**, 8819-8827 (1997)

HERMOSO J., PIGNOL D., PENEL S., ROTH M., CHAPUS C., FONTECILLA-CAMPS J.C. Neutron crystallographic evidence of lipase-colipase complex activation by a micelle.
EMBO Journal **18**, 5531-5536 (1997)

HICKL P., BALLAUFF M., LINDNER P., JADA A. Interaction of blockcopolymer micelles as probed by small angle neutron and by small angle x-ray scattering.
Colloid and Polymer Science **275**, 1027-1034 (1997)

HICKL P., BALLAUFF M., SCHERF U., MÜLLEN K., LINDNER P. Characterization of a ladder polymer by small-angle x-ray and neutron scattering.
Macromolecules **30**, 273-279 (1997)

HIESS A., BONNET M., BURLET P., RESSOUCHE E., SANCHEZ J.P., BOURDAROT F., WAERENBORGH J.C., ZWIRNER S., WASTIN F., REBIZANT J., LANDER G.H., SUARD E., SMITH J.L. Magnetic structures of $NpBe_{13}$ and $NpPd_2Al_3$.
Physica B **234-236**, 893-894 (1997)

HIESS A., BOUCHERLE J.X., GIVORD F., SCHWEIZER J., LELIEVRE-BERNA E., TASSET F., GILLON B., CANFIELD P.C. Magnetization density in the intermediate valence compound $YbAl_3$.
Physica B **234-236**, 886-887 (1997)

HIESS A., BOURDAROT F., BURLET P., RESSOUCHE E., SANCHEZ J.P., WASTIN F., REBIZANT J., LANDER G.H., SUARD E. Magnetic structure of $NpPd_2Al_3$: relevance to the coexistence of superconductivity and magnetism in UPd_2Al_3.
Physical Review B **55**, 1138-1141 (1997)

HIESS A., HAVELA L., PROKES K., ECCLESTON R.S., LANDER G.H. Magnetic response function in URhAl.
Physica B **230-232**, 89-91 (1997)

HIESS A., ZOBKALO I., BONNET M., SCHWEIZER J., LELIEVRE-BERNA E., TASSET F., ISIKAWA Y., LANDER G.H. On the magnetisation density of CeNiSn.
Physica B **230-232**, 687-689 (1997)

HIESS A., ZOBKALO I., BONNET M., SCHWEIZER J., LELIEVRE-BERNA E., TASSET F., ISAKAWA Y., LANDER G.H. Polarized neutron studies of CeNiSn.
Journal of Physics Condensed Matter **9**, 9321-9332 (1997)

HINES J.D., FRAGNETO G., THOMAS R.K., GARRETT P.R., RENNIE G.K., RENNIE A.R. Neutron reflection from mixtures of sodium dodecyl sulfate and dodecyl betaine adsorbed at the hydrophobic solid/aqueous interface.
Journal of Colloid and Interface Science **189**, 259-267 (1997)

HLINKA J., QUILICHINI M., CURRAT R., LEGRAND J.F. Phason dispersion in the incommensurate phase of betaine calcium chloride dihydrate.
Journal of Physics Condensed Matter **9**, 1461-1475 (1997)

HOFMANN M., HULL S., MCINTYRE G.J., WILSON C.C. A neutron diffraction study of the superionic transition in $(Ca_{1-x}Y_x)F_{2+x}$ with x=0.06.
Journal of Physics Condensed Matter **9**, 845-857 (1997)

HØGHØJ P., ANDERSON I.S., EBISAWA T., TAKEDA T. Fabrication and performance of a large wavelength band multilayer monochromator.
Journal of the Physical Society of Japan **65 Suppl. A**, 296-298 (1996)

HOPE S., LEE J., ROSENBUSCH P., LAUHOFF G., BLAND J.A.C., ERCOLE A., BUCKNALL D., PENFOLD J., LAUTER H.J., LAUTER V., CUBITT R. Thickness dependence of the total magnetic moment per atom in the Cu/Ni/Cu/Si(001) system.
Physical Review B **55**, 11422-11431 (1997)

HORDEQUIN C., LELIEVRE-BERNA E., PIERRE J. Magnetization density in the half-metallic ferromagnet NiMnSb.
Physica B **234-236**, 602-604 (1997)

HORDEQUIN C., PIERRE J., CURRAT R. How do magnetic excitations behave in half metallic ferromagnets ? The case of NiMnSb.
Physica B **234-236**, 605-607 (1997)

HORSEWILL T., JOHNSON M.R., TROMMSDORFF H.P. Proton tunnelling in intermolecular hydrogen bonds.
Europhysics News **28**, 140-142 (1997)

HUANG B., GINGL F., FAUTH F., HEWAT A.W., YVON K. New tetragonal metal hydrides $BaMg_2TH_8$ (T=Ru, Os) containing octahedral $[TH_6]^{4-}$ complex anions and hydride anions.
Journal of Alloys and Compounds **248**, 13-17 (1997)

HUMBLOT H., HEIL W., LELIEVRE-BERNA E., TASSET F. The ^{3}He neutron spin filter at ILL.
Neutron News **8**, 27-32 (1997)

HUNT J.F., MCCREA P.D., ZACCAI G., ENGELMAN D.M. Assessment of the aggregation state of integral membrane proteins in reconstituted phospholipid vesicles using small angle neutron scattering.
Journal of Molecular Biology **273**, 1004-1019 (1997)

HUXLEY A., BOUCHERLE J.X., BONNET M., BOURDAROT F., SCHUSTLER I., CAPLAN D., LELIEVRE-BERNA E., BERNHOEFT N.R., LEJAY P., GILLON B. The magnetic and crystalline structure of the Laves phase superconductor $CeRu_2$.
Journal of Physics Condensed Matter **9**, 4185-4195 (1997)

IBARRA M.R., DE TERESA J.M., BLASCO J., ALGARABEL P.A., MARQUINA C., GARCIA J., STANKIEWICZ J. Lattice effects, stability under a high magnetic field, and magnetotransport properties of the charge-ordered mixed-valence $La_{0.35}Ca_{0.65}MnO_3$ perovskite.
Physical Review B **56**, 8252-8256 (1997)

JANOT C. Atomic clusters, local isomorphism, and recurrently localized states in quasicrystals.
Journal of Physics Condensed Matter **9**, 1493-1508 (1997)

JANOT C. Quasicrystals as self similar packing of atomic clusters.
In: 'Proceedings of the Science and Technology of Atomically Engineered Materials', JENA P. et al. (Eds.) (World Scientific, 1996) pp. 221-229

JANOT C., PATERA J. Simple physical generation of quasicrystals.
Physics Letters A **233**, 110-114 (1997)

JANSSEN S., NATTER H., HEMPELMANN R. The mechanism of hydrogen diffusion in nanocrystalline palladium: a quasielastic neutron scattering study.
Swiss Neutron News **11**, 27-35 (1997)

JANSSEN S., NATTER H., HEMPELMANN R., STRIFFLER T., STUHR U., WIPF H., HAHN H., COOK J.C. Hydrogen diffusion in nanocrystalline Pd by means of quasielastic neutron scattering.
Nanostructured Materials **9**, 579-582 (1997)

JANSSEN S., WAGNER J., NATTER H., PREWO J., RUPP R., LÖFFLER J., ECKERLEBE H., MAY R.P., MEIER G., HEMPELMANN R. Small angle neutron scattering experiments on nanostructured matter using contrast variation.
Nanostructured Materials **9**, 327-330 (1997)

JAVORSKY P., BURLET P., SECHOVSKY V., ARONS R.R., RESSOUCHE E., LAPERTOT G. Neutron diffraction study of magnetic ordering in RNiAl compounds.
Physica B **234-236**, 665-666 (1997)

JENSEN P., LARRALDE H., PIMPINELLI A. Effect of monomer evaporation on a simple model of submonolayer growth.
Physical Review B **55**, 2556-2569 (1997)

JERKE G., PEDERSEN J.S., EGELHAAF S.U., SCHURTENBERGER P. Structure and flexibility of worm-like micelles.
Physica B **234-236**, 273-275 (1997)

JIMENEZ M., MARTINEZ J.L., HERRERO E., ALONSO J.A., PRIETO C., DE ANDRES A., VALLET-REGI M., GONZALES-CALBET J., FERNANDEZ-DIAZ M.T. Structural and magnetoresistance study of $La_xMn_yO_{3\pm z}$.
Physica B **234-236**, 708-709 (1997)

JOBIC H. Neutron techniques.
In: 'Handbook of Heterogeneous Catalysis. Volume 2', ERTL G. et al. (Eds.) (VCH Verlagsgesellschaft Publishers, 1997) pp. 574-582

JOBIC H. Vibrational spectroscopy with neutrons.
In: 'Catalysis by metals', RENOUPREZ A.J., JOBIC H. (Eds.) (Les Editions de Physique/Springer Verlag, 1997) pp. 182-200

JOBIC H., FITCH A.N. Vibrational study of benzene adsorbed in NaY zeolite by neutron spectroscopy.
In: 'Progress in Zeolite and Microporous Materials', CHON H. et al. (Eds.) (Elsevier Science Publishers, 1997) pp. 559-566

JOBIC H., HAHN K., KÄRGER J., BEE M., TUEL A., NOACK M., GIRNUS I., KEARLEY G.J. Unidirectional and single-file diffusion of molecules in one-dimensional channel systems. A quasi-elastic neutron scattering study.
Journal of Physical Chemistry B **101**, 5834-5841 (1997)

JOBIC H., TUEL A., KROSSNER M., SAUER J. Water in interaction with acid sites in H-ZSM-5 zeolite does not form hydroxonium ions. A comparison between neutron scattering results and ab initio calculations.
Journal of Physical Chemistry **100**, 19545-19550 (1996)

JOENSEN K.D., GORENSTEIN P., HØGHØJ P., SUSINI J., ZIEGLER E., FREUND A.K., CHRISTENSEN F.E., WOOD J., GUTMAN G. Broad-band hard x-ray reflectors.
Nuclear Instruments and Methods in Physics Research B **132**, 221-227 (1997)

JOHNSON M.R., NEUMANN M., NICOLAI B., SMITH P., KEARLEY G.J. The origin and temperature dependence of the single particle, methyl-group rotational potential in acetic acid.
Chemical Physics **215**, 343-353 (1997)

JOLIE J., STRITT N., BÖRNER H.G., DOLL C., JENTSCHEL M., ROBINSON S.J., KESSLER E.G. The neutrino induced Doppler broadening technique and its application to the study of phonon creation in solids.
Zeitschrift für Physik B **102**, 1-7 (1997)

KAHLERT H., FREY F., BOYSEN H., PROFFEN T., MASON S.A., WEPPNER W. Structural investigations of the ionic conductivity in zirconia single crystals by neutron diffraction at high temperatures and simultaneously applied electric field.
Ionics **2**, 88-96 (1996)

KAHN T., VON EGIDY T., HARTMANN F.J., OTT J., JENTSCHEL M. Gamma-ray induced Doppler shift attenuation after (n, γ) reactions in Si and Ti.
Nuclear Instruments and Methods in Physics Research A **385**, 100-107 (1997)

KASSAPIDOU K., JESSE W., KUIL M.E., LAPP A., EGELHAAF S.U., VAN DER MAAREL J.R.C. Structure and charge distribution in DNA and poly(styrenesulfonate) aqueous solutions.
Macromolecules **30**, 2671-2684 (1997)

KAZAKOV S.M., CHAILLOUT C., BORDET P., CAPPONI J.J., NUNEZ-REGUEIRO M., RYSAK A., THOLENCE J.L., RADAELLI P.G., PUTILIN S.N., ANTIPOV E.V. Discovery of a second family of bismuth-oxide-based superconductors.
Nature **390**, 148-150 (1997)

KAZAKOV S.M., PACHOT S., KOPNIN E.M., PUTILIN S.N., ANTIPOV E.V., CHAILLOUT C., CAPPONI J.J., RADAELLI P.G., MAREZIO M. Synthesis, neutron diffraction study and cation substitutions in $Sr_{n-1}Cu_{n+1}O_{2n}$ (n=3, 5).
Physica C **276**, 139-146 (1997)

KEARLEY G.J., TOMKINSON J., NAVARRO A., LOPEZ GONZALEZ J.J., FERNANDEZ GOMEZ M. Symmetrised quantum-mechanical force-fields and INS spectra: s-triazine, trichloro-s-triazine and pyrazine.
Chemical Physics **216**, 323-335 (1997)

KEIMER B., AKSAY I.A., BOSSY J., BOURGES P., FONG H.F., MILIUS D.L., REGNAULT L.P., REZNIK D., VETTIER C. Spin excitations and phonons in $YBa_2Cu_3O_{6+x}$: a status report.
Physica B **234-236**, 821-829 (1997)

KEMALI M., MERCER M., SUN D., ROSS D.K., LANGAN P. Neutron diffraction measurements on the C15 Laves phase TaV_2D_x.
Physica B **234-236**, 945-948 (1997)

KERN N., FOURCADE B. Vesicles decorated with magnetic particles.
Europhysics Letters **38**, 395-400 (1997)

KILCOYNE S.H., RITTER C. The influence of Al on the magnetic properties of synthetic goethite.
Physica B **234-236**, 620-621 (1997)

KITAZAWA H., DÖNNI A., FISCHER P., TANG J., KIDO G., FAUTH F., ZOLLIKER M. Magnetic properties of NdPtAl.
Physica B **234-236**, 644-646 (1997)

KÖBLER U., SCHWEIZER J., CHIEUX P., LORENZ T., BÜCHNER B., SCHNELLE W., DELOIE F., ZINN W. Evidence for biquadratic exchange interactions in $GdAg_{1-x}Zn_x$.
Journal of Magnetism and Magnetic Materials **170**, 110-128 (1997)

KREYSSIG A., LÖWENHAUPT M., MÜLLER K.H., FUCHS G., HANDSTEIN A., RITTER C. Influence of magnetic order on superconducting properties of $Ho_xY_{1-x}Ni_2B_2C$.
Physica B **234-236**, 737-738 (1997)

KRIMMEL A., LOIDL A., SCHOBER H., CANFIELD P.C. Single-crystal neutron diffraction studies on $CeCu_2Ge_2$ and $CeCu_{1.9}Ni_{0.1}Ge_2$.
Physical Review B **55**, 6416-6420 (1997)

KRIMMEL A., LOIDL A., SEVERING A. The evolution of the crystal-field states upon increasing hybridization in $Ce(Cu_{1-x}Ni_x)_2Ge_2$.
Journal of Physics Condensed Matter **9**, 873-880 (1997)

KRIMMEL A., SEVERING A., SPITZFADEN R., GRAUEL A., BUSCHINGER B., GEIBEL C., LOIDL A. Magnetic relaxation in $UCu_{4+x}Al_{8-x}$.
Zeitschrift für Physik B **102**, 9-14 (1997)

KULDA J., BAUER R., STERNER H., STRAUCH D. Eigenvectors of the [111] longitudinal phonons in diamond.
Physica B **234-236**, 124-125 (1997)

LANGAN P. Neutron fibre diffraction: recent advances at the ILL.
Physica B **234-236**, 213-214 (1997)

LANGRIDGE S., LANDER G.H., BERNHOEFT N.R., STUNAULT A., VETTIER C., GRÜBEL G., SUTTER C., BERGEVIN F. DE, NUTTALL W.J., STIRLING W.G., MATTENBERGER K., VOGT O. Separation of the spin and orbital moments in antiferromagnetic UAs.
Physical Review B **55**, 6392-6398 (1997)

LANZARA A., SAINI N.L., BIANCONI A., HAZEMANN J.L., SOLDO Y., CHOU F.C., JOHNSTON D.C. Temperature-dependent modulation amplitude of the CuO_2 superconducting lattice in $La_2CuO_{4.1}$.
Physical Review B **55**, 9120-9124 (1997)

LANZARA A., SAINI N.L., BRUNELLI M., NATALI F., BIANCONI A., RADAELLI P.G. From manganites to cuprates : a comparative study of the local lattice instability.
Zeitschrift für Physik B **104**, 699-702 (1997)

LATROCHE M., NOTTEN P.H.L., PERCHERON-GUEGAN A. In situ neutron diffraction study of solid gas desorption of non-stoichiometric AB5 type hydrides.
Journal of Alloys and Compounds **253-254**, 295-297 (1997)

LE CAËR G., DELCROIX P., MALAMAN B., WELTER R., FULTZ B., RESSOUCHE E. Comparison of disorder induced thermally and by ball milling in Ni_2MnSn.
Materials Science Forum **235-238**, 583-588 (1997)

LEES M.R., CHANG L.J., BARRATT J., BALAKRISHNAN G., TOMY C.V., PAUL D. MCK., DEWHURST C.D., RITTER C. The structural, magnetic and transport properties of $Pr_{0.6}(Ca_{1-x}Sr_x)_{0.4}MnO_3$.
Physica B **230-232**, 313-316 (1997)

LEHNERT H., BOYSEN H., FREY F., HEWAT A.W., RADAELLI P.G. A neutron powder investigation of the high-temperature structure and phase transition in stoichiometric $LiNbO_3$.
Zeitschrift für Kristallographie **212**, 712-719 (1997)

LEHNERT H., BOYSEN H., HEWAT A.W., RADAELLI P.G. Neutronenpulver-Untersuchungen der Hochtemperaturphase und des Phasenübergangs in $LiNbO_3$.
Zeitschrift für Kristallographie Supplement **11**, 158 (1996)

LIAUD P., SCHRECKENBACH K., KOSSAKOWSKI R., NASTOLL H., BUSSIERE A., GUILLAUD J.P., BECK L. The measurement of the beta asymmetry in the decay of polarized neutrons.
Nuclear Physics A **612**, 53-81 (1997)

LIESERT S., FRUCHART D., DE RANGO P., RIVOIRARD S., SOUBEYROUX J.L., PERRIER DE LA BATHIE R., TOURNIER R. HDDR process of Nd-Fe-B with an excess of intergranular Nd-rich phase under magnetic field.
Journal of Alloys and Compounds **262-263**, 366-371 (1997)

LIESERT S., FRUCHART D., DE RANGO P., SOUBEYROUX J.L. The hydrogenation-disproportionation-desorption-recombination process of $Nd_2Fe_{14}B$ studied by in-situ neutron diffraction and thermomagnetic measurements.
Journal of Alloys and Compounds **253-254**, 140-143 (1997)

LINE C.M.B., KEARLEY G.J., SUARD E., FITCH A.N., SWAINSON I. Water in wairakite: a water-zeolite model system.
Physica B **234-236**, 79-81 (1997)

LISS K.D., MAGERL A., HOCK R., REMHOF A., WAIBEL B. Towards a new (Q,t) regime by time-resolved x-ray diffraction: ultra-sound excited crystals as an example.
Europhysics Letters **40**, 369-374 (1997)

LISS K.D., MAGERL A., REMHOF A., HOCK R. Ultrasound-induced gradient crystals observed by high-energy x-rays.
Acta Crystallographica A **53**, 181-186 (1997)

LOBBAN C., FINNEY J.L., KUHS W.F. The structure of a new phase of ice.
Nature **391**, 268-270 (1997)

LOHSTROH W., SCHULTE O., KLOSE F., MÜNZENBERG M., FELSCH W., MALETTA H., LAUTER H.J. Non-collinear spin structures in CeH_2/Fe.
Physica B **234-236**, 477-479 (1997)

LORENZO J.E., REGNAULT L.P., HENNION B., AÏN M., BOURDAROT F., KULDA J., DHALENNE G., REVCOLEVSCHI A. Spin dynamics in the spin-Peierls compound $CuGeO_3$.
Journal of Physics Condensed Matter **9**, L211-L217 (1997)

LOSILLA E.R., ARANDA M.A.G., MARTINEZ-LARA M., BRUQUE S. Reversible triclinic-rhombohedral phase transition in $LiHf_2(PO_4)_3$: crystal structures from neutron powder diffraction.
Chemistry of Materials **9**, 1678-1685 (1997)

LYONNARD S., CODDENS G., HENNION B., CALVAYRAC Y. Dynamics of phason hopping in AlFeCu and AlMnPd quasicrystals.
Physica B **234-236**, 28-29 (1997)

MADERN D., ZACCAI G. Stabilisation of halophilic malate dehydrogenase from *Haloarcula marismortui* by divalent cations.
European Journal of Biochemistry **249**, 607-611 (1997)

MALAMAN B., VENTURINI G., EL IDRISSI B.C., RESSOUCHE E. Magnetic properties of $NdMn_6Sn_6$ and $SmMn_6Sn_6$ compounds from susceptibility measurements and neutron diffraction study.
Journal of Alloys and Compounds **252**, 41-49 (1997)

MAREZIO M., RADAELLI P.G. Aspetti strutturali dei composti $La_{1-x}Ca_xMnO_3$ a struttura perovskitica.
Notiziaro Neutroni e Luce di Sincrotrone **2**, 7-15 (1997)

MARINI M., PISTOLESI F., STRINATI G.C. Analytic results for the crossover from BCS superconductivity to Bose-Einstein condensation.
Physica C **282-287**, 1817-1818 (1997)

MARMEGGI J.C. Use of an image plate for the study of phase transitions with the neutron Laue method.
Physica B **234-236**, 1087-1089 (1997)

MARMEGGI J.C., LANDER G.H., CURRAT R., ZEYEN C.M.E. Soft phonons and the charge-density-wave transition in alpha uranium.
Physica B **234-236**, 129-130 (1997)

MASON S.A. Neutron instrumentation for biology (Abstract).
In: 'Neutrons in Biology', SCHOENBORN B.P., KNOTT R.B. (Eds.) (Plenum Press, 1996) pp. 105

MAY T., STRAUCH D. Anharmonic lattice dynamics and neutron-scattering spectra in BCC-Ti.
Physica B **234-236**, 131-132 (1997)

MAY T., STRAUCH D., SCHOBER H., DORNER B. Lattice dynamics of Cr_2O_3.
Physica B **234-236**, 133-134 (1997)

MAYERHOFER U., VON EGIDY T., KLORA J., LINDNER H., BÖRNER H.G., JUDGE S., KRUSCHE B., ROBINSON S., SCHRECKENBACH K., SUKHOVOJ A.M., KHITROV V.A., BONEVA S.T., PAAR V., BRANT S., PEZER R. The nucleus ^{198}Au investigated with neutron capture and transfer reactions. II. Construction of the level scheme and calculation of level densities.
Fizika B **5**, 229-253 (1996)

MEDARDE M., MESOT J., ROSENKRANZ S., LACORRE P., MARSHALL W., KLOTZ S., LOVEDAY J.S., HAMEL G., HULL S., RADAELLI P.G. Pressure-induced orthorhombic-rhombohedral phase transition in $NdNiO_3$.
Physica B **234-236**, 15-17 (1997)

MEDARDE M., RODRIGUEZ CARVAJAL J. Oxygen vacancy ordering in $La_{2-x}Sr_xNiO_{4-\delta}$ ($0 \le x \le 0.5$): the crystal structure and defects investigated by neutron diffraction.
Zeitschrift für Physik B **102**, 307-315 (1997)

MENDES E., SCHÄDLER V., MARQUES C.M., LINDNER P., WIESNER U. Electrostatics in the self-assembly of macromolecular surfactants.
Europhysics Letters **40**, 521-526 (1997)

MENSHIKOV A.Z., SCHWEIZER J. The transverse magnetization components in the ground state of invar γ-$Ni_{1-c}Fe_c$ alloys.
Solid State Communications **100**, 251-255 (1996)

MERGIA K., AL HAZMI F., STEWART R.J., MESSOLORAS S. *In-situ* small-angle neutron scattering study of the growth and dissolution of precipitates in Al-Li alloys.
Philosophical Magazine A **75**, 939-958 (1997)

MERMET A., DUVAL E., SUROVTSEV N.V., JAL J.F., DIANOUX A.J., YEE A.F. Localized fast relaxation in poly(methyl methacrylate) glass.
Europhysics Letters **38**, 515-520 (1997)

MESOT J., BÖTTGER G., BERASTEGUI P., MUTKA H., FURRER A. Temperature dependence of crystal-field transitions in underdoped superconductors: evidence for a pseudogap in the normal state.
Physica C **282-287**, 1377-1378 (1997)

MICHAUDON A. Use of ultracold neutrons for condensed-matter studies.
Los Alamos National Laboratory (1997)
LA-13197-MS

MIDDENDORF H.D., MILLER A. Neutron scattering studies of the dynamics of biopolymer-water systems using pulsed-source spectrometers.
In: 'Neutrons in Biology', SCHOENBORN B.P., KNOTT R.B. (Eds.) (Plenum Press, 1996) pp. 239-265

MIHALKOVIC M., DUGAIN F., SUCK J.B. Vibrational density of states of decagonal $Al_{70}Co_{15}Ni_{15}$.
Journal of Non-Crystalline Solids **205-207**, 701-705 (1996)

MILES P.A., KENNEDY S.J., MCINTYRE G.J., GU G.D., RUSSELL G.J., KOSHIZUKA N. Diffuse features in neutron diffraction studies of high quality Bi-2212 single crystals.
Physica C **280**, 66-70 (1997)

MIREBEAU I., SUARD E., HENNION M., FERNANDEZ-DIAZ M.T., DAOUD-ALADINE A., NATEPROV A. Chemical and magnetic order in $ZnMn_2As_2$ as studied by neutron diffraction.
Journal of Magnetism and Magnetic Materials **175**, 290-298 (1997)

MIRMELSTEIN A., PODLESNYAK A., BOBROVSKII V.I., MITBERG E., GOSHCHITSKII B.N., MUZYCHKA A., SASHIN I., ECCLESTON R.S., MESOT J., ZOLLIKER M., HENGGELER W., FURRER A. Neutron spectroscopic study of crystalline electric-field in infinite-layer $Sr_{1-x}Nd_xCuO_2$.
Physica C **282-287**, 1335-1336 (1997)

MOMPEAN F.J., GARCIA HERNANDEZ M., MARTINEZ J.L., GARCIA-MATRES E., PRIETO C., DE ANDRES A., SAEZ-PUCHE R., ECCLESTON R.S., SCHOBER H. Spin dynamics in 1D antiferromagnetic system $Y_2BaNi_{1-x}Zn_xO_5$
Physica B **234-236**, 572-573 (1997)

MORALES M.F., ARTIGAS M., BACMANN M., FRUCHART D., SOUBEYROUX J.L., WOLFERS P. Relationship between the structural and the magnetic properties of $ErMn_{12-x}Fe_x$ compounds.
Journal of Alloys and Compounds **262-263**, 134-140 (1997)

MORELLON L., ALGARABEL P.A., IBARRA M.R., RITTER C. Magnetic structures and magnetic phase diagram of $Nd_xTb_{1-x}Mn_2Ge_2$.
Physical Review B **55**, 12363-12374 (1997)

MOS B., VERKERK P., BAFILE U., BENMORE C.J., SUCK J.B., BAROCCHI F., COOK J.C., ANDERSEN K.H. Neutron Brillouin scattering in liquid ^{36}Ar.
Physica B **234-236**, 308-310 (1997)

MÜLLER K.H., KREYSSIG A., HANDSTEIN A., FUCHS G., RITTER C., LÖWENHAUPT M. Magnetic structure and superconductivity in $(Ho_xY_{1-x})Ni_2B_2C$.
Journal of Applied Physics **81**, 4240-4242 (1997)

MÜLLER M., ASMUSSEN B., PRESS W., SENKER J., JACOBS H., BÜTTNER H.G., KOCKELMANN W., IBBERSON R.M. Dynamics of the amide ions in potassium amide: orientational order and disorder.
Physica B **234-236**, 45-47 (1997)

MÜLLER M., VOGL G., SCHOBER H., CHANZY H., HEUX L. Inelastic neutron scattering study on different types of cellulose.
In: 'Biological Macromolecular Dynamics', CUSACK S. et al. (Eds.) (Adenine Press, 1997) pp. 99-103

MURANI A.P. Paramagnetic scattering from heavy and moderately heavy fermions.
Neutron News **8**, 21-27 (1997)

MURANI A.P. Paramagnetic spectral response from the magnetic and 'non-magnetic' Ce sites in the compound Ce_2Sn_5.
Physica B **230-232**, 259-262 (1997)

MURANI A.P., ECCLESTON R.S. Evidence for single-ion spectral response from a strongly hybridised Anderson-lattice: $CeRh_2$.
Physica B **230-232**, 126-129 (1997)

MURANI A.P., ECCLESTON R.S. High-energy neutron scattering from heavy-fermion systems $Ce(In_{1-x}Sn_x)_3$ and $Ce(Pt_{1-x}Rh_x)_2$.
Physica B **234-236**, 888-890 (1997)

MURANI A.P., STUNAULT A. Evidence for paramagnetic scattering from nonmagnetic Ce sites in the compound Ce_2Sn_5.
Physical Review B **55**, 12518-12521 (1997)

NATTER H., SCHMELZER M., JANSSEN S., HEMPELMANN R. Nanocrystalline materials. Nanocrystalline metals and oxides I: pulsed electrodeposition.
Berichte der Bunsengesellschaft für Physikalische Chemie **101**, 1706-1713 (1997)

NEDER R., BURGHAMMER M., SCHULZ H., CHRISTENSEN A.N., KRANE H.G., BELL A.M.T., HEWAT A.W., ALTOMARE A. Crystal structure determination of barium oxalate, $BaC_2O_4.3.5H_2O/D_2O$.
Zeitschrift für Kristallographie **211**, 305-309 (1997)

NEUMANN M., JOHNSON M.R. Methyl group tunneling - A *quantitative* probe of atom-atom potentials.
Journal of Chemical Physics **107**, 1725-1731 (1997)

NEUMANN M., JOHNSON M.R., TROMMSDORFF H.P. Rotational tunneling of methyl groups: probes of intermolecular potentials.
Journal of Luminescence **72-74**, 459-461 (1997)

NEUMANN M., KEARLEY G.J. Rotation/precession of NH_3 groups in Hofmann clathrates.
Chemical Physics **215**, 253-260 (1997)

NICOLAI B., KEARLEY G.J., RANDL O.G., FILLAUX F., TROMMSDORFF H.P. Intramolecular rotational coupling of inequivalent CH_3 groups.
Physica B **234-236**, 76-78 (1997)

NIIMURA N., MINEZAKI Y., NONAKA T., CASTAGNA J.C., CIPRIANI F., HØGHØJ P., LEHMANN M.S., WILKINSON C. Neutron Laue diffractometry with an imaging plate provides an effective data collection regime for neutron protein crystallography.
Nature Structural Biology **4**, 909-914 (1997)

NIRAIMATHI A.M., GMELIN E., ALLENSPACH P., RITTER C. Magnetic structure and ordering of Nd ions in Ga substituted $NdBa_2Cu_3O_7$ (abstract).
Journal of Applied Physics **79**, 5869 (1996)

NIRAIMATHI A.M., RITTER C., GMELIN E. Structural properties of Ga substituted Nd123 compounds.
Physica B **234-236**, 23-25 (1997)

NORLIDAH M.N., VENTURINI G., MALAMAN B., RESSOUCHE E. Magnetic properties of the new $TbFeSi_2$ -type $NdRhCu_{0.5}Si_{1.5}$ and $PrRhCu_{0.5}Si_{1.5}$ compounds from magnetic measurements and neutron diffraction.
Journal of Alloys and Compounds **257**, 30-35 (1997)

NORLIDAH M.N., VENTURINI G., MALAMAN B., RESSOUCHE E. Neutron diffraction study of the $TbFeSi_2$-type $NdMnCu_{0.5}Ge_{1.5-x}Si_x$ ($0 \le x \le 1.5$) solid solution.
Journal of Alloys and Compounds **259**, 11-23 (1997)

NORLIDAH M.N., VENTURINI G., MALAMAN B., RESSOUCHE E. The *x*-T magnetic phase diagram of the $LaMn_{2-x}Fe_xGe_2$ ($0 \le x \le 1$) system by neutron diffraction study.
Journal of Alloys and Compounds **248**, 112-120 (1997)

OBBADE S., FRUCHART D., BOUOUDINA M., MIRAGLIA S., SOUBEYROUX J.L., ISNARD O. About hydrogen insertion in $ThMn_{12}$ type alloys.
Journal of Alloys and Compounds **253-254**, 298-301 (1997)

OBERSTEDT S. γ-decay above the shape-isomeric ground state of ^{239}U.
Physik der Hadronen und Kerne, 1997-02-24 / 28, Göttingen, Germany (Abstract)

OBERSTEDT S. Retrospective indoor aerosol-particle characterization.
In: 'Proceedings of the european conference on protection against radon at home and work' (1997)

OED A. Ortsempfindliche Gasdetektoren mit Mikrostreifenelektroden.
Physikalische Blätter **53**, 681-683 (1997)

OHTA T., IZUMI F., ONODA M., ISOBE M., TAKAYAMA-MUROMACHI E., HEWAT A.W. Modulated structure of the composite crystal $Ca_{13.6}Sr_{0.4}Cu_{24+y}O_{41+z}$.
Journal of the Physical Society of Japan **66**, 3107-3114 (1997)

OHTA T., IZUMI F., TOKIWA-YAMAMOTO A., TANABE K., HEWAT A.W.
Oxygen configuration and disordering in the superconductor $(Hg_{0.7}Tl_{0.3})_2Ba_2(Y_{0.8}Ca_{0.2})Cu_2O_{8+\delta}$.
Physica C **281**, 228-236 (1997)

OHTA T., TOKIWA-YAMAMOTO A., IZUMI F., HEWAT A.W., TANABE K. Crystal structure of $(Hg_{0.7}Tl_{0.3})_2Ba_2(Y_{0.8}Ca_{0.2})Cu_2O_{8-\delta}$ synthesized at high pressure.
Physica C **282-287**, 911-912 (1997)

OLEKSYN O., SCHOBINGER-PAPAMANTELLOS P., RITTER C., DE GROOT C.H., BUSCHOW K.H.J. Structure and magnetic ordering in the defect compound $ErGe_{1.83}$.
Journal of Alloys and Compounds **252**, 53-58 (1997)

OLEKSYN O., SCHOBINGER-PAPAMANTELLOS P., RITTER C., DE GROOT C.H., BUSCHOW K.H.J. Crystallographic and magnetic structure of the novel compound $ErGe_{1.83}$.
Physica B **234-236**, 652-653 (1997)

OLEKSYN O., SCHOBINGER-PAPAMANTELLOS P., RITTER C., DE GROOT C.H., BUSCHOW K.H.J. Antiferromagnetic ordering in the novel Dy_3Ge_4 and $DyGe_{1.3}$ compounds studied by neutron diffraction and magnetic measurements.
Journal of Alloys and Compounds **262-263**, 492-497 (1997)

OLEKSYN O., SCHOBINGER-PAPAMANTELLOS P., RITTER C., JANSSEN Y., BRÜCK E., BUSCHOW K.H.J. Antiferromagnetic ordering in the novel Tb_3Ge_4 (two-step) and $TbGe_{2-\delta}$ (AlB_2-type) compounds studied by neutron diffraction and magnetic measurements.
Journal of Physics Condensed Matter **9**, 9993-10008 (1997)

OULADDIAF B., SCHMITT D., WADA H. Antiferromagnetic structure of $EuAl_2$.
Journal of the Physical Society of Japan **66**, 3242-3243 (1997)

PAIXAO J.A., LANGRIDGE S., SORENSEN S.A., LEBECH B., GONCALVES A.P., LANDER G.H., BROWN P.J., BURLET P., TALIK E. Unusual magnetic interactions in compounds with the $ThMn_{12}$ structure.
Physica B **234-236**, 614-616 (1997)

PAIXAO J.A., LEBECH B., GONCALVES A.P., BROWN P.J., LANDER G.H., BURLET P., DELAPALME A., SPIRLET J.C. Magnetic sublattice interactions in UFe_4Al_8.
Physical Review B **55**, 14370-14377 (1997)

PALACIO F., ANTORRENA G., CASTRO M.A., BURRIEL R., RAWSON J., SMITH J.N.B., BRICKLEBANK N., NOVOA J., RITTER C. High-temperature magnetic ordering in a new organic magnet.
Physical Review Letters **79**, 2336-2339 (1997)

PAUL A., RÖTTGER S., KEYSER U., LOHENGRIN-COLLABORATION. Q_β values of the low and high spin isomer of ^{146}La.
In: 'International Workshop on Research with Fission Fragments', VON EGIDY T. et al. (Eds.) (World Scientific, 1997) pp. 252-257

PAUL-BONCOUR V., GUENEE L., LATROCHE M., ESCORNE M., PERCHERON-GUEGAN A., REICHL C., WIESINGER G. Structural and magnetic study of new YFe_2D_x compounds ($0 < x \le 3.5$).
Journal of Alloys and Compounds **253-254**, 272-274 (1997)

PELLAUX R., SCHMALLE H.W., DECURTINS S., FISCHER P., FAUTH F., OULADDIAF B., HAUSS T. Magnetic structure of two- and three-dimensional supramolecular compounds.
Physica B **234-236**, 783-784 (1997)

PELLAUX R., SCHMALLE H.W., HUBER R., FISCHER P., HAUSS T., OULADDIAF B., DECURTINS S. Molecular-based magnetism in bimetallic two-dimensional oxalate-bridged networks. An x-ray and neutron diffraction study.
Inorganic Chemistry **36**, 2301-2308 (1997)

PENDLEBURY J.M. Review of particle electric dipole moments.
In: 'Proceedings of the Workshop on K Physics - Comptes Rendus sur la Physique des K', ICONOMIDOU-FAYARD L. (Ed.) (Editions Frontieres, 1997) pp. 135-148

PENEL S., LEGRAND P. MAINDEX. Manual indexation for area-detector crystallographic data.
Journal of Applied Crystallography **30**, 206 (1997)

PETIT S., MOUDDEN A.H., HENNION B., VIETKIN A., REVCOLEVSCHI A. Spin dynamics study of $La_{2-x}Sr_xCuO_4$ by inelastic neutron scattering.
Physica B **234-236**, 800-802 (1997)

PETITGRAND D., CASALTA H., BOURGES P., IVANOV A.S. Low-energy magnetic excitations in Nd_2CuO_4.
Physica B **234-236**, 806-807 (1997)

PIERRE J., GUZIK A., KACZMARSKA K., MURANI A.P. Spin dynamics in cerium ternary stannides and antimonides.
Physica B **234-236**, 870-871 (1997)

PIERRE J., SKOLOZDRA R.V., TOBOLA J., KAPRZYK A.S., HORDEQUIN C., KOUAKOU M.A., KARLA I., CURRAT R., LELIEVRE-BERNA E. Properties on request in semi-Heusler phases.
Journal of Alloys and Compounds **262-263**, 101-107 (1997)

PIGNON F., MAGNIN A., PIAU J.M., CABANE B., LINDNER P., DIAT O. Yield stress thixotropic clay suspension: investigations of structure by light, neutron and x-ray scattering.
Physical Review E **56**, 3281-3289 (1997)

PIONKE M., MONO T., SCHWEIKA W., SCHOBER H., SPRINGER T. Proton diffusion in $Ba[Ca_{(1+x)/3}Nb_{(2-x)/3}]O_{3-x/2}$ studied by quasielastic neutron scattering.
Physica B **234-236**, 95-96 (1997)

PIONKE M., MONO T., SCHWEIKA W., SPRINGER T., SCHOBER H. Investigation of the hydrogen mobility in a mixed perovskite: $Ba[Ca_{(1+x)/3}Nb_{(2-x)/3}]O_{3-x/2}$ by quasielastic neutron scattering.
Solid State Ionics **97**, 497-504 (1997)

PLAZA I., PALACIOS E., BARTOLOME J., ROSENKRANZ S., RITTER C., FURRER A. Neutron diffraction study of the magnetic ordered Nd^{3+} in $NdCoO_3$ and $NdInO_3$ below 1K.
Physica B **234-236**, 632-634 (1997)

PLAZA I., PALACIOS E., BARTOLOME J., ROSENKRANZ S., RITTER C., FURRER A. Neutron diffraction study of $NdScO_3$ below 1K. Magnetic structure and hyperfine enhanced polarization of Nd.
Physica B **234-236**, 635-636 (1997)

PODLESNYAK A., MIRMELSTEIN A., BOBROVSKII V.I., GOSHCHITSKII B.N., MITBERG E., MUZYCHKA A., SASHIN I., ECCLESTON R.S., MESOT J., ZOLLIKER M., ROSENKRANZ S., HENGGELER W., FURRER A. Neutron spectroscopic studies of crystalline electric field in infinite-layer $Sr_{1-x}Nd_xCuO_2$.
Physica B **234-236**, 794-796 (1997)

PODLESNYAK A., MIRMELSTEIN A., BOBROVSKII V.I., VORONIN V., KARKIN A., ZHDAKHIN I., GOSHCHITSKII B.N., MIDBERG E., ZUBKOV V., D'YACHKOVA T., KHLYBOV E., GENOUD J.Y., ROSENKRANZ S., FAUTH F., HENGGELER W., FURRER A. New elaboration technique, structure and physical properties of infinite-layer $Sr_{1-x}Ln_xCuO_2$ (Ln=Nd, Pr).
Physica C **258**, 159-168 (1996)

PONTILLON Y., OVCHARENKO V.I., RESSOUCHE E., REY P., SCHLEGER P., SCHWEIZER J. Spin density in the tetrahedral copper complex of an enaninoketon nitroxide.
Physica B **234-236**, 785-787 (1997)

PONTILLON Y., RESSOUCHE E., ROMERO F., SCHWEIZER J., ZIESSEL R. Spin density in the free radical NitPy (C≡C-H).
Physica B **234-236**, 788-789 (1997)

PRAGER M., HAVIGHORST M., CODDENS G., BÜTTNER H.G. NH_3 on the MgO{100} surface: the concentration dependence of tunnelling spectra.
Journal of Physics Condensed Matter **9**, 43-52 (1997)

PRAGER M., HAVIGHORST M., CODDENS G., BÜTTNER H.G. Rotational tunnelling and structural phase transitions of NH_3 adsorbed as a submonolayer on MgO{100} surfaces.
Physica B **234-236**, 170-172 (1997)

PRASSIDES K., VAVEKIS K., KORDATOS K., TANIGAKI K., BENDELE G.M., STEPHENS P.W. Loss of cubic symmetry in low-temperature Na_2RbC_{60}.
Journal of the American Chemical Society **119**, 834-835 (1997)

PRATESI G., SUCK J.B. Collective atomic dynamics in liquid $Rb_{95}Sb_5$.
Journal of Physics Condensed Matter **9**, 11035-11043 (1997)

PRINCE E., WILKINSON C., MCINTYRE G.J. Comparison of the $\sigma(I)/I$ and least-squares methods for integration of Bragg reflections.
Journal of Applied Crystallography **30**, 133-137 (1997)

PTASIEWICZ-BAK H., OLOVSSON I., MCINTYRE G.J. Charge density in orthorhombic $NiSO_4{\cdot}7H_2O$ at room temperature and 25K.
Acta Crystallographica B **53**, 325-336 (1997)

PYKA N.M., LÖWENHAUPT M., METZ A., HIEN N.T. Magnetic correlations in heavy fermion $Nd_{1.85}Ce_{0.15}CuO_4$.
Physica B **234-236**, 808-809 (1997)

RADAELLI P.G., COX D.E., MAREZIO M., CHEONG S.W. Charge, orbital, and magnetic ordering in $La_{0.5}Ca_{0.5}MnO_3$.
Physical Review B **55**, 3015-3023 (1997)

RADAELLI P.G., IANNONE G., MAREZIO M., HWANG H.Y., CHEONG S.W., JORGENSEN J.D., ARGYRIOU D.N. Structural effects on the magnetic and transport properties of perovskite $A_{1-x}A'_xMnO_3$ (x=0.25,0.30).
Physical Review B **56**, 8265-8276 (1997)

RAINFORD B.D. Magnetic excitations studied with time-of-flight spectroscopy.
In: 'New Instruments and Science Around SINQ. Lecture Notes of the '4th Summer School on Neutron Scattering' PSI Proceedings 96-02 (PAUL SCHERRER INSTITUTE, 1996) pp. 361-377

RAMOS M.A., VIEIRA S., BERMEJO F.J., DAWIDOWSKI J., FISCHER H.E., SCHOBER H., GONZALEZ M.A., LOONG C.K., PRICE D.L. Quantitative assessment of the effects of orientational and positional disorder on glassy dynamics.
Physical Review Letters **78**, 82-85 (1997)

RANDL O.G., FRANZ H., GERSTENDÖRFER T., PETRY W., VOGL G., MAGERL A. How to rejuvenate an old lady: new crystals for the backscattering spectrometer IN10.
Physica B **234-236**, 1064-1065 (1997)

RANDL O.G., JOHNSON M.R. IN10B. Neutron backscattering up to high energy transfers.
Neutron News **8**, 11-14 (1997)

RANDL O.G., PETRY W., VOGL G., BÜHRER W., HENNION B. Lattice dynamics and related diffusion properties of intermetallics: II. Ni3Sb.
Journal of Physics Condensed Matter **9**, 10283-10292 (1997)

RATHGEBER S., ZIRKEL A., WILLNER L., RICHTER D., BRULET A., FARAGO B. Dynamics of bimodal polymer melts in the crossover-region from Rouse- to reptation-like behaviour - A study with NSE-spectroscopy.
Physica B **234-236**, 258-259 (1997)

RAUM K., WEBER M., GÄHLER R., ZEILINGER A. Gravity and inertia in neutron crystal optics and VCN interferometry.
Journal of the Physical Society of Japan **65 Suppl. A**, 277-280 (1996)

RAYMOND S., REGNAULT L.P., KADOWAKI H., NAKAMOTO G., TAKABATAKE T., FLOUQUET J. Magnetic excitations in CeNiSn under high magnetic field.
Physica B **230-232**, 667-669 (1997)

RAYMOND S., REGNAULT L.P., KAMBE S., MIGNOT J.M., LEJAY P., FLOUQUET J. Magnetic correlations in $Ce_{0.925}La_{0.075}Ru_2Si_2$.
Journal of Low-Temperature Physics **109**, 205-224 (1997)

RAYMOND S., REGNAULT L.P., SATO T., KADOWAKI H., PYKA N., NAKAMOTO G., TAKABATAKE T., FUJII H., ISIKAWA Y., LAPERTOT G., FLOUQUET J. An inelastic neutron scattering study of the Kondo semiconductor CeNiSn in high magnetic field.
Journal of Physics Condensed Matter **9**, 1599-1608 (1997)

REAT V., ZACCAI G., FERRAND M., PFISTER C. Functional dynamics in purple membrane.
In: 'Biological Macromolecular Dynamics', CUSACK S. et al. (Eds.) (Adenine Press, 1997) pp. 117-122

REEHUIS M., OULADDIAF B., JEITSCHKO W., VOMHOF T., ZIMMER B., RESSOUCHE E. Magnetization and neutron diffraction studies of the magnetic order in the compounds $Pr_2Co_{12}P_7$, $Nd_2Co_{12}P_7$, $Ho_2Co_{12}P_7$ and $Lu_2Co_{12}P_7$.
Journal of Alloys and Compounds **261**, 1-11 (1997)

REGNAULT L.P. Structural fluctuations and magnetic excitations in the spin-Peierls system $CuGeO_3$.
Physica B **234-236**, 528-533 (1997)

REGNAULT L.P., RENARD J.P. Spin dynamics under high magnetic field in the Haldane-gap system NENP.
Physica B **234-236**, 541-543 (1997)

REIF T., LÖWENHAUPT M., SVOBODA P., SCHWEIKA W., GRATZ E., ROTTER M., MCINTYRE G.J. Diffuse magnetic neutron scattering in $NdCu_2$.
Physica B **234-236**, 640-641 (1997)

REJMANKOVA P., BARUCHEL J., KULDA J. Investigation of $KTiOPO_4$ crystals under an electric field by synchrotron x-ray topography.
Philosophical Magazine B **75**, 871-886 (1997)

REMHOF A., LISS K.D., MAGERL A. Neutron diffraction from sound-excited crystals.
Nuclear Instruments and Methods in Physics Research A **391**, 485-491 (1997)

RENKER B., SCHOBER H., HEID R. Lattice dynamics of RbC_{60}, RbC_{70} and phase transitions in $A1C_{60}$: a neutron scattering study.
Applied Physics A **64**, 271-281 (1997)

RENKER B., SCHOBER H., HEID R., STEIN P.V. Pressure and charge induced polymerisation of C_{60}: a comparative study of lattice vibrations.
Solid State Communications **104**, 527-530 (1997)

REQUARDT H., CURRAT R., MONCEAU P., LORENZO J.E., DIANOUX A.J., LASJAUNIAS J.C., MARCUS J. The phonon density of states and low-temperature specific heat: the blue bronze $K_{0.3}MoO_3$ and the platinum chain compound KCP.
Journal of Physics Condensed Matter **9**, 8639-8655 (1997)

REYNOLDS P.A., FIGGIS B.N., FORSYTH J.B., TASSET F. Covalence and spin polarisation in tetraphenylarsonium tetrachloronitridotechnetate(VI) studied by polarised neutron diffraction.
Journal of the Chemical Society Dalton Transactions , 1447-1453 (1997)

RICHTER D., SCHNEIDERS D., MONKENBUSCH M., WILLNER L., FETTERS L.J., HUANG J.S., LIN M., MORTENSEN K., FARAGO B. Polymer aggregates with crystalline cores: the system polyethylene-poly(ethylenepropylene).
Macromolecules **30**, 1053-1068 (1997)

RITTER C., CYWINSKI R., KILCOYNE S.H. Structural distortions in doped YMn_2 compounds.
Physica B **234-236**, 596-598 (1997)

RITTER C., IBARRA M.R., DE TERESA J.M., ALGARABEL P.A., MARQUINA C., BLASCO J., GARCIA J., OSEROFF S., CHEONG S.W. Influence of oxygen content on the structural, magnetotransport, and magnetic properties of $LaMnO_{3+\delta}$.
Physical Review B **56**, 8902-8911 (1997)

RITTER C., RADAELLI P.G., LEES M.R., BARRATT J., BALAKRISHNAN G., PAUL D. MCK. A new monoclinic perovskite allotype in $Pr_{0.6}Sr_{0.4}MnO_3$.
Journal of Solid State Chemistry **127**, 276-282 (1996)

ROESSLI B., FÅK B., FERNANDEZ-DIAZ M.T., SABLINA K., PETRAKOVSKII G. Polarization analysis of spin waves in Bi_2CuO_4.
Physica B **234-236**, 726-727 (1997)

ROUF-GEORGE C., MUNCH J.P., SCHOSSELER F., POUCHELON A., BEINERT G., BOUE F., BASTIDE J. Thermal and quenched fluctuations of polymer concentration in poly(dimethylsiloxane) gels.
Macromolecules **30**, 8344-8359 (1997)

ROUTSI C.D., YAKINTHOS J.K., RESSOUCHE E. Crystal and magnetic structure of $TbCo_3Ga_2$.
Journal of Alloys and Compounds **256**, 61-64 (1997)

SALVADO M.A., PERTIERRA P., GARCIA-GRANDA S., GARCIA J.R., RODRIGUEZ J., FERNANDEZ-DIAZ M.T. Neutron powder diffraction study of α-$Ti(HPO_4)_2.H_2O$ and α-$Hf(HPO_4)_2.H_2O$; H-atom positions. Erratum [Acta Cryst. (1996), B52, 896-898)].
Acta Crystallographica B **53**, 188 (1997)

SAROUN J., KULDA J. RESTRAX. A program for TAS resolution calculation and scan profile simulation.
Physica B **234-236**, 1102-1104 (1997)

SATO N., ASO N., LANDER G.H., ROESSLI B., KOMATSUBARA T., ENDOH Y. Spin fluctuations in the heavy fermion superconductor UPd_2Al_3 studied by neutron inelastic scattering.
Journal of the Physical Society of Japan **66**, 1884-1887 (1997)

SATO N., ASO N., LANDER G.H., ROESSLI B., KOMATSUBARA T., ENDOH Y. Possible spin-fluctuation mediated superconductivity in UPd_2Al_3.
Journal of the Physical Society of Japan **66**, 2981-2984 (1997)

SATULA D., DOBRZYNSKI L., WALISZEWSKI J., SZYMANSKI K., RECKO K., MALINOWSKI A., BRÜCKEL T., SCHÄRPF O., BLINOWSKI K. Structural and magnetic properties of Fe-Cr-Al alloys with DO_3-type structure.
Journal of Magnetism and Magnetic Materials **169**, 240-252 (1997)

SAUVAJOL J.L., BORMANN D., PALPACUER M., LERE-PORTE J.P., MOREAU J.J.E., DIANOUX A.J. Low and high-frequency vibrational dynamics as a function of structural order in polythiophene.
Synthetic Metals **84**, 569-570 (1997)

SAUVAJOL J.L., PAPANEK P., FISCHER J.E., DIANOUX A.J., MCNEILLIS P.M., MATHIS C., FRANCOIS B. Dynamics of pristine and doped conjugated polymers: a combined inelastic neutron scattering and computer simulation analysis.
Synthetic Metals **84**, 941-942 (1997)

SAVARIAULT J.M., ROZIER P. Evidence of lithium ordering in ε-$Li_xV_2O_5$ phase.
Physica B **234-236**, 97-99 (1997)

SCHEFER J., SCHWARZENBACH D., FISCHER P., KOETZLE T., HAUSSÜHL S., RÜDLINGER M. Single-crystal and powder neutron diffraction investigations of thermal motions in K_2PtCl_6 as a function of temperature.
Physica B **234-236**, 137-138 (1997)

SCHEFER J., WOIKE T., HAUSSÜHL S., FERNANDEZ-DIAZ M.T. Population and structural changes of the metastable state II in sodiumnitroprusside $(Na_2[Fe(CN)_5NO].2H_2O)$ at 60K.
Zeitschrift für Kristallographie **212**, 29-33 (1997)

SCHELLHORN U., RUPP R.A., BREER S., MAY R.P. The first neutron interferometer built of holographic gratings.
Physica B **234-236**, 1068-1070 (1997)

SCHERBAKOVA I.V., ZGURSKAYA E.I., FAN L.X., SERDYUK I.N., ZACCAI G. Metabolic regulation of selective deuterium incorporation into RNA and protein components of the ribosome.
In: 'Biological Macromolecular Dynamics', CUSACK S., BÜTTNER H.G. et al. (Eds.) (Adenine Press, 1997) pp. 165-169

SCHEYER Y., LEVELUT C., PELOUS J., COOK J.C., JOHNSON M.R., PROCHAZKA F., DURAND D. Relaxations versus crosslink density in glass- and gel-forming polyurethane.
Physica B **234-236**, 445-447 (1997)

SCHLEGER P., PUIG-MOLINA A., RESSOUCHE E., RUTTY O., SCHWEIZER J. A general maximum-entropy method for model-free reconstructions of magnetization densities from polarized neutron diffraction data.
Acta Crystallographica A **53**, 426-435 (1997)

SCHLENKER M., BARUCHEL J. Neutron topography.
In: 'X-ray and Neutron Dynamical Diffraction - Theory and Applications', AUTHIER A. et al. (Eds.) (Plenum Press, 1996) pp. 177-186

SCHLENKER M., GUIGAY J.P. Dynamical theory of neutron scattering.
In: 'X-ray and Neutron Dynamical Diffraction - Theory and Applications', AUTHIER A. et al. (Eds.) (Plenum Press, 1996) pp. 63-72

SCHMIDT W. Analytical resolution calculation beyond the Gaussian limit.
Physica B **234-236**, 1105-1106 (1997)

SCHOBER H., RENKER B. Spectroscopic evidence for dimer formation in Rb_1C_{70} compounds.
Solid State Communications **104**, 609-613 (1997)

SCHOBER H., RENKER B., HEID R., GOMPF F., TÖLLE A. Microscopic dynamics of A_1C_{60} compounds.
In: 'Complex Behaviour of Glassy Systems', RUBI M., PEREZ-VICENTE C. (Eds.) (Springer Verlag, 1997) pp. 62-81

SCHOBER H., RENKER B., HEID R., TÖLLE A. Dynamics and phase transitions in $A1C_{60}$ compounds.
Physica B **234-236**, 13-14 (1997)

SCHOBER H., TÖLLE A., RENKER B., HEID R., GOMPF F. Microscopic dynamics of AC_{60} compounds in the plastic, polymer, and dimer phases investigated by inelastic neutron scattering.
Physical Review B **56**, 5937-5950 (1997)

SCHOBINGER-PAPAMANTELLOS P., FAUTH F., BUSCHOW K.H.J. Uniaxial antiferromagnetic ordering in $HoNiSi_2$. A neutron and magnetic study.
Journal of Alloys and Compounds **252**, 50-52 (1997)

SCHOBINGER-PAPAMANTELLOS P., FAUTH F., MIDDLETON D.P., BUSCHOW K.H.J. Magnetic ordering of $TbNi_3Ga_2$ studied by neutron diffraction and magnetic measurements.
Journal of Alloys and Compounds **252**, 16-19 (1997)

SCHOBINGER-PAPAMANTELLOS P., OLEKSYN O., RITTER C., DE GROOT C.H., BUSCHOW K.H.J. Canted antiferromagnetic structure of the novel compound Er_3Ge_4 by neutron diffraction and magnetic measurements.
Journal of Magnetism and Magnetic Materials **169**, 253-260 (1997)

SCHWEIZER J. Magnetic scattering of neutrons: a technique with a real future.
In: 'Magnetism and Synchrotron Radiation', BEAUREPAIRE E. et al. (Eds.) (Les Editions de Physique, 1997) pp. 275-284

SCHWEIZER J. Spin densities in magnetic molecular compounds (invited paper).
Physica B **234-236**, 772-779 (1997)

SERDYUK I.N., ZACCAI G. Triple isotopic substitution method in small angle neutron scattering: application to some problems of structural biology.
Journal of Applied Crystallography **30**, 787-791 (1997)

SETTLES M., DOSTER W. Anomalous diffusion of adsorbed water: a neutron scattering study of hydrated myoglobin.
Faraday Discussions **103**, 269-279 (1996)

SETTLES M., DOSTER W. Iterative calculation of the vibrational density of states from incoherent neutron scattering data with the account of double scattering.
In: 'Biological Macromolecular Dynamics', CUSACK S. et al. (Eds.) (Adenine Press, 1997) pp. 3-8

SHOTTON M.W., POPE L.H., FORSYTH V.T., LANGAN P., DENNY R.C., GIESEN U., DAUVERGNE M.T., FULLER W. A high-angle neutron fibre diffraction study of the hydration of deuterated A-DNA.
Biophysical Chemistry **69**, 85-96 (1997)

SIMONET V., KLEIN H., BELLISSENT R., HIPPERT F., AUDIER M. Magnetism and local order in AlPdMn liquid alloys.
Physica B **234-236**, 594-595 (1997)

SKRIPOV A.V., COOK J.C., KARMONIK C., HEMPELMANN R. Localized motion of hydrogen in C15-type TaV_2: nuclear magnetic resonance and neutron scattering study.
Journal of Alloys and Compounds **253-254**, 432-434 (1997)

SMITH G.D., PAUL W., YOON D.Y., ZIRKEL A., HENDRICKS J., RICHTER D., SCHOBER H. Local dynamics in a long-chain alkane melt from molecular dynamics simulations and neutron scattering experiments.
Journal of Chemical Physics **107**, 4751-4755 (1997)

SONNTAG R., MELZER R., WESSELS T., RADAELLI P.G. $Cs_3H(SeO_4)_2$ at 300 K by high-resolution neutron powder diffraction.
Acta Crystallographica C **53**, 1529-1531 (1997)

SOSNOWSKA I., BUCHENAU U., REICHENAUER G., GRAETSCH H., IBEL K., FRICK B. Structure and dynamics of the opal silica-water system.
Physica B **234-236**, 455-457 (1997)

STAUB U., FAUTH F., GUTMANN M., KAGUNYA W.W. Magnetic properties of Tb doped in $YBa_2Cu_3O_8$.
Physica B **234-236**, 841-842 (1997)

STAUB U., SODERHOLM L., SKANTHAKUMAR S., OSBORN R., FAUTH F. Importance of the magnetic ground state of Pr for T_c suppression in high-T_c superconductors.
Europhysics Letters **39**, 663-668 (1997)

STAUB U., SODERHOLM L., SKANTHAKUMAR S., ROSENKRANZ S., RITTER C., KAGUNYA W.W. Quasi two-dimensional magnetic order of Tb^{3+} spins in $Pb_2Sr_2Tb_{1-x}Ca_xCu_3O_8$ (x=0 and 0.5).
Zeitschrift für Physik B **104**, 37-43 (1997)

STEGMANN R., MANAKOVA E., AXMANN S., RÖSSLE M., HERMANN T., MAY R.P., WIEDENMANN A., PLÜCKTHUN A., HEUMANN H. Conformational changes and spatial arrangement of the *E.coli* chaperones GroEL and GroES.
Physica B **234-236**, 220-222 (1997)

STEINER T., MASON S.A., TAMM M. Neutron diffraction study of aromatic hydrogen bonds: 5-ethynyl-5H-dibenzo[a,d]cyclohepten-5-ol at 20K.
Acta Crystallographica B **53**, 843-848 (1997)

STEYERL A., MALIK S.S., GELTENBORT P., NEUMAIER S., NESVIZHEVSKY V.V., UTSURO M., KAWABATA Y. Spectral evolution during ultracold neutron storage.
Journal de Physique III **7**, 1941-1954 (1997)

STOCKERT O., LÖHNEYSEN H.V., SCHROEDER A., LÖWENHAUPT M., PYKA N., GAMMEL P.L., YARON U. Incommensurate antiferromagnetism and magnetic correlations in $CeCu_{6-x}Au_x$.
Physica B **230-232**, 247-249 (1997)

STRITT N., JOLIE J., JENTSCHEL M., BÖRNER H.G. Study of atomic motion in oriented EuO single crystals using neutrino induced Doppler broadening.
Physical Review Letters **78**, 2592-2595 (1997)

STRITT N., JOLIE J., MASER H., PITZ H.H. A MeV tunable gamma-ray source by Compton scattering.
Nuclear Instruments and Methods in Physics Research A **381**, 443-452 (1996)

STUHR U., STRIFFLER T., WIPF H., NATTER H., WETTMANN B., JANSSEN S., HEMPELMANN R., HAHN H. An investigation of hydrogen diffusion in nanocrystalline Pd by neutron spectroscopy.
Journal of Alloys and Compounds **253-254**, 393-396 (1997)

STUHRMANN S., BARTELS K.S., BRAUNWARTH W., DOOSE R., DAUVERGNE F., GABRIEL A., KNÖCHEL A., MARMOTTI M., STUHRMANN H.B., TRAME C., LEHMANN M.S. Anomalous dispersion with edges in the soft x-ray region: first results of diffraction from single crystals of trypsin near the *K*-absorption edge of sulfur.
Journal of Synchrotron Radiation **4**, 298-310 (1997)

STUNAULT A., LANGRIDGE S., VETTIER C., GIBBS D., BERNHOEFT N.R. Near-surface effects at the antiferromagnetic phase transition in uranium phosphide.
Physical Review B **55**, 423-438 (1997)

SUARD E., MIREBEAU I., CAIGNAERT V., IMBERT P., BALAGUROV A.M. Influence of a deoxygenation process on the magnetic diagram of iron doped $YBa_2Cu_3O_x$ phases: a neutron diffraction study.
Physica C **288**, 10-20 (1997)

SUCK J.B. Temperature dependence of the generalized vibrational density of states of melt spun $Zr_{65}Cu_{27.5}Al_{7.5}$.
Materials Science and Engineering A **226-228**, 479-482 (1997)

SUCK J.B. Temperature dependence of the total dynamic structure factor of the metallic glass $Ni_{33}Zr_{67}$.
Journal of Non-Crystalline Solids **205-207**, 592-596 (1996)

SUCK J.B., SCHOBER H., GÜNTHERODT H.J. The generalised vibrational density of states and total dynamic structure factor of the metallic glass $Zr_{65}Cu_{17.5}Ni_{10}Al_{7.5}$ measured at room temperature.
Journal of Non-Crystalline Solids **205-207**, 733-736 (1996)

SUGENO H., TAKAMURA Y., SAKURAI H., NOMA M., GUNJI S., GELTENBORT P. A study of the rise time in a microstrip gas proportional counter for the development of an x-ray polarimeter.
IEEE Transactions on Nuclear Science **44**, 979-984 (1997)

SUNDARESAN A., CAIGNAERT V., RAVEAU B., SUARD E. Nuclear and magnetic structures in new distorted perovskites $Pr_{0.5-x}Ce_xSr_{0.5}MnO_3$ (x=0.1 and 0.2).
Solid State Communications **104**, 489-493 (1997)

SVOBODA P., REIF T., LÖWENHAUPT M., ROTTER M., GRATZ E., MCINTYRE G.J. Observation of higher-order harmonics in AF2 phase of $NdCu_2$.
Physica B **234-236**, 642-643 (1997)

SWENSON J., SMALLEY M.V., THOMAS R.K., CRAWFORD R.J., BRAGANZA L.F. Intermediate interlayer structure in butylammonium vermiculites.
Langmuir **13**, 6654-6657 (1997)

SZYTULA A., KOLENDA M., RESSOUCHE E. Magnetic structures of the $R_2Ni_3Si_5$ compounds (R=Tb, Dy, Ho).
Physica B **234-236**, 663-664 (1997)

SZYTULA A., KOLENDA M., RESSOUCHE E., SIKORA W. Neutron diffraction studies of magnetic structures of $R_2Ni_3Si_5$ (R=Tb, Dy, Ho) compounds.
Journal of Physics Condensed Matter **9**, 6651-6663 (1997)

SZYTULA A., KOLENDA M., RESSOUCHE E., ZYGMUNT A. Magnetic properties of RPdGe (R=Ce, Pr and Tb) compounds.
Journal of Alloys and Compounds **259**, 36-41 (1997)

TAKEDA T., SETO H., KOMURA S., GHOSH S.K., NAGAO M., MATSUBA J.I., KOBAYASHI H., EBISAWA T., TASAKI S., ZEYEN C.M.E., ITO Y., TAKAHASHI S., YOSHIZAWA H. A neutron spin echo spectrometer with an assembly of position sensitive detectors.
Journal of the Physical Society of Japan **65 Suppl. A**, 189-194 (1996)

THOMS M., LEHMANN M.S., WILKINSON C. The optimization of the neutron sensitivity of image plates.
Nuclear Instruments and Methods in Physics Research A **384**, 457-462 (1997)

TIETZE-JAENSCH H., KAMP R.V.D., SCHMIDT W., GEICK R., TREUTMANN W., VORDERWISCH P. The magnetic excitation spectrum of Rb_2MnCl_4.
Physica B **234-236**, 564-566 (1997)

TIETZE-JAENSCH H., SCHMIDT W., GEICK R. Evaluation of the ROTAX spectrometer.
Physica B **234-236**, 1152-1154 (1997)

TILS P., LÖWENHAUPT M., LOONG C.K., SCHOBER H. Crystal fields and exchange interactions in HoT_4Al_8 with T= Mn and Fe.
Physica B **234-236**, 739-740 (1997)

TIMMINS P.A., PEBAY-PEYROULA E. Protein-detergent interactions in single crystals of membrane proteins studied by neutron crystallography.
In: 'Neutrons in Biology', SCHOENBORN B.P., KNOTT R.B. (Eds.) (Plenum Press, 1996) pp. 267-272

TÖLLE A., SCHOBER H., WUTTKE J., FUJARA F. Coherent dynamic structure factor of orthoterphenyl around the mode coupling crossover temperature T_c.
Physical Review E **56**, 809-815 (1997)

TÖLLE A., SCHOBER H., WUTTKE J., FUJARA F., RANDL O.G. Incoherent dynamical structure factor of the compressed fragile liquid orthoterphenyl.
Physica B **234-236**, 428-430 (1997)

TOMKA G.J., KAPUSTA C., RITTER C., RIEDI P.C., CYWINSKI R., BUSCHOW K.H.J. Magnetic structure and transitions of $SmMn_2Ge_2$.
Physica B **230-232**, 727-730 (1997)

TOMY C.V., CHANG L.J., PAUL D. MCK., RITTER C. The nature of magnetic ordering in $TbNi_2B_2C$.
Physica B **230-232**, 872-875 (1997)

TONDEUR F., GARADY I., POFFIJIN A., MEESEN G., VANMARCKE H., OBERSTEDT S., PARIDAENS J., FLEMAL J.M., DEBAUCHE A., LELLIS C. DE Belgian intercomparison of solid state radon measurements.
In: 'Proceedings of the European Conference on Protection Against Radon at Home and Work' (1997)

TOPERVERG B.P., DORNER B., SONNTAG A., PETITGRAND D. Quantum paramagnetic fluctuations in $RbFeCl_3$ in a magnetic field applied perpendicular to the anisotropy axis.
Physical Review B **55**, 983-993 (1997)

TORTET L., GAVARRI J.R., NIHOUL G., DIANOUX A.J. Proton mobilities in brushite and brushite/polymer composites.
Solid State Ionics **97**, 253-256 (1997)

TORTET L., GAVARRI J.R., NIHOUL G., DIANOUX A.J. Study of protonic mobility in $CaHPO_4.2H_2O$ (brushite) and $CaHPO_4$ (monetite) by infrared spectroscopy and neutron scattering.
Journal of Solid State Chemistry **132**, 6-16 (1997)

TRABELSI M., COULOMB J.P., DEGENHARDT D., LAUTER H.J. Structures of the nitrogen monolayer adsorbed on MgO (100).
Surface Science **377-379**, 38-44 (1997)

UDOVIC T.J., RUSH J.J., HUANG Q., ANDERSON I.S. Neutron scattering studies of the structure and dynamics of rare-earth hydrides and deuterides.
Journal of Alloys and Compounds **253-254**, 241-247 (1997)

VACHER R., PELOUS J., COURTENS E. Mean free path of high-frequency acoustic excitations in glasses with application to vitreous silica.
Physical Review B **56**, R481-R484 (1997)

VAN DIJK N.H., BOURDAROT F., FÅK B., LAPIERRE F., REGNAULT L.P., BURLET P., BOSSY J., PYKA N., MENOVSKY A.A. Magnetic order of the heavy-fermion URu_2Si_2 in a field of 12T.
Physica B **234-236**, 692-693 (1997)

VELLETTAZ N., ASSAF J.E., OED A. Two-dimensional gaseous microstrip detector for thermal neutrons.
Nuclear Instruments and Methods in Physics Research. A **392**, 73-79 (1997)

VENTURINI G., IJJAALI I., RESSOUCHE E., MALAMAN B. Neutron diffraction study of the HoMnSi, LuMnSi and $Sc_{0.9}Lu_{0.1}MnSi$ compounds.
Journal of Alloys and Compounds **256**, 65-75 (1997)

VENTURINI G., MALAMAN B., RESSOUCHE E. Neutron diffraction study of the $Tb_3Mn_4Ge_4$ compound.
Journal of Alloys and Compounds **248**, 101-105 (1997)

VERON M., BASTIE P. Strain induced directional coarsening in nickel based superalloys: Investigation on kinetics using the small angle neutron scattering (SANS) technique.
Acta Materiala **45**, 3277-3282 (1997)

VILLAIN J., WÜRGER A., FORT A., RETTORI A. Effet tunnel dans les systèmes magnétiques: de la description microscopique et déterministe à l'équation maîtresse.
Journal de Physique I **7**, 1583-1594 (1997)

VORDERWISCH P., HAUTECLER S., KEARLEY G.J., KUBANEK F. Influence of the guest molecule on the rotational motions of ammonia groups in Hofmann clathrates.
Physica B **234-236**, 68-69 (1997)

WAGEMANS C., LOISELET M., BIEBER R., DENECKE B., REHER D., GELTENBORT P. Preparation, characterization and testing of implanted ^{37}Ar-layers.
Nuclear Instruments and Methods in Physics Research A **397**, 22-25 (1997)

WAGNER J.L., CHMAISSEN O., JORGENSEN J.D., HINKS D.G., RADAELLI P.G., HUNTER B.A., JENSEN W.R. Multiple defects in overdoped $Tl_2Ba_2CuO_{6+\delta}$: effects on structure and superconductivity.
Physica C **277**, 170-182 (1997)

WALTERS J.K., KUEHN M., SPAETH C., FISCHER H., RICHTER F., NEWPORT R.J. Neutron-diffraction studies of amorphous CN_x materials.
Physical Review B **56**, 14315-14321 (1997)

WEBSTER G.A., EZEILO A.N. Principles of the measurement of residual stress by neutron diffraction.
In: 'New Instruments and Science Around SINQ. Lecture Notes of the '4th Summer School on Neutron Scattering' PSI Proceedings 96-02 (PAUL SCHERRER INSTITUTE, 1996) pp. 217-234

WEIDENTHALER C., FISCHER R.X., ABRAMS L., HEWAT A.W. Zeolite rho loaded with methylamines. I. Monomethylamine loadings.
Acta Crystallographica B **53**, 429-439 (1997)

WEIDENTHALER C., FISCHER R.X., ABRAMS L., HEWAT A.W. Zeolite rho loaded with methylamines. III. Trimethylamine loadings.
Acta Crystallographica B **53**, 444-450 (1997)

WEIK M., ZACCAI G., DENCHER N.A., OESTERHELT D., HAUSS T. Structure and hydration of the M-state of the bacteriorhodopsin mutant D96N studied by neutron diffraction.
Journal of Molecular Biology **275**, 625-634 (1998)

WEIS R., ENSS C., WÜRGER A., LUTY F. Coherent tunneling of lithium defect pairs in KCl crystals.
Annalen der Physik **6**, 263-286 (1997)

WESS T.J., WESS L., MILLER A. The chemical reactivity and structure of collagen studied by neutron diffraction.
In: 'Neutrons in Biology', SCHOENBORN B.P., KNOTT R.B. (Eds.) (Plenum Press, 1996) pp. 369-383

WILLIAMS S., BECERRO A.I., CASTRO M.A., THOMAS R.K. Arrangement of surfactant molecules in the internal surfaces of layered materials.
Physica B **234-236**, 1096-1098 (1997)

WILSON J.E., ANSELL S., ENDERBY J.E., NEILSON G.W. Water structure around chloride ions in the presence of biological macromolecules.
Chemical Physics Letters **278**, 21-25 (1997)

WINTER R., LANDWEHR A., BRAUNS T., ERBES J., CZESLIK C., REIS O. High-pressure effects on the structure and phase behavior of model membrane systems.
In: 'High Pressure Effects in Molecular Biophysics and Enzymology' (1996) pp. 274-297

WOLFERS P., BACMANN M., FRUCHART D. Low-temperature structures of the $Er_2Fe_{14}B$ ferromagnetic compound.
Physica B **234-236**, 654-655 (1997)

WORCESTER D.L., HAMACHER K., KAISER H., KULASEKERE R., TORBET J. Intercalation of small hydrophobic molecules in lipid bilayers containing cholesterol.
In: 'Neutrons in Biology', SCHOENBORN B.P., KNOTT R.B. (Eds.) (Plenum Press, 1996) pp. 215-226

WÜRGER A. Dissipative tunneling in insulators: noninteracting blip approximation and beyond.
Physical Review Letters **78**, 1759-1762 (1997)

WÜRGER A. Perturbation theory for the spin-phonon model.
Journal of Physics Condensed Matter **9**, 5543-5560 (1997)

WUTTKE J., CHANG I., FUJARA F., PETRY W. Viscous glycerol.
Physica B **234-236**, 431-432 (1997)

ZACCAI G. Towards inelastic neutron scattering in biology.
In: 'Cold Neutrons: Large Scale - High Resolution. Lecture Notes of the 5th Summer School on Neutron' PSI Proceedings 97-01 (Paul Scherrer Institute, 1997)

ZAWADOWSKI A., ZARAND G., NOZIERES P., VLADAR K., ZIMANYI G.T. Instability of the marginal commutative model of tunneling centers interacting with a metallic environment: role of the electron-hole symmetry breaking.
Physical Review B **56**, 12947-12960 (1997)

ZEISKE T., HARRIS M.J., ZINKIN M.P. Antiferromagnetic fluctuations in a modified pyrochlore.
Physica B **234-236**, 766-767 (1997)

ZEYEN C.M.E., KAKURAI K., NISHI M., NAKAJIMA K., SAKAGUCHI T., KAWAMURA Y., WATANABE S., BERNERON M., SASAKI K., ENDOH Y. Thermal neutron spin echo three-axis spectrometer with μeV resolution.
Neutron News **8**, 7-10 (1997)

ZEYEN C.M.E., OTAKE Y., TABARU T., TOPERVERG B. Search for neutron EDM using crystal techniques.
Journal of the Physical Society of Japan **65 Suppl. A**, 177-182 (1996)

Books published

CUSACK S., BÜTTNER H.G., FERRAND M., TIMMINS P.A. Biological macromolecular dynamics.
Adenine Press, 1997

GEBHARD F.
The Mott metal-insulator transition. Models and methods.
Springer Verlag, 1997
ISBN 3-540-61481-8

ZACCAI G., GARREC C.
Structure et fonction des protéines et acides nucléiques.
Editions Nathan, 1998

Theses and Habilitations

CHENET A. Ein Phasenschieber für Laserlicht für das VCN-Interferometer am ILL in Grenoble.
Diplomarbeit zur Erlangung des Titels Magister rerum naturalium. Institut für Experimentalphysik Universität Innsbruck, Institut Laue-Langevin, Grenoble (1997)

CICOGNANI G. Etude d'un détecteur gazeux à micropistes avec lecture à pixels.
Institut Laue-Langevin, Grenoble, France. Thèse présentée en vue d'obtenir le titre de Docteur de l'Université Joseph Fourier, Grenoble 1 (1997)

COLE J.M. Structural studies of organic and organometallic compounds using x-ray and neutron techniques.
University of Durham (1997)

DUBOS O. Effets d'interférence sur la loi de diffusion des phonons, un exemple le Zirconium cubique centré.
Thèse présentée en vue d'obtenir le titre de Docteur de l'Université de Picardie Jules Vernes (1996)

DUBOS P. Interaction entre un peptide et une bicouche de phospholipides.
Institut Laue-Langevin et Laboratoire de Spectrométrie Physique, Grenoble, France (1997)

FISCHER H.E. Mémoire présenté pour l'obtention d'une habilitation à diriger les recherches.
Institut Laue-Langevin, Grenoble, France (1997)

FISCHER H.E. Soutenance de DHDR (Diplome d'Habilitation à diriger les recherches).
Université Joseph Fourier Grenoble I, France (1997)

FUSELLIER G. Rheology of aqueous suspensions of a fibrous clay: sepiolite.
Institut National Polytechnique, Grenoble, France (1997)

GÖCKING K.D. Untersuchung lamellarer Phasen von Mikroemulsionen mit Neutronenstreuung.
Westfälische Wilhelms-Universität Münster (1997)

HIESS A. Untersuchungen zur Konkurrenz der magnetischen Wechselwirkungen in elektronisch hochkorrelierten Metallen. Neutronenstreuung - Magnetische Röntgendiffraktion - Mössbauer-Spektroskopie - Magnetisierungsexperimente.
Vom Fachbereich Physik der Technischen Hochschule Darmstadt zur Erlangung des Grades eines Doktors der Naturwissenschaften (1996)

PIGNON F. Rheology of thixotropic aqueous dispersions of a hectorite-type clay.
Institut National Polytechnique, Grenoble, France (1997)

SCHEYER Y. Transition vitreuse dans les gels de polyuréthane: étude de la dynamique par diffusion inélastique de la lumière et des neutrons.
Université de Montpellier II, France (1997)

TANG K.T. Studies of ^{158}GD by thermal neutron capture reactions and by IBA-1 model calculations.
University of Brighton and Institut Laue-Langevin (1997)

TÖLLE A. Relaxationen in viskosem Orthoterphenyl - Ein Test der Modenkopplungstheorie mit Hilfe der dynamischen Neutronenstreuung.
Dissertation zur Erlangung des Grades eines Doktors der Naturwissenschaften des Fachbereichs Physik der Universität Dortmund (1997)

ZANOTTI J.M. Structure et dynamique de l'eau interfaciale. Rôle de l'eau d'hydratation dans la dynamique des protéines globulaires.
Thèse de Doctorat de l'Université Paris XI pour obtenir le grade de Docteur de l'Université Paris XI (1997)

Editors: Herma G. Büttner, Alan J. Leadbetter
Design and typesetting: Soft Office – www.softoffice.fr
Photography by J.L. Baudet, H.G. Büttner, S. Claisse, J. Italia (ILL), Studio de la Revirée
Printing: V8
April 1998

Acknowledgement
We would like to thank all the people who helped make this report.

Further copies can be obtained from:
Institut Laue-Langevin
Scientific **C**oordination **O**ffice (SCO)
BP 156 – F-38042 Grenoble Cedex 9 (France)
tel: +33 (0)4 76 20 72 40 – fax: +33 (0)4 76 48 39 06
email: kjenkins@ill.fr or sco@ill.fr
web: www.ill.fr

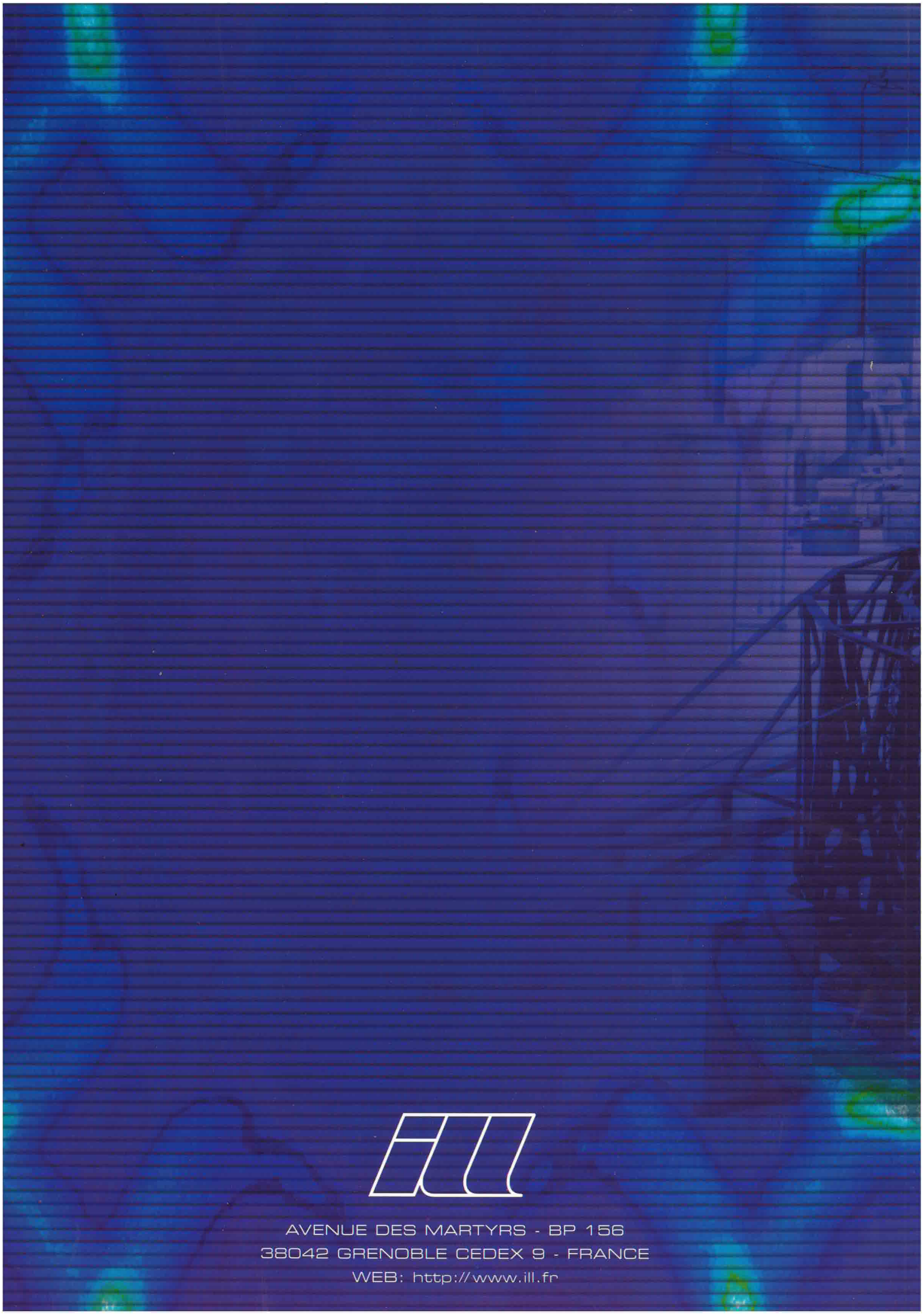

AVENUE DES MARTYRS - BP 156
38042 GRENOBLE CEDEX 9 - FRANCE
WEB: http://www.ill.fr